acta physica slovaca vol. 60 No. 3, 259 – 391 **June 2010**

RELATIVISTIC EFFECTS IN ATOMIC AND MOLECULAR PROPERTIES *

Miroslav Iliaš,[a,1] **Vladimír Kellö,**[b,2] **Miroslav Urban**[b,c,3]

[a] *Department of Chemistry, Faculty of Natural Sciences, Matej Bel University, Tajovského 40, SK–974 00 Banská Bystrica, Slovakia*

[b] *Department of Physical and Theoretical Chemistry, Faculty of Natural Sciences, Comenius University, Mlynská dolina, SK–842 15 Bratislava, Slovakia*

[c] *Slovak University of Technology in Bratislava, Faculty of Materials Science and Technology in Trnava, Institute of Materials Science, Bottova 25, SK–917 24 Trnava, Slovakia.*

Received 17 May 2010, accepted 1 June 2010

This paper is dedicated to the memory of our friend, prof. Andrzej J. Sadlej, with whom we had a privilege and pleasure to collaborate for decades in many areas of theoretical and computational chemistry. We are particularly indebted to Andrzej for introducing us to the area of relativistic effects and their importance in atomic and molecular properties. Senior authors will remember forever days and nights of joint work and discussions on chemistry, physics and life.

We present an overview of basic principles and methods of the relativistic quantum chemistry. Practical aspects of different methods will be discussed stressing their capability of providing accurate predictions of molecular properties, particularly in species containing a heavy metal element. We will present a series of examples showing the importance of relativistic effects in a variety of molecular properties including electron affinities, ionization potentials, reaction and dissociation energies, electric, spectroscopic and other properties. It is possible to recognize a link between these properties and behaviour of materials in some cases. Particular attention is paid to relativistic calculations of the nuclear quadrupole moments for which accurate theoretical electric field gradient is combined with data from the microwave spectra. Important aspect of the present paper is understanding of trends in electronically related atoms throughout the Mendeleev Periodic Table rather than focusing on highly accurate numbers. We will show that relativistic effects represent an unavoidable instrument for explaining some unexpected properties of heavy metal containing compounds. We will also discuss an interplay between the many–electron correlation and relativistic effects.

DOI: 10.2478/v10155-010-0003-1

PACS: 31.15.A-, 31.15.aj, 31.15.ap, 31.15.bw, 31.15.V-, 31.30.jc, 31.30.jp, 32.10.Hq

KEYWORDS: Relativistic effects, Electron correlation, Change of picture, Ionization potentials, Electron affinities, Excitation energies, Dipole moments and polarizabilities, Electric field gradients, Nuclear quadrupole moments, Multiple bonds, Intermolecular interactions, NMR.

*The reference [71] was corrected by the authors after the paper had been printed out.

[1] E-mail address: ilias@fpv.umb.sk

[2] E-mail address: kelloe@fns.uniba.sk

[3] E-mail address: urban@fns.uniba.sk; miroslav.urban@stuba.sk

Contents

1 Introduction

Until the seventies of the 20th century it was generally accepted that for a description of the electronic structure of atoms and molecules and, therefore, for the whole chemistry and for the substantial part of physics, relativistic theory is not needed. According to Sheldon L. Glashow [1], Nobel Prize Winner for Physics, 1979, *"Modern elementary–particle physics is founded upon the two pillars of quantum mechanics and relativity. I have made little mention of relativity so far because, while the atom is very much a quantum system, it is not very relativistic at all. Relativity becomes important only when velocities become comparable to the speed of light. Electrons in atoms move rather slowly, at a mere of one percent of light speed. Thus it is that a satisfactory description of the atom can be obtained without Einstein's revolutionary theory."* Possibly these beliefs were initiated by Dirac himself [2], who wrote in 1929 that *"Relativistic effects are therefore of no importance in the consideration of atomic and molecular structure and ordinary chemical reactions"*. In the last thirty years the situation has changed considerably. Presently, it is generally accepted that relativistic effects must be considered in compounds containing heavy metal elements. Even understanding of the Mendeleev Periodic Table is impossible without utilizing the ideas of theory of relativity along, of course, with quantum physics. When talking about the relativistic theory of atoms and molecules we mean, of course, the special theory of relativity discovered by Einstein in 1905. It was in the same year in which he published the theory of the photo–electric effect, which is one of pillars on which the quantum mechanics was founded few years later. Therefore, both fundamental theories of the electronic structure of atoms and molecules were discovered and developed about at the same time, in first few years of the twenties century. Quantum physics was accepted as a basic theory for understanding of atomic and molecular properties almost immediately after its discovery. The first theory of the chemical bond formulated by Heitler and London in 1927 [3], is considered as the "birthday" of quantum chemistry. Theory of relativity, however, was awaiting for recognition of its fundamental importance in molecular physics and chemistry much longer. It took several decades after Dirac's formulation of his fundamental relativistic quantum mechanics in 1928 [4] until his theory was developed as a tool for the treatment of many–electron molecular systems. Currently, it is generally accepted that both, quantum mechanics and the special theory of relativity, are essential in the description and understanding of molecular properties. Clearly, relativity is increasingly important for molecules containing an element with high atomic number. However, even accurate description of properties of the lightest hydrogen molecule, as performed by Kołos and Wolniewicz in 1961 [5] showed that careful treatment of relativistic effects is unavoidable. Solutions of the Dirac–Fock equations [6,7] for many–electron systems with atomic numbers up to 120 was presented by Desclaux in 1973 [8]. An important milestone on a long way towards recognizing the importance of the relativistic quantum theory in understanding general trends of molecular properties is a paper entitled "Relativity and the Periodic System of elements" published by Pyykkö and Desclaux in 1979 [9]. This work was followed by many other reviews on the development of the relativistic quantum theory and its applications in quantum molecular sciences by Pyykkö, Kutzelnigg, Schwerdtfeger, Schwarz and other authors [10–22], to name at least a few. A further development of relativistic quantum chemistry in molecular sciences was greatly affected by excellent books published recently, particularly *Relativistic electronic structure theory, Part 1. Fundamentals* and *Part 2. Applications*, edited by Schwerdtfeger [23, 24] and books by Dyall and Fægri [25] and by Reiher and Wolf [26].

The purpose of this review is a short description of basic nonrelativistic theories, including most important methods for treating the many–electron correlation problem. An essential part of this paper is devoted to a transparent overview of relativistic many–electron theories in which the electron correlation problem (very difficult to treat accurately even at the nonrelativistic level) will be considered at the relativistic level. Rigorous four–component relativistic many–electron calculations for larger molecules are hardly tractable in the spirit of the four–component Dirac relativistic quantum mechanics [4,27]. Approximate extensions applicable to many–electron systems including electron correlation are feasible but very tedious. Methodologies which give rise to a variety of two–component Hamiltonians and allow treating larger molecular systems will be discussed in more detail in Section 4 and specifically in Section 4.6. For practical purposes it is important to note that in many applications it is sufficient to consider relativistic effects even at the no–pair one–component level. This is frequently denoted as ”scalar” relativistic level. This is a pragmatic attitude toward the many–electron correlated relativistic treatment of molecules. Great advantage is that scalar relativistic effects can be taken into account within common nonrelativistic many–electron wave function methods, with only a small modification. One– and two–component methods are frequently called also as ”quasi–relativistic”. Spin–orbit (SO) effects are neglected within the one–component framework but applications may go to as large molecules as it is possible in the nonrelativistic case, still using sophisticated many–electron wave function methods. We will demonstrate this approach in many applications to problems in which spin–orbit effects are unimportant. A large part of relativistic quantum chemistry calculations is performed using the density functional theory (DFT) which is applicable to truly large systems, although the control of accuracy is to some extent questionable.

In comparison with scalar relativistic effects, rigorous four–component many–electron relativistic theories employing sophisticated treatment of the electron correlation, like relativistic Coupled Cluster (CC) theories, are very tedious in most cases. Nevertheless, there is a large progress in making these theories (or their theoretically well founded approximations) applicable to a larger variety of systems of chemical and physical importance. We will pay attention to these theories and to their transformation to two–component treatments which are better applicable to larger many–electron calculations still allowing sufficiently accurate treatment of spin–orbit effects.

Somewhat out of the main scope of this review are fine structure problems, *e.g.*, spectra of atoms and molecules, Lamb shift, Quantum Electron Dynamics (QED) effects to which pay large attention some experts in relativistic many– electron theories. Of course, there exists a rich literature on QED effects in simple systems. Less is known about the importance of these effects on properties and reactivity of many–electron atoms and molecules. Presently, some results indicate that QED effects may eventually lead to interesting chemical and physical consequences but the knowledge in this area still remains quite limited [28, 29].

2 Manifestation of relativistic effects on atomic properties. Basic notes.

Historically, a breakdown in understanding of the chemical and physical behaviour of elements and their compound goes back to the formulation of the periodic law and the Periodic Table of elements by D. I. Mendeleev in 1869 [30]. The impact of his discovery on chemistry and molecular physics can be hardly exaggerated. As the greatest (we believe) theoretical chemist in the history, Mendeleev was able to systematise the accumulated knowledge, to interpret the facts and to predict chemical properties of elements and their compounds. Yet, he has failed in placing some elements at proper positions. As we can see in Fig. 2.1, in which we reproduce the Mendeleev Periodic Table from his 1869 paper published in Germany [31] which was abstracted from the original Russian paper [30], most elements have proper location. It corresponds to our present knowledge of the isoelectronic valence electronic structure of elements belonging to the same group in the Periodic Table. As we can see, incorrect location concerns in fact exclusively

Ueber die Beziehungen der Eigenschaften zu den Atomgewichten der Elemente. Von D. Mendelejeff. — Ordnet man Elemente nach zunehmenden Atomgewichten in verticale Reihen so, dass die Horizontalreihen analoge Elemente enthalten, wieder nach zunehmendem Atomgewicht geordnet, so erhält man folgende Zusammenstellung, aus der sich einige allgemeinere Folgerungen ableiten lassen.

			Ti = 50	Zr = 90	? = 180
			V = 51	Nb = 94	Ta = 182
			Cr = 52	Mo = 96	W = 186
			Mn = 55	Rh = 104,4	Pt = 197,4
			Fe = 56	Ru = 104,4	Ir = 198
			Ni = Co = 59	Pd = 106,6	Os = 199
H = 1			Cu = 63,4	Ag = 108	Hg = 200
	Be = 9,4	Mg = 24	Zn = 65,2	Cd = 112	
	B = 11	Al = 27,4	? = 68	Ur = 116	Au = 197?
	C = 12	Si = 28	? = 70	Sn = 118	
	N = 14	P = 31	As = 75	Sb = 122	Bi = 210?
	O = 16	S = 32	Se = 79,4	Te = 128?	
	F = 19	Cl = 35,5	Br = 80	J = 127	
Li = 7	Na = 23	K = 39	Rb = 85,4	Cs = 133	Tl = 204
		Ca = 40	Sr = 87,6	Ba = 137	Pb = 207
		? = 45	Ce = 92		
		?Er = 56	La = 94		
		?Yt = 60	Di = 95		
		?In = 75,6	Th = 118?		

1. Die nach der Grösse des Atomgewichts geordneten Elemente zeigen eine stufenweise Abänderung in den Eigenschaften.
2. Chemisch-analoge Elemente haben entweder übereinstimmende Atomgewichte (Pt, Ir, Os), oder letztere nehmen gleichviel zu (K, Rb, Cs).
3. Das Anordnen nach den Atomgewichten entspricht der *Werthigkeit* der Elemente und bis zu einem gewissen Grade der Verschiedenheit im chemischen Verhalten, z. B. Li, Be, B, C, N, O, F.
4. Die in der Natur verbreitetsten Elemente haben *kleine* Atomgewichte

Fig. 2.1. Mendeleev Periodic Table as published in 1869, Ref. [31].

elements with a high atomic weight, or, as we are saying nowadays, with a high atomic number. Most striking examples are mercury, gold, lead, or thallium. Mendeleev was able to recognize that atomic weights of some elements (one of ingredients on which his Table is founded) are incorrect. His knowledge about the chemical and physical behaviour of elements and their compounds was essential but what is really admirable, is his fascinating intuition. All this did not help him in properly placing some heavy elements in the Table. Presently, the reason is well known. It is relativity which changes chemical and physical behaviour of atoms and molecules substantially. Throughout the Periodic Table there are some irregularities which were difficult to explain before the era of an extended exploitation of the relativistic quantum mechanics in the theory of atoms and molecules. We demonstrate some of these irregularities in Tab. 2.1.

Very transparent example is a behaviour of the coinage elements, Cu, Ag, and Au. In the seventieth, we could find in textbooks (see, *e.g.*, Ref. [34]) a description of their properties as "...quite different in spite of the same valence electron structure, (n-1)s^2(n-1)p^6(n-1)d^{10}ns^1. We have no reasonable explanation of this behaviour...". Concerning copper, it is characterized by much smaller energy gap between the $3d^{10}$ and $4s^1$ orbitals than is the analogous energy gap between $4d^{10}$ and $5s^1$ orbitals in Ag. Cu behaves like a first group transition metal and exhibits larger electron correlation effects than Ag. Different chemical and physical properties of Au and Ag result mainly from large relativistic effects in Au. Many properties, even the yellow colour of the metallic gold, are caused by relativistic effects. If relativistic effects were negligible or absent, a saying "a nonrelativistic gold would be a silver" is quite appropriate. One example are large relativistic effects in gold leading to "irregularities" or "V–shaped" pattern of ionization potentials (IP's) in the series Cu, Ag, and Au [33], as shown in Fig. 2.2. It is well known that atomic ionization potentials vary within the Periodic Table according to their valence electronic structure. For a group of atoms characterized by the same valence electrons, like (n-1)s^2(n-1)p^6(n-1)d^{10}ns^1 in Cu, Ag, and Au one expects that ionization of the ns^1 electron would be easier with increasing atomic number. That means, the expected sequence of IP's should be Cu$<$Ag$<$Au. Experimental data in Tab. 2.1 show that IP of Ag is lower than IP of Cu, as expected. However, on the contrary to our expectations, IP of gold is the largest within the family of coinage metals. This experimental finding can be understood by employing three approximations with gradually improved theoretical levels for calculating ionization potentials, as demonstrated in Fig. 2.2. The lowest theoretical level is the nonrelativistic Restricted Open

Tab. 2.1. Common anomalies in the periodic system, coinage metal elements. Data from Ref. [32].

Property	Cu	Ag	Au
Melting point [$^\circ$C]	1085	962	1064
Boiling point [$^\circ$C]	2562	2162	2856
Electron affinity [eV]	1.235	1.302	2.309
Ionization potential [eV]	7.726	7.576	9.225
Standard specific electrical resistivity [$10^{-8}\Omega$m]	1.712	1.617	2.255
Polarizability^a [a.u.]	46.5	52.46	36.06

^{a} Ref. [33]

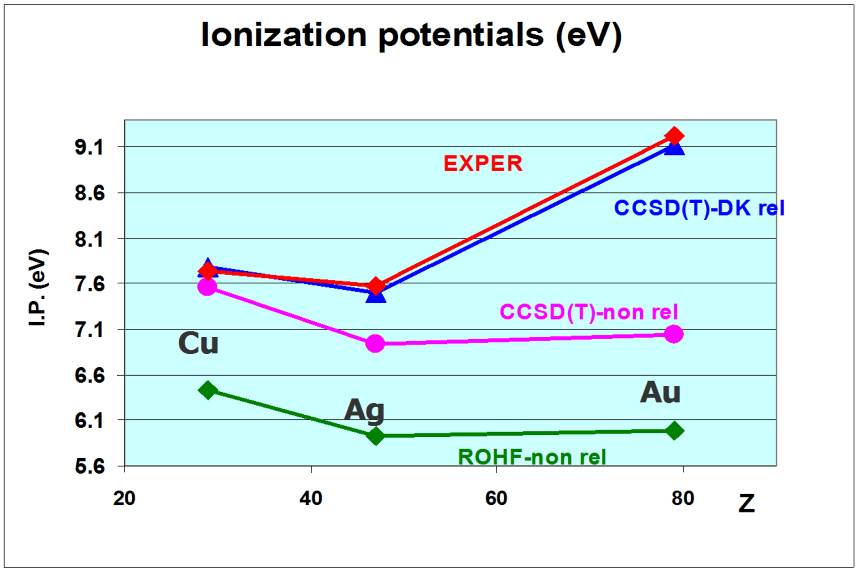

Fig. 2.2. Electron correlation and relativistic effects in ionization energies (eV) of the coinage elements Cu, Ag, and Au. The ROHF nonrelativistic data represent calculations using a single determinant Restricted Open shell Hartree Fock calculation. Electron correlation is treated by the Coupled Cluster CCSD(T) method and relativistic effects are calculated by the no–pair spin–free Douglas–Kroll–Hess method. Data from Ref. [33].

Shell Hartree–Fock one–electron calculation (ROHF), which treats inter–electronic interactions only approximatively. This model is completely insufficient in describing IP's of any of the three coinage metals. The error is larger than 1 eV. Clearly, electron correlation effects are inevitable.

Sophisticated description of the electron correlation provides the Coupled Cluster CCSD(T) method in which amplitudes of the single and double excitations with respect to the single determinant ROHF wave function are treated iteratively. Computationally demanding triple excitations employ the resulting CCSD amplitudes perturbatively in a single noniterative step. Normally, this is an excellent many–electron model [35–40] capable of interpreting and predicting atomic and molecular properties very accurately, see Section 3.2.5. The difference between nonrelativistic ROHF and CCSD(T) results is largest for Cu, followed by Au. Nevertheless electron correlation effects, as represented by the difference between ROHF and CCSD(T) calculations, are similar for all three valence isoelectronic coinage metals. IP of Cu calculated using the nonrelativistic CCSD(T) method agrees with experiment reasonably well. When relativistic effects are neglected for Ag, the CCSD(T) result deviates from experiment considerably, by about 0.5 eV, while for Au is the nonrelativistic result completely misleading. Considering the no–pair one–component scalar relativistic approximation, used in calculations presented in Fig. 2.2 is quite satisfactory for reproducing and predicting ionization potentials of Cu, Ag, Au, and many other atoms and molecules. This approximation works quite well for states that are not affected by other relativistic effects, particularly spin–orbit effects, significantly. The electronic state of Cu, Ag, and Au and their ions is ^{2}S and ^{1}S (a closed–shell), respectively, which are not split into spin–orbit components. It is good to remind already now, that SO effects may contribute even for the closed–shell singlet or some doublet states (like ^{2}S states). Although these states do not split by SO effects, their core–valence d and f, *etc.* orbitals do [8]. When working within true four–component theories, valence s–orbitals (which have obviously only one SO component) feel different field from different SO components of orbitals with higher orbital momenta. This effect may contribute to atomic or molecular properties, when accurate final results are required. Calculations as presented in Fig. 2.2 represent a scheme which will be used in this paper quite frequently. In order to recognize the importance of relativistic effects we will start our treatment with the nonrelativistic Hamiltonian and the nonrelativistic Hartree–Fock wave function or, alternatively, using a sophisticated wave function in which electron correlation is considered reasonably accurately. This $\hat{H}_0$ Hamiltonian is then supplemented by a relativistic term, $\hat{H}_{relativistic}$. As we will show later, there are numerous approximations to the relativistic Hamiltonian. Occasionally we can consider in the first step scalar relativistic effects corrected subsequently by SO or higher relativistic effects. We note that the electron correlation, relativistic, and SO contributions are not independent and, therefore, are not additive. We also stress, that when talking about relativistic effects, atoms and molecules are neither nonrelativistic or relativistic. Relativistic effects are present in all species, irrespective whether participating atoms have low or very high atomic numbers. The difference is only the magnitude of relativistic effects related to the accuracy which is required for a property under consideration. Therefore, when talking about "nonrelativistic" or "relativistic" atoms and molecules and their theoretical description, we have in mind just different models representing their Hamiltonian and the corresponding wave function. In the nonrelativistic representation we refer to the world where the speed of light c would be infinite. In reality, it is finite and this is the real world of atoms and molecules.

Returning now to Fig. 2.2, the enhancement of IP of gold (and to a lesser extent also of Cu and Ag) can be rationalized in quite transparent terms. A summary of basic effects encountered in the real world of the finite speed of light has been formulated by Pyykkö [9]. The three most frequently occurring relativistic effects are the relativistic shrinking and stabilization of s orbitals (and to a lesser extent also p orbitals), the spin–orbit splitting of p, d, *etc.* orbitals, and third, the relativistic self–consistent expansion and destabilization of d and f orbitals. Electrons in d and f subshells are far from the nucleus and their velocities are much lower than the speed of light. Therefore, the last effect, relativistic radial expansion and destabilization of d and f electronic shells is indirect and follows from relativistically affected screening of nucleus by s and p electrons. Since their radial distribution shrinks, the d and f subshells expand. Now, since inner shell $1s$ electrons of Au move near the nucleus with the velocity comparable to the speed of light, these electrons are relativistically stabilized and corresponding orbitals shrink. In many–electron systems all electrons up to valence electrons "feel" this effect, being stabilized and shrunk as well. Consequently, removing an electron from the valence $6s$ orbital is hindered by this stabilization and leads to an enhanced ionization potential. The same mechanism explains a relativistically enhanced electron affinity (EA) of coinage metals and particularly of Au, so that Au has a larger electron affinity than other coinage metals, see Tab. 2.1. The relativistic modification of the shape of the valence electrons of Au and particularly shrinking of the $6s$ orbital affects also its dipole polarizability. Consequently, the polarizability of this atom is lower than is the polarizability of Cu or Ag, in spite of a higher atomic number and the expected

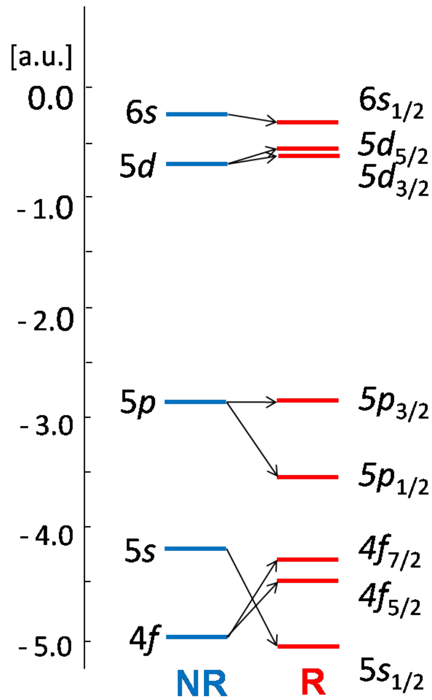

Fig. 2.3. Nonrelativistic and relativistic Hartree–Fock energies of outer orbitals of Hg. Data from Ref. [41].

largest volume of Au. This has important consequences in intermolecular interactions with a participation of a heavy metal element. How relativistic effects affect atomic orbital energies of, *e.g.*, the mercury atom is schematically shown in Fig. 2.3. This scheme follows from pioneering Dirac–Fock calculations of Desclaux and Kim [41] and is quite general.

Note that the energy gap between the valence $6s$ and $5d$ orbitals diminishes significantly. At the same time, $5p$ and $5s$ orbitals are relativistically stabilized and $4f$ orbitals destabilized. The consequence is the reversed sequence of some components of $4f$ and $5s$ orbitals. Clearly, relativistic stabilization/destabilization of orbitals may affect the energy differences between the ground and excited states of atoms and molecules and alter in this way their spectra and other properties. The scheme as presented in Fig. 2.3 is quite useful for qualitative discussion of ionization potentials and electron affinities of the coinage elements which have very simple valence electronic structure. A dominating role in processes which determine IP and EA of Cu, Ag, and Au, play ns electrons. Stabilization of these orbitals is quite general so that qualitative assessment of relativistic effects in such species is simple.

More complicated is the situation when there are partly occupied valence p, d, *etc.* shells. These shells split up due to spin–orbit effects and resulting different components behave differently when considering relativistic effects. Note, *e.g.*, $p_{1/2}$ orbitals shrink and are stabilized more than $p_{3/2}$ orbitals. Noteworthy is the Z-dependence of the orbital shifts. The stabilization

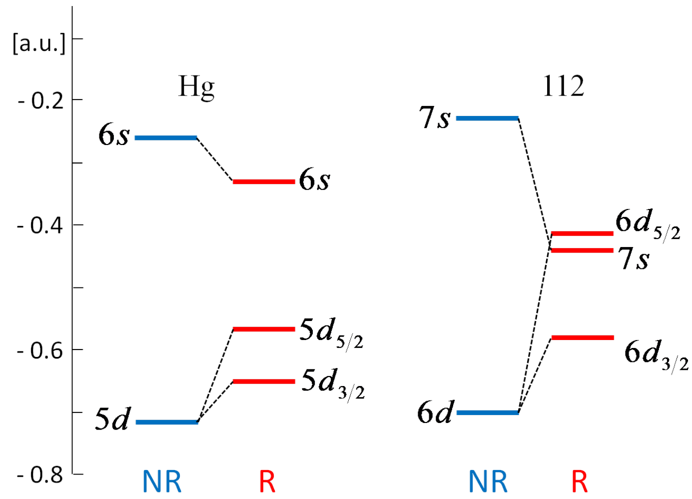

Fig. 2.4. Nonrelativistic and relativistic valence(n-1)d and ns orbital energies for the mercury element and the superheavy element 112 derived from HF and DHF calculations. Data from Ref. [41] (Hg) and Ref. [17] (the 112 element).

of the $7s$ orbital and the destabilization of the $6d_{5/2}$ orbital of the superheavy element with the atomic number 112 is so strong that the $7s$ orbital lies between the two $6d$ components, $d_{5/2}$ and the lower $d_{3/2}$ component [17]. A schematic comparison of the valence orbitals stabilization/destabilization of Hg and its valence isoelectronic analogue, the element 112, is shown in Fig. 2.4. Theoretical methods of relativistic quantum chemistry are capable of treating and predicting electronic properties of superheavy elements. One should take care about the valence electronic structure since for heavy and superheavy elements the valence electronic structure of orbitals frequently differs from our expectation based on the experience with lighter elements.

Details of the (valence) electronic structure of all species which participate at processes under consideration, including the electron correlation and spin–orbit effects must be carefully considered in qualitative estimates of relativistic effects in atomic and molecular properties. Since relativistic and electron correlation effects are not additive, they can not be treated separately. Particularly demanding are qualitative considerations and accurate theoretical calculations of systems in which participate transition metal elements.

The orbital pattern of the halogen molecules split due to relativistic effects is schematically shown in Fig. 2.5.

2.1 Z–dependence of the relativistic effects

Relativistic effects can be expressed as the difference between the corresponding relativistic and the nonrelativistic description of a quantum chemical system. This difference is just the consequence of applying different physical models. In computational practice we asses which theoret-

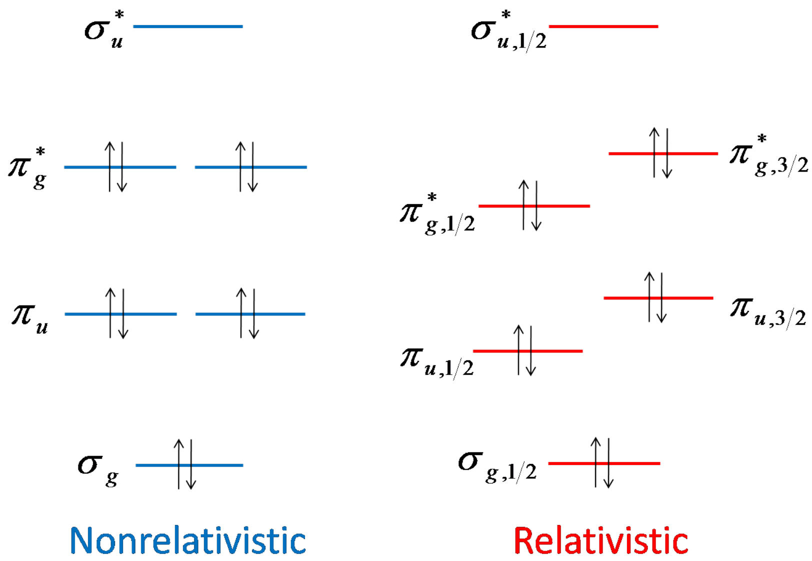

Fig. 2.5. Nonrelativistic and relativistic orbital scheme for halogen dimer molecules.

ical model is more suitable for describing studied chemical system.

Dirac himself at the time of the publishing his famous relativistic wave equation did not foresee the importance of his theory for chemical systems. He wrote [2] *"The general theory of quantum mechanics is now almost complete, the imperfections that still remain being in connection with the exact fitting in of the theory with relativity ideas. This give rise to difficulties only when high–speed particles are involved, and therefore* ***of no importance in the consideration of atomic and molecular structure and ordinary chemical reactions****, in which it is, indeed, usually sufficiently accurate if one neglects relativity variation of mass with velocity..."*

Before proceeding to rigorous relativistic quantum theory whose foundations are credited to Dirac himself, it is worth to present few semi–quantitative arguments in order to shed some light on the importance of relativistic effects for the electronic structure.

First, let us have a closer look at the "Bohr radius" meaning extension, or characteristic size of the atomic orbital what is dealt in Bohr's model [42],

$$a_0 = \frac{n^2 4\pi\epsilon_0\hbar^2}{mZe^2}, \tag{2.1}$$

where n is the principal quantum number, Z is the atomic number, m is the mass of the particle, and the rest are common constants. Next, as was promoted by Einstein [43], the inert mass of any fast–moving particle, including electron, is increasing with its speed as

$$m = \frac{m_0}{\sqrt{1-\frac{v^2}{c^2}}}, \tag{2.2}$$

where m_0 is the rest mass, v and c are velocities of the particle and of the light. For small velocity v remains m very close to m_0, but as v is increasing, the relativistic mass m goes to infinity. The speed of light, c, may be derived from Maxwell's equations [44] and in SI units has the form of $c^2 = 1/\mu_0\epsilon_0$ with μ_0 and ϵ_0 being the vacuum permeability and permittivity, respectively. The exact value of the speed of light in vacuum can be found in the latest set of CODATA recommended values of fundamental physical constants [45]. The relativistic mass enhancement, Eq. 2.2, has profound influence on the electronic structure. For the simple, semi–quantitative demonstration, let us assume $1s$ electron in an atom with the nuclear charge Z. According to the Bohr's simple model [42], by solving $mvr = n\hbar$, inserting Eq.2.1 for r and by considering atomic units, a.u., convenient for quantum chemistry ($e = m_0 = \hbar = 4\pi\epsilon_0 = 1$, see Appendix 6) the speed of the electron is then

$$v_{1s} = Z. \tag{2.3}$$

It is evident from Eq. 2.3 that in heavy elements inner shell electrons move with a speed comparable with the speed of light ($c \simeq 137.036$ a.u.), the velocity being proportional to the atomic number Z and therefore the relativistic description particularly of heavy elements is necessary.

Relativistic mass appearing in the denominator of Eq.2.1 shrinks core orbitals. For instance, the $1s$ electron of the Rn atom ($Z = 86$) has the ratio v/c (for v we apply Eq. 2.3) of $86/137 \simeq 0.63$, implying the radial shrinking approximately by 22%. It is important to realize that relativistic effects do not concern only fast moving inner shell electrons. Real atoms and molecules are many–electron systems. The valence electrons "feel" relativistically altered average field of inner shell electrons. The complete picture is a bit complicated. Nevertheless a simplified view tells us that the higher s shells are also contracted as these must be orthogonal to lower ones.

Note that the above mentioned semi–quantitative arguments for importance of relativistic effects are based upon very primitive atomic model. Also, present considerations concern just radial distribution of orbitals. The dependence of relativistic effects in bond energies and other properties [19] on the atomic number Z is more complicated. Following perturbational arguments, Schwarz *et al.* [19] arrived at the conclusion that for hydrogen–like states relativistic corrections to valence properties scale with the nuclear charge as $Z^2\alpha^2$, where

$$\alpha = \frac{1}{c}. \tag{2.4}$$

Relativistic alteration in the electron correlation contribution is also proportional approximately to $Z^2\alpha^2$. Clearly, relativistic effects are very complex for many–electron systems. Note that methods of quantum mechanics which suppose the finite speed of light are called relativistic and those in which the infinite speed of light is supposed are called nonrelativistic. Relativistic effects are defined as the difference between results following from these two approaches. We stress, again, that atoms and molecules are in fact governed by laws of the relativistic quantum mechanics. When talking about relativistic effects we have in mind just a model which is applied to a specific problem.

2.1.1 Semi–classical estimate of spin–orbit effects

The spin–orbit (SO) coupling is one of the most common manifestation of relativistic effects in molecular sciences. Individual orbital and spin quantum numbers are not good quantum numbers any more since the orbital and spin operators do not commute with the Hamiltonian (only the total angular momentum does). We note that the notion of the spin itself is a consequence of the relativistic character of electrons. Here we present a qualitative introduction of the coupling between the spin and the orbital angular momentum. A simple demonstration of the SO coupling can be obtained employing the classical expression for the interaction of the spin of a single electron and the magnetic field which has the source in its orbital motion. An electron moving around a nucleus with a speed v is producing the classical magnetic field, $\mathbf{B}$:

$$\mathbf{B} = \mathbf{E} \times \frac{\mathbf{v}}{c^2}, \tag{2.5}$$

where the electric field, $\mathbf{E}$, for a central potential $V(\mathbf{r})$ is given by

$$\mathbf{E} = \frac{1}{r}\frac{\partial V}{\partial r}\mathbf{r}. \tag{2.6}$$

The intrinsic magnetic moment of the electron is (in a.u.)

$$\boldsymbol{\mu} = -g_s \mu_B \mathbf{s}, \tag{2.7}$$

where $\mathbf{s}$ is the spin moment, see Section 3.1.2. The term

$$\mu_B = \frac{e\hbar}{2m_e} \tag{2.8}$$

is the Bohr magneton and $g_s \simeq 2$ is the electron spin g–factor. Its precise value is derived from quantum electrodynamics. Now, the interaction energy operator of the magnetic moment of the electron, Eq. 2.7, with the magnetic field, Eq. 2.5, can be expressed as (employing a.u.):

$$\Delta H_{SO} = -\boldsymbol{\mu} \cdot \mathbf{B} = \frac{\mu_B}{c^2 r}\frac{\partial V}{\partial r}(\mathbf{l} \cdot \mathbf{s}). \tag{2.9}$$

$\mathbf{l}$ is the angular momentum of the electron, see Section 3.1.1. The product $\mathbf{l} \cdot \mathbf{s}$ can be written in the operator form utilizing the definition of the square of the total momentum valid for the hydrogen–like systems, $\hat{\mathbf{j}}^2 = (\hat{\mathbf{l}} + \hat{\mathbf{s}})^2$. Therefore, the product $\hat{\mathbf{l}} \cdot \hat{\mathbf{s}}$ can be written in the operator form as

$$\hat{\mathbf{l}} \cdot \hat{\mathbf{s}} = \frac{1}{2}(\hat{j}^2 - \hat{l}^2 - \hat{s}^2), \tag{2.10}$$

which allows to estimate SO–splittings by using quantum numbers j, l and s, related to $\hat{j}^2$, $\hat{l}^2$ and $\hat{s}^2$ operators in Eq. 2.10, see Sections 3.1.1 and 3.1.2.

The Hamiltonian of a hydrogen–like atom with the central field potential $V(r) = Z/r$ can be written as the zero–order Hamiltonian and the SO perturbation, $\hat{H} = \hat{H}_0 + W(r) \cdot \hat{\mathbf{l}} \cdot \hat{\mathbf{s}}$. For the hydrogen atom the first order perturbation contribution due to $W(r) \cdot \hat{\mathbf{l}} \cdot \hat{\mathbf{s}}$ can be calculated employing analytical expressions for the unperturbed H–atom radial and spherical wave functions (for more details and a very instructive analysis, see, *e.g.*, [46]). Qualitatively, for hydrogen–like atoms $W(r)$ is proportional to Z/r^3. Since $1/r^3$ is proportional to Z^3, the SO splitting in hydrogen–like atoms scales as Z^4 (see also Eq. 2.9). For the $2p$ orbital of H, He^+, Li^{2+}, *etc.*

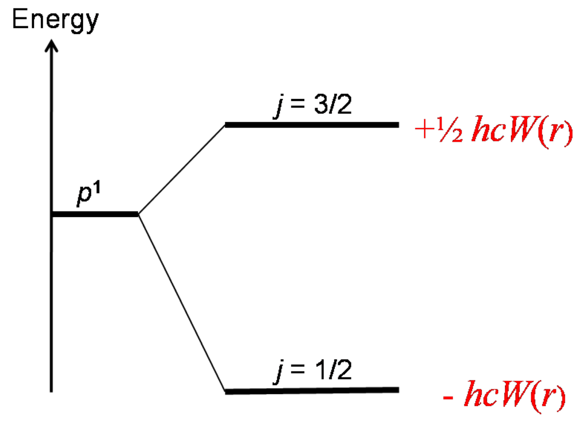

Fig. 2.6. Spin–orbit splitting of the p orbital of hydrogen–like atom into $p_{1/2}$ and $p_{3/2}$ states.

is the ratio, $\Delta H_{SO}/Z^4$ constant, 0.3652 cm^{-1}. Considering the eigenvalues of $\hat{j}^2$, $\hat{l}^2$ and $\hat{s}^2$ operators in Eq. 2.10, *i.e.* $j(j+1)$, $l(l+1)$, and $s(s+1)$ in a.u., it is clear that s–orbitals do not split. The $2p$ orbital splits into $2p_{1/2}$ and $2p_{3/2}$ states, the ratio of the energy shift with respect to the unperturbed energy being -2:1, Fig. 2.6.

The SO splitting in many–electron atoms can be approximated as the sum of the one electron operators,

$$\hat{W} = \sum_i \zeta(r_i)\hat{\mathbf{l}}_i \cdot \hat{\mathbf{s}}_i, \tag{2.11}$$

with $\zeta(r_i)$ taken as an analogue of $W(r)$ above. The total angular momentum J for lighter atoms is frequently considered by a LS coupling, and the first order corrections due to the SO perturbation are calculated as the eigenvalues of the matrix within the degenerate subspace. At this level of approximation we employ $\zeta(LS)$ regarded as parameters to be determined by experiment.

A rigorous treatment of the SO coupling requires relativistic approach and will be described in Section 4.7.

3 Basic notes on nonrelativistic electronic structure methods for many–electron atoms and molecules

Proper description of relativistic effects in atoms and molecules and a quantitative (or frequently even qualitative) account of their importance in atomic and molecular properties require the treatment of many–electron correlation methods at the relativistic level. One should realize that the reasonably accurate quantum mechanical consideration of many–atomic and many–electron systems is tremendously difficult even at the nonrelativistic level. The analytical solutions of the Schrödinger equation in the nonrelativistic case, just as the solutions of the Dirac equation in the relativistic case, are possible only for one electron hydrogen–like systems. For description of properties of all other atoms and molecules we are faced with the many–particle problem for which solutions are necessarily only approximate. Before proceeding into the description of the relativistic many–electron quantum theory it may be useful to recall the solutions of the simplest hydrogen atom at the nonrelativistic level. Quantum numbers which follow from the solutions of the Dirac equation at the relativistic level are related to the quantum numbers of the solutions of the Schrödinger equation. We note that the energy spectra in the nonrelativistic and relativistic case, respectively, are different. Further on, we wish to draw attention to the relation between the eigenvalues and eigenfunctions of the basic angular and the spin momentum operators for one electron systems. More difficult is the quantum mechanics of the many–electron atoms and molecules at both the nonrelativistic and relativistic level. The description of the relativistic methods for many–electron systems in which the so called electron correlation is treated approximately will be a main body of our theoretical overview and should help the reader in understanding the limits of accuracy attainable by present day electron correlated relativistic approaches.

3.1 Schrödinger equation and the hydrogen–like atoms

The Schrödinger equation, published in 1926, is a fundamental equation of the nonrelativistic quantum physics [47]. It is a general equation describing the behaviour of not only atoms and molecules but is fundamental for describing all systems in the micro–world as well. The quantum mechanical (and relativistic) behaviour of atoms and molecules affects also properties of systems at the macroscopic level and leads eventually to many present days technologies.

For a system exposed to an external potential $V(\mathbf{r})$ the time–dependent Schrödinger equation (from this point we are using a.u., that is $\hbar$ omitted) is

$$i\frac{\partial}{\partial t}\Psi_n(\mathbf{r},t) = \hat{H}\Psi_n(\mathbf{r},t) = (-\frac{1}{2}\Delta + \hat{V}(\mathbf{r}))\Psi_n(\mathbf{r},t), \tag{3.1}$$

where $\mathbf{r} = \mathbf{r}(x,y,z)$ is the position of the particle in the 3–dimensional space, Δ is the Laplace operator, $\hat{V}(\mathbf{r})$ is the potential energy operator of the particle at a given position $\mathbf{r}$ and $\Psi_n(\mathbf{r},t)$ is the time–dependent wave function representing a system in the quantum state n. In the theory of atoms and molecules in which the Hamiltonian frequently does not depend explicitly on time the Schrödinger equation can be transformed into the time–independent form describing stationary states:

$$\hat{H}\Psi_n(\mathbf{r}) = E\Psi_n(\mathbf{r}). \tag{3.2}$$

Exact solutions of the Schrödinger equation for one–electron hydrogen–like atoms is notoriously known topic in standard textbooks of quantum physics. The Schrödinger equation is first transformed into spherical coordinates, which allows its separation into radial and angular parts. One–electron wave functions, the product of the radial $R_{nl}(r)$ and the $Y_{lm}(\theta, \phi)$ angular parts, are referred to as hydrogen–like atomic functions:

$$\psi_{nlm}(r, \theta, \phi) = R_{nl}(r) Y_{lm}(\theta, \phi). \tag{3.3}$$

Integers n, l, m are quantum numbers which characterize the quantum state of the system. The number n is the principal quantum number (n can have values $1, 2...$) and determines the nonrelativistic energy of the hydrogen–like atom with the atomic number Z as $E_n = -Z/2n^2$ a.u. The angular part of the wave function, $Y_{lm}(\theta, \phi)$, is represented by the spherical harmonic functions. Since for the hydrogen–like atoms the nonrelativistic Hamiltonian commutes with the square of the angular momentum operator $\hat{l}^2$ and both commute with its z–component, the $\hat{\mathbf{l}}_z$ operator, the spherical harmonic functions $Y_{lm}(\theta, \phi)$ are eigenfunctions of all three fundamental operators.

3.1.1 Angular momentum

Eigenvalues (in a.u.) and eigenfunctions of the square of the angular momentum operator, $\hat{l}^2$, $\hat{l}^2 = \hat{l}_x^2 + \hat{l}_y^2 + \hat{l}_z^2$, are determined by the equation (in a.u.)

$$\hat{l}^2 Y_{lm} \; = \; l(l+1) Y_{lm}. \tag{3.4}$$

The z–component $\mathbf{l}$ of the angular momentum is quantized as

$$\hat{l}_z Y_{lm} = m Y_{lm}. \tag{3.5}$$

The angular quantum number l, with $l = 0, 1, 2, ...(n-1)$ determines the magnitude of the angular momentum. The "magnetic" quantum number m (more frequently denoted as m_l) can have values $-l, (-l+1), ..., (l-1), l$ and determines the projection of the angular momentum into the (arbitrarily chosen) z–axis. The nonrelativistic hydrogen–like orbitals ψ_{nlm} are traditional building stones (serving as basis sets) in the nonrelativistic theory of the chemical bond, particularly in the theory of molecular orbitals and in many other areas (note, nevertheless, that in modern quantum chemistry we are using modified and more general basis sets, mostly Gaussian basis sets). The radial and angular distributions of the eigenfunctions of the hydrogen atom, say, s, p, d, *etc.* orbitals and their density distributions are very well known to students of physics or chemistry and need not be reproduced here. We note, however, that not only the energy spectrum of the hydrogen–like systems but also the shape of their wave functions and orbitals in the nonrelativistic and relativistic theory are different. Later on (Section 4) we will show that nonrelativistic electronic orbitals are frequently unsatisfactory for modelling of chemical bonds for systems containing heavy elements and that they are to be replaced by relativistically obtained wave functions.

3.1.2 Spin momentum

The electron, the proton and other particles as well, posses an intrinsic angular momentum. First direct observation of the electron's intrinsic angular momentum was achieved in the Stern–Gerlach experiment [48]. Another experimental evidence are closely spaced doublets in the hydrogen spectrum examined at a very high resolution, what is known as the fine–structure splitting.

The intrinsic momentum of the electron is denoted as the "spin 1/2" [49] and is established as the fourth quantum number in the nonrelativistic framework. With some imagination it could be approximately compared to a ball spinning around its own axis.

Regarding the pioneering work leading to the discovery of the spin of the electron, nice stories are described in the book by Pišút and Zajac [50], see also [51]. It was Wolfgang Pauli who first noticed that there must be a fourth quantum number which is related to the "two–valuedness" behaviour of an electron. He has initiated a new theory for the explanation of the doubling of the spectral lines related to transitions of the valence electron of the sodium atom. The theory of the electron spin was published by two young scientists, George Uhlenbeck and Samuel Goudsmit, prompted by another distinguished theoretician, Paul Ehrenfest. Initially, Uhlenbeck and Goudsmit did not trust their theory and wanted to withdraw their German written paper [52]. However, in the meantime, Ehrenfest has forwarded their paper to Naturwissenschaften accompanied by his supporting comment. An English written paper on spin by these two pioneers, Ref. [49], followed approximately one year later.

If one measures the component of the spin momentum of a single electron along a selected direction one finds the value of $\pm\frac{\hbar}{2}$ (in a.u. just $\pm\frac{1}{2}$). Note that the angular orbital momentum mentioned before can have only integer quantum numbers in contrast to the spin eigenvalues, see Eqs. 3.4, 3.5. Further on, spinning distribution of a charge has a magnetic moment.

Similarly as it is expressed for the angular momentum in Eq. 3.4, the square of the spin operator acts on a spin function as (in a.u.)

$$\hat{s}^2\eta = s(s+1)\eta \ , \ \eta = (\alpha, \beta). \tag{3.6}$$

The spin of a single electron is associated with Pauli spin matrices [53] :

$$\hat{\boldsymbol{\sigma}} = \left(\begin{bmatrix} 0 & 1 \\ 1 & 0 \end{bmatrix} ; \begin{bmatrix} 0 & -i \\ i & 0 \end{bmatrix} ; \begin{bmatrix} 1 & 0 \\ 0 & -1 \end{bmatrix} \right) . \tag{3.7}$$

The Pauli matrices, $\hat{\sigma}_{x,y,z}$, are complex Hermitian and unitary. Except for a factor of $1/2$ they can be viewed as representations of the $\hat{\mathbf{s}}_{x,y,z}$ spin operators, where α and β spin functions are taken as column vectors.

$$\hat{\mathbf{s}}_z \ = \ \frac{1}{2}\hat{\sigma}_z; \ \ \hat{\mathbf{s}}_z\alpha \ = \ \hat{\mathbf{s}}_z \begin{pmatrix} 1 \\ 0 \end{pmatrix} \ = \ \frac{1}{2}\begin{pmatrix} 1 \\ 0 \end{pmatrix}; \ \ \hat{\mathbf{s}}_z\beta \ = \ \hat{\mathbf{s}_z} \begin{pmatrix} 0 \\ 1 \end{pmatrix} \ = \ -\frac{1}{2}\begin{pmatrix} 0 \\ 1 \end{pmatrix} . \tag{3.8}$$

The α and the β are eigenfunctions of the $\hat{\mathbf{s}}_z$ operator (for comparison see Eq. 3.5) with eigenvalues of $m_s = 1/2 \ a.u.$ and $m_s = -1/2 \ a.u.$, respectively. The Pauli spin matrices satisfy the identities

$$\hat{\sigma}_p^2 = \mathbf{I} \ ; \ \hat{\sigma}_p\hat{\sigma}_q + \hat{\sigma}_q\hat{\sigma}_p = 2\delta_{pq}\mathbf{I} \ ; \ \hat{\sigma}_p\hat{\sigma}_q = \mathbf{I}\delta_{pq} + i\epsilon_{pqr}\sigma_r \ ; (p,q,r) = (x,y,z), \tag{3.9}$$

where ϵ_{pqr} is the permutation symbol (also called as the Levi-Civita symbol) which is 1 if (p, q, r) is and even permutation, -1 if it is an odd permutation or 0 if any index is repeated. The $\mathbf{I}$ represents the 2×2 unit matrix

$$\mathbf{I} \ = \ \begin{bmatrix} 1 & 0 \\ 0 & 1 \end{bmatrix} . \tag{3.10}$$

Later on, in Section 4.3.1, we will show that the spin arises naturally as the solution of the Dirac equation. Let us mention that all operators related to the solutions of the Schrödinger equation are defined differently within the Dirac equation.

3.2 Many-electron systems

The first step in reducing theoretical and computational demands needed for solving the Schrödinger equation for many–electron molecules and their clusters is the decoupling of the motion of the electrons from that of nuclei. The same is desirable also at the relativistic level. This is most frequently achieved by the Born–Oppenheimer (BO) approximation [54]. The computationally simplest way is using the clamped nuclei Hamiltonian. We note that the BO approximation leads to reasonably accurate results when electronic energy differences between the electronic ground state and low–lying excited states are much larger than are differences between vibrational states. Details of the interactions between electronic, vibrational and rotational movements can be found, *e.g.*, in the book by Piela [51]. The Schrödinger equation for the many–electron wave function is solved in the field of fixed positions of nuclei. The electronic energy $E_e(R)_n$ for a specific spectroscopic state n plays the role of the potential energy for oscillations. When treated numerically, electronic energies calculated for different positions of nuclei allow finding the minima on the potential energy hypersurface and equilibrium geometries, vibrational frequencies and some other spectroscopic characteristics. Having energies, geometries, vibrational and other spectroscopic data for atoms and molecules participating in chemical reactions, we can calculate reaction and activation energies, enthalpies and free energies, ionization potentials, electron affinities and other properties (vibrationally corrected, if desired). Similar approach is behind the energetics in intermolecular interactions or in energetics of clusters. Geometries and vibrational frequencies are presently mostly calculated by analytical derivatives of electronic energies with respect to the nuclear coordinates Using appropriate operators we can also calculate electric properties, like dipole moments, dipole and higher polarizabilities, magnetic properties *etc.*, by numerical derivatives of electronic energies with respect to an external perturbation (like the electric field). Modern methods are based on response theories for obtaining molecular properties [39, 40].

The nonrelativistic Hamiltonian for an n-electron system in which electrons are exposed to the field of N nuclei, $I = 1, 2, ...N$, at their fixed positions within the BO approximation is

$$\hat{H}_e(1, 2...n) = \sum_{i}^{n} \hat{h}_i + \sum_{i<j}^{n} \frac{1}{r_{ij}} + \sum_{I<J}^{N} \frac{Z_I Z_J}{R_{IJ}} \qquad \hat{h}(i) = -\frac{1}{2}\Delta_i - \sum_{I}^{N} \frac{Z_I}{r_{iI}}. \tag{3.11}$$

The first term in Eq. 3.11, $\hat{h}_i$, represents the kinetic energy of an i-th electron plus the interaction between an electron and all nuclei. This is the one–electron part of the Hamiltonian expressed as the sum of one–electron contributions. The second term represents a sum of two–electron contributions, $\frac{1}{r_{ij}}$, describing the inter-electronic interactions. The last term in the Hamiltonian, $\frac{Z_I Z_J}{R_{IJ}}$, represents the contribution of electrostatic interactions between nuclei. Within the Born-Oppenheimer approximation it is a constant, depending only on the fixed geometry of the system.

Now, it is appropriate to present a starting form of the wave function, $\Phi_0(1, 2, ...n)$ which would be a solution of the stationary Schrödinger equation for a many–electron system. A common way is expressing the wave function in the form of Slater determinant [55]

$$\Phi_0(1,2,...n) = \frac{1}{\sqrt{n!}} \begin{vmatrix} \lambda_1(1) & \lambda_1(2) & ... & \lambda_1(n) \\ \lambda_2(1) & \lambda_2(2) & ... & \lambda_2(n) \\ . & . & ... & . \\ . & . & ... & . \\ . & . & ... & . \\ \lambda_n(1) & \lambda_n(2) & ... & \lambda_n(n) \end{vmatrix}. \tag{3.12}$$

It is a very convenient form. First, it obeys the Pauli principle, *i.e.* it is antisymmetric with respect to permutations of any pair of electrons. Second, it is expressed in the form of a product of (antisymmetrized) one–electron terms. This reflects the statistical interpretation of quantum mechanics for many–electron systems. Each electron in the nonrelativistic realm occupies a spinorbital λ, which is the product of the one–electron spatial function, ϕ, and the electron spin function, η:

$$\lambda_i(\mathbf{r},\sigma) = \phi_i(\mathbf{r})\eta; \;\; \eta = (\alpha,\beta). \tag{3.13}$$

In the many–electron theory it is advantageous to write the molecular nonrelativistic Hamiltonian in the second quantization form [39]:

$$\hat{H} = \sum_{pq} h_{pq}\hat{p}^+\hat{q} + \frac{1}{2}\sum_{pqrs} g_{pqrs}\hat{p}^+\hat{r}^+\hat{s}\hat{q} + h_{\rm nuc}. \tag{3.14}$$

where $\hat{p}^+, \hat{r}^+, ..., \hat{q}, \hat{s}$ ...., are creation and anihilation operators, respectively; One– and two–electron integrals, h_{pq} and g_{pqrs}, respectively, can be expressed over spinorbitals p,q,r, and s, Eq. 3.13, in the usual notation as

$$h_{pq} = \langle\lambda_p(1)|\hat{h}(1)|\lambda_q(1)\rangle \tag{3.15}$$

$$\begin{aligned} g_{pqrs} &= \langle\lambda_p(1)\lambda_q(2)|\frac{1}{r_{12}}|\lambda_r(1)\lambda_s(2)\rangle - \langle\lambda_p(1)\lambda_q(2)|\frac{1}{r_{12}}|\lambda_s(1)\lambda_r(2)\rangle \\ &= \langle pq||rs\rangle \end{aligned} \tag{3.16}$$

$$h_{\rm nuc} = \frac{1}{2}\sum_{I\neq J}\frac{Z_I Z_J}{R_{IJ}}. \tag{3.17}$$

Note that the second term in g_{pqrs} results from the electron exchange. Employing the standard rules for integration over spin variables we are left with integrals over spatial coordinates. We will see later that the two–electron integrals are real "trouble makers" in many–electron calculations. In sophisticated calculations we go beyond the single–determinant approximation of the wave function. In that case we need not only integrals over occupied spinorbitals but also integrals over frequently enormous number of virtual spinorbitals. The initial wave function $\Phi_0(1,2,...n)$ for a closed–shell system in the nonrelativistic case can be expressed in terms of spatial orbitals only, each one occupied by two electrons having spin α and β, respectively, and the same spatial part (in the spinorbital formulation both α and β electrons are allowed to have different spatial part). Therefore, the number of orbitals entering into the Slater determinant is one half of the number of spinorbitals. The number of two–electron integrals carrying indices of four orbitals which must be calculated and used in the wave function and energy calculations is reduced considerably. This is much more important in post-Hartree-Fock calculations than in the HF step.

3.2.1 The independent–electron model: The Hartree–Fock method

The Hartree–Fock (HF) method [56–58] represents a basic approximation for determining the wave function of a many–electron system. It is also called the self–consistent field (SCF) method, which reflects the way in which the HF solution is searched. The most frequently used HF method assumes that the wave function Φ_0 can be approximated by a single determinant, Eq. 3.12. The energy functional, expressed by a Slater determinant of, say, the ground state of a system and the nonrelativistic Hamiltonian,

$$E_0^{HF} = \frac{\langle \Phi_0 | \hat{H}_e | \Phi_0 \rangle}{\langle \Phi_0 | \Phi_0 \rangle}, \tag{3.18}$$

is minimized, varying occupied one–electron functions, used for the construction of the Slater determinant, *i.e.* spinorbitals or orbitals. An additional condition is that so obtained orbitals remain orthogonal, *i.e.* $\langle \phi_i(1) | \phi_j(1) \rangle = \delta_{ij}$, where δ_{ij} is the Kronecker delta. The procedure leads to the set of one-electron equations [51], known as the Hartree–Fock equations:

$$\hat{f}(1)\phi_i(1) = \varepsilon_i \phi_i(1) \; , \tag{3.19}$$

where the general structure of the Fock operator (in the basis of spinorbitals, Eq. 3.13) is

$$\hat{f} = \hat{h} + \sum_i^{occ} (\hat{J}_i - \hat{K}_i). \tag{3.20}$$

In Eq. 3.20 $\hat{h}$ is the one–electron operator, see Eq. 3.11, $\hat{J}_i$ and $\hat{K}_i$ are the Coulomb and exchange operators, respectively. Summation runs over indices of occupied orbitals, the only orbitals which determine the HF energy. The coulomb and exchange operators can be formally defined as one–electron operators,

$$\hat{J}_i(1)\lambda_j(1) = \int \lambda_i(2)\lambda_i(2) \frac{1}{r_{12}} dr_2 \lambda_j(1) \tag{3.21}$$

$$\hat{K}_i(1)\lambda_j(1) = \int \lambda_i(2)\lambda_j(2) \frac{1}{r_{12}} dr_2 \lambda_i(1) \tag{3.22}$$

the integration being over the coordinates of electron 2 only. Matrix elements of the $\hat{J}$ and $\hat{K}$ operators are $J_{ij} = \langle \lambda_i(1)\lambda_j(2) | \frac{1}{r_{12}} | \lambda_i(1)\lambda_j(2) \rangle$ and $K_{ij} = \langle \lambda_i(1)\lambda_j(2) | \frac{1}{r_{12}} | \lambda_j(1)\lambda_i(2) \rangle$. By introducing the $\hat{J}$ and $\hat{K}$ operators we are able to formally decouple the two–electron problem into a series of one–electron problems. The physical picture adopted in the HF method is that each electron is exposed to the field of all nuclei and a mean field created by all remaining electrons. Since the mean field is initially unknown (note that both $\hat{J}$ and $\hat{K}$ operators contain spinorbitals which are to be determined) HF solutions are searched iteratively until a threshold selected for the accuracy of the SCF energy or the HF orbitals is achieved, starting usually from just a one–electron part of the Fock operator, Eq. 3.20 . We will see later that in the relativistic theory the Fock operator is substituted by the Dirac–Fock operator which leads to the Dirac–Hartree–Fock set of one–electron solutions of the many–electron problem, an analogue of the Hartree–Fock equations in the nonrelativistic case.

For the closed-shell systems having n electrons, in which we use the doubly occupied molecular orbitals with the same spatial functions for α and β electrons respectively, the Fock operator (after the spin integration) can be written as

$$\hat{f} = \hat{h} + \sum_{i}^{n/2}(2\hat{J}_i - \hat{K}_i). \tag{3.23}$$

Depending upon restrictions imposed on one–electron functions entering into the Slater determinant, Eq. 3.12, we define different variants of the HF method. The most natural selection for closed–shell molecules is using doubly occupied orbitals, mentioned above. The advantage of using the same spatial orbitals for a pair of α and β electrons can be partly employed for open–shell systems as well, *i.e.* pair of electrons corresponding to the doubly occupied orbitals are restricted to have the same spatial part. Remaining orbitals are singly occupied (in so called high spin open–shell systems treated by a single determinant HF method are unpaired electrons defined as α electrons). Clearly, this restriction brings additional approximation into the wave function, but it allows creating a more efficient computer code for open–shell systems than it is possible within the fully spinorbital formulation. Such defined HF method is the Restricted Open Shell HF method, or, in short, the ROHF method [59]. If there are no restrictions other than creating spinorbitals as a product of the spatial and the spin state for a single electron, Eq. 3.13, allowing different spatial part for a spinorbital having α or β spin, we talk about the Unrestricted HF method, UHF [60]. This is conceptually the simplest HF method, used mostly for treating open–shell molecules or for describing the dissociation processes of both closed–shell and open–shell molecules. The two drawbacks of the UHF method are the following. First, the UHF wave function is not a proper wave function of the total spin operator, $\hat{S}^2$ (it is "spin contaminated"). Second, we have to treat two–electron integrals over spinorbitals. However, there is two times more spinorbitals than orbitals for closed–shell systems (almost the same also applies to open–shells treated by the ROHF method). Treating just occupied and virtual orbitals resulting from HF or ROHF equations instead of twice as much spinorbitals in UHF is crucial when going beyond the one–electron HF approximation, *i.e.* in sophisticated many–electron methods like CC methods. Even if the computer code is simpler when the reference wave function is UHF, calculations are about four or three times more time consuming than with the RHF (for closed–shell) or ROHF (for open–shell) reference wave functions. Considerations on adopting the one–electron functions, orbitals or spinorbitals, in the nonrelativistic theory would not be complete without mentioning already now that the number of integrals correspondingly increases with using four–spinors in relativistic calculations. In any case, there is much space for improved theoretical formulations and computer codes focused particularly on an efficient treatment of difficult terms containing two–electron integrals at any level of the many–electron theory. Finally, we should note that some atomic and molecular states can not be represented by a single determinant wave function. Typical examples are excited singlet states which need at least two determinants to define a reference wave function.

3.2.2 Algebraic approximation

With just a few exceptions, HF equations of atoms and molecules are solved within the so called algebraic approximation. This means that the spatial part of spinorbitals or orbitals, ϕ_i, entering into the Slater determinant are expanded in terms of properly selected basis sets, χ_ν:

$$\phi_i = \sum_\nu c_{\nu i}\chi_\nu , \tag{3.24}$$

In early days of molecular quantum mechanics χ_ν were mostly Slater–type orbitals, resembling the orbitals resulting from the analytical solutions of the hydrogen–like atoms. In line with this, the first orbital theory of the chemical bond, not yet the HF theory, was called the MO–LCAO theory, (Linear Combination of Atomic Orbitals). Note, however, that the first theory of the chemical bond was the Heitler–London valence bond theory [51]. Presently, basis sets are more general, even though they mostly remain linked with specific atoms which are components of a molecule or the molecular complex. Molecular calculations are highly dominated by expansions in terms of Gaussian–type basis functions (GTF's). A general shape of the so called Cartesian primitive Gaussian basis function located at the point A (usually but not necessarily at the point nucleus) is

$$g(\alpha, A, i, j, k) = N_{\alpha,i,j,k} x_A^i y_A^j z_A^k \mathrm{e}^{-\alpha r_A^2} \, . \tag{3.25}$$

The orbital exponents α of Gaussian basis sets are optimized in atomic calculations, i, j, k are positive integers. Gaussians having i=j=k=0 represent s–type functions, when i=1, j=k=0 we talk about p_x functions *etc.* The reason why Boys [61] has suggested using Gaussians as basis functions is that calculations of two–electron integrals with GTF's are much easier than with exponential Slater–type basis functions with a radial part $\mathrm{e}^{-\zeta r_A}$ (ζ is an optimized orbital exponent). The basic advantage of the Slater–type orbitals is their proper shape in the vicinity of nuclei. Due to the singularity of the potential at a *point* nucleus with nuclear charge Z, the wave function must have a cusp at the nucleus, *i.e.* its derivative at $r = 0$ should be $-Z$. Obviously, Gaussian functions have qualitatively wrong behaviour at the nucleus. They also have inaccurate behaviour at long distances. This disadvantage can be largely eliminated by expanding ϕ_i by more Gaussians than would correspond to Slater–type basis functions. However, having more basis functions means a need to calculate and to treat much more two–electron integrals. This is eliminated by "contracting" some primitive Gaussian functions into fixed groups with coefficients determined by simpler atomic calculations. Contracted Gaussian basis functions, CGTF's, are then used in more demanding molecular calculations. The description of this technique can be found in the literature [39, 62]. Most applications at the relativistic level rely on CGTF's as well. However, nonrelativistic basis sets are not directly applicable to relativistic calculations. Basis sets for relativistic calculations must be optimized having in mind a specific relativistic Hamiltonian. Concerning the wrong behaviour of Gaussian functions in the vicinity of the nucleus, it is interesting to note that this is traditionally considered as a drawback of these basis sets in nonrelativistic calculations. In the relativistic theory the nucleus is actually not a point charge. In fact, its shape can be approximated by Gaussians (see Section 4.3.3)

Once having basis functions we are ready to calculate the molecular orbitals expansion coefficients $c_{\nu i}$. Within the HF–SCF method coefficients $c_{\nu i}$ are determined variationally. Inserting the basis set expansion, Eq. 3.24, into HF equations we obtain Roothaan equations [51, 63]:

$$\mathbf{FC} = \mathbf{SC}\boldsymbol{\epsilon}, \tag{3.26}$$

where $\mathbf{F}$ is the Fock matrix (which depends on the coefficients $\mathbf{C}$ due to electron–electron interaction terms, see Section 3.2.1), $\mathbf{C}$ is a molecular orbital matrix, $\boldsymbol{\epsilon}$ is the (diagonal) matrix of orbital energies, and $\mathbf{S}$ is the overlap matrix of the basis functions. The dimension of the $\mathbf{C}$ matrix is determined by the size of the basis set used in the MO expansion, Eq. 3.24. Therefore, for reasonably large basis sets we obtain much more orbitals than is the number of electrons. Clearly, the number of occupied orbitals (spinorbitals), which determine the HF energy, unambiguously follows from the number of electrons. Remaining (virtual) orbitals or spinorbitals are empty in the HF wave function. Their shape in terms of basis set expansion, Eq. 3.24, is determined by requiring their orthogonality to the space of occupied orbitals. A space of virtual orbitals is important in post–Hartree–Fock correlation calculations. As a rule, the number of virtual orbitals (N_v) is much larger than N_o, the number of occupied orbitals. Very large space of virtual orbitals leads to enormously large number of two-electron integrals needed in post–Hartree–Fock calculations. If we forget indices restrictions, the number of two–electron integrals over virtual orbitals, $\langle \phi_p(1)\phi_r(2)|\frac{1}{r_{12}}|\phi_q(1)\phi_s(2)\rangle$, scales as N_v^4. Considering that in modern post HF calculations can N_v be as large as 1000 [64], we realize that not only calculations of the two–electron integrals (via transforming through integrals over the atomic basis functions) but also managing large files is a problem. We will return to this issue in the next Section. By imposing the diagonalization of the matrix $\boldsymbol{\epsilon}$ we create so called canonical HF orbitals. This is straightforward in closed–shell RHF and open–shell UHF calculations, but a bit tricky in ROHF calculations [40, 65, 66]. Most convenient in post–Hartree–Fock correlation calculations of open–shell systems is using so called semicanonical orbitals which means that diagonal are *blocks* within the space of occupied and virtual orbitals, respectively.

The HF method is said to be a *”best independent–electron approximation of a many–electron system”*. It recovers more that 99% of the total electronic energy. Yet, this is not enough for obtaining results with a high and controlled accuracy. The two–electron part of the Hamiltonian is just a good approximation, even if it is considered through the Coulomb and exchange operators as in the HF method. Results are frequently quite satisfactory, but may fail even qualitatively in predicting some molecular properties, reaction and activation energies and so on. The HF method is not applicable to calculations of, *e.g.*, van der Waals interactions. For dispersion forces and many other applications proper treatment of atoms and molecules requires many–electron methods for considering the electron correlation problem. HF solution is a good starting point for so called post–Hartree–Fock methods, which use the HF wave function as the zero–order approximation.

3.2.3 Electron correlation in the nonrelativistic theory of many electron systems

The correlation energy can be well defined [67] for closed–shell systems as a difference between the exact nonrelativistic energy and the Restricted Hartree–Fock energy of a many–electron system:

$$E_{corr} = E_{exact} - E_{RHF}. \tag{3.27}$$

This definition can be extended to open–shell molecules with some caution since there are few variants of the independent–electron models for open–shells.

The physical origin of the electron correlation arises from the approximate description of the mutual repulsion of electrons within the independent–electron model. In the Hartree–Fock method is the movement of an electron considered in the average field of other electrons and this model does not describe their instantaneous interactions accurately. Notable deficiency of the HF description consists in the fact that two electrons with opposite spins are not prevented from occupying the same region of space at the same time. In contrast, the probability of finding two electrons with the same spin at a point r is zero, which is a direct consequence of the Pauli principle which the HF wave function obeys. In most systems, particularly in closed–shell systems with the RHF reference the inaccuracy arising from the approximate treatment of electron interactions is dominated by the dynamical effects related to the instantaneous movement of electrons. This represents a *dynamical* electron correlation. When the HF wave function is not a satisfactory representation of the wave function, that is when a single determinant wave function is not "good enough", we talk about the *nondynamical* correlation. This is topical in quasi degenerate systems, when several electronic states of a atom or an molecule have similar energies. In this case the starting (or zero–order) wave function should be represented by several determinants (having the same symmetry and spin states in the nonrelativistic theory) which represent near degenerate states. Examples are low–lying excited states, frequently open–shell systems. In the relativistic theory near degeneracies frequently result from spin–orbit effects. Special is a class of systems, like atoms and molecules in some excited singlet states, which can by no means be represented by a single determinant wave function. As a rule, a single RHF determinant wave function is inadequate for a description of a molecule with stretched chemical bonds (far from the equilibrium geometry), with the exception when the molecule and all fragments have a closed–shell electronic structure. In all such cases the reference wave function for the post–HF treatment should be represented by a multiconfigurational SCF (MC SCF) wave function. Alternatively, the reference HF wave function can be expressed in the UHF form and all subsequent calculations can be performed within the spinorbital formalism. However, the UHF wave function has another theoretical disadvantages mentioned in Section 3.2.1.

3.2.4 Configuration interaction

The exact solution of the Schrödinger equation can be expressed in terms of a linear combination of *all* Slater determinants obeying just the spin and symmetry restrictions which can be constructed from a selected one–electron basis in the n–electron Fock space:

$$\Psi_{FCI} = C_0\Phi_0 + \sum_{i,a} C_i^a \Phi_i^a + \sum_{i<j,a<b} C_{ij}^{ab}\Phi_{ij}^{ab} + \ldots, \tag{3.28}$$

where Φ_i^a are mono–excited configurations, Φ_{ij}^{ab} are bi–excited configuration *etc.* (up to n–tuple excitations according to the number of electrons of the system under consideration) with respect to a reference wave function, Φ_0. The $i, j...$ and $a, b, ...$ represent occupied and virtual spinorbitals, respectively. *Linear* expansion coefficients C_0, C_i^a, C_{ij}^{ab} are calculated variationally. The CI wave function means an expansion in terms of a linear combination of spin and symmetry adapted Slater determinants, or, more generally, Configuration State Functions, CSFs. Ψ_{FCI}, when no other than the spin and symmetry restrictions are imposed, represents the Full Configuration Interaction (FCI) expansion. It gives the accurate solution corresponding to the selected basis set within the algebraic approximation. The FCI energy would converge to the exact energy with gradually increasing the size of the basis set. However, the number of configuration functions in Eq. 3.28 grows drastically with the number of electrons and with the size of the basis set. Therefore, the FCI expansion is attainable only for relatively small systems and small basis sets. Yet, FCI solutions are very useful as benchmark results for other methods.

For practical use the FCI expansion must be truncated at some level of the excitation operator $\hat{C}$ with respect to the reference Φ_0, which defines the Ψ_{CI} wave function. Truncation at the single– and double–excitation level, *i.e.* $\hat{C} = \hat{C}_1 + \hat{C}_2$, with respect to a reference Φ_0 wave function, defines the most common variational post–HF method, the single determinant reference CISD:

$$\Psi_{CISD} = (1 + \sum_i \hat{C}_i)\Phi_0 = \Phi_0 + \sum_{i,a} C_i^a \Phi_i^a + \sum_{i<j,a<b} C_{ij}^{ab} \Phi_{ij}^{ab}. \tag{3.29}$$

We note that the reference function Φ_0 must not necessarily be a HF determinant, even if this is usually the case. Orbitals which enter the reference function and all Φ_i^a, Φ_{ij}^{ab} *etc.* are known (resulting from a HF solution) which means that also Slater determinants entering into the CI expansion are known. The only variables which must be determined are the *linear* expansion CI coefficients C_i^a, C_{ij}^{ab} and eventually coefficients of higher excitations, triple, quadruple, *etc.* which defines the CISDT, CISDTQ *etc.* methods. They are determined by the Ritz variational method requiring that the CI energy is a minimum, solving the eigenvalue problem

$$\mathbf{HC} = E\mathbf{C}, \tag{3.30}$$

where H_{ij} are CI matrix elements over Slater determinants. The lowest solution represents the energy and wave function of the ground state, higher solutions represent excited states. One should realize, however, that at this level all the states refer to different vectors of the $\mathbf{C}$ matrix but with Slater determinants constructed for all states from the same set of orbitals.

Consider now, with some simplification, the physical meaning of a linear expansion represented by Eqs. 3.28 and 3.29. Should the reference function Φ_0 be a single determinant HF reference means that electrons occupy orbitals (spinorbitals) which define the Slater determinant and interact mutually just through their average field. The HF energy is solely determined by occupied orbitals $i, j....$ However, in the CI expansion we allow electrons to occupy more space exploiting also virtual orbitals $a, b, c...$ through the single and double excitation in CISD (or higher excitations in a more general CI expansion). Clearly, allowing electrons to occupy more space means a relief of their mutual repulsion, *i.e.* their movement is better correlated.

The CI method represents a basic and conceptually straightforward post Hartree–Fock model for the treatment of the electron correlation [51,68]. The problem is the computational tractability. Presently, the number of configurations in CI goes up to billions! This was not possible until B. Roos [69] has discovered an iterative alternative to the straightforward Ritz variational method. In a sense this resembles techniques employed in the Many Body Perturbation Theories (MBPT) and the Coupled Cluster (CC) theory. Even if the excitation space with respect to the reference is restricted to single and double excitations, for many–electron atoms and molecules are computational demands unbearable. So we usually do not consider all electrons in the correlated treatment. Electrons in lowest–lying orbitals are usually well separated from valence electrons and so they contribute to the atomic and molecular properties very little. In most processes (for example in reaction or interaction energies) is their contribution cancelled. Therefore, we leave these so called "inner shell" electrons uncorrelated. We talk that about these electrons as about the "frozen core" electrons. Similarly, we do not allow electrons to occupy the highest lying virtual orbitals. These computational tricks are well under control since we can verify the inaccuracy caused by omitting inner shell electrons from the correlation treatment. In molecules with atoms as C, N, O, ..., the obvious selection of the frozen core are $1s$ orbitals. Some caution must be payed to so called semi–core–valence correlation. For example, it is insufficient to correlate just ns^2np^1 electrons of Ga, In, or Tl. Definitively, also (n-1)d^{10} shell must be correlated. For, say, the gold atom, we usually correlate valence and core–valence $5p^6 5d^{10} 6s^1$ electrons. Special caution needs selection of frozen orbitals in relativistic calculations. For Au (and, similarly for Pt, Tl, and other atoms) relativistic shifts of orbital energies alters the order of orbital energies, see Fig. 2.3. Also, different components of, *e.g.*, f orbitals, may belong to different symmetries, depending of the symmetry of the molecule. Therefore, we either do not correlate $5s^2$ and $4f$ shells or correlate both (which is demanding).

For more accurate solutions of excited states, for simultaneous solving the problem of the dynamical and nondynamical electron correlation, in cases when taking just one determinant is inadequate for representing a reference wave function *etc.*, the Multireference CI (MR CI) is a method of the choice. In this case the reference wave function Φ_0 is created as a set of determinants, not just as a single determinant. The selection of this wave function is not always straightforward and needs some experience. Since excitations (again, mostly singles and doubles) refer to all determinants in the MR wave function, the MR CI method becomes quickly intractable with the size of the MR space (so called model space). In general, all determinants which are quasi–degenerate must be included. The MR CI method is particularly useful in calculations of the bond breaking processes on the hypersurfaces, demanding are problems with conical intersections which may appear in the treatment of reactions in excited states *etc.* [70].

3.2.5 Coupled Cluster theory

The CI theory discussed in the previous Section was a leading instrument for the high level treatment of the electron correlation problem in many–electron atoms and molecules for a long time. Up to the eighties the variational upper bound property, typical for SCF and CI, was considered as a principal requirement imposed on molecular many–electron methods. For this reason the emerging Many–body Perturbation Theories (MBPT) were considered for the electron correlation calculations as less convenient. This view was quite general even though, for example, the fourth order MBPT method was that time appreciated as clearly very accurate and computationally much less demanding alternative to CISD [37,62]. Another bottleneck of truncated CI is the problem of size–consistency, or proper scaling of energy with the size of the system. Size consistency means [40] that if the subsystems A and B are far apart, and if energies of A, B, and AB are computed in an equivalent way, the computed energies satisfy $E(AB) = E(A) + E(B)$. Related to the size consistency is the concept of the size extensivity, which has its analogue in thermodynamics. In many–electron systems was the importance of the size extensivity and the advantage in using an exponential *ansatz* first realized by nuclear physicists. A quantum mechanical model is said to be extensive if the energy of a system computed with this model scales correctly with the size of the system. We recommend the reader to study a detailed analysis of these and related problems in the literature, see Refs. [40, 71]. One has to be familiar with consequences of the errors caused by these effects when calculating intermolecular interactions, reaction energies, bond strength and in many other molecular properties by truncated CI methods, including CISD. Correction can be achieved by including quadruple excitations, at least approximately .

Unlike truncated CI methods, MBPT and Coupled cluster methods provide properly size consistent descriptions. Also, with CC methods higher excitations are considered more effectively than in CI methods. Therefore it is worthwhile to pay more attention to CC methods used frequently also at the relativistic level. Particular attention should be paid to the CCSD(T) method [35, 36] which is presently accepted as a ”golden standard” of quantum chemistry. Another reason of our attention to the CC theory is that CC methods have been most often used in our own calculations of molecular properties. The Many Body Perturbation Theory will be shortly discussed in the correlated–relativistic Section 4.5.1.

The Coupled Cluster theory was invented in fifties initially as a tool for understanding correlation effects in the electron gas [72–75]. Čížek's pioneering implementation of the CC theory to many–electron systems [76–78] represents a real breakthrough in the development of methods for the treatment of the electron correlation in atoms and molecules [37–40, 71, 79]. The many–body diagrammatic formulation of MBPT and CC theories as presented in a detailed form by Paldus and Čížek already in 1975 [80, 81] is up to now a wonderful tool for a transparent order by order analysis of the energy and the wave function. The diagrammatic technique also facilitates the formulation of final CC equations that obey the requirements of the size consistency and an efficient implementation thanks to clever factorization that alleviates the unpleasant scaling of CC with the number of correlated electrons and the number of virtual orbitals [37, 40, 71, 82]. Presently, the CC theory is extremely useful tool for solving a variety of many–body problems starting from small systems as atomic nuclei, up to large polyatomic molecules, from weakly bound atoms and molecules up to strongly bound systems as atomic nuclei. Most recent comprehensive and authoritative account of the CC theory and its applications, including relativistic theory [83, 84] represents a book edited by Čársky, Paldus and Pittner [85].

The essence of the CC theory lies in the exponential expansion of the wave function,

$$\Psi_{CC} = \exp(\hat{T})\Phi_0, \tag{3.31}$$

where $\hat{T}$ is the excitation operator acting on the *known* reference state Φ_0, which is in most cases represented by a single–determinant HF wave function. The excitation operator can be expressed using the Taylor expansion, so that Ψ_{CC} can be written as

$$\Psi_{CC} = (1 + \hat{T} + \hat{T}^2/2 + \hat{T}^3/3! + \dots)\Phi_0. \tag{3.32}$$

Expressing the excitation operator $\hat{T}$ as a sum of all possible excitation operators (up to the number of electrons),

$$\hat{T} = \hat{T}_1 + \hat{T}_2 + \hat{T}_3 + \dots, \tag{3.33}$$

leads to different variants of the CC method according to the truncation of the total excitation operator $\hat{T}$ at a specific excitation level. Note that upon including all excitation operators the CC wave function and the corresponding energy are accurate within a selected one–electron basis set which defines the reference wave function Φ_0. This is equivalent to full CI. The effect of the single, double, *etc.* excitation operators, $\hat{T}_1$, $\hat{T}_2$, *etc.*, acting on Φ_0 can be expressed in terms of the excitation amplitudes $t_{ij\cdots}^{ab\cdots}$ defined as

$$\hat{T}_1\Phi_0 = \sum_i \sum_a t_i^a \hat{a}^+ \hat{i}|\Phi_0\rangle = \sum_i \sum_a t_i^a \Phi_i^a$$

$$\hat{T}_2\Phi_0 = (1/4)\sum_{i,j}\sum_{a,b} t_{ij}^{ab}\hat{a}^+\hat{b}^+\hat{j}\hat{i}|\Phi_0\rangle = \sum_{i>j}\sum_{a>b} t_{ij}^{ab}\Phi_{ij}^{ab} \tag{3.34}$$

($\hat{a}^+, \hat{b}^+, ..., \hat{i}, \hat{j}$ ...., are creation and annihilation operators, respectively, acting on a Slater determinant). More generally, $\hat{T}_n\Phi_0 = 1/(n!)^2 \sum_{i,j,k...;a,b,c...} t_{ijk...}^{abc...}\Phi_{ijk..}^{abc...}$. Note that in many–electron theories we prefer to deal with the n–electron reference determinant Φ_0 rather than the true vacuum state. In the above equations indices $i, j, k, ...$ and $a, b, c...$ *etc.* refer to occupied and virtual spinorbitals in Φ_0, respectively, and $\Phi_{ijk...}^{abc...}$ are determinants representing single, double, *etc.* excitations from occupied to virtual spinorbitals. General indices will be denoted as $p, q, r, s, ...$

To get the energy corresponding to the CC wave function $|\Psi_{CC}\rangle$ defined in the exponential form, Eq. 3.31, we have to solve the Schrödinger equation,

$$\hat{H}\exp(\hat{T})|\Phi_0\rangle = E\exp(\hat{T})|\Phi_0\rangle. \tag{3.35}$$

Next, we multiply Eq. 3.35 from left by $\exp(\hat{T})$ and obtain:

$$\exp(-\hat{T})\hat{H}\exp(\hat{T})|\Phi_0\rangle = E|\Phi_0\rangle. \tag{3.36}$$

The Hamiltonian $\bar{H} = \exp(-\hat{T})\hat{H}\exp(\hat{T})$ is a similarity transformed Hamiltonian $\hat{H}$. It facilitates calculations of nested commutators of the Hamiltonian $\hat{H}$ with the cluster operator $\hat{T}$ needed for obtaining algebraic expressions for the CC energy and the wave function in terms of one– and two– electron integrals. By projecting Eq. 3.36 onto a reference determinant, $|\Phi_0\rangle$, we obtain the CC energy. The CC excitation amplitudes, $t_{ij...}^{ab...}$ and the corresponding CC wave function can be obtained by projecting Eq. 3.36 onto all excited determinants, $|\Phi_{ij...}^{ab...}\rangle$:

$$\langle\Phi_0|\exp(-\hat{T})\hat{H}\exp(\hat{T})|\Phi_0\rangle = E_{CC} \tag{3.37}$$

$$\langle\Phi_{ij...}^{ab...}|\exp(-\hat{T})\hat{H}\exp(\hat{T})|\Phi_0\rangle = 0. \tag{3.38}$$

At this point it is profitable to employ the Hamiltonian in the normal–ordered second quantization form as

$$\hat{H} = \sum_{pq} f_{pq}\{\hat{p}^+\hat{q}\} + \frac{1}{4}\sum_{pqrs}\langle pq||rs\rangle\{\hat{p}^+\hat{q}^+\hat{s}\hat{r}\} + \langle\Phi_0|\hat{H}|\Phi_0\rangle = \hat{f}_N + \hat{W}_N + \langle\Phi_0|\hat{H}|\Phi_0\rangle. \tag{3.39}$$

Antisymmetrized two–electron integrals $\langle pq||rs\rangle$ are defined in Section 3.2, see Eq. 3.16. Curly brackets $\{...\}$ denote a normal–ordered string of the second–quantized operators (see, *e.g.* [40, 71, 81]). Subtracting $\langle\Phi_0|\hat{H}|\Phi_0\rangle$, the energy of the Hartree–Fock reference state, we have the normal–ordered form of the Hamiltonian,

$$\hat{H}_N = \hat{f}_N + \hat{W}_N = \hat{H} - \langle\Phi_0|\hat{H}|\Phi_0\rangle. \tag{3.40}$$

Using $\hat{H}_N$ we obtain the CC correlation energy and the wave function,

$$\triangle E_{CC} = \langle\Phi_0|\hat{H}_N \exp(\hat{T})|\Phi_0\rangle_C \tag{3.41}$$
$$0 = \langle\Phi_{ij\ldots}^{ab\cdots}|\hat{H}_N \exp(\hat{T})|\Phi_0\rangle_C, \tag{3.42}$$

Eqs. 3.41 and 3.42 may be expressed using the diagrammatic representation of $\hat{H}_N$ and $\hat{T}_1$, $\hat{T}_2$, ... $\hat{T}_n$, see *e.g.*, Refs. [40, 71, 80, 81]. The subscript C in Eqs. 3.41 and 3.42 indicates that only those terms in which the Hamiltonian is connected to the every cluster operator on its right should be included in the algebraic representation of the expression. Since $\hat{H}_N$ involves merely one– and two–electron parts, the expansion of the excitation operator $\exp(\hat{T})$ is truncated. That means, no higher than double excitations, *i.e.* no higher excitation operators than $\hat{T}_1$, $\hat{T}_2$ and the product $\hat{T}_1\hat{T}_1$ (this would correspond to CC with singles and doubles excitations, *i.e.* CCSD) may appear in any CC energy expression:

$$\triangle E_{CC} = \langle\Phi_0|\hat{H}_N(\hat{T}_1 + \hat{T}_2 + 1/2\hat{T}_1\hat{T}_1)|\Phi_0\rangle_C\,. \tag{3.43}$$

The algebraic representation of Eq. 3.43 in spinorbitals is

$$\triangle E_{CC} = \sum_{ia} f_{ia}t_i^a + \frac{1}{4}\sum_{ijab}\langle ij||ab\rangle t_{ij}^{ab} + \frac{1}{2}\sum_{ijab}\langle ij||ab\rangle t_i^a t_j^b\,. \tag{3.44}$$

We stress that above expressions for the CC energy are general. The expression for the CC energy remains the same when along with $\hat{T}_1$ and $\hat{T}_2$ also $\hat{T}_3$, $\hat{T}_4$, and so on would be included in the cluster expansion of $\hat{T}$, Eq. 3.33. Of course, the energy itself would be different, since for any truncation of $\hat{T} = \hat{T}_1 + \hat{T}_2 + \hat{T}_3 + \ldots$ different amplitudes enter into Eq. 3.44.

Eqs. 3.42, which determine the $t_{ij\ldots}^{ab\cdots}$ excitation amplitudes are truncated by the excitation level as well. This time, however, we have to consider which operators are included in the CC exponential expansion, Eq. 3.33. The most common is the CCSD method [86] (Coupled Cluster Singles and Doubles), approximating $\hat{T}$ as $\hat{T} = \hat{T}_1 + \hat{T}_2$. This means, that we have to determine the single and double excitation amplitudes, t_i^a and t_{ij}^{ab}, respectively. Again, due to the existence of solely one– and two–electron parts in $\hat{H}_N$ the exponential expansion of the CCSD wave function contains no higher contributions than those from the triple and quadruple excitations

$$\begin{aligned}|\Psi_{CCSD}\rangle \quad \Longleftarrow \quad & \left[1 + \hat{T}_1 + \left(\hat{T}_2 + \frac{1}{2}\hat{T}_1^2\right) + \left(\hat{T}_1\hat{T}_2 + \frac{1}{6}\hat{T}_1^3\right)\right.\\ & \left.+\left(\frac{1}{2}\hat{T}_2^2 + \frac{1}{2}\hat{T}_2\hat{T}_1^2 + \frac{1}{24}\hat{T}_1^4\right)\right]|\Phi_0\rangle.\end{aligned} \tag{3.45}$$

By the symbol $\Longleftarrow$ we are giving a notice that terms listed in Eq. 3.45 contribute to the CCSD energy and the wave function. The exponential expansion of the wave function is in fact infinite and terminates only upon projecting on Φ_0, singles and doubles, respectively, see Eqs. 3.41 and 3.41. Note that the expansion, Eq. 3.45, contains not only terms easily recognized as single and double excitations which arise from the so called *connected* clusters (terms $\hat{T}_1$ and $\hat{T}_2$) but also their products, *disconnected* clusters $\hat{T}_1\hat{T}_1$, $\hat{T}_1\hat{T}_2$, $\hat{T}_2\hat{T}_2$, up to $\hat{T}_1^4$. $\hat{T}_1\hat{T}_2$ represents a part of contributions due to triple excitations, $\hat{T}_2\hat{T}_2$ represents a dominating disconnected contribution due to quadruple excitations. For their calculations we need, however, only amplitudes of the single and double excitations. This explains the advantage of expressing the wave function as an exponential expansion in CC as compared with the linear expansion in CI (along with the size–extensivity of CC). The CI coefficients and CC amplitudes can be symbolically related by equations,

$$
\begin{aligned}
C_1 &= T_1 \\
C_2 &= T_2 + (1/2)T_1T_1 \\
C_3 &= T_3 + T_1T_2 + (1/6)T_1T_1T_1 \\
C_4 &= T_4 + (1/2)T_2T_2 + T_1T_3 + (1/24)T_1T_1T_1T_1 \\
&\dots
\end{aligned}
\tag{3.46}
$$

Theoretical and computational implementation of $\hat{T}_3$, $\hat{T}_4$ and even higher excitation operators (which introduce connected contributions of triple and quadruple excitations) is available [82,87–89], but iterative CCSDT, CCSDTQ and higher level methods are prohibitively demanding for other than benchmark calculations of smaller molecules. The algebraic representation of Eq. 3.42 is quite complicated even for the CCSD method. The reader is referred to the literature, see *e.g.*, [37, 40, 71, 80]. We just mention that the single and double excitation amplitudes in CCSD, t_i^a and t_{ij}^{ab}, have to be determined in an iterative process starting from the simplest amplitudes, which are the first–order wave function t_{ij}^{ab} amplitudes ($t_{ij}^{ab(1)}$). Let us assume that we work with canonical HF orbitals, for which $\langle p|\hat{f}|q\rangle = \epsilon_p\delta_{pq}$. In the spinorbital form $t_{ij}^{ab(1)}$ amplitudes are represented by a simple formula,

$$
t_{ij}^{ab(1)} = \frac{\langle ij||ab\rangle}{\epsilon_i + \epsilon_j - \epsilon_a - \epsilon_b} . \tag{3.47}
$$

The denominator in Eq. 3.47 , (denoted in the following as $D_{ij\dots}^{ab\dots}$)

$$
D_{ij\dots}^{ab\dots} = (f_{ii} + f_{jj} + \dots) - (f_{aa} + f_{bb} + \dots) = \epsilon_i + \epsilon_j + \dots - \epsilon_a - \epsilon_b - \dots \tag{3.48}
$$

results from the one–electron part of $\hat{H}_N$. For the reference determinant with canonical HF orbitals, Eq. 3.19, the only nonzero terms are diagonal Fock matrix elements, *i.e.* orbital energies. We should add that the single excitation amplitudes t_i^a appear for the first time as the second–order terms (however, they are the first order terms for open–shells with the ROHF reference). It is easily recognized that with $t_{ij}^{ab(1)}$ defined in Eq. 3.47 we obtain the second order MBPT correlation energy (MBPT2),

$$
\triangle E_{MBPT}^{(2)} = \frac{1}{4}\sum_{ijab}\langle ij||ab\rangle t_{ij}^{ab(1)} = \sum_{i<j,a<b}\frac{\langle ij||ab\rangle^2}{\epsilon_i + \epsilon_j - \epsilon_a - \epsilon_b} . \tag{3.49}
$$

The expression is pair additive, that means the correlation energy can be expressed in terms over pairs of occupied (virtual) orbitals. Higher orders of MBPT do not exhibit such additivity. Note that the expression for $\triangle E_{MBPT}^{(2)}$ is formally the same as is the second term in the $\triangle E_{CC}$ energy. The only difference is that the amplitudes in $\triangle E_{CC}$ are the infinite–order t_{ij}^{ab} CC amplitudes while in $\triangle E^{(2)}_{MBPT}$ there are the first–order double excitation amplitudes (terms with t_i^a are zero in the MBPT2 energy, since they appear for the first time in the second–order wave function). We will use this simplest nonrelativistic expression for the correlation energy in Section 4.5.1 as a starting point for discussing the theoretical and computational demands when going from the nonrelativistic to the relativistic correlated treatment of atoms and molecules. This instructive example may give the reader some idea of what can be expected with higher electron correlation methods at the four–component relativistic level.

Realizing that all iterative methods lying higher in the hierarchy of the CC methods are computationally much more demanding than CCSD, we have to ask a question of including connected triples and quadruples in a more approximate way. CCSD contains disconnected contributions of triples and quadruples, but for accurate results are important connected triples and for quasidegenerate systems also connected quadruples. The importance of triples was for the first time documented by Paldus, Shavitt and Čížek [78]. The first systematic inclusion of triple excitations into the CC theory was studied by Lee, Kucharski and Bartlett [90]. Their approximate iterative CCSDT–1 method was largely extended to a series of the CCSDT–n approximations of the full CCSDT by Urban *et al.* [35] based on the careful order–by–order CC wave function analysis. Full iterative CCSDT was implemented by Noga and Bartlett [87]. Higher level CC calculations are also available [40, 91], albeit obtaining an algebraic representation of CC equations beyond CCSDT is extremely tedious. The problem was alleviated by using diagrammatic techniques and the second quantization formalism, leading to the string-based coupled cluster theory and automated generation of computer codes [89], as pioneered by Li and Paldus [92]. The critical need for including triples in an economical fashion culminated by introducing the famous CCSD(T) method. The idea was that the main contributions from triple excitations (4–th order energy terms in the perturbation theory), that are missing in CCSD can be effectively added via perturbation–based technique non–iteratively, using all the "correlation" information available from the converged T_1 and T_2 CCSD amplitudes. The CCSD(T) method [35–37], represents perhaps the best compromise between accuracy and efficiency for treating high–level electron correlation problem for small and medium size molecules represented by a good single determinant reference. As many comparisons with experiment and benchmark FCI and higher level CC methods showed, it is accurate enough and still allowing the usage of sufficiently large basis sets. For its safe use it is recommended checking the suitability of a single determinant reference by inspecting the t_i^a and t_{ij}^{ab} CCSD amplitudes which should not be larger than 0.20 or to use the diagnostics for single excitation amplitudes (the T_1 diagnostics, [71]). We note, however, that even CCSD(T) remains computationally very demanding for large scale calculations. Its importance, besides being an excellent tool for predicting molecular properties lies also in its role as a source of benchmark results for DFT methods, which are missing a systematic test of accuracy.

In CCSD(T) calculations with large basis sets the most demanding step remains the triples step, even though it is noniterative (in contrast to the iterative CCSD). It should be interesting to realize that CCSD(T) for open–shells and for four–component relativistic calculations is even more demanding than are nonrelativistic closed–shell calculations. Therefore we will show a few equations in order to demonstrate the scaling of triples with the number of occupied (N_o) and virtual (N_v) spinorbitals.

The CCSD(T) energy is represented by a sum of the converged CCSD energy plus contributions from connected triples calculated noniteratively using the perturbative MBPT arguments (for more details see [36, 37, 40, 71]:

$$E_{CCSD(T)} = E_{CCSD} + E_T^{(CCSD)} + E_{ST}^{(CCSD)}, \tag{3.50}$$

where $E_T^{(CCSD)}$ is the correction from triple excitations calculated in the fourth order MBPT fashion,

$$E_T^{(CCSD)} = \sum_{i<j<k} \sum_{a<b<c} t_{ijk}^{abc} D_{ijk}^{abc} t_{ijk}^{abc}. \tag{3.51}$$

D_{ijk}^{abc} is the denominator defined by Eq. 3.48. The triple excitation amplitudes are calculated using the expression (see, *e.g.* [37, 40, 71])

$$D_{ijk}^{abc} t_{ijk}^{abc} = \hat{P}(i/jk)\hat{P}(a/bc) \sum_d \langle bc||di\rangle t_{jk}^{ad} - \hat{P}(i/jk)\hat{P}(a/bc) \sum_l \langle la||jk\rangle t_{il}^{bc}. \tag{3.52}$$

All these equations are presented in the simplest spinorbital form. Eqs. 3.51 and 3.52 look like the MBPT equations which define the fourth order energy contribution from the triple excitation amplitudes. However, triples in CCSD(T) are calculated using the converged CCSD t_{ij}^{ab} infinite order amplitudes instead of the first order $t_{ij}^{ab(1)}$ double excitation amplitudes. $\hat{P}$ is the permutation operator. The $E_T^{(CCSD)}$ contribution which supplements the $\triangle E_{CCSD}$ correlation energy (or E_{CCSD} in a shorter notation) defines the CCSD + T(CCSD) method [35] which is a forerunner of the CCSD(T) method. The difference is that Pople *et al.* [36] have incorporated in CCSD(T) a single fifth order contribution, $E_{ST}^{(CCSD)}$ (all other fifth order energy contributions were neglected), which represents an interaction of singles and triples:

$$E_{ST}^{(CCSD)} = \sum_{i,j<k} \sum_{a,b<c} \langle bc||jk\rangle t_{ijk}^{abc} t_i^a. \tag{3.53}$$

The $E_{ST}^{(CCSD)}$ contribution is an analogue of the fifth order contribution to the MBPT energy, $E_{ST}^{(5)}$, comprising the single and triple excitations. In CCSD(T) is $E_{ST}^{(CCSD)}$ calculated, again, employing the converged CCSD t_i^a infinite order single excitation amplitudes instead of the second order wave function single excitation MBPT amplitudes. Formally the second order MBPT wave function triples amplitudes t_{ijk}^{abc} are calculated using Eq. 3.52 from the infinite order CCSD t_{ij}^{ab} doubles. We note that the t_i^a singles are first order wave function amplitudes for open–shells with the ROHF (or any other non–HF) reference. For details see [38, 40, 65, 66, 71].

No doubt, the most frequently used CC method, CCSD(T), is computationally much more demanding than are the SCF or the Density Functional Theory (DFT) calculations. Even more demanding are CCSDT, CCSDTQ *etc.* methods and their variants. The role of CC methods and particularly the CCSD(T) method as a source of benchmark results for *e.g.*, tuning less demanding DFT methods can be hardly overestimated. Enormous importance of CC methods lies in their potential for obtaining results with high and controlled accuracy, *i.e. good results for a good reason*. This follows from the fact that CC methods form a natural perturbative–like hierarchy [35, 37–40, 71] employing gradually more accurate wave functions in more efficient way than in other (for example variational) methods. The efficiency follows from utilizing the exponential *ansatz* for the wave function, Eq. 3.31. At the same time this *ansatz* guarantees the size–extensivity of CC energies [40, 71]. We note that an instrument for controlling the accuracy and reliability of frequently used DFT methods is missing. Another problem with DFT is plenty of functionals used in calculations of a specific property and difficulties of DFT in representing, *e.g.*, dispersion forces in Van der Waals interactions, diffuse parts of the electron distribution needed for proper treatment of electron affinities, *etc.*

Should CCSD(T) results for smaller molecules serve as a benchmark for other methods, reasonably large basis sets for accurate description of occupied orbitals are required. The number of occupied orbitals (spinorbitals) is strictly determined by the number of electrons. Large basis sets create large space of virtual orbitals and, therefore, enhanced computational demands in the treatment of the correlated calculations. With the UHF reference the most demanding steps for obtaining the single and double excitation amplitudes in CCSD scale with the number of occupied (N_o) and virtual spinorbitals N_v as $N_o^2 N_v^4$ in an iterative process. Resulting single and double excitation CCSD amplitudes are afterwards used in the *noniterative* approximate determination of the triple excitations. Calculations of the triple excitation amplitudes, Eq. 3.52, is the most demanding part in CCSD(T) with large basis sets (for large basis sets is $N_v \gg N_o$). The t_{ijk}^{abc} amplitudes are carrying three target indices of occupied orbitals and three indices of virtuals. Adding the summation over index of the occupied or virtual orbital leads to unfavorable scaling $\approx N_o^3 N_v^4$ and $N_o^4 N_v^3$. The final calculation of the energy resulting from triples is slightly less demanding, scaling as $N_o^3 N_v^3$, see Eqs. 3.51 and 3.53. Worst steps in the rigorous iterative CCSDT would need arithmetic operations which scale as $N_o^3 N_v^5$ in each iteration. Approximate CCSDT–n methods are a bit simpler but still very demanding. Another problem with CCSDT and CCSDT–n is also storing of $N_o^3 N_v^3$ triples amplitudes.

For closed–shell systems the computational cost of CCSD(T) calculations can be reduced by about a factor of 4 when working with orbitals instead of spinorbitals (the number of occupied/virtual orbitals for closed–shells is one half of the number of spinorbitals). Substantial reduction of computer demands for open–shell systems with respect to the UHF reference can be achieved using the ROHF reference [65]. Theoretical background of the ROHF CCSD(T) method with the spin adapted amplitudes is more complicated [66, 93] than with the UHF reference or methods for the closed–shells with the RHF reference. Theoretical reduction of the computer time for closed–shells or for open–shells with the ROHF reference does not correspond to the expected factor of reducing the number of orbitals by one half since it is hampered by more complicated structure of the final equations after applying the spin integration. Clearly, working with four–component spinors makes relativistic CCSD(T) calculations even more demanding than are nonrelativistic calculations utilizing doubly occupied orbitals for closed–shells or one–component spinorbitals with the UHF reference.

Modern formulations of the CC theory, sophisticated factorization of complicated equations for obtaining CC amplitudes, combined with a quickly enhanced computer power accompanied with a high level of parallelism allow calculations of gradually larger and larger molecules with a high and controlled accuracy [64]. Techniques exploited in modern approaches utilize many mathematical ”tricks” and physically well founded approximations like Choleski decomposition for more efficient treatment of the two–electron integrals (which is a bottleneck in all sophisticated many–electron methods), optimization and subsequent reduction of normally very large space of virtual orbitals (OVOS, Optimized Virtual Orbitals Space), the symmetry constrains etc. [64]. Using of CC methods based on the Douglas–Kroll–Hess Hamiltonian [18, 94, 95], in which the scalar–relativistic effects are included needs modified integrals over basis functions (forgetting for a need of modified contractions of basis sets) but otherwise it is quite straightforward. Very efficient are approaches relying on the idea of localized orbitals and also explicitly correlated CC methods [96] working with the r_{12} variables in the wave function. Eventually, CC methods approach in some cases an almost linear scaling with the size of a molecule, which is a dream goal of the quantum chemistry methods for many–electron systems.

Large progress is observed in developments of the Multireference CC methods (MR CC) and approaches capable of treating quasidegenerate systems [38, 88, 97–99]. MR CC approaches are very important in relativistic calculations particularly for the SO coupling or QED effects [84]. Relativistic CC methods will be discussed in more detail in Section 4.5.2.

3.2.6 CASSCF, RASSCF, and CASPT2 methods

The physical origin of the electron correlation was summarized in Section 3.2.3. We have already introduced a concept of the dynamical and nondynamical correlation. Clearly, both effects can not be entirely separated and mean just a possible way for understanding a difficult problem of the treatment of inter–electronic interactions in many electron systems. The problem can be somewhat simplified if the starting wave function for high level calculations can be just a single Slater determinant which is a solution of the HF equations. The single determinant methods for treating the dynamic correlation were discussed in previous sections. In this part we will summarize some methods applicable to problems which require two or more Slater determinants which represent a reasonable starting wave function of a system under consideration. As mentioned in Section 3.2.3 this occurs in investigations of the bond breaking processes, in many open–shell systems, particularly in low–spin excited states, and other. First indication that the single determinant reference is insufficient is a small energy gap between the SCF occupied and virtual orbitals in a single Slater determinant wave function (if used as a reference). In the CISD wave function the leading determinant must be strictly dominating (by more than 90%) and the singly and doubly excitation amplitudes in CCSD must be not larger than 0.2 for calculations with a single determinant reference. A trivial example of problems with a single determinant reference is the bond breaking in the hydrogen molecule. It is perfectly well represented by a single determinant around the equilibrium bond distances R_e. Upon stretching the bond length the potential energy curve (calculated within the Born–Oppenheimer approximation) has a reasonable shape up to distance of about 1.5 R_e. For longer distances the energy gap between the bonding σ_g and the antibonding σ_u orbitals gets narrow and the potential energy curve deteriorates. At the full separation is the situation simple - dissociation products are just two hydrogen atoms. In medium distances, however, we need at least two determinants, corresponding to the electronic configurations σ_g^2 and σ_u^2 (having the same spin and the same state symmetry). Analogous orbitals participate also in the bond breaking in the F_2 molecule. More complicated is the situation when breaking (or forming) the double or triple bonds in which participate π orbitals. Examples are the dissociation of the ethylene molecule into two methylene radicals or bond breaking of the triple–bonded N_2 molecule. The fact that the electronic potential energy curves around minima are for many molecules well represented by energies obtained from the correlated single determinant reference wave functions and methods, like CCSD(T), can be documented numerically: In most cases the polynomial fit over energies around the minima leads to reasonably accurate harmonic vibrational frequencies (alternatively they can be obtained by analytical derivatives at R_e). Anharmonicity is occasionally less accurate with a single determinant reference, since it depends on energies more apart from the equilibrium. Careful analysis of participating determinants is also needed for many excited states and radicals.

Basic method for obtaining a linear combination of Slater determinants needed for a physically correct description of the reference wave function is the Multi–Configuration SCF method (MC SCF). Several or many Slater determinants are chosen to guarantee a qualitatively correct description of all states and electronic configurations. So selected set of Slater determinants leads to the description of the nondynamical electron correlation. The dynamical correlation must be added by the CI method in which the reference is the MC SCF wave function. So defined MR CI is mostly computationally very demanding.

The MC SCF wave function for the electronic state I is a linear expansion in terms of a set of pre–selected Slater determinants Φ_P,

$$\Psi_I = \sum_P C_P \Phi_P. \tag{3.54}$$

The variational parameters C_P are optimized *simultaneously* with the expansion coefficients $c_{\nu p}$ of the spatial part of molecular orbitals ϕ_p which define the Slater determinants Φ_P. Molecular orbitals (either occupied or virtual) are expressed within the algebraic approximation, $\phi_p = \sum_\nu c_{\nu p}\chi_\nu$, Eq. 3.24. Resulting molecular orbitals are the same for the ground state (the lowest solution of the eigenvalue problem) and for excited states. Their shape is, so to say a compromise between the accuracy and effectivity. Obviously, selecting a set of determinants for a MC SCF wave function, Eq. 3.54, may be in some cases difficult and to some extent arbitrary. Selecting too many Slater determinants as a reference makes the subsequent MR CISD calculation quickly intractable.

Presently, MC SCF–type methods are dominated by the CASSCF (Complete Active Space SCF) approach. In CASSCF the user selects the set of *active* orbitals and the number of electrons in active orbitals instead of pre–selected Slater determinants. Clearly, for a regular user of the computational chemistry programs thinking in terms of orbitals is easier than in terms of determinants. Selected orbitals are those which actively participate in the process under consideration or which participate in electronic states which are to be considered (for example, the ground state and several low–lying excited states). The CASSCF wave function is defined [100] by selecting a set of active orbitals and active electrons and is constructed as a linear expansion in the set of configuration state functions (CSFs) that can be generated by occupying the active orbitals in all possible ways consistent with a spin and state symmetry. Therefore, they form full CI within active orbitals. This is very advantageous since the wave function is then fully variational, both in orbitals and in CSFs and satisfies some important requirements, as the Hellmann–Feynman theorem, which allows, *e.g.*, calculations of electric properties as expectation values. In some difficult cases we may need for a proper representation of the process or a state under consideration so many CSFs in the CASSCF wave function that calculations become computationally too demanding. To alleviate the problem, the active space is split into three subspaces, listed below. Some excitations from/to orbitals in the RAS1 and RAS3 space, respectively, are somewhat restricted. Methods has an acronym RASSCF. When the RAS1 and RAS3 spaces are empty, the RASSCF method is equivalent to CASSCF.

Partitioning of the occupied molecular orbitals in RASSCF and the participation of orbitals in CASPT2 (which will be defined later in this Section) can be summarized as follows:

- **Frozen orbitals:** Orbitals that are doubly occupied in all configurations in CASSCF and PT2.
- **Inactive orbitals:** Orbitals that are doubly occupied in all configurations in CASSCF. Allowed are excitations in the PT2 step.
- **Active orbitals:** These orbitals are subdivided into three separate groups:
  - **RAS1 orbitals:** Orbitals that are doubly occupied except for a maximum number of holes allowed in this orbital subspace.
  - **RAS2 orbitals:** In these orbitals all possible occupations are allowed (former Complete Active Space orbitals).
  - **RAS3 orbitals:** Orbitals that are unoccupied except for a maximum number of electrons allowed in this subspace.
- **Secondary orbitals:** Virtual orbitals that are inactive in CASSCF. Excitations to these orbitals are allowed in the PT2 step.

The CASSCF method can handle the near–degeneracies very effectively and is particularly suitable as a starting point for applications to processes on the energy hypersurfaces and in the electronic spectroscopy [100]. The extension of CASSCF to the relativistic domain and particularly to the spin–orbit interactions will be treated in Section 4.7.2.

The CASSCF wave function is not capable of treating the dynamic correlation effects satisfactorily (unless the active space would be unrealistically large). Therefore, CASSCF is used as a zero–order wave function (a root function) for the multiconfigurational second–order perturbation theory, which defines the CASPT2 method [64, 100, 101]. CASPT2 uses orbital excitation operators applied to the root wave function to express the first–order perturbation function. With respect to the structure of the active space we should add that within the PT2 perturbation treatment also excitations from inactive orbitals are allowed. They do not participate, however, in optimization of the C_I coefficients in the expansion, Eq. 3.54. The same holds for so called secondary orbitals which can be employed in the excitation process in the PT2 step. Finally, as with CI and CC methods there are frozen orbitals that are not used in any excitation process and remain doubly occupied in both the CASSCF and in the PT2 step. Analogously, some highest lying virtual orbitals are neglected in the PT2 dynamic electron correlation calculations

The problem which had to be solved [100,101] is the definition of the zero–order Hamiltonian $\hat{H}_0$. A good choice in defining the simple enough $\hat{H}_0$ is a generalization of the zero–order Hamiltonian based on the HF operator, usual in a single determinant reference perturbation theory. We refer the reader to the original literature [100, 101].

CASSCF, CASPT2, RASPT2 and their generalizations to the relativistic domain, RASSI [102, 103] have been successfully applied to a large variety of problems in chemistry and molecular physics. These methods are implemented into the famous MOLCAS computer package [64]. When the active space is selected properly, the method is sufficiently accurate and reliable. Possible problems may occur due to an inadequate choice of active orbitals [104]. Alternative selection/extension of the active space is also a tool for controlling the accuracy. Relativistic treatments include the scalar–relativistic methods based on the Douglas–Kroll–Hess Hamiltonian [18, 94, 95]. The RASSI method for the treatment of spin–orbit effects will be discussed in Section 4.7.2. Important is also availability of basis sets for both nonrelativistic and relativistic [105, 106] calculations.

4 Relativistic theory of many–electron atoms and molecules

While the Schrödinger nonrelativistic description, Section 3.1, is sufficient for light elements, here we focus ourselves on the derivation of a more general equation fulfilling the principles of the theory of relativity.

4.1 Lorentz transformations

When Maxwell published his four equations for electromagnetism [44], in contrast to Newtonian physics these were not invariant with respect to the Galilean transformation which serves for transformation between the coordinates of two reference frames differing only by constant relative motion. The Galilean transformation, acting in the realm of the Newtonian physics, relates two different reference systems with coordinates $\mathbf{r}$ and $\mathbf{r}'$, moving with a relative velocity $\mathbf{v}$,

$$\mathbf{r}' = \mathbf{r} - \mathbf{v}t. \tag{4.1}$$

The space–time Galilean transformation between two systems can be written as follows

$$\begin{pmatrix} \mathbf{r}' \\ t' \end{pmatrix} = \begin{pmatrix} 1 & -\mathbf{v} \\ 0 & 1 \end{pmatrix} \begin{pmatrix} \mathbf{r} \\ t \end{pmatrix}. \tag{4.2}$$

Lorentz proposed the following transformation [107] to make Maxwell's equations invariant:

$$\begin{pmatrix} \mathbf{r}' \\ t' \end{pmatrix} = \gamma \begin{pmatrix} 1 & -\mathbf{v} \\ -\frac{v}{c^2} & 1 \end{pmatrix} \begin{pmatrix} \mathbf{r} \\ t \end{pmatrix}. \tag{4.3}$$

γ is the relativistic scaling factor

$$\gamma = \sqrt{1 - \frac{v^2}{c^2}}, \tag{4.4}$$

which approaches the value of 1 in the nonrelativistic limit when velocities are negligible in comparison to the speed of light.

The Lorentz transformation illustrates how, in line with the theory of the special relativity, two observers' varying measurements of space and time can be turned into each other's frame of reference. Though the Lorentz transformations were invented in a somehow *ad hoc* manner, they may be also introduced if two basic postulates are taken into account:

1. The Principle of Relativity: The physical laws are the same in all inertial reference frames.
2. The Principle of Invariant Light Speed: Light in free space is propagated with a constant velocity, regardless of any relative motion of observer and of the source.

These postulates were first suggested by Henri Poincaré [108], but it is Albert Einstein [43] who is credited with discovering and promoting the full impact of the new theory of relativity. Note, that the second postulate claiming the invariance of the speed of light, c, can also be derived from Maxwell's equations. The constant speed of light in all inertial frames can be viewed as the central theme in relativity. By applying these presuppositions it can be shown that physical laws should be invariant under the Lorentz transformation, Eq. 4.3, rather than under the old Galileo transformation, Eq. 4.2.

4.2 Klein–Gordon equation

The Einstein theory of relativity [43, 109] gives the total energy expression in terms of the momentum and of the rest mass, m_0:

$$E^2 \;=\; p^2c^2 + m_0^2c^4; \qquad\qquad E \;=\; \pm\sqrt{p^2c^2 + m_0^2c^4}. \tag{4.5}$$

This equation may be utilized to form the classical free particle Hamiltonian, Section 4.3. The corresponding quantum mechanical expression is derived by substituting the classical momentum, p, by its (three component) quantum mechanical operator, $\hat{\mathbf{p}} = -i\hbar\nabla$. The same holds for the total energy which is replaced by the energy operator, $i\hbar\frac{\partial}{\partial t}$.

We insert these operators into the square root of energy expression, Eq. 4.5, and get:

$$i\hbar\frac{\partial\Psi(\mathbf{r},t)}{\partial t} \;=\; \pm c\sqrt{(-\hbar^2\nabla^2 + m_0^2c^2)}\Psi(\mathbf{r},t). \tag{4.6}$$

The resulting wave equation is known as the Klein–Gordon equation [110, 111] and is manifestly Lorentz covariant. However, other aspects of the equation are problematic. It is difficult to interpret the square root operator. The Taylor expansion is possible, but it would lead to all powers of the derivative operator and thus to a nonlocal theory. Negative energy solutions have negative probability densities. Neither does the Klein–Gordon equation handle the spin nature of the electron. These facts lead to rejection of the equation, but in 1934 it found its place as the relativistic wave equation for spin–less charged particles [112].

4.3 Dirac equation

Above mentioned weaknesses motivated Dirac to take the right track and derive a single particle equation overcoming all these problems. Though there were several attempts to formulate the theory that would couple principles of relativity with those of quantum mechanics, it was Dirac who invented relativistic quantum mechanics for one–electron systems.

Dirac tried to derive an Lorentz invariant equation in the general, time–dependent form (in a.u.)

$$i\frac{\partial\Psi}{\partial t} \;=\; \hat{h}_D\Psi \tag{4.7}$$

which can be turned, as in the nonrelativistic case (see Section 3.1), into the time–independent form:

$$\hat{h}_D\Psi = E\Psi. \tag{4.8}$$

Eq. 4.7 is linear in the first derivative with respect to time. The Lorentz invariance requires the Hamiltonian to be linear in the first derivatives with respect to space as well. Such equation is expected to have the form (in a.u.)

$$i\frac{\partial\Psi}{\partial t} \;=\; -ic(\hat{\alpha}_x\frac{\partial\Psi}{\partial x} + \hat{\alpha}_y\frac{\partial\Psi}{\partial y} + \hat{\alpha}_z\frac{\partial\Psi}{\partial z}) \;+\; \beta c^2\Psi, \tag{4.9}$$

where newly introduced $\hat{\boldsymbol{\alpha}}$ and β terms must be determined by additional criteria. One of them is that solutions of the new equation must still fulfil the Klein–Gordon equation, Eq. 4.6. Paul Dirac commented on the topic: *"It took me quite a while...before I suddenly realized that there was no need to stick to quantities $\hat{\boldsymbol{\sigma}}$...with just two rows and columns. Why not go to four rows and columns?"* [113]. In this way Dirac found missing terms,

$$\hat{\boldsymbol{\alpha}} = \begin{bmatrix} 0 & \hat{\boldsymbol{\sigma}} \\ \hat{\boldsymbol{\sigma}} & 0 \end{bmatrix}; \quad \beta = \begin{bmatrix} \mathbf{I} & 0 \\ 0 & -\mathbf{I} \end{bmatrix}, \tag{4.10}$$

with mutual relations

$$[\hat{\alpha}_p, \hat{\alpha}_q]_+ = 2\delta_{pq}\ ,\ [\hat{\alpha}_q, \beta]_+ = 0\ , \qquad \hat{\alpha}_q^2 = \beta^2 = 1\ , \qquad (p,q) = (x,y,z), \tag{4.11}$$

where expression in "$[]_+$" parenthesis is the anticommutator, $[a,b]_+ = ab + ba$, and δ_{pq} is the Kronecker delta symbol. $\hat{\boldsymbol{\sigma}}$ are 2×2 Pauli matrices, mentioned in Section 3.1.2, and $\mathbf{I}$ is the 2×2 unit matrix, Eq. 3.10.

Dirac equation posses the form of a 4×4 matrix. Further usage of the notation *four–component Hamiltonian* means the Dirac based energy operator. For the free–electron it can be written as (in a.u.):

$$\hat{h}_D^{fe} = c\hat{\boldsymbol{\alpha}} \cdot \hat{\mathbf{p}} + \beta c^2 = \begin{pmatrix} c^2\mathbf{I} & c\hat{\boldsymbol{\sigma}} \cdot \hat{\mathbf{p}} \\ c\hat{\boldsymbol{\sigma}} \cdot \hat{\mathbf{p}} & -c^2\mathbf{I} \end{pmatrix}. \tag{4.12}$$

The Dirac relativistic wave function has four degrees of freedom besides the space–time variable: spin–up (α) and spin–down (β) both for electron and its positively charged conjugated partner. It is called the four–component spinor, or shortly four–spinor.

$$\Psi = \begin{pmatrix} \Psi^L \\ \Psi^S \end{pmatrix} = \begin{pmatrix} \Psi^{L\alpha} \\ \Psi^{L\beta} \\ \Psi^{S\alpha} \\ \Psi^{S\beta} \end{pmatrix}. \tag{4.13}$$

The Ψ^L and Ψ^S in the Dirac four–spinor are two–component spinors containing large (L) and small component functions (S), respectively. The probability density is given as the product of four–component vectors:

$$\Psi^\dagger\Psi = (\Psi^{L\alpha})^*\Psi^{L\alpha} + (\Psi^{L\beta})^*\Psi^{L\beta} + (\Psi^{S\alpha})^*\Psi^{S\alpha} + (\Psi^{S\beta})^*\Psi^{S\beta}, \tag{4.14}$$

where $\Psi^\dagger$ is a one–row vector:

$$\Psi^\dagger = ((\Psi^{L\alpha})^*,\ (\Psi^{L\beta})^*,\ (\Psi^{S\alpha})^*,\ (\Psi^{S\beta})^*). \tag{4.15}$$

The current density vector, $\mathbf{j}$, can be expressed as (in a.u.)

$$\mathbf{j} = c\Psi^\dagger\hat{\boldsymbol{\alpha}}\Psi. \tag{4.16}$$

Contrary to the Dirac equation, its nonrelativistic Schrödinger counterpart, Section 3.1, is of the second order in momentum. One could say that the Schrödinger equation is suitable for the description of a universe where - hypothetically speaking - the speed of light is infinitely high.

4.3.1 Nonrelativistic limit of the Dirac equation

In general it is important to understand relations between relativistic and nonrelativistic theories. For that reason we establish the connection towards the nonrelativistic limit of the Dirac equation. First, we write the free–particle Dirac equation in the shortened form of two–component spinors:

$$\hat{h}_D^{fe}\begin{pmatrix}\Psi^L\\ \Psi^S\end{pmatrix} = E\begin{pmatrix}\Psi^L\\ \Psi^S\end{pmatrix}. \tag{4.17}$$

In the next step we express the Dirac equation for the free electron, Eq. 4.12, as a simple set of two (2×2)–dimensional matrix equations (in a.u.):

$$\begin{aligned}(c^2 - E)\Psi^L \;+\; c(\hat{\boldsymbol{\sigma}} \cdot \hat{\mathbf{p}})\Psi^S \;=\; 0,\\ c(\hat{\boldsymbol{\sigma}} \cdot \hat{\mathbf{p}})\Psi^L \;-\; (c^2 + E)\Psi^S \;=\; 0.\end{aligned} \tag{4.18}$$

The small component can be obtained from the second expression of Eq. 4.18

$$\Psi^S \;=\; \frac{c(\hat{\boldsymbol{\sigma}} \cdot \hat{\mathbf{p}})}{(c^2 + E)}\Psi^L, \tag{4.19}$$

and inserted it into the first equation:

$$[(c^2 - E) + \frac{c^2(\hat{\boldsymbol{\sigma}} \cdot \hat{\mathbf{p}})(\hat{\boldsymbol{\sigma}} \cdot \hat{\mathbf{p}})}{(c^2 + E)})]\Psi^L \;=\; 0. \tag{4.20}$$

We make now the key approximation to approach the nonrelativistic framework: the nonrelativistic energy, ϵ, is positive and very small compared to c^2 (in a.u.):

$$E \;=\; c^2 \;+\; \epsilon \approx c^2. \tag{4.21}$$

After neglecting the energy contribution ϵ in the denominator, Eq. 4.20, we get

$$[-\epsilon + \frac{(\hat{\boldsymbol{\sigma}} \cdot \hat{\mathbf{p}})(\hat{\boldsymbol{\sigma}} \cdot \hat{\mathbf{p}})}{2}]\Psi^L \;=\; 0. \tag{4.22}$$

Utilizing the identity

$$(\hat{\boldsymbol{\sigma}} \cdot \hat{\mathbf{p}})(\hat{\boldsymbol{\sigma}} \cdot \hat{\mathbf{p}}) \;=\; \hat{p}^2, \tag{4.23}$$

we get a two–component equation for Ψ^L, which is in fact the Schrödinger equation, Section 3.1, for a free electron (in a.u.):

$$[-\epsilon + \frac{\hat{\mathbf{p}}^2}{2}]\Psi^L \;=\; 0. \tag{4.24}$$

Thus, the large component Ψ^L can be interpreted as the nonrelativistic limit ($c \to \infty$) of the four–component solution. Moreover, its two–component solutions

$$\Psi^L \;=\; c^\alpha \alpha \Psi^{L\alpha} + c^\beta \beta \Psi^{L\beta}, \tag{4.25}$$

where α and β are defined in Eq. 3.8, and are carrying information about the spin–orientation of a particle. In this way we have shown that the Dirac equation contains inherently the spin quantum number. This demonstration can also be carried out for a particle in an external field. In the Schrödinger description of the electronic structure the spin quantum number (see Section 3.1.2) must be added *ad hoc*. Note that since the kinetic energy operator, $\hat{\mathbf{p}}^2/2$, is mathematically equivalent, according to Eq. 4.23, to $(\hat{\boldsymbol{\sigma}} \cdot \hat{\mathbf{p}})^2/2$, it may be stated that the electron spin is actually present in the nonrelativistic case. Therefore, if the kinetic energy term is present in the form of $(\hat{\boldsymbol{\sigma}} \cdot \hat{\mathbf{p}})^2/2$ in the Schrödinger equation, than the electron spin is involved in the nonrelativistic case. This would have consequences only in the presence of a magnetic field.

Regarding the small component, Eq. 4.19, by employing the approximation of Eq. 4.21, we get (in a.u.)

$$\Psi^S \approx \frac{(\hat{\boldsymbol{\sigma}} \cdot \hat{\mathbf{p}})}{2c}\Psi^L. \tag{4.26}$$

Values of small component, Ψ^S, are $\frac{1}{c}$–times smaller (in a.u.) than those of large component, Ψ^L.

Negative energy solutions According to Eq. 4.5 solutions for a free particle are symmetric with respect to zero. They are of continuum type and energies span the range below $-mc^2$ and above mc^2 (or just $-c^2$ and c^2 in a.u.). The spectrum is thus not bounded from below and from above.

Negative energy solutions worried Dirac: *"One gets over the difficulty on the classical theory by arbitrarily excluding those solutions that have a negative E. One cannot do this in the quantum theory, since in general a perturbation will cause transitions from states with E positive to states with E negative."* [4].

Negative solutions seemed to be problematic, since it was assumed that a particle has a positive energy. Dirac introduced that the vacuum is the many–body quantum state in which all the negative–energy electron eigenstates are occupied. Negative states are occupied with particles (*i.e.* they form the physical vacuum), so that electrons of positive energy do not spontaneously fall into negative states with the release of energy. This description of the vacuum as a "sea" of electrons is called the Dirac sea. Transitions down into the "Dirac sea" are forbidden by the Pauli exclusion principle. Any additional electron therefore would be forced to occupy a positive–energy eigenstate. However, there is no need to assume infinite number of particles in the vacuum since the modern relativistic theory describes both particles and antiparticles in a way that only the total charge is conserved, but not the total number of all particles and antiparticles.

Dirac stated that if energy higher than $2c^2$ a.u. is applied on an "electron" in a negative energy state this electron could jump into a positive energy state where it could be observed as an ordinary electron. The remaining "hole", *i.e.* positively charged electron (positron), in the negative energy state could also be observed. If an electron with positive energy eventually falls into this "hole", both would disappear with releasing of the energy higher that $2c^2$ a.u. Dirac's relativistic theory predicted the existence of the positron, the particle of the weight of an electron but with the positive charge. This brought a great success for his theory when this particle was discovered in the cosmic radiation by Carl Anderson in 1932 [114].

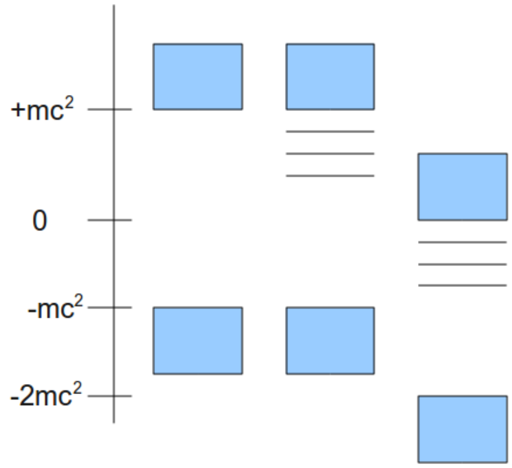

Fig. 4.1. Scheme of the Dirac energy spectrum for a free particle (left) and for an electron in the nuclear field (centre). On the right hand side of the figure there is an energy spectrum with the scale shifted with respect to the zero energy reference, Eqs. 4.34,4.35.

4.3.2 Solution of the Dirac equation for the hydrogen–like atom

The explicit solution of the Dirac equation for a hydrogen–like atom (in a.u),

$$\hat{h}_D = \beta c^2 + c\hat{\boldsymbol{\alpha}} \cdot \hat{\mathbf{p}} + \hat{V}\mathbf{I}, \tag{4.27}$$

was first published by Darwin [115] in 1928. He honoured Dirac's outstanding works, Refs. [4, 27], with words *"...one of the great papers in physics in this century"*. Excellent modern presentations can be found in later monographs, for instance Bethe and Salpeter [116], Moss [117], Rose [118] or Messiah [119].

Finding four–component solutions, Eq. 4.13, of the Dirac equation is similar to that for solving the Schrödinger analogue, Section 3.1. Eigenfunctions are written as products of radial and angular terms what leads to the separation into individual angular and radial equations (for comparison see Eq. 3.3).

The eigenspectrum of the Dirac hydrogen–like operator, Eq. 4.27 (see Fig. 4.1), has three separated parts: i) the continuum of negative energy states from $-\infty$ to $-mc^2$ ($-c^2$ in a.u.), ii) another continuum of positive energy states from $+mc^2$ ($+c^2$ in a.u.) to $+\infty$, and iii) a discrete spectrum of states between both continuum, leaned towards the bottom of the positive continuum. In the case of the Dirac free particle (Eq. 4.12), the part of the energy spectrum iii) is empty.

Dirac quantum numbers There are four quantum numbers required to specify the state of a Dirac hydrogen–like atom. These are similar, but not exactly the same as those of the Schrödinger

one–electron atom, Section 3.1, where only three parameters are needed to determine the state of the electron. The Dirac quantum numbers are:
i) The principal quantum number, n, which can have values of $1, 2, 3....$
ii) The azimuthal quantum number, l, with values of $0, 1, 2, ..., (n-1)$. This parameter is usually denoted by the alphabetical symbols s, p, d, f... However, contrary to the Schrödinger description of the atom, the l number does not represent the orbital angular momentum.
iii) The angular quantum number, j. It can carry at most two values, $|l \pm 1/2|$. This parameter is written as a subscript of the alphabetical symbol of the azimuthal quantum number l.
iv) The last parameter is the magnetic quantum number, m, taking all half–odd integer values from $-j$ to $+j$.

Regarding pictures of the electron distribution of the Dirac atom, they were published shortly after the Dirac's paper. In 1931 White [120] presented, as continuations to his famous electron–cloud pictures of a nonrelativistic Schrödinger atom, the electron–cloud illustrations of the corresponding Dirac atom. For more recent pictures of spinors of the Dirac hydrogen–like atom the reader is referred to works like that of Szabo [121].

Shapes of four–component Dirac electronic wave functions are determined by quantum numbers j and m. Orbitals with identical values of j and m have the same shape, or identical angular distribution. The $s_{1/2}$ spinor is spherically symmetrical like the $p_{1/2}$ one. The pair of $d_{3/2}$ spinors has the same angular distribution as the pair of $p_{3/2}$. Furthermore, the $p_{3/2,1/2}$ $(j = 3/2, m = 1/2)$ resembles a "dog–bone" rather than two touching ellipsoids. Some chemists from the "old school" might be a little upset to learn that nonrelativistic perpendicular p orbitals are no longer degenerate and look like a sphere $p_{1/2}$, a "doughnut" $p_{3/2,3/2}$, and a "dog–bone" $p_{3/2,1/2}$. All Dirac spinors have electron densities symmetrical about the z–axis and all have a plane of symmetry perpendicular to the z–axis. However, *none* have nodal planes [121,122]. The mathematical reason for the absence of nodes is due to the fact that all four components of the wave function Ψ (Eq. 4.13) never have nodes all in the same place, because the probability density, Eq. 4.14, is never zero. From a physical point of view this feature is a natural consequence of the correct handling of the angular dependence for an electron with spin. Schrödinger angular distributions with nodes are caused by a nonexistent spin–less electron. Likewise no nodes can be observed already in the simplest case of an electron in a one–dimensional box [116], because whenever the large component has a node, the small component remains nonzero. Thus, the answer to a would–be question of a student - *'How does a p electron pass from one lobe to another?'* - is that the physically more general Dirac theory is without nodes. Note, that the correct nodeless results would be obtained already through the Pauli two–component theory. And it is even possible to construct Schrödinger–type orbitals from certain linear combination of the Dirac four–spinors.

For the determination of nonrelativistic spectroscopic states of chemical systems one needs eigenvalues of the angular and spin operators. However, the usual angular momentum operator of the nonrelativistic theory, Section 3.1.1, does not commute with the Dirac Hamiltonian. It is the operator, called the total angular momentum for a relativistic particle

$$\hat{\mathbf{j}} = \hat{\mathbf{l}} + \frac{1}{2}\hat{\mathbf{\Sigma}}, \tag{4.28}$$

which does. It has the spin–component containing the Pauli matrices, Eq. 3.7, of the form:

$$\hat{\mathbf{\Sigma}} = \begin{pmatrix} \hat{\boldsymbol{\sigma}} & \mathbf{0} \\ \mathbf{0} & \hat{\boldsymbol{\sigma}} \end{pmatrix}. \tag{4.29}$$

Components of the operator of Eq. 4.28 satisfy all commutation rules for the angular momentum operators:

$$[\hat{j}_p, \hat{j}_q] = i\hat{j}_r, \tag{4.30}$$

where (p, q, r) labels correspond to cyclic permutations of (x, y, z) components. Analogous to the relations of the nonrelativistic Hamiltonian, and the angular operators, the square of the total angular momentum and the z–component of the $\hat{\mathbf{j}}$–operator commutes with the Dirac Hamiltonian, Eq. 4.27 :

$$[\hat{h}_D, \hat{j}_z] = 0\,, [\hat{h}_D, \hat{j}^2] = 0. \tag{4.31}$$

As for the nonrelativistic counterpart, $\hat{\mathbf{l}}^2$, there is a similar eigen equation for the $\hat{\mathbf{j}}^2$:

$$\hat{\mathbf{j}}^2 Y_4(\vartheta, \varphi) = j(j+1) Y_4(\vartheta, \varphi), \tag{4.32}$$

where the eigenfunction $Y_4(\vartheta, \varphi)$ is the four–component spinor function depending on spherical angles ϑ and φ.

The Dirac equation is rigorous only for a one particle system since it obeys all the requirements of the special relativity and quantum mechanics. With the hydrogen like atom as the analytically solvable model serves as the conceptual background for relativistic theories of many–electron systems.

4.3.3 Finite nucleus

In the nonrelativistic theory the electron–nuclei interaction is usually described by the simple Coulomb interaction, $\hat{V} = -\frac{Z}{r}$ (in a.u.), where r is the distance of the electron from the *point* nucleus with the charge Z. Nonrelativistic orbitals have zero amplitude at the nuclei (centre) except for s–orbitals involving small exponential cusp of the form $\sim exp(-\alpha r)$.

In relativistic calculations, however, the $s_{1/2}$ and $p_{1/2}$ spinors have a weak singularity at the nucleus [123]. Thus it is customary to employ a physically more realistic finite–nucleus model which also improves the basis set convergence [124]. Perhaps the most popular nucleus model is based on Gaussian distribution, as was proposed by Visser *et al.* [125]. The nuclear distribution, ρ, and the potential, $\hat{V}$, are given by (in a.u.)

$$\rho = Z(\frac{\lambda}{\pi})^{\frac{3}{2}} exp(-\lambda r^2)\,, \qquad V = -\frac{Z}{r} erf(\sqrt{\lambda} r), \tag{4.33}$$

where $erf(x)$ is the error function. The nuclear exponent λ is chosen in such a way that the nuclear model has the same root–mean–square radius as the experimental value for the nucleus. Recommended values for nuclear parameters were published by Visscher and Dyall [126].

The choice of the nuclear model has negligible effect in cases where only valence spinors are important for chemical properties. However, there are cases of properties where spinors close to the nuclei are important and the nuclear model may have large influence, and one should avoid unphysical point nucleus. Note that the computational implementation of nuclear attraction integrals is easy as these are only modified two–electron integrals expressed in a Gaussian basis set.

4.4 Four component relativistic quantum chemistry

The relativistic theory of chemical systems appears to be more challenging with respect to established nonrelativistic methods based on the Schrödinger equation. Corresponding four–component computational methods are not as good developed as their nonrelativistic counterparts. The ”reward” for the development of more complex relativistic apparatus is its generality, which fully recovers the nonrelativistic realm in the limit of $c \to \infty$, providing in this way the test of the correctness of the implementation. For this reason it is worth to have both nonrelativistic and relativistic energy scales aligned.

The rest energy of the free electron, Eq. 4.21, mc^2, is equal to 0.511 MeV. This value, which is much higher that the binding energy of the hydrogen atom - 13.6 eV, is defined as zero in the nonrelativistic framework. Accordingly, the zero point in the relativistic energy scale is obtained by subtracting the free electron rest energy. At the operator level this is achieved by subtracting the diagonal 4×4 matrix from the β term, Eq. 4.10, and using the modified β' instead of in the Dirac Hamiltonian

$$\beta' = \begin{bmatrix} \mathbf{0} & \mathbf{0} \\ \mathbf{0} & -2\mathbf{I} \end{bmatrix} . \tag{4.34}$$

Now we can write the Dirac equation for one electron in a molecular field as

$$\begin{bmatrix} \hat{V} & c\,(\hat{\boldsymbol{\sigma}} \cdot \hat{\mathbf{p}}) \\ c\,(\hat{\boldsymbol{\sigma}} \cdot \hat{\mathbf{p}}) & \hat{V} - 2c^2 \end{bmatrix} \begin{bmatrix} \psi^L \\ \psi^S \end{bmatrix} = \begin{bmatrix} \psi^L \\ \psi^S \end{bmatrix} E, \tag{4.35}$$

where $\hat{V}$ represents the electrostatic interaction of the electron with the clamped nuclei. Here we wish to shed more light on the distinction between electron and positron solutions of the Dirac equation, as it is not often precisely clarified in the literature. All solutions of the Dirac equation, *i.e.* both of positive and negative energies, are truly electronic because the introduction of potential by the principle of minimal electromagnetic coupling [127] requires specification of charge [128]. For chemical purposes one sets the charge of the electron $e = -1$ a.u. and not the charge of the positron, $e = +1$ a.u. This assignment was used by Dirac himself [129]. The observable positron solutions of the same potential can be obtained by choosing by the charge conjugation of the negative–energy solutions of the electronic problem, or are calculated by explicitly choosing the positron charge in the potential.

4.4.1 The relativistic electron–electron interaction

The Dirac equation is valid only for the one–electron system. To extend it for many–electron systems the proper relativistic electron–electron interaction is to be taken into account. The straightforward approach is to augment the one–electron Dirac operator with a two–electron interaction term. When we consider the Coulomb interaction, what is the simplest case, this term is not Lorentz invariant. Although an invariant interaction potential can be derived from quantum electrodynamics (QED), the fully Lorentz invariant form of the electron–electron interaction term can not be written in a closed form [123]. Therefore, in practise one prefers truncation to the so called Breit operator [130],

$$\hat{g}_{ij}^{Breit} \;=\; -\frac{1}{2r_{ij}}\Big[\hat{\boldsymbol{\alpha}}_i \cdot \hat{\boldsymbol{\alpha}}_j \;+\; \frac{(\hat{\boldsymbol{\alpha}}_i \cdot \mathbf{r}_{ij})(\hat{\boldsymbol{\alpha}}_j \cdot \mathbf{r}_{ij})}{r_{ij}^2}\Big], \tag{4.36}$$

which is added to the Coulomb interaction term, $\frac{1}{r_{ij}}$. The Breit operator accounts for magnetic interactions and retardation effects up to the order of $\frac{1}{c^2}$.

The first term in brackets on the right–hand side of Eq. 4.36 is the Gaunt interaction term [131], often used as an approximation of the Breit operator since it includes the largest portion of the full Breit form. The Gaunt operator contains spin–spin, orbit–orbit and spin–orbit contributions, while the second term in Eq. 4.36 is the gauge interaction representing retardation effects induced by the finite speed of light. Though the Gaunt term itself is not gauge invariant, it is easy to implement within two–electron integral generating codes.

4.4.2 The Dirac–Coulomb–Breit/Gaunt Hamiltonian

The Dirac–Coulomb–Breit/Gaunt (DCB/DCG) operator represents nowadays the most rigorous representation for many–electron relativistic effects. It is formed by selecting the Dirac operator in a molecular field as the one–electron operator and the Coulomb term, possibly extended by the Gaunt or the full Breit two–electron term, Eq. 4.36. Keeping the lowest order Coulomb term is the often used approximation of the electron–electron interaction because the two–electron magnetic interaction terms are typically small.

For the purpose of relativistic quantum chemical calculations one works within the Born–Oppenheimer approximation [54] as in the nonrelativistic framework, Section 3.2. This approximation introduces very small errors in the relativistic quantum mechanical treatment, but corrections can be applied in the same manner as in the nonrelativistic theory [132].

The aim is to solve the molecular Dirac equation for n electrons localized in the static field of N nuclei. The Dirac–Coulomb–Breit/Gaunt Hamiltonian for this general system is

$$\hat{H}_{DCB/DCG} \;=\; \sum_{i}^{n} \hat{h}_D(i) \;+\; \frac{1}{2}\sum_{i \neq j}^{n} \hat{g}_{ij}^{Breit/Gaunt} \;+\; \sum_{I<J}^{N} \frac{Z_I Z_J}{R_{IJ}}. \tag{4.37}$$

The one–particle operator, $\hat{h}_D(i)$, is identical with the operator in Eq. 4.35 where the external potential is created by static atomic nuclei. Note that the classical potential of the electron in the point nuclear field is usually replaced by the finite nuclear distribution, Section 4.3.3.

In comparison to the nonrelativistic many–electron Hamiltonian, Eq. 3.11, it is the one–electron operator that makes the difference which is sometimes accompanied with the $\hat{g}_{ij}$ electron–electron interaction term in its relativistically specified form, see Section 4.4.1.

Brown and Ravenhall problem. A discussion arose about the validity of the DCB/DCG operator. The one–electron Dirac equation is not bounded from below and the same holds for the many–electron case. Brown and Ravenhall [133] argued that one can not find stable stationary states for this Hamiltonian (what is called as the "Brown–Ravenhall disease"). This is due to the fact that when the electron–electron interaction is treated as a perturbation, one can construct an infinite number of states for electrons as well as for positrons, causing final states to be completely delocalized. For the case of a two–electron system (like the helium atom) this can be demonstrated as follows: Let us assume a double excitation from an orbital, where one electron ends in the negative energy continuum and the other lands in the positive energy continuum. The sum of their orbital energies is the same (or very close to) as the initial unperturbed energy. Theoretically, when the Coulomb electron–electron interaction is turned on, what would happen is transition to these doubly excited states and subsequent decay of former two–electron bound state into the continuum. However, the real helium atom does not disintegrate into electrons in the positive and negative continuum bands. As a remedy Brown and Ravenhall suggested to restrict the Hamiltonian only for positive energy states by applying projection operators. Once negative energy ("positron") solutions are abandoned, the corresponding theory becomes what is sometimes called as the four–component theory "for electrons only", or the *no pair* approach. However, later it has been found that for practical four–component calculations it is sufficient to have a proper basis set (see Section 4.4.6) and keep only positive energy solutions [134].

4.4.3 The Dirac–Hartree–Fock method

The relativistic analogue of the Hartree–Fock self-consistent field method (see Section 3.2.1), the Dirac–Fock–Breit method, was first formulated by Bertha Swirles [6] in 1935. The story goes that suggestion came to her by Douglas R. Hartree, who is associated with the Hartree–Fock theory [57, 58], when they were waiting at the London train station [135].

The resulting theory has been implemented first to atoms [7]. Molecular closed–shell formalism where four–component spinors were used as basis functions were proposed by Malli and Oreg [136] in 1975. Later more flexible basis sets were employed for both components coupled by the kinetic balance condition [137–139], see Section 4.4.6.

Both Hartree–Fock and Dirac–Hartree–Fock methods are independent particle models where each electron "feels" the field of nuclei and the average field of other electrons. The derivation of Dirac–Hartree–Fock equations is the same as in the nonrelativistic framework. Shortly, one seeks the wave function Φ_0, which makes the energy functional (for comparison see Eq. 3.18), stationary

$$E_{DHF} \;=\; \frac{\langle\Phi_0|\hat{H}_{DCB/DCG}|\Phi_0\rangle}{\langle\Phi_0|\Phi_0\rangle}. \tag{4.38}$$

The Φ_0 wave function is the antisymmetrized product (the Slater determinant, Eq. 3.12) of relativistic one–particle functions, in this case built of four–component spinors, Eq. 4.13. Here we will label the $\phi(i)$ as the four–component spinor representation of the one–electron state. The expectation value of the energy can be written as

$$E_{DHF} \;=\; \sum_{i=1}^{N_{occ}}\langle\phi_i|\hat{h}_D|\phi_i\rangle \;+\; \frac{1}{2}\sum_{i,j}^{N_{occ}}(\langle\phi_i\phi_j|\hat{g}_{ij}|\phi_i\phi_j\rangle \;-\; \langle\phi_i\phi_j|\hat{g}_{ij}|\phi_j\phi_i\rangle). \tag{4.39}$$

The Dirac–Fock operator has the same structure as its nonrelativistic analogue, Eq.3.20:

$$\hat{f}_{DHF}\phi(i) \;=\; (\hat{h}_D + \hat{u}_{DHF})\phi(i) \;=\; \epsilon_i\phi(i), \tag{4.40}$$

where the Coulomb and exchange operators involved in the $\hat{u}_{DHF}$ term depend on four–spinors, and are determined in a self–consistent manner.

Since we are seeking electronic states solutions, orthogonal spinors for the Fock operator, Eq. 4.40, must be taken from the *positive* part of the spectrum. And as we do not allow electrons to enter negative (”positron”) states, the four–component energy operator remains bounded from below (also thanks to the kinetic balance condition, see Section 4.4.6), and clear separation between negative and positive part of the energy spectrum is retained. The so called Brown–Ravenhall problem, Section 4.4.2, is not relevant for Dirac–Hartree–Fock calculations, although this so called continuum dissolution was a discussed topic in the early eighties.

For the single determinant open–shell system one may employ, for instance, the average configurations formalism [140, 141]. Available is also the four–component multi–configuration SCF version [142, 143], see also Ref. [144].

Solutions of the DHF–equations couple one-electron spin s and orbital l angular momenta through the j–j or ω–ω coupling. Atomic j–j split shells are as follows: $s^{(2)}_{1/2}$, $p^{(2)}_{1/2}$, $p^{(4)}_{3/2}$, $d^{(4)}_{3/2}$, $d^{(6)}_{5/2}$, $f^{(6)}_{5/2}$, $f^{(8)}_{7/2}$ *etc.*, for comparison see Figs. 2.3 and 2.4. Example of molecular ω–ω coupled shells ($\sigma^{(2)}_{1/2}$, $\pi^{(2)}_{1/2}$, $\pi^{(2)}_{3/2}$) is given in Fig. 2.5.

Relativistic effects (see Section 2), which are observable already in solutions of the hydrogen Dirac equation, Section 4.3.2, are for chemical systems fully manifested within the DHF method. Besides the spin–orbit splitting of $l > 0$ shells these can be briefly summarized as i) contraction and stabilization of s and p shells which leads to the strengthening of the chemical bond, and ii) relativistic expansion of d and f spinors causing the weakening of the bond.

4.4.4 Symmetry aspects

Computational costs of calculating the energy and properties of any chemical system can be greatly reduced by considering the symmetry of the molecule in question.

Kramers symmetry Since we are in the relativistic domain, the spin–symmetry, Section 3.1.2, can not be used for this type of relativistic operator. Note, however, that by removing spin–orbit interaction terms from the relativistic Hamiltonian, *i.e.* keeping the spin–free form, one can employ the spin–symmetry and single–point group symmetry.

The relativistic replacement of the spin–symmetry is called the time reversal symmetry [119], and is represented by the anti–unitary time–reversal operator which has the form

$$\hat{K} \;=\; -i\begin{pmatrix} \hat{\sigma}_y & 0 \\ 0 & \hat{\sigma}_y \end{pmatrix}\hat{K}_0, \tag{4.41}$$

where $\hat{K}_0$ is the complex conjugation operator. The time–reversal operator commutes, in the absence of the magnetic field, with four–component energy operator, Eqs. 4.37 and 4.40.

Due to the time–reversal symmetry Dirac–Hartree–Fock solutions come out in degenerate pairs, known as Kramers pairs [145, 146]. This is the consequence of the Kramers theorem [145] claiming that energy levels of a system with half–integer spin are at least doubly degenerate, and any degeneracy is even–fold. The theorem does not hold in the presence of magnetic field. Relation between two degenerate spinors, representing one–electron states, ϕ and $\bar{\phi}$, is

$$\hat{K}(a\phi) \;=\; a^{*}\bar{\phi}, \;\; \hat{K}\bar{\phi} \;=\; -\phi, \tag{4.42}$$

where a is an arbitrary complex number.

Double–group symmetry In the nonrelativistic theory one deals with point group symmetry operations acting only on spatial parts of the chemical system. However, with the Dirac Hamiltonian invariant under symmetry operations, these must be a product of spatial and spin operations, as this four–component operator is coupling both. Therefore, a more general point group comprising both spatial and spin coordinates has to be introduced. To found the ground for the new group theory, rotation by 2π is treated not as an identity operation but as a symmetry operation. Any ordinary rotation group is expanded by taking the product of this new operation. The number of symmetry operations is thus doubled and these groups are called double groups. Besides the irreducible representations (irreps) used in the nonrelativistic theory, called boson irreps, there are also irreps that describe one–electron functions of the Dirac–Coulomb Hamiltonian, known as fermion irreps. The number of fermion irreps is lower than the number of boson irreps. For example, a molecule of the D_{2h} symmetry has eight boson irreps but only two two–dimensional fermion irreps, $E_{1/2g}$ and $E_{1/2u}$. Likewise the symmetry group of water, C_{2v}, has four different (one–dimensional) boson irreps, but only one (two–dimensional) fermion irrep, $E_{1/2}$. This means that fewer two–electron integrals are zero due to the double group symmetry. For that reason the rigorous four–component symmetry apparatus has to be applied appropriately. Let us consider a molecule that has only light elements and its energy is computed by using the Dirac–Coulomb Hamiltonian in the double group symmetry. Calculations are much more demanding due to many two–electron integrals which need to be computed, while most of them are nearly zero. In this case it is sufficient to resort to one–component quantum chemical methods with adapted single point group symmetry.

The theory for the double group symmetry was first presented by Bethe [147]. There are several books [148, 149] of this subject available to the reader, together with many works on the usage of double groups for constructing relativistic orbitals like Refs. [150–157]. Peng *et al.* [158] published recently scheme for constructing Kramers paired double group symmetry functions.

4.4.5 Classification of relativistic electronic states of atoms and molecules

For atomic systems one takes into consideration also the so called j–j coupling convention as the Dirac Hamiltonian commutes with the operator of the total angular momentum, Eq. 4.31. One adds the third number, J, representing the size of the total angular momentum, to the spin (S) and angular (L) quantum numbers. For example, the ground state of the thallium atom is $\mathrm{X}^2\mathrm{P}_{1/2}$, meaning that the valence $6p^{(1)}$ electron occupies the $6p_{1/2}$ ($l = 1, s = 1/2, j = 1/2$) relativistic spinor. The lowest excited state is $^2\mathrm{P}_{3/2}$ ($l = 1, s = 1/2, j = 3/2$). Note that the $^2\mathrm{P}_{1/2}$ – $^2\mathrm{P}_{3/2}$ spin–orbit interaction splitting serves as a testing ground for a variety of quasirelativistic methods, see Ref. [159].

Another case is the lead atom with the valence configuration of $6p^{(2)}$. While in the spin–free framework we have X^{3}P, ^{1}D, and ^{1}S states, the spin–orbit coupling gives rise of more states (in ascending order): X^{3}P$_0$, ^{3}P$_1$, ^{3}P$_2$, ^{1}D$_2$, and ^{1}S$_0$.

For diatomic molecules one employs the so called ω–ω coupling where the total angular momentum is

$$\Omega \;=\; |\Lambda + S|. \tag{4.43}$$

The Ω number is assigned by the group theory as a direct product between the irreducible representation of the spin and the irreducible representation of the total angular momentum. First, let us have a look at the correspondence between nonrelativistic and relativistic symmetry states. In the $\omega - \omega$ notation the Σ^+ irrep is designed as 0^+, Σ^- as 0^-, and Π, Δ, Φ... as 1, 2, 3... The $E_{1/2}$ double group representation is labelled as $\frac{1}{2}$, the $E_{3/2}$ as one $\frac{3}{2}$ in the $\omega - \omega$ notation. As an example consider a $^3\Sigma^-$ state of a diatomic. The spatial symmetry (angular momentum) is Σ^-, the triplet spin–symmetry (S=1) spans Σ^- and Π irreps. The direct product of the spin and spatial symmetries is $\Sigma^-(spin) \otimes \Sigma^-(spatial) = \Sigma^+$ and $\Pi(spin) \otimes \Sigma^-(spatial) = \Pi$. So the spin–orbit interaction splits a $^3\Sigma^-$ state into 0^+ (Σ^+) and 1 (Π) states.

In the $^2\Pi$ nonrelativistic state the doublet spin corresponds to $E_{1/2}$ double group representation. Multiplying the spin and spatial irreducible representations, $E_{1/2}(spin) \otimes \Pi(spatial) = E_{1/2} + E_{3/2}$, gives $\Omega = \frac{1}{2}$ and $\frac{3}{2}$ electronic states, respectively.

And in the last example, shortly, the $^3\Pi$ state of some diatomic molecule leads to these ω–ω split states (in ascending order): 0^+, 0^-, 1, 2. The reader can found more in Ref. [160].

4.4.6 Four–component relativistic basis set functions

A common way of solving the molecular Dirac–Fock problem, Section 4.4.3, lies in the expansion of molecular spinors in a set of analytic basis set functions. This is "borrowed" from the nonrelativistic realm where the basis set expansion of the HF–SCF one–electron wave functions, Eq. 3.24, was introduced by Roothaan [63].

In the relativistic domain the one–particle four–spinors are expanded in a separate scalar basis functions set for large (L) and for small (S) components:

$$\phi_p = \begin{pmatrix} \phi_p^{L\alpha} \\ \phi_p^{L\beta} \\ \phi_p^{S\alpha} \\ \phi_p^{S\beta} \end{pmatrix} = \begin{pmatrix} \sum_i \chi_i^L c_{ip}^{L\alpha} \\ \sum_i \chi_i^L c_{ip}^{L\beta} \\ \sum_i \chi_i^S c_{ip}^{S\alpha} \\ \sum_i \chi_i^S c_{ip}^{S\beta} \end{pmatrix}. \tag{4.44}$$

The four sets of coefficients, $\{c^{L\alpha}\}$, $\{c^{L\beta}\}$, $\{c^{S\alpha}\}$, and $\{c^{S\beta}\}$ are in general complex. The upper (L) and lower (S) components of a four–component molecular spinor are expanded as a linear combination of primitive Cartesian Gaussian type of orbitals,

$$\chi_i^L \;=\; N_i^L x^{k_i^L} y^{m_i^L} z^{o_i^L} exp(-\alpha_i^L r^2) \;\;,\;\; \chi_i^S \;=\; N_i^S x^{k_i^S} y^{m_i^S} z^{o_i^S} exp(-\alpha_i^S r^2), \tag{4.45}$$

where N is a normalization constant and k, m, o are parameters whose sum gives the angular momentum of the atomic orbital.

The large $\{\chi^L\}$ and small $\{\chi^S\}$ component basis functions are related through the so called *kinetic balance condition* [137–139]:

$$\{\chi^S\} \;=\; -\frac{1}{2c}(\hat{\boldsymbol{\sigma}} \cdot \hat{\mathbf{p}})\{\chi^L\}. \tag{4.46}$$

This condition is nowadays, starting from a given (decontracted) large component set, χ^L, used for constructing the relativistic small component basis set. Note that Eq. 4.46 is derived in the same way as Eq. 4.26 with employing the shifted energy scale, Eqs. 4.34 and 4.35. In pioneering years of the relativistic electronic structure theory the negative energy continuum was sometimes considered to be "guilty" for the failure to get upper bounds of the total energy what was known as so called "variational collapse". However, this was caused by a poor basis set causing bad finite matrix representations of relativistic operators [139]. By employing the balanced basis the "unphysical positronic" solutions of the DHF method are easily identified according to their eigenvalues which are about (in absolute value) $2c^2$ a.u.

Thanks to the basis set expansion, Eq. 4.44, the Dirac–Hartree–Fock problem, Eq. 4.40, can be reformulated into the matrix representation (analogous with Eq. 3.26)

$$\mathbf{F}_{DHF}\mathbf{C} = \mathbf{SC}\epsilon, \tag{4.47}$$

which is suitable for an efficient computer implementation. Dyall and coworkers [161–165] are nowadays intensively developing basis sets for all–electron four–component relativistic calculations.

The small component depends on the operator $\hat{\boldsymbol{\sigma}} \cdot \hat{\mathbf{p}}$, acting as a partial derivative with respect to x, y, z coordinates. By applying Eq. 4.46 on large component of Eq. 4.45 with angular momentum l one obtains two small component functions with angular momentum $l-1$ and $l+1$. The kinetic balance prescription generates the small component basis set which is about two–times of the size of the corresponding large component basis set. This already indicates that solving a DHF problem can be quite expensive when compared to the nonrelativistic counterpart. For the construction of the two–electron Fock(–Dirac) matrix two–electron atomic integrals (over the Coulomb interaction operator) are sorted into three classes, $(LL|LL$, $(LL|SS)$, and $(SS|SS)$. Dyall and Fægri stated [25] that in addition to approximately equal number of $(LL|LL)$ integrals comparing to the nonrelativistic framework, the number of $(LL|SS)$ integrals is about 13 times larger than $(LL|LL)$ integrals and the number of $(SS|SS)$ integrals is approximately 39 times larger. The overall computational cost for a DHF calculation in an *uncontracted* basis set is about 53 times larger than in the corresponding nonrelativistic domain. However, the effect of $(SS|SS)$ integrals is often negligible and their number can be reduced substantially by adopting simple Coulombic correction [166]. In the nonrelativistic limit ($c \to \infty$) small component basis functions, χ^S, according to Eq. 4.46, disappear and one works with the large component basis set only.

4.5 Relativistic correlation methods

The starting point in four–component relativistic correlation methods is the Dirac–Coulomb–Breit/Gaunt Hamiltonian, Eq. 4.37, in the no–pair approximation, *i.e.*, neglecting positron–electron pair creation. Only electronic states are treated in relativistic correlation calculations.

By using Kramers unrestricted spinors which correspond to spinorbitals in the nonrelativistic theory, the second quantized form of the Hamiltonian can be expressed by Eq. 3.40. In the relativistic case the f_{pq} are matrix elements over the Fock–Dirac operator, Eq. 4.40. Regarding the two–electron integrals, the obvious step in correlated calculations is their transformation from atomic orbital basis to molecular orbitals (spinors) basis. Expression for two–electron integrals in the basis of the four–component Kramers unrestricted spinors, based on the expansion of Eq. 4.44, can be written as

$$\langle \phi_p \phi_q | \phi_r \phi_s \rangle \;=\; \sum_{X,Y} \sum_{\sigma,\gamma} \sum_{i,j,k,l} C_{ip}^{X\sigma *} C_{jq}^{Y\gamma *} C_{kr}^{X\sigma} C_{ls}^{Y\gamma} \langle \chi_i^X \chi_j^Y | \chi_k^X \chi_l^Y \rangle, \tag{4.48}$$

where X and Y run over large (L) and small (S) components, σ and γ over α and β components. The ϕ_p, ϕ_q... are four–spinors of arbitrary electronic states, either Kramers restricted or not, coming out of the Dirac–Hartree–Fock procedure, Section 4.4.3, and $\langle \chi_i^X \chi_j^Y | \chi_k^X \chi_l^Y \rangle$ are two–electron integrals over $(L/S)-$atomic basis functions, described by Eq. 4.45. Due to the presence of atomic basis functions over small component basis functions obtained by Eq. 4.46, the transformation of four–component spinors, Eq. 4.48, is usually computationally most expensive part of correlated relativistic calculations. Various speed–ups have been reported, like that of Abe *et al.* [167].

4.5.1 Second–order Kramers restricted MP2 method

The simplest and relatively tractable correlation correction to the Hartree–Fock theory is the second order Møller–Plesset (MP2) energy [168], given by the general expression for the nonrelativistic Hamiltonian

$$E^{(2)} \;=\; \frac{1}{4} \sum_{ij}^{N_{occ}} \sum_{ab}^{N_{virt}} \frac{|\langle ij \| ab \rangle^2|}{\epsilon_i + \epsilon_j - \epsilon_a - \epsilon_b} \,. \tag{4.49}$$

In connection with four–component relativistic methods we refer the implementation for the Kramers restricted closed–shell DHF wave function as was done by Lærdahl *et al.* [169]. Being in the relativistic domain, it employs the relation between degenerate Kramers partners, Eq. 4.42, connecting two–electron integrals with 'barred' and 'unbarred' spinors:

$$\begin{array}{ll} \langle ij \| ab \rangle^* = \langle \overline{i}\overline{j} \| \overline{a}\overline{b} \rangle, & \langle ij \| \overline{a}\overline{b} \rangle^* = \langle \overline{i}\overline{j} \| ab \rangle, \\ \langle i\overline{j} \| a\overline{b} \rangle^* = \langle \overline{i}j \| \overline{a}b \rangle, & \langle i\overline{j} \| \overline{a}b \rangle^* = \langle \overline{i}j \| a\overline{b} \rangle, \\ \langle ij \| \overline{a}b \rangle^* = -\langle \overline{i}\overline{j} \| a\overline{b} \rangle, & \langle ij \| a\overline{b} \rangle^* = -\langle \overline{i}\overline{j} \| \overline{a}b \rangle, \\ \langle i\overline{j} \| \overline{a}\overline{b} \rangle^* = -\langle \overline{i}j \| ab \rangle, & \langle i\overline{j} \| ab \rangle^* = -\langle \overline{i}j \| \overline{a}\overline{b} \rangle. \end{array} \tag{4.50}$$

Inserting these formulas into Eq. 4.49 and carrying out algebraic manipulations we get the simplified expression for the Kramers restricted MP2 correlation energy

$$\begin{aligned} E^{(2)} \;=\; \frac{1}{2} \sum_{ij}^{N_o/2} \sum_{ab}^{N_v/2} \frac{1}{\epsilon_i + \epsilon_j - \epsilon_a - \epsilon_b} & (|\langle ij \| ab \rangle|^2 + |\langle \overline{i}j \| ab \rangle|^2 + \\ & + |\langle i\overline{j} \| ab \rangle|^2 + |\langle ij \| \overline{a}b \rangle|^2 + |\langle ij \| a\overline{b} \rangle|^2 + \\ & + |\langle i\overline{j} \| a\overline{b} \rangle|^2 + |\langle ij \| \overline{a}\overline{b} \rangle|^2 + |\langle i\overline{j} \| \overline{a}b \rangle|^2). \end{aligned} \tag{4.51}$$

The formula Eq. 4.51 is implemented in a direct and parallelized way in the DIRAC [170] program suite. For that reason an average cost for calculation of the relativistic Kramers restricted MP2 energy is negligible with respect to the cost of the full four–index transformation, Eq. 4.48, which is necessary for higher level correlation methods, Section 4.5.2, even when employing the Kramers restriction.

By replacing the Kramers restricted spinors, Eq. 4.42, with pure spin restricted spinorbitals, Eq. 3.13, one can further reduce the MP2 expression to the form of the nonrelativistic limit. This is due to the spin–orthogonality, where densities $(p\overline{q}) = (p\alpha q\beta)$ with an odd numbers of bars (equivalent to β–spin) have no contributions. This leads to the simplified expression

$$
\begin{aligned}
E^{(2)} \; = \; & \frac{1}{2} \sum_{ij}^{N_o/2} \sum_{ab}^{N_v/2} \frac{1}{\epsilon_i + \epsilon_j - \epsilon_a - \epsilon_b} (|\langle ij \| ab \rangle|^2 + \\
& + |\langle ij \| \overline{a}\overline{b} \rangle|^2 + 2 |\langle i\overline{j} | a\overline{b} \rangle|^2),
\end{aligned}
\tag{4.52}
$$

and, after the spin–integration we finally get the familiar nonrelativistic expression:

$$
E^{(2)}_{NR} \; = \; \frac{1}{2} \sum_{ij}^{N_{occ}/2} \sum_{ab}^{N_{virt}/2} \frac{\langle ij|ab\rangle (2\langle ij|ab\rangle - \langle ij|ba\rangle)}{\epsilon_i + \epsilon_j - \epsilon_a - \epsilon_b}. \tag{4.53}
$$

To compare the effectivity of nonrelativistic and four–component relativistic MP2 calculations one has to take into consideration the transformation over small component basis functions as the main computational bottleneck, both at the Dirac–Hartree–Fock and the correlated MP2 levels, together with higher number of terms in Eq. 4.51 in comparison to Eq. 4.53. The relativistic complete active space second order perturbation theory with the four–component Dirac Hamiltonian has been reported by Abe *et al.* [171].

4.5.2 Relativistic Coupled Cluster and Configuration Interaction methods

The Kramers unrestricted Coupled Cluster method with singles, doubles and noniterative connected triples CCSD(T), applicable for a wide scale of atomic and molecular systems, was implemented by Visscher and coauthors [172]. Authors utilized the spinorbital form of the CC equations (see Section 3.2.5) in the framework of the effectively implemented double–group symmetry. Parallelization of the code was carried out by Pernpointer and Visscher [173]. The Kramers restricted CC version was also reported [174], but this program is much less used.

There is another group of relativistic CC methods based on the Fock–space Kramers unrestricted CC expansion, which give a variety of excited states, see Refs. [175–179].

Relativistic Kramers restricted CI methods are discussed in Refs. [180–183]. Note, that the comprehensive theory on the generalized Kramers restriction of spinors applicable for open–shell systems was published by Fleig [184].

4.6 Transformations to two–component Hamiltonians

Four–component Dirac–based theories are connecting ”positron–like” and ”electron–like” degrees of freedom. In addition, four–component description of the shell structure is always associated with small component basis functions, as mentioned in Section 4.4.6, what increase computational time. Without the coupling between the states with negative energy (”positrons”) and the states of positive energy (”electrons”) one would have a possibility to focus on the latter and work solely with the electronic two–component wave function. A high computational cost of four–component methods is the stimulus towards the development of less demanding two–component Hamiltonians dealing with electronic states only, and without the need of small–component basis functions. Methodologies for decoupling charge conjugated degrees of freedom leads to the appearance of a variety of two–component Hamiltonians accurate to various orders of some expansion parameters.

The following attributes are required for approximate relativistic Hamiltonians: i) They should be accurate enough to give close enough results to corresponding four–component operators. ii) They are to be well balanced for treating chemical systems containing a wide variety of atoms, *i.e.* both heavy and light. iii) Variational stability together with effectiveness to apply them to moderate and large molecules containing heavy elements.

For two–component methods which include spin–orbit coupling at the orbital level formation the Kramers restriction and the double–group symmetry, Section 4.4.4, is applicable. Hence one can utilize the very same (four–)spinors based correlation apparatus, like MP2, Section 4.5.1, CI or CC methods, Section 4.5.2. Let us stress that the main computational saving is due to abandoning small component basis functions, both at the Hartree–Fock level and at the transformation level, Eq. 4.48, what makes them attractive for ’everyday’ relativistic calculations.

Two–component methods can be divided into all–electron and pseudo–potential methods. We focus here on the former group, regarding the latter, we refer the reader to the literature like Ref. [185–189].

In subsequent section we present two known approximate decoupling schemes, the Foldy–Wouthuysen transformation and the Douglas–Kroll transformation. Afterwards we demonstrate how to perform the decoupling transformation up to the infinite order.

4.6.1 Foldy–Wouthuysen transformation

The idea of Foldy and Wouthuysen (FW) [190] was to separate the electronic and positronic solutions of the Dirac equation by the Van Vleck type unitary decoupling transformation of the Dirac Hamiltonian in the form

$$\hat{H}'_{2comp} = U\hat{H}_{4comp}U^{\dagger}. \tag{4.54}$$

The Foldy-Wouthuysen transformation can be specified in a number of different forms. The most common is the exponential form. Moreover, it can be also expressed as a product of a series of unitary transformations, $U = ...U_2U_1U_0$.

For one particle in an external potential $\hat{V}_{ext}$ and within the single transformation, $U = U_0 = exp(iS)$ one gets, after applying the Taylor expansion in the fine structure constant 1/c, the following one–electron terms:

$$\hat{h}^{BP} = (mc^2 + \hat{V}_{ext} + \frac{\hat{p}^2}{2m}) - \frac{\hat{p}^4}{8m^3c^2} + \frac{1}{8m^2c^2}(\hat{p}^2\hat{V}_{ext}) + \frac{1}{4m^2c^2}\hat{\boldsymbol{\sigma}}(\boldsymbol{\nabla}\hat{V}_{ext} \times \hat{\boldsymbol{p}}) + ... \tag{4.55}$$

The definition of S in the exponential above, $U_0 = exp\big(\beta\frac{\boldsymbol{\alpha p}}{p}\omega(p)\big)$ with a yet unknown parameter $\omega(p)$, as used by Foldy and Wouthuysen [190] in their original work is described in the literature, see Ref. [15, 26]. It is the mandatory starting point for all decoupling schemes employing unitary transformations of the Dirac Hamiltonian. The first terms in parenthesis in Eq. 4.55 represent the usual nonrelativistic Hamiltonian, then the second one is the so called mass–velocity term, the third is called the Darwin term and the fourth operator describes the spin–orbit interaction. It can be analytically proved that the scalar mass–velocity and Darwin terms are unbounded from below [15]. Carrying out the FW transformation on the entire Dirac–Coulomb–Breit Hamiltonian, Eq. 4.37, one obtains the full two–component Breit–Pauli (BP) operator, which in short notation has the form

$$\hat{H}^{BP} = \sum_i \hat{h}^{BP}(i) + \sum_{i<j} \hat{g}_{ij}^{BP}. \tag{4.56}$$

The transformed electron–electron interaction operator, $\hat{g}_{ij}^{BP}$ contains the Coulomb, spin–orbit and also other interaction terms, like spin–spin and orbit–orbit terms along with numerous high order terms.

The main disadvantage of the resulting Breit–Pauli Hamiltonian, also known as the first order relativistic Hamiltonian, is that its terms are highly singular and variationally unstable. Therefore this operator is suitable to be used in the first order perturbation theory.

4.6.2 Douglas–Kroll transformation

Douglas and Kroll (DK) pointed out that the FW transformation in an external field yields highly singular operator which is not suitable for practical calculations. Their approach decouples the large and small components of the Dirac four–spinors in the presence of an external potential through successive unitary transformations. The DK transformation is adopting the external potential, $\hat{V}_{ext}$, as an expansion parameter rather than the speed of light, c, in the FW transformation.

The very first step in the DK transformation is the free–particle FW transformation of the Dirac Hamiltonian with the external potential, Eq. 4.27, in the momentum space. Such a term is often referred as the first order DK Hamiltonian, but is unsuitable for practical computations. The DK–proposed operator is of the type

$$\hat{U}_n \; = \; (1 + W_n^2)^{1/2} + W_n, \tag{4.57}$$

which is unitary if W_n is anti–Hermitian. We shall not go into details of the derivation, but rather give a final form of the DK–transformed operator. The two–component one–electron Hamiltonian is then

$$\hat{h}^{DK} \; = \; E_i + \hat{V}^{eff}(i) \; = \; E_i + A_i(\hat{V}_{ext}(i) + Q_i \hat{V}_{ext}(i) Q_i) A_i - \frac{1}{2}[[E_i, W_1(i)]_+, W_1(i)]_+, \tag{4.58}$$

where $[a,b]_+$ is the anticommutator. Exact form of the E_i, A_i, Q_i, $W_1(i)$ terms is beyond the scope of the present work and the reader can found them in the literature, like Ref. [15].

Applying the free–electron transformation on a two–electron operator, including the Breit interaction, Eq. 4.36, we get the two–electron Douglas–Kroll operator:

$$\hat{H}^{DK} \; = \; \sum_i (E_i + \hat{V}^{eff}(i)) \; + \; \sum_{i<j} \hat{V}_{ij}^{eff}. \tag{4.59}$$

We point to the Dirac relation enabling separation of the spin and spatial operator terms

$$(\hat{\boldsymbol{\sigma}} \cdot \hat{\mathbf{a}})(\hat{\boldsymbol{\sigma}} \cdot \hat{\mathbf{b}}) \;=\; \hat{\mathbf{a}} \cdot \hat{\mathbf{b}} \;+\; i\hat{\boldsymbol{\sigma}} \cdot (\hat{\mathbf{a}} \times \hat{\mathbf{b}}), \tag{4.60}$$

which gives individual spin and scalar (spatial) parts of the Douglas–Kroll transformed operator:

$$\hat{H}^{DK} \;=\; \sum_i (E_i + \hat{V}^{sf}_{eff}(i) + \hat{h}^{DK}_{SO}(i)) + \sum_{i \neq j} (\hat{V}^{eff-sf}_{ij} + \hat{g}^{DK}_{SO\,ij}), \tag{4.61}$$

where $\hat{h}^{DK}_{SO}(i)$ and $\hat{g}^{DK}_{SO\,ij}$ are one– and two–electron spin–orbit terms, respectively. For a detailed meaning of the terms we refer the reader to the specialized literature, like Ref. [191].

The DK transformation to the second order in the external potential has been extensively studied by Hess and coworkers [95, 192]. The third order (DK3) was implemented by Nakajima and Hirao [193], who applied the DK3 transformation onto the two–electron Coulomb term [194]. Previously Park and Almlöf [195] applied only the first order spin–free DK transformation on the Coulomb interaction operator.

In recent years the Douglas–Kroll–Hess (DKH) transformation has been enhanced up to higher orders. Van Wüllen reported the generalized transformation through the sixth order [196]. Reiher and Wolf invented a generalized transformation scheme up to the infinite order [197, 198].

4.6.3 Exact decoupling

We shall give here alternative derivation of an 'exact' two–component Hamiltonian and show afterwards its truncation to known approximate forms. First we show equivalence of two approaches for the exact decoupling of negative and positive energy solutions of the DIRAC equation: i) elimination of small components and ii) unitary decoupling transformation.

Similarly as was done for the free particle, Eq. 4.18, we express the Dirac equation for a charged particle in the potential field, Eq. 4.35, as a system of coupled equations for large and small components:

$$\begin{aligned} \hat{h}_{11}\Psi^L \;+\; \hat{h}_{12}\Psi^S \;&=\; E\Psi^L \\ \hat{h}_{21}\Psi^L \;+\; \hat{h}_{22}\Psi^S \;&=\; E\Psi^S. \end{aligned} \tag{4.62}$$

Let us introduce the operator $\hat{R}$ representing the exact coupling between small and large components:

$$\Psi^S \;=\; \hat{R}\Psi^L. \tag{4.63}$$

First we eliminate small components in Eq. 4.62 by using Eq. 4.63. We get

$$(\hat{h}_{11} \;+\; \hat{h}_{12}\hat{R})\Psi^L \;=\; E\Psi^L. \tag{4.64}$$

Than one has to introduce the normalization of individual large–components since these are not normalized, although enveloping four–component wave functions are normalized to themselves. The normalization operator, $\hat{N}_+$, can be extracted from normalization condition of the four–component wave function

$$\langle\Psi|\Psi\rangle = \langle\Psi^L|\Psi^L\rangle + \langle\Psi^S|\Psi^S\rangle = (1 + \hat{R}^\dagger\hat{R})\langle\Psi^L|\Psi^L\rangle = 1, \tag{4.65}$$

and is equal to

$$\hat{N}_+ = \sqrt{(1+\hat{R}^\dagger\hat{R})}. \tag{4.66}$$

The resulting exact Hamiltonian for the normalized two–component wave function $\phi = \hat{N}_+\Psi^L$ thereby becomes (the subscript $+$ is representing positive energy solutions, $-$ negative solutions):

$$\hat{h}_+ = \hat{N}_+\left[\hat{h}_{11} + \hat{h}_{12}\hat{R}\right]\hat{N}_+^{-1} = \sqrt{1+\hat{R}^\dagger\hat{R}}\left[\hat{h}_{11} + \hat{h}_{12}\hat{R}\right]\frac{1}{\sqrt{1+\hat{R}^\dagger\hat{R}}}. \tag{4.67}$$

We are looking for unitary transformation $\hat{U}$ to decouple solutions of positive and of negative energy. The general form (for comparison see also Eq. 4.54) comes from Heully *et al.* [199]:

$$\hat{U}^\dagger\begin{bmatrix}\hat{h}_{11} & \hat{h}_{12}\\ \hat{h}_{21} & \hat{h}_{22}\end{bmatrix}\hat{U} = \begin{bmatrix}\hat{h}_+ & 0\\ 0 & \hat{h}_-\end{bmatrix}. \tag{4.68}$$

Kutzelnigg [200] found the advantage of writing the unitary operator matrix as the product of two transformations

$$\hat{U} = \hat{W}_1\hat{W}_2: \quad \hat{W}_1 = \begin{bmatrix}1 & -\hat{R}^\dagger\\ \hat{R} & 1\end{bmatrix}; \quad \hat{W}_2 = \begin{bmatrix}\hat{N}_+^{-1} & 0\\ 0 & \hat{N}_-^{-1}\end{bmatrix}; \quad \begin{array}{lcl}\hat{N}_+ & = & \sqrt{1+\hat{R}^\dagger\hat{R}}\\ \hat{N}_- & = & \sqrt{1+\hat{R}\hat{R}^\dagger}\end{array}. \tag{4.69}$$

The first transformation with $\hat{W}_1$ leads to the decoupling:

$$\begin{bmatrix}\hat{h}_{11} + \hat{h}_{12}\hat{R} + \hat{R}^\dagger\hat{h}_{21} + \hat{R}^\dagger\hat{h}_{22}\hat{R} & -\hat{h}_{11}\hat{R}^\dagger + \hat{h}_{12} - \hat{R}^\dagger\hat{h}_{21}\hat{R} + \hat{R}^\dagger\hat{h}_{22}\\ -\hat{R}\hat{h}_{11} - \hat{R}\hat{h}_{12}\hat{R} + \hat{h}_{21} + \hat{h}_{22}\hat{R} & \hat{R}\hat{h}_{11}\hat{R}^\dagger - \hat{R}^\dagger\hat{h}_{12} - \hat{h}_{21}\hat{R}^\dagger + \hat{h}_{22}\end{bmatrix}. \tag{4.70}$$

It is clear for the exact decoupling the off–diagonal elements, which are Hermitian conjugated, have to be equal to zero. This gives relation which is valid *only* for the exact $\hat{R}$:

$$\hat{h}_{21} + \hat{h}_{22}\hat{R} = \hat{R}\hat{h}_{11} + \hat{R}\hat{h}_{21}\hat{R}. \tag{4.71}$$

The second transformation $\hat{W}_2$ introduces the renormalization, thus ensuring the unitarity of the transformation. In this final step we obtain the Hamiltonian for the positive–energy solutions

$$\hat{h}_+ \;=\; \frac{1}{\sqrt{1+\hat{R}^\dagger\hat{R}}}\left[\hat{h}_{11} + \hat{h}_{12}\hat{R} + \hat{R}^\dagger\left(\hat{h}_{21} + \hat{h}_{22}\hat{R}\right)\right]\frac{1}{\sqrt{1+\hat{R}^\dagger\hat{R}}}, \tag{4.72}$$

which is identical to Eq. 4.67, when we use the coupling equation, Eq. 4.71.

We have shown the equivalence between the elimination of the small components and the unitary decoupling transformation for the case of the *exact* coupling between the large and small components represented by $\hat{R}$.

Regarding the two–component wave functions, we consider the decoupling transformation, Eq. 4.68, of the *matrix of four–component eigenvectors*,

$$\hat{U}^{\dagger}\Psi \;=\; \hat{W}_2^{\dagger}\hat{W}_1^{\dagger}\left[\begin{array}{cc}\psi_+^L & \psi_-^L\\ \psi_+^S & \psi_-^S\end{array}\right], \tag{4.73}$$

which gives

$$\left[\begin{array}{cc}\widetilde{\psi}_+^L & \widetilde{\psi}_-^L\\ \widetilde{\psi}_+^S & \widetilde{\psi}_-^S\end{array}\right] = \hat{W}_2^{\dagger}\left[\begin{array}{cc}\psi_+^L + \hat{R}^{\dagger}\psi_+^S & \psi_-^L + \hat{R}^{\dagger}\psi_-^S\\ \psi_+^S - \hat{R}\psi_+^L & \psi_-^S - \hat{R}\psi_-^L\end{array}\right]. \tag{4.74}$$

After the exact decoupling small component wave functions for positive energies and large component wave functions for negative energies are zero, $\widetilde{\psi}_+^S = 0$ and $\widetilde{\psi}_-^L = 0$. This implies (after making off-diagonal blocks of Eq. 4.74 equal to zero):

$$\psi_+^S = \hat{R}\psi_+^L; \quad \psi_-^L = -\hat{R}^{\dagger}\psi_-^S, \tag{4.75}$$

One sees that $\hat{R}$ couples the large and small positive–energy eigenvectors. The final renormalized nonzero two–component functions for separated positive and negative states therefore are :

$$\widetilde{\psi}_+^L = \sqrt{1+\hat{R}^{\dagger}\hat{R}}\,\psi_+^L \qquad \widetilde{\psi}_-^S = \sqrt{1+\hat{R}\hat{R}^{\dagger}}\,\psi_-^S. \tag{4.76}$$

The exact coupling between the large and small components of the Dirac equation, Eq. 4.35, can be expressed as

$$\hat{R} = \frac{1}{2mc}\widehat{B}(E)\,(\hat{\boldsymbol{\sigma}}\cdot\hat{\mathbf{p}})\,; \quad \widehat{B}(E) = \left[1+\frac{E-V}{2mc^2}\right]^{-1}. \tag{4.77}$$

This coupling is, however, energy–dependent and thus *state–specific*. Heully *et al.* [199] developed a *state–universal* quadratic equation. The coupling equation obtained in a kinetically balanced basis set (Eq. 4.46) forms the basis of the iterative XQR scheme proposed by Kutzelnigg and Liu [201]. The $\hat{R}$ in Eq. 4.63 will refer to the *state universal* coupling operator, in agreement with the notation used in the paper by Heully *et al.* [199]. Finally, one may note that the resulting working equation for electronic states,

$$\hat{h}_+\widetilde{\psi}_+^L = E\widetilde{\psi}_+^L, \tag{4.78}$$

can be rearranged to

$$\left[\hat{h}_{11} + \hat{h}_{12}\hat{R} + \hat{R}^{\dagger}\left(\hat{h}_{21} + \hat{h}_{22}\hat{R}\right)\right]\psi_+^L = E\left(1+\hat{R}^{\dagger}\hat{R}\right)\psi_+^L. \tag{4.79}$$

This corresponds to the Normalized Elimination of Small Components (NESC) [202–204].

Truncation to approximate schemes Several two–component relativistic Hamiltonians can be obtained using approximate couplings, for which Eq. 4.71 is no longer valid. The previously mentioned Breit–Pauli Hamiltonian, Eq. 4.55, is extracted using the approximation

$$\hat{R} \sim \frac{1}{2mc}\left(\hat{\boldsymbol{\sigma}}\cdot\hat{\mathbf{p}}\right), \tag{4.80}$$

and keeping terms to the order of O(c^{-2}). Difficulties due to the unboundedness and singularity of the Pauli operator are avoided in regular approximations (RA). These are constructed upon the approximation

$$\hat{R} \sim \frac{c}{2mc^2 - \hat{V}} \left(\hat{\boldsymbol{\sigma}} \cdot \hat{\mathbf{p}}\right). \tag{4.81}$$

The ZORA (Zero–Order Relativistic Approximation) Hamiltonian is obtained from decoupling with Eq. 4.81 and no renormalization [205–207]. Insertion of the approximate coupling, Eq. 4.81, into the NESC equation, Eq. 4.79, gives the IORA (Infinite Order Regular Approximation) equation [208]. A precursor to IORA was the scaled ZORA approach [209], which is an approximation to IORA obtained by replacing the operator product $\hat{R}^\dagger \hat{R}$ in Eq. 4.79 by its expectation value. Comparing the exact coupling, Eq. 4.77, with the regular approximation, Eq. 4.81, one sees that the latter is obtained from the former simply by setting the energy to zero. Note that most recently ZORA was implemented in a new relativistic treatment in the Quantum Monte Carlo technique [210].

There is another decoupling strategy: performing first the free–particle Foldy–Wouthuysen transformation [190] which gives a two–component kinetic energy operator on square root form what ensures the variational stability of the resulting operator. Subsequent decoupling in orders of the external potential V (or in the inverse speed of light in c^{-1}) defines the previously mentioned Douglas–Kroll–Hess [94, 95, 192], Section 4.6.2, and Barysz–Sadlej–Snijders [211–216] transformations, respectively. Alternatively, the small components may be eliminated and the exact coupling obtained through iterative procedures [217–219].

4.6.4 Infinite order two–component Hamiltonian (IOTC)

One may obtain the *exact coupling* [211, 213, 214, 216] in the finite basis approximation by solving the Dirac equation, Eq. 4.35, in some suitable basis set. The exact decoupling can be carried out in a single step starting from a matrix representation of the Dirac operator in a molecular field.

The coupling relations, Eq. 4.75, are in a finite basis set transformed into two systems of linear equations

$$Y_+^S = \hat{R} Y_+^L; \quad Y_-^L = -\hat{R}^\dagger Y_-^S, \tag{4.82}$$

where $Y_{+(-)}^{L(S)}$ is the block of the eigenvector matrix corresponding to the large (small) components of the positive (negative) energy solutions of the Dirac equation. The coupling operator $\hat{R}$, Eqs. 4.63, 4.77, now in a *matrix* form (without the "hat" symbol), can be obtained directly by solving the first of system of equations, but in practice it turns out to be better to take the Hermite conjugate of the second system and premultiply it by Y_-^S giving

$$AR = B; \quad A = \left[Y_-^S Y_-^{S\dagger}\right]; \quad B = -\left[Y_-^S Y_-^{L\dagger}\right]. \tag{4.83}$$

The A matrix is positive–definite and Hermitian. The system can accordingly be solved by a Choleski decomposition. The unitary transformation can now be constructed and the Dirac Hamiltonian decoupled in matrix form.

Another important point is that in a rigorous construction of a two–component relativistic Hamiltonian the decoupling transformation should be defined with respect to the complete electronic Hamiltonian, Eq. 4.37, not only to the one–electron part, as is usually done in the literature. Evidently, not only the one–electron part, but the two–electron part as well should be subject to the change of picture transformation. However, this would bring the computational cost back to the four–component level [194, 195]. Therefore, in the two–component electronic Hamiltonian one prefers untransformed two–electron Coulomb term, which implies that two–electron spin–orbit contributions (see Section 4.7) are neglected.

Calculation of properties. Change of picture. Till now various transformations to the two–component form have been demonstrated solely on the Dirac energy operator. In the relativistic quantum mechanics, however, one works with a variety of four–component property operators. For this reason, to be physically fully consistent at the two–component level, all relativistic property operators have to undergo the very same transformation as the 'parental' Dirac Hamiltonian. Clearly, when 'descending' to the two–component framework, one has to adapt any four–component operator accordingly. The adaptation of the operator with respect to the wave function is known as the change of picture [220, 221].

For the IOTC case the picture change transformation matrix U, Eq. 4.69, can be applied not only for the Dirac operator, but also for any four–component property operators in matrix representation as well. Thus the picture change transformation of a four–component property operator in the basis set, X^{4c}, can be done easily:

$$U^{\dagger} X^{4c} U \;\rightarrow\; X^{2c}_{++} \,. \tag{4.84}$$

It should be stressed, however, that the decoupling transformation U is constructed to block–diagonalize a specific one–electron Hamiltonian, defined by the external scalar potential $\hat{V}$ appearing in Eq. 4.35. Hence, in general, the decoupling transformation does not block–diagonalize an arbitrary operator. Therefore, elements of the two–component operator, X^{2c}_{++}, are obtained by selecting the $(++)$–matrix block, see Eq. 4.73, of the transformed operator. This corresponds to projecting the four–component operator onto the space spanned by the positive–energy solutions of the particular Hamiltonian defining the decoupling transformation. At the algebraic IOTC level the importance of the change of picture for expectation values was reported by Kędziera *et al.* [222]. Note that relativistic picture change transformations of the two–electron interaction term have been reported in Refs. [194, 195, 223].

Implementation of the IOTC method The implementation was described by one of us (MI) [224] and is distributed within the DIRAC08 program suite [170].

The Dirac equation, Eq. 4.35, is solved in the orthonormal (MO) basis [225] and subsequently the IOTC Hamiltonian with positive energy solutions only is then projected back onto the large component AO–basis. This algorithm runs as follows:

1. Setting up the Dirac equation on matrix form in the AO–basis

$$h^{AO} c_i^{AO} = S^{AO} c_i^{AO} \varepsilon_i; \quad S^{AO} = \begin{bmatrix} S^{LL} & 0 \\ 0 & S^{SS} \end{bmatrix}, \tag{4.85}$$

where S^{AO} is the overlap matrix. Uncontracted Gaussian basis functions are used in the implementation.

2. Transforming to an orthonormal basis using the non–unitary transformation

$$h^{MO} c_i^{MO} = c_i^{MO} \varepsilon_i; \quad V = \begin{bmatrix} V^{LL} & 0 \\ 0 & V^{SS} \end{bmatrix}; V^\dagger S^{AO} V = I. \tag{4.86}$$

   In our implementation the so called restricted kinetic balance (RKB) is enforced in this step by embedding the transformation to Dyall's modified Dirac equation [225, 226] in the transformation $\hat{V}$, as described in Refs. [128, 225].

3. The eigenvalue problem, Eq. 4.86, is solved by the diagonalization and the coupling matrix R is extracted using Eq. 4.83. The transformation matrix U, Eq. 4.69, is constructed, and subsequently the positive–energy two–component relativistic Hamiltonian h_+^{MO}, Eq. 4.72, is obtained in the matrix form.

4. In the final step the Hamiltonian is projected back onto the large component AO–basis

$$h_+^{AO} = \left[V^{LL;\dagger}\right]^{-1} h_+^{MO} \left[V^{LL}\right]^{-1}; \quad \left[V^{LL}\right]^{-1} = V^{LL;\dagger} S^{LL;AO}. \tag{4.87}$$

   The matrix representation of the IOTC Hamiltonian, h_+^{AO}, is then written to file with whatever transformed property operators are needed and all the subsequent calculations continue in the two–component framework.

In comparison to the scheme proposed by Jensen and Iliaš [227] the preliminary free–particle FW transformation is completely avoided. Since this transformation was used by Barysz and coworkers [211–214], we will refer to the two–step approach as BSS. The direct construction of the coupling matrix emphasised here was already proposed by Dyall [204] as well as Kutzelnigg and Liu [201, 228], although the latter authors seem to prefer an iterative approach. The noniterative algebraic approach to the IOTC relativistic theory was published by Kędziera and Barysz [229]. In the same group it has been shown recently how to recover four–component solutions by the inverse transformation of the IOTC wave function [230].

Tab. 4.1 displays ionization energies and electron affinities of the radon atom computed with the Fock–space Coupled–Cluster method, see Section 4.5.2. We utilized four–component DC, and two–component BSS and IOTC Hamiltonians, all of them including both scalar and spin–orbit effects. The IOTC and BSS Hamiltonians give results closely matching the DC data.

Tab. 4.2 shows NMR shielding constants (see also Section 5.7), magnetizabilities and polarizabilities of the Rn atom calculated with the DC, IOTC and BSS Hamiltonians. These properties were obtained upon the DC/IOTC/BSS Hartree–Fock wave function with the second order linear–response module [232]. Two–component IOTC and BSS results agree with each other and follow the corresponding four–component DC values.

4.7 Spin–orbit effects

The four–component Dirac Hamiltonian contains by default both scalar and spin–orbit effects. Note that its modification is possible in order to distinguish between those relativistic effects according to K. Dyall [226]. Dyall's adaptation of the Dirac Hamiltonian was enhanced by adopting the so called quaternion symmetry by Visscher and Saue [225]. Although leaving out spin–orbit effects creates some computational speed up in the four–component framework due to the use of the single point group symmetry, small component basis set functions still remain and cause a computational bottleneck.

Therefore a better way is transforming the four–component Hamiltonian to a two–component form, Section 4.6, and afterwards separate spin–orbit terms according to Eq. 4.60. Here we give three examples of SO Hamiltonians. Note that in following formulas for spin–orbit operators we prefer to use Pauli matrices (see Section 3.1.2) instead of spin operators, utilized in Eq. 2.11.

i) Applying the FW transformation on the DCB Hamiltonian, Section 4.6.1, one can extract (from Eq. 4.56) the full spin–orbit Breit–Pauli Hamiltonian [53] of the form

$$\hat{H}_{SO}^{BP} = \frac{e^2\hbar}{4m^2c^2}\Big(\sum_i\sum_I Z_I\frac{\mathbf{r}_{iI}\times\hat{\mathbf{p}}_i}{r_{iI}^3}\cdot\hat{\boldsymbol{\sigma}}_i - \sum_{i\neq j}\frac{\mathbf{r}_{ij}\times\hat{\mathbf{p}}_i}{r_{ij}^3}\cdot(\hat{\boldsymbol{\sigma}}_i + 2\hat{\boldsymbol{\sigma}}_j)\Big). \tag{4.88}$$

Tab. 4.1. Ionization energies (IE) of the Rn atom and excitation energies (EE) of the Rn^+ cation calculated by the Fock–space CCSD method [in eV]. Absolute differences from DC values in parentheses. Data from Ref. [224].

	DC	IOTC	BSS
IE of Rn[a]			
$^1S_0 - {}^2P_{3/2}$	10.5614	10.5304	10.5304
		(-0.0310)	(-0.0310)
EE of Rn^+			
$^2P_{3/2} - {}^2P_{1/2}$	3.7706	3.8967	3.8953
		(0.1261)	(0.1247)
$^2P_{3/2} - {}^2S_{1/2}$	14.8708	14.8427	14.8420
		(-0.0281)	(-0.0288)

[a] Experimental value of the first IE ($^1S_0 - {}^2P_{3/2}$) is 10.7485 eV, Ref. [231].

Tab. 4.2. Magnetic and electric properties of the Rn atom. Absolute differences from DC values are in parentheses. Data from Ref. [224].

Property	DC	IOTC	BSS
NMR shielding[a]	23348.4	23373.6 (25.2)	23372.4 (24.0)
Magnetizability[b]	-12.7160	-12.7230 (-0.0070)	-12.7236 (-0.0076)
Polarizability[c]	27.066	27.119 (0.053)	27.122 (0.056)

[a] NMR shielding constants in ppm.
[b] Magnetizabilities in a.u.
[c] Polarizabilities in a.u.

ii) Through the Douglas–Kroll–Hess (DKH) transformation, Section 4.6.2, one may separate (by adopting Eq. 4.61) the variationally stable spin–orbit Hamiltonian

$$\hat{H}_{SO}^{DK} = e^2\hbar\Big(\sum_i\sum_I B_i\frac{Z_I}{r_{iI}^3}\hat{\boldsymbol{\sigma}}_i\cdot(\mathbf{r}_i\times\hat{\mathbf{p}}_i)B_i - \sum_{i\neq j}(B_iA_j\frac{\mathbf{r}_{ij}\times\hat{\mathbf{p}}_i}{r_{ij}^3}\cdot\hat{\boldsymbol{\sigma}}_iB_iA_j + 2B_iA_j\frac{\mathbf{r}_{ij}\times\hat{\mathbf{p}}_i}{r_{ij}^3}\cdot\hat{\boldsymbol{\sigma}}_jB_jA_i)\Big). \tag{4.89}$$

The Douglas–Kroll SO Hamiltonian, Eq. 4.89, contains projector operators and the Breit–Pauli spin–orbit Hamiltonian, Eq. 4.88, can be obtained by expanding and truncating the kinematic factors A_i and B_i in both one– and two–electron operators, see, *e.g.*, Ref. [15]. Note that the two–electron SO terms appearing in Eqs. 4.88,4.89 are known as the spin–same–orbit (SSO) and spin–other–orbit (SOO) terms, respectively. Both of them are an approximation of the full Coulomb–Breit/Gaunt interaction operator, see Section 4.4.1.

iii) Since it is difficult to compute different types of two–electron spin–orbit integrals, as a cheap alternative one can utilize an effective one–electron spin–orbit operator of the general form:

$$\hat{H}_{SO}^{eff} = \frac{e^2\hbar}{4m^2c^2}\sum_i\sum_I Z_I^{eff}\frac{\mathbf{r}_{iI}\times\hat{\mathbf{p}}_i}{r_{iI}^3}\cdot\hat{\boldsymbol{\sigma}}_i, \tag{4.90}$$

where Z^{eff} is a parameter. However, since the two–electron contribution does not scale as the one–electron spin–orbit term, this SO–operator is state dependent and therefore less accurate.

4.7.1 Mean–field spin–orbit operator

Calculation of many–centre two–electron spin–orbit integrals is costly [159, 191, 233] and is approximately equal to the cost of two–electron integrals over small–component basis functions, Section 4.4.6. This disadvantage has been overcome by introducing a pseudo one–electron Fock type spin–orbit operator, called as the mean–field spin–orbit operator, MFSO. It is an effective one–centre operator obtained from the full DKH atomic spin–orbit Hamiltonian [234], Eq. 4.89.

Atomic matrix elements of the MFSO operator have the form:

$$\begin{gathered}\langle i|\hat{h}^{MFSO}|j\rangle_c \;=\; \langle i|\hat{h}_{SO}^{DK}(1)|j\rangle_c \;+\; \tfrac{1}{2}\textstyle\sum_M^{mf-orbs} n_M(2\langle iM|\hat{g}_{SO}^{DK}(1,2)|jM\rangle_c - \\ \langle iM|\hat{g}_{SO}^{DK}(1,2)|Mj\rangle_c - \langle Mi|\hat{g}_{SO}^{DK}(1,2)|jM\rangle_c)\;,\; c=(x,y,z),\end{gathered} \tag{4.91}$$

where one– and two–electron spin–orbit terms are given in Eq. 4.61. The two–electron part of this operator is represented as the summation running over occupied (mean–field) spatial $M(l,m_l)$ atomic orbitals; n_M are occupation numbers. The orbitals M can be taken either from contractions of the basis set, or, what was preferred here, from an interfaced internal atomic SCF code producing scalar relativistic orbitals for a given set of orbital exponents.

A two–component Hamiltonian accounting for both scalar and spin–orbit relativistic effects can be simply constructed by combining available operators. In the previous work [235] we have employed the no–pair Hamiltonian containing the one–electron spin–free Douglas–Kroll–Hess term, DKH2sf, which is accurate to the second order in the external potential, together with the MFSO operator, Eq. 4.91. Note that from Section 5 onward the acronym DKH is used solely for the DKH2sf operator. The two–electron interaction was represented by the standard nonrelativistic Coulomb interaction term.

$$\hat{H}^{DKH2sf+MFSO} = \sum_i (\hat{h}^{DKH2sf}(i) + \hat{h}^{MFSO}(i)) + \sum_{i<j} \frac{1}{r_{ij}}. \tag{4.92}$$

The mean–field spin–orbit operator can be expressed as:

$$\hat{h}^{MFSO} = \hat{h}^{MFSO(x)}\hat{\sigma}_x + \hat{h}^{MFSO(y)}\hat{\sigma}_y + \hat{h}^{MFSO(z)}\hat{\sigma}_z. \tag{4.93}$$

The spin–orbit term in the Hamiltonian is the reason why one can not utilize the spin symmetry and work with spinorbitals. One has to resort to general two–component spinors, Ψ^L of Eq. 4.13. The platform for the implementation was another four–component relativistic program suite, MOLFDIR [236], which fully utilizes the relativistic double–group symmetry, Section 4.4.4. MOLFDIR performs Kramers restricted four– and two–component single determinant HF–SCF calculation on closed– or open–shell system (see Section 4.4.3), followed by electron correlation methods, Section 4.5. MOLFDIR was slightly modified in such a way that its two–component mode handles external one–electron integrals of the $\hat{h}^{DKH2sf}$ and $\hat{h}^{MFSO}$ operators.

The effectiveness of this operator was demonstrated on FO and ClO molecules in Tabs. 4.3 and 4.4. For these light systems DKH2sf+MFSO results follow closely four–component DCG counterparts. However, for treating heavier elements one has to resort to the Hamiltonian infinite in both scalar and spin–orbit terms, Section 4.6.3.

Tab. 4.3. Spin-orbit splitting of the $^2\Pi$ state of the FO molecule [cm^{-1}]. Calculated in decontracted basis sets, $1s$ spinors of fluorine and $1s$ spinors of oxygen were frozen. Data from Ref. [235].

Method/Hamiltonian	DKH2sf+MFSO	DCG
SCF	183.5	184.9
CCSD(T)	194.1	194.4
Experiment	193.81	

Tab. 4.4. Spin–orbit splitting of the $^2\Pi$ ground state of the ClO molecule [cm^{-1}]. Calculated in decontracted basis sets, two sets of spinors, $1s$ spinors of oxygen and $1s$, $2s$, $2p$ spinors of chlorine were frozen. Data from Ref. [235].

Method/Hamiltonian	DKH2sf+MFSO	DCG
SCF	223.3	225.2
CCSD(T)	310.7	312.6
Experiment	318	

4.7.2 RASSI–SO

The so called RASSI–SO [102] method belongs to the group where spin–orbit relativistic effects are treated *a posteriori* in the so called L–S or Russell–Saunders coupling scheme [237], see also Ref. [233], which is based on the combination of many–electron states with the resultant angular and spin momentum numbers, L and S, respectively, leading to a new wave function of a total angular number J. The spin–orbit interaction in accounted for through a multiconfigurational interaction approach, which employs the Complete Active Space (CASSCF) or Restricted Active Space (RASSCF) wave functions as a reference.

Relativistic effects are treated in two steps as follows: First, the CASSCF/RASSCF wave function is calculated for a specified total spin S, and can be viewed as a common representative of all possible spin states within the given multiplet. Its advantage is that this spin–free basis can involve many wave functions, and these may use individually optimized molecular orbitals. Such determined scalar relativistic wave functions include both static (through the use of the multideterminantal RASSCF/CASSCF method) and dynamic correlation effects (using the multiconfigurational perturbation theory, CASPT2).

In the second step, one computes eigenstates of a two–component quasirelativistic Hamiltonian in a basis set of spin–free (scalar) wave functions. The matrix over spin–free states, where the Hamiltonian operator contains the Douglas–Kroll–Hess scalar term together with the AMFI operator, Eq. 4.91, is calculated by an extension of the Restricted Active Space Interaction (RASSI) method, and is utilizing the Wigner–Eckart theorem due to the spin–orbit operator.

To include the dynamic correlation within, one can employ the multi state (MS) CASPT2 method in the RASSI–SO procedure for calculation of spin–orbit matrix elements. The MS–CASPT2 method is mixing CASSCF states and the resulting SOC wave functions are mixtures of CASSCF functions of different space and spin symmetry.

Matrix elements over the original basis as well as over the eigenstates can involve also other property operators, and can be used to calculate, for example, transition strengths.

4.8 Fine effects, Lamb shift

Although the Dirac theory predicts the entire spectrum of the hydrogen–like atom, some cases of the fine splitting are not covered. Lamb and Retheford [238] discovered (1947) in a microwave experiment that the $2s_{1/2}$ level was higher than the $2p_{1/2}$ level by 1.060 MHz. According to the Dirac theory, both states, $^2\mathrm{S}_{1/2}$ and $^2\mathrm{P}_{1/2}$ should have equal energy. Bethe [239] was the first to explain the very small shift, called the Lamb shift, in the hydrogen spectrum. This was the beginning of modern Quantum Electrodynamics, QED.

Dirac's theory does not deal with the possibility of creating and destroying particles, which is one of the basic consequences of the theory of relativity. An extension using the quantized electromagnetic field leads to the theory of quantum electrodynamics, which fixes this difficulty. According to the QED theory electrons and positrons appear as quanta of the quantized Dirac field. Vacuum fluctuations are perceived as zero point oscillations of this field. The interaction of an electron with zero–point oscillations of the electromagnetic field creates its self–energy, which is, together with effect of vacuum polarization, observed experimentally. The self–energy is the largest QED correction reducing the binding energy of an electron due to the exchange of virtual photons with the nucleus. The vacuum polarization contribution causes shift in the binding energy of an electron due to the creation and annihilation of virtual e^-–e^+ pairs in the vacuum. It increases the binding energy mostly of the time and is the second largest correction. In the two excellent reviews published recently by Lindgren, Salomonson a Hedendahl [83] and Eliav and Kaldor [84] discussed physical aspects of QED effects in physics and chemistry and present computational tools for incorporating of QED within the Coupled Cluster formalism for electron correlation effects.

The value of the Lamb shift scales as the fourth power with respect to the nuclear charge Z, thus is rather important for heavy systems. For instance, a good example is the U^{91+} cation, where the shift is of the order of 10^5 cm^{-1}, what was confirmed experimentally [240].

It appears that QED corrections may be chemically important in the electron binding energy of the eka–radon (Z=118) amounting to a 9% reduction of this property [241]. Eka–radon is a superheavy element for which a relatively large QED effect is not so much surprising. However, in compounds with rather light atoms as BF_3, AlF_3, and GaF_3 it appears that the Lamb shift to the atomization energies may be in the range of 3–5% of the scalar relativistic contribution [242] and may be important for higher accuracy calculations particularly for molecules containing heavy elements. Hirao *et al.* [243] calculated ionization energies of Zn and Mo^{12+} and conclude that unprecedented accuracy can be achieved by using the fully relativistic many–body treatment including the Lamb shift.

When working in relativistic molecular calculations with the *no pair* approximation (*i.e.* one works with electronic states only), all QED effects are thus neglected.

5 Relativistic effects in atoms and molecules, their properties and interactions

Accurate calculations of atomic and molecular properties require sophisticated many–electron theories for treatment of the electron correlation problem. This is computationally very demanding even at the nonrelativistic level for medium or larger molecules. In so called wave function methods the starting point is the HF wave function expressed most frequently in the form of the Slater determinant, Eq. 3.12, as a reference. A single–determinant HF reference wave function is usually sufficient for closed–shell atoms and molecules. For high–spin open–shell systems the simplest reference is the single–determinant ROHF wave function. In quasidegenerate situations the reference is a combination of Slater determinants. Many problems require a reference consisting of more than a single–determinant reference. This is the case of quasidegenerate systems, like calculations on the hypersurface far from the equilibrium geometry or many excited states. A multideterminant reference is also needed for treatment of the SO coupling.

Let us remind (see Section 3.2.5) that at the simplest single–determinant level most demanding steps in sophisticated many–electron methods, like CCSD, scale with the number of occupied (N_o) and virtual orbitals N_v as $N_o^2 N_v^4$ in an iterative process. Number of operations required for triples scales as $N_o^3 N_v^4$. When using the spinorbital basis for open–shell systems with the UHF (Unrestricted Hartree Fock) reference, we have to treat twice as much spinorbitals when compared to the number of closed–shell or ROHF open–shell orbitals. The number of operations further increases for calculations in which we work with 4–spinors (see Section 4). In spite of an enormous progress in technology of CC calculations (see, *e.g.*, our implementation of CCSD(T) in the MOLCAS program [64]), they still remain computationally demanding, particularly, when combined with specific requirements on the construction of basis sets with some relativistic Hamiltonian. This explains that rigorous computational applications of ideas of the relativistic theory for many–electron atoms and molecules is much more complicated than it is in the nonrelativistic case.

Orbitals or spinorbitals in the Slater determinant, Eq. 3.12, are in practical nonrelativistic calculations expressed in the form of the linear combination of atomic basis functions, mostly contracted Gaussians, [39, 51, 62, 244]. Selection of basis sets for practitioners of relativistic many–electron calculations is rather delicate. In Section 4.4.6 we learned that there are specific requirements on basis sets which are capable of representing the large and small components of the Dirac spinors. Nonrelativistic basis sets are not applicable for such calculations. A small component set of exponents is obtained from the large component set and leads to basis sets which are too large for practical use. Also, in most calculations of atomic and molecular properties we need just a large component. The remedy is the Foldy–Wouthuysen transformation to a two–component Hamiltonian. Theoretical background of these methods is described in Section 4.6. Most frequently used relativistic calculations employ no–pair DKH methods which provide excellent results in situations when the spin–orbit coupling can be safely avoided. Such calculations are very appealing since they require nothing more than standard methods and computer programs of nonrelativistic many–electron quantum chemistry, just supplemented with relativistic integrals. Yet, using of standard nonrelativistic contracted Gaussian basis sets is not recommended. In fact, to be rigorous, we should say that any specific Hamiltonian requires a specific basis set. This is clearly not practical for extensive applications of relativistic methods. A good compromise is using standard exponents of the primitive Gaussians optimized at the nonrelativistic level. When left uncontracted, the flexibility is sufficient for quite different Hamiltonians.

This, however, would be of little help, since uncontracted basis sets are too large. Sadlej, in collaboration also with our group has developed a counterpart of popular nonrelativistic polarized basis sets. The family of Pol basis sets [245–256] was constructed having in mind nonrelativistic calculations of molecular electric properties, which represent a response of the wave function to the external electric field and thus suitable, especially, for calculations of molecular dipole and quadrupole moments, dipole polarizabilities, higher polarizabilities, *etc.* Due to the presence of diffuse Gaussians these basis sets are suitable also for calculations of electron affinities, weak intermolecular interactions, *etc.* Their relativistic counterparts, the Pol–DK family of basis sets [255–262], share the same exponents as nonrelativistic Pol basis sets, but are contracted differently. Contraction coefficients are obtained from atomic DKH calculations and therefore "feel" the relativistic change of corresponding orbitals. Review of basis sets for relativistic calculations can be found in [263]. Another newer series of relativistic basis sets which are generally available are aug–cc–pVTZ–DK [264, 265], ANO–RCC [105, 106]. Efficient are bases connected with pseudopotentials. Frequently used are the Stuttgart group effective core potentials and corresponding basis sets, see *e.g.*, Refs. [186–188]. These basis sets and corresponding methods are designed to simulate cores of heavy atoms in valence–only calculations with a formally nonrelativistic Hamiltonian. Direct relativistic effects, including spin–orbit interactions, on the valence electron systems as well as indirect effects due to relativistic changes within the core, are implicitly incorporated into the pseudopotential (PP). Two–component energy–consisted pseudopotentials in atomic Fock–space Coupled Cluster calculations [189] were successfully applied in calculations of accurate (to within a few hundred wavenumbers) ionization potentials, electron affinities, and excitation energies of the group 11 and 12 as well as the 13 and 14 post–d main group elements. Treatment of just valence electrons within relativistic pseudopotentials leads to substantial savings of computer time with usually small loss of accuracy with respect to all–electron correlated calculations.

The density functional theory (DFT), originally formulated by Hohenberg, Kohn and Sham [266, 267], was later extended also to high–Z systems within the framework of quantum electrodynamics [268–271]. DFT covers important part of the relativistic treatment of atomic and molecular properties of systems with heavy atoms. This is due to well known advantages of DFT, its simple mathematical formalism and less demanding computational implementation (*e.g.*, very favourable scaling with the number of electrons). Both these aspects make DFT attractive for large many–electron atoms, molecules, clusters and/or solids. In similarity with the HF–SCF method, Section 3.2.1, the Kohn–Sham DFT paves the way for the electron density of the ground state of system of independent particles moving in the effective one–particle external potential.

The key point and the stumbling block in DFT is the unknown exchange–correlation functional that describes the electron–electron interactions. There is a large spectrum of functionals ranging from local density approximation, gradient corrected functionals to hybrid ones. The latter class can be classified as having a semiempirical flavour, since all hybrid functionals are products of some kind of calibration or fitting with respect to accurate data obtained from wave function based methods (mostly CCSD(T)). They provide quite reasonable properties like geometries, harmonic frequencies, proton affinities, ionization potentials and work well in thermochemistry. Their performance in more sensitive properties like electron affinities, dipole moments and/or polarizabilities is less satisfactory [272]. Although there is no well defined systematic hierarchy of improved approximations in DFT (compared to wave function based methods), it seems that for medium and large molecular systems (including heavy atoms) the DFT is and will still remain the only method of choice in the near future. We are convinced that combining the advantages of both approaches in a smart way one can arrive to reasonable molecular relativistic properties. Wavefunction based data used as benchmarks for small systems can provide valuable numerical control for DFT applied in extended systems. Implementation of the DFT method at the relativistic four–component level together with applications for molecular properties are reported in Refs. [273–276].

An important idea of this paper is to show how molecular properties are affected by relativistic effects. Working with models including nonrelativistic and relativistic Hamiltonians allows us to assess the difference of both results and estimate the importance of specific relativistic contributions. Clearly such model is approximate. One reason is that we can not use the same basis set for different models. We just believe that our basis sets lead to results which are not too far from the basis set limit and the basis set effects are small.

5.1 Ionization potentials, electron affinities and excitation energies

Ionization potentials, together with electron affinities and other properties are important quantities in calculating chemical potentials, electronegativity and other values useful in chemistry or physics. How relativistic effects affect ionization potentials, electron affinities, and excitation energies will be discussed in this Section.

5.1.1 Ionization potentials

An interesting "V" shaped dependence of ionization potentials of Cu, Ag, and Au on the atomic number Z, Fig. 2.2, was used in Section 2 as an introductory demonstration of relativistic effects on atomic property. Similar behaviour as seen in Fig. 5.1 is quite common, at least for atoms with similar valence electronic structure.

In Tab. 5.1 are presented calculations of ionization potentials of alkali metal elements, which are based on three different sources [277–279]. The nr–CCSD(T) values and the first line DKH–CCSD(T) values are calculated in equivalent basis sets and thus their comparison show us how big is the scalar relativistic effect. This effect is growing from 0.017 eV for K up to 0.435 eV for Fr and for the 119 element it is even 1.226 eV. Qualitatively, the pattern of IP's is similar as for elements in the group 11. Note, however, that the difference of IP between Cs and Fr is much smaller than is the analogous difference for Ag and Au. The second series of DKH–CCSD(T) values are calculated in a better basis set and this improvement accounts for about 0.1 eV. The spin–orbit effect is much smaller, than is the basis set effect. Even though it is small, its inclusion via the two–component pseudopotential ARPP–CCSD(T) method and particularly via the relativistic Fock–space Coupled Cluster singles and doubles approximation starting from the Dirac–Coulomb Hamiltonian RCC(C) method, decently improves agreement with experiment.

Tab. 5.2 with calculations of ionization potentials of an extended series of atoms gives us another paradigm for relativistic effects. We can follow several trends. The first one is increasing magnitude of relativistic effects with the increasing Z number within the groups, which varies from 0.3% for Ca up to 30% for Au. The second trend is that while nonrelativistic ionization potentials are monotonously, mostly, decreasing with Z, relativistic values exhibit extremes in the series and the last members, *i.e.* IP's of Ra, Au, and Hg are larger than the previous ones. However, this is not true for elements in the group 15, where IP's are going monotonously down.

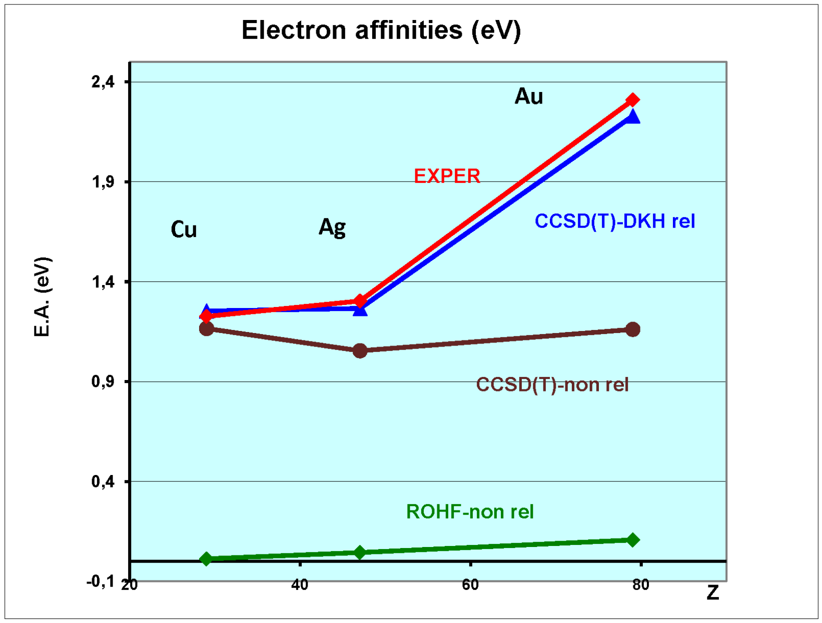

Fig. 5.1. Electron correlation and relativistic effects on electron affinities [eV] of the coinage elements Cu, Ag, and Au. The ROHF nonrelativistic data represent calculation using a single determinant Restricted Hartree Fock calculation. Electron correlation is treated by the CCSD(T) method and relativistic effects are calculated by the spin–free Douglas–Kroll–Hess method.

This group differs from other presented groups by the fact that outermost occupied orbitals are of p–type with the p^3 occupancy. In general, p orbitals exhibit smaller stabilization and contraction than s orbitals which are outermost ones in the other groups. In the particular case of Bi, in the group 15, the electronic structure means that the electron is occupying the relativistically *destabilized* $6p_{3/2}$ orbital, similar as in Section 5.5, is the situation schematically shown for Hg in Fig. 2.3 in Section 2. Of course, the important role is also played by the interplay between the electron correlation and relativistic effects in obtaining quantitative values of IP's. With high level correlated relativistic methods there is mostly a reasonable agreement between relativistically calculated ionization potentials and experiment. This gives a confidence in predicted value of IP of the superheavy element 119, as shown in Tab. 5.1.

5.1.2 Electron affinities

Now, let us analyse relativistic effects on electron affinities. Before going into details, let us stress that obtaining EA accurately is more difficult than obtaining accurate values of IP's. Frequently, the electron configuration of an anion is more complicated than that of the mother molecule. Second, to accommodate an extra electron in the originally unoccupied orbital requires specific diffuse basis sets, that means more extended bases than are normally required. One has to be careful since many states of an anion represent a situation when the electron is in fact unbound.

In practice, obtaining AE of seemingly simple (but extremely important) molecule like the O_2 molecule by quantum chemistry methods with accuracy better than, say. 0.005 eV is a torture [284]. Interestingly, even if oxygen is a light element, both scalar [284] and spin–orbit [172] relativistic effects matter in EA of the O_2 molecule (together with many other effects) if the above mentioned accuracy should be achieved. The relief for theoreticians is that experimental determination of the electron affinity is very difficult as well.

In spite of a previous general note, obtaining reasonably accurate electron affinities for Cu, Ag, and Au (as a counterpart to their IP's) is relatively simple. The DKH–CCSD(T) data are presented in Fig. 5.1. We note that EA's obtained by the independent Hartree–Fock model are completely meaningless. At the nonrelativistic HF level all three EA's are close to zero, completely out of experiment. Electron correlation treated by CCSD(T) helps a lot for Cu, but the true remedy for Au is CCSD(T) with at least scalar relativistic effects at the DKH level. This treatment leads to reasonable agreement of theoretical and experimental data and represent the trend with respect to the atomic number excellently.

Supplementary insight into electron affinities offer data in Tab. 5.3. Here we compare the pattern of EA's for elements of the group 11 and 14. In contrast to the Cu, Ag, and Au series, EA's of the group 14 elements go down monotonically (data for Si and Ge can be found in the original literature [285]). The decrease is rather slow when going from Si to Ge and Sn, but is enhanced for Pb. This is attributed to the relativistic *destabilization* of the $6p_{3/2}$ orbital and is analogous to the effect commented already in IP of bismuth, Tab. 5.2. Extrapolating to larger atomic numbers Borschewski *et al.* [285] predict that no electron binding will occur

Tab. 5.1. Ionization potentials of alkali atoms [eV].

Atom	nr–CCSD(T)^a	DKH–CCSD(T)	ARPP–CCSD(T)^c	RCC(C)^d	experiment^e
Group 1 [ns]					
K	4.267	4.284^a			
		4.336^b	4.333	4.343	4.347
Rb	4.068	4.137^a			
		4.167^b	4.161	4.181	4.171
Cs	3.681	3.821^a			
		3.881^b	3.884	3.898	3.899
Fr	3.542	3.977^a			
		4.038^b	4.013	4.072	4.073
119	3.312	4.538^a			
		4.713^b	4.333	4.181	

^{a} Ref. [277].
^{b} Ref. [278].
^{c} Two–component pseudopotential method [278].
^{d} Relativistic Fock–space coupled cluster singles and doubles approximation starting from Dirac–Coulomb Hamiltonian [279].
^{e} All experimental data from Ref. [280].

in the element 114. They predict that this element is expected to be highly inert and volatile. This is related to an adsorption process on gold (and other) surfaces of chromatography column detectors, using the gas–phase chromatography techniques.

Our next example of relativistic effects in calculations of EA of the PbO molecule demonstrates essential importance of the spin–orbit effects. Data in Tab. 5.4 represent the adiabatic detachment energy. The PbO^- anion is more stable than is the mother molecule. The adiabatic

Tab. 5.2. Ionization potentials of selected atoms [eV].

Atom	nonrelativistic	relativistic	experiment[a]
Group 2 [ns^2]	nr-CCSD(T)	DKH-CCSD(T)	
Ca[b]	6.074	6.093	6.1132
Sr[b]	5.607	5.678	5.6949
Ba[b]	5.054	5.194	5.2117
Ra[b]	4.815	5.238	5.2784
Group 10 [(n-1)d^8ns^2]	nr-CCSD(T)	DKH-CCSD(T)	
Ni[c]	7.676	8.302	7.6398
Group 11 [(n-1)d^{10}ns]	nr-CCSD(T)	DKH-CCSD(T)	
Cu[d]	7.555	7.733	7.7264
Ag[d]	6.934	7.461	7.5762
Au[d]	7.035	9.123	9.2255
Group 12 [(n-1)d^{10}ns^2]	nr-CCSD(T)	DKH-CCSD(T)	
Zn[e]	9.167	9.363	
		(9.393)	9.3942
Cd[e]	8.351	8.851	
		(8.941)	8.9938
Hg[e]	8.326	10.285	
		(10.362)	10.4375
Group 15 [ns^2np^3]		MSIH	
As[f]		9.660	9.7284
Sb[f]		8.487	8.6084
Bi[f]		7.284	7.2855

[a] All experimental data from Ref. [280].
[b] Ref. [281].
[c] Ref. [282].
[d] Ref. [33].
[e] Data in parentheses are with estimated contribution from correlating of inner shell electrons on top of the correlation of 18/17 electrons, [283].
[f] Relativistic mixed sector intermediate Hamiltonian (MSIH) Fock–space coupled cluster calculations [175].

Tab. 5.3. Electron affinities of selected atoms [eV].

Atom	relativistic	experiment[a]
Group 11 [(n-1)d^{10}ns]	DKH-CCSD(T)	
Cu[b]	1.236	1.235
Ag[b]	1.254	1.302
Au[b]	2.229	2.309
Group 14 [ns^2np^2]	MSIH	
Sn[c]	1.085	1.112
Pb[c]	0.383	0.364
114[c]	no EA[d]	

[a] All experimental data from Ref. [32].
[b] Ref. [33].
[c] Relativistic calculations in the framework of the projected Dirac–Coulomb-Breit Hamiltonian. Mixed sector intermediate Hamiltonian (MSIH) Fock–space coupled cluster calculations with spin–orbit effect included [285].
[d] The 114 element does not bind an extra electron.

detachment process is denoted in Fig. 5.2 by the solid line connecting the electronic minima of both species. For comparison with experiment the energy difference must be corrected by vibrational contributions. The vertical EA is denoted by the dotted line. The PbO molecule is not split due to SO effects. The SO states of the anion and both separated atoms are inserted in the ovals.

Both electron correlation and relativistic effects are important in calculations of EA of PbO. Our data show that at the SCF level one obtains no better EA than is 0.31 eV, less than half of the experimental value. Our best result follows from the BSS–CCSD(T) calculation with the large decontracted ANO–RCC basis. Calculated EA, 0.696 eV, agrees reasonably well with the experimental value, 0.714 eV. We note that the experimental electron affinity for the ground vibrational state of PbO, 0.722 eV [287], was corrected considering the zero point energies, 0.045 eV and 0.037 eV for the PbO ground state and the negative ion, PbO^-, respectively. Harmonic vibrational frequencies were taken from experiment. The reliability of the BSS–CCSD(T) result is supported by the good agreement of BSS–CCSD(T) and DC–CCSD(T) results with the Pol–DK basis set. Both EA's agree to within 0.01 eV. It is fair to mention that our best BSS–CCSD(T) results with ANO–RCC basis sets were obtained after deleting virtual spinors with energies higher than 10 a.u., which introduces some uncertainty in the final EA. Spin–free DKH–CCSD(T) data in Tab. 5.4 show, however, that deleting virtuals affects EA very little. We believe that the same is valid with methods treating spin–orbit effects as well. The estimate of the basis set effect is another issue that has to be considered. Spin–free CCSD(T) results with the two basis sets, Pol–DK and ANO–RCC, differ by 0.01 and 0.005 eV with the DC and BSS Hamiltonians, respectively. When considering the basis set effect with the SO coupling within BSS–CCSD(T), that is the difference of results with the Pol–DK and ANO–RCC basis sets, it is estimated to be 0.1 eV.

Proper consideration of the relativistic effects including the spin–orbit coupling is a must for calculations of EA for PbO. Results presented in this work show that due to the SO coupling the magnitude of EA increases by 0.17 - 0.20 eV with the Pol–DK basis set with BSS–CCSD(T) and DC–CCSD(T) methods. With larger decontracted ANO–RCC basis set the SO effect increases to 0.23 eV. Lower SO effect was obtained when comparing the spin–free and the spin–orbit coupling CASSCF/CASPT2/RASSI–SO results, 0.607 eV and 0.659 eV, respectively. In this comparison the CASPT2/RASSI–SO calculations for PbO^- were performed using the contracted ANO–RCC Pb$[9s8p6d4f3g]$ and O$[5s4p3d2f1g]$ basis set for the two components of the $^2\Pi$ state. The spin–orbit calculation included only these states. The ground state level is $^2\Pi_{1/2}$, which is separated from the $^2\Pi_{3/2}$ state by 0.42 eV. It is possible that a more elaborate study would increase the spin–orbit coupling somewhat and would subsequently increase the SO effect on the electron affinity. In any case, it is important to realize that EA of PbO is affected dominantly by SO states of the anion and the Pb atom. The oxygen atom contributes much less, as expected. Reasonable agreement of EA following from the RASSI–SO method (which uses DKH orbitals instead of spinors) and BSS or DC CCSD(T) methods shows that SO splitting of reference orbitals do not deteriorate the accuracy significantly. One should not forget that the electron correlation treatment is different in CASPT2/RASSI–SO and CCSD(T) methods.

5.1.3 Excitation energies

There are many examples of relativistic effects on excitation energies (EE) available in the literature, see at least results obtained by the RASSI–SO, the four–component Fock–space CC, ZORA

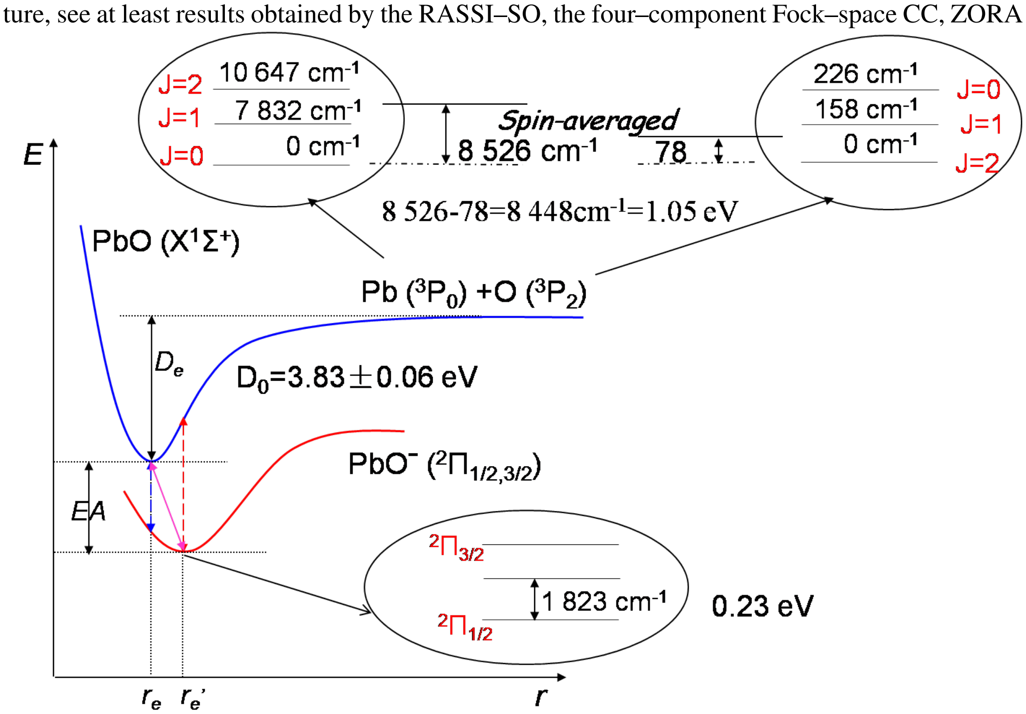

Fig. 5.2. Spin–orbit effects on the dissociation energy and the electron affinity of PbO. Data from Ref. [286].

and other methods [102, 103, 105, 189, 290, 291]. In this Section we will restrict ourselves just to an interesting example of the excitation energy between the ground state of the Fe atom and its first excited state. Another example, low–lying states of InN, will be discussed in the next Section together with SO effects affecting the potential energy curves of the two states of this molecule.

We tried to calculate EE of the Fe atom some years ago [292] using a simple MVD (Mass–Velocity–Darwin) approach, *i.e.* we have omitted SO effects. Considering that Fe is relatively light element, we were surprised to observe that approximately considered relativistic effect enhanced EE of Fe by about 0.3 eV. Now, we present newly obtained more accurate results which confirm our previous experience. Nonrelativistic, scalar relativistic and relativistic results including the SO contribution are compared with experimental energy splitting between the ^{5}D ground state and the first excited ^{5}F state of the Fe atom in Fig. 5.3. The NR value was calculated by the MRCI–SD method using the ANO–L–VQZP basis set [293]. REL represents the scalar relativistic DKH MRCI–SD value and the SO column represents the spin–orbit effect included via the RASSI–SO method [102]. Both REL and SO values were calculated with the relativistic ANO–RCC–VQZP basis set [106]. Clearly, the scalar relativistic effect alters the excitation energy of Fe significantly. Neglecting SO effects exaggerates the relativistic correction with re-

Tab. 5.4. Electron affinity of the PbO molecule [eV]. Data from Ref. [286].

Method	DKHsf	BSSsf	DCsf	BSS	DC
Pol–DK basis					
SCF	0.182	0.180	0.178	0.312	0.307
CCSD(T)^a(700)	0.377	0.382	0.380	0.594	0.584
ANO-RCC basis					
SCF	0.160	0.157	0.156	0.291	0.285
CCSD(T)^a(10)	0.463	0.470		0.696	
CCSD(T)^a(700)	0.466				
CCSD(T)^a(10)^b		0.472		0.696	
contracted ANO-RCC basis					
CASPT2/RASSI-SO^c	0.607^d			0.659	
Experiment^e					0.714

^{a} Values in parentheses denote energy limit [a.u.] of deleted virtual orbitals.
^{b} PbO and PbO$^-$ molecules are in the CCSD(T) optimized distances. Otherwise experimental geometries are used.
^{c} Used the spin–free CASPT2/SOC–CASPT2 optimized distances.
^{d} Result neglecting the spin–orbit coupling.
^{e} The given EA$_e$ value is recalculated from the adiabatic EA$_0$ value of 0.722 eV from Ref. [287], using experimental values of ω_e.

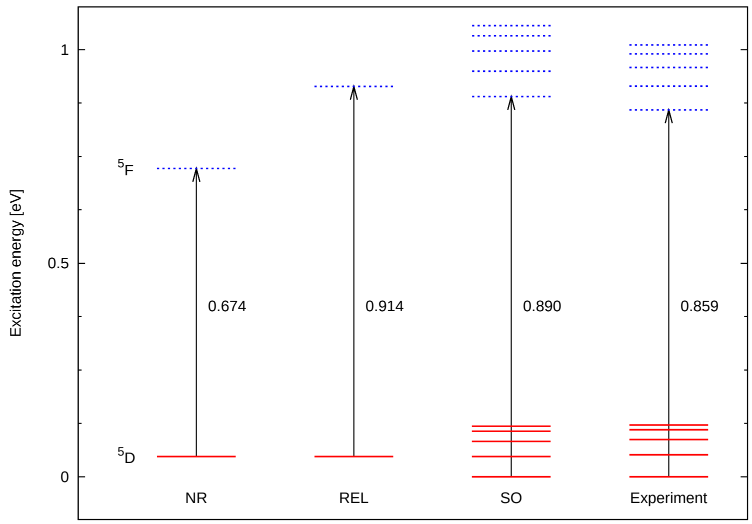

Fig. 5.3. Comparison of calculated nonrelativistic, spin–free relativistic, spin–orbit relativistic and experimental values of excitations between the two lowest electronic terms of the Fe atom. Data from Ref. [288].

spect to experiment. Proper treatment of both scalar relativistic and SO effects leads to very good agreement of theoretical values with experiment. More quantitative account is presented in Tab. 5.5 in which we collect excitation energies of individual spectroscopic levels of these two

Tab. 5.5. Spin–orbit splitting for the two lowest electronic terms of the Fe atom [cm^{-1}]. Data from Ref. [288].

Configuration	Term	J	level	
			RASSI-SO	experiment[a]
$3p^6 3d^6 4s^2$	^{5}D	4	0	0
		3	382	416
		2	669	704
		1	860	888
		0	956	978
$3p^6 3d^7 (^4\mathrm{F}) 4\mathrm{s}$	^{5}F	5	7 180	6 928
		4	7 657	7 376
		3	8 040	7 728
		2	8 326	7 986
		1	8 517	8 155

[a] Ref. [289].

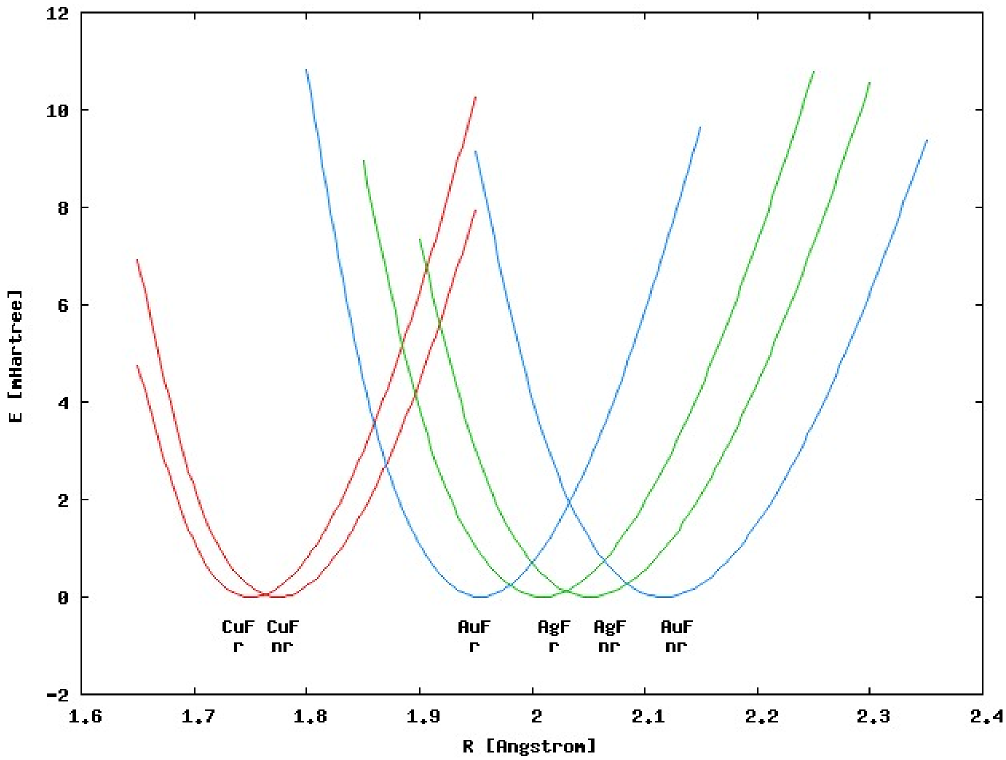

Fig. 5.4. Contractions of bond lengths in coinage metal fluorides due to relativistic effects.

electronic terms. The calculated total spin–orbit splitting for the ground state term ^{5}D differs from experiment by 22 cm^{-1} and for the ^{5}F term by 110 cm^{-1}.

5.2 Relativistic effects on molecular geometries

One can easily understand that due to the relativistic shrinking and expanding of orbitals participating in molecular bonds, due to the shift of orbital energies and other effects, as mentioned already in Section 1, molecular geometries must also undergo changes due to relativistic effects. A simple example (which, nevertheless reflects the situation in many other cases) is presented in Fig. 5.4. Here are depicted contractions of bond lengths in coinage metal fluorides due to relativistic effects calculated by the IOTC–CCSD(T) method with 18 electrons correlated. There were used completely uncontracted Pol basis sets for coinage metals [254] and for fluorine [245]. While for CuF the contraction is 0.02 Å, for AuF it is already 0.17 Å. This leads to the fact that the bond length of AuF is much shorter than that of AgF, which is clearly against trivial "non-relativistic" expectations and fully in line with other effects (like relativistic effects in IP and EA discussed in the preceding Section), which follow from the relativistic contraction and stabiliza-

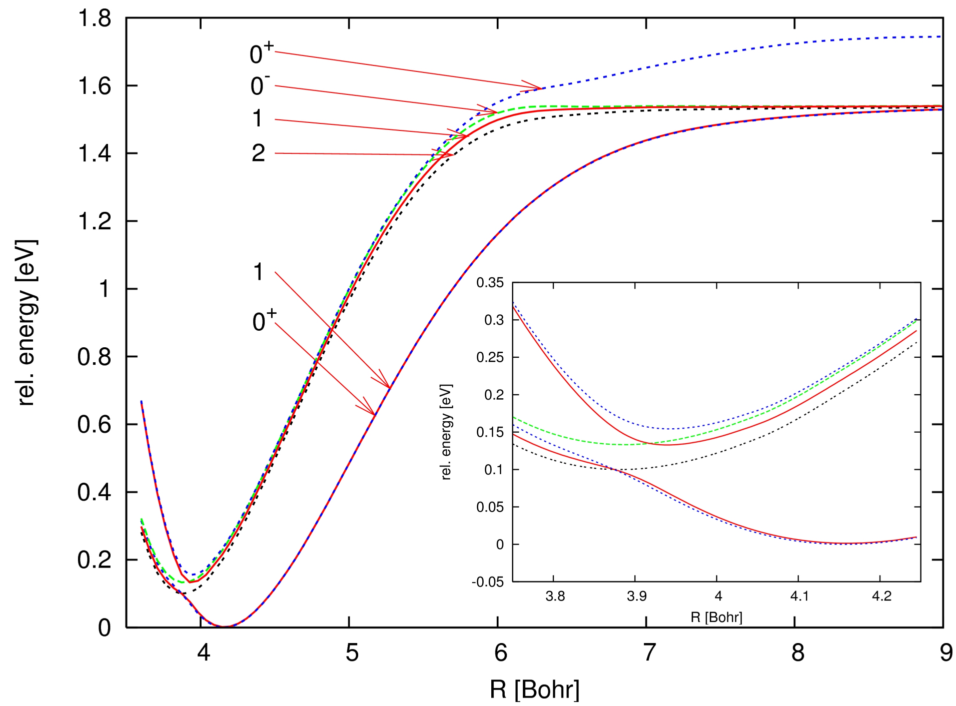

Fig. 5.5. Potential energy curves of the InN molecule calculated by the RASSI–SO method. Taken from Ref. [294].

tion of valence $6s$ electrons of gold. Of course, relativistically altered potential energy curves alter vibrational frequencies as well.

More complicated are the potential energy curves of the InN molecule with relatively light In atom. In Fig. 5.5 we present potential energy curves of the ground $X^3\Sigma^-$ state and the low–lying $^3\Pi$ state of InN. Six different relativistic SO states arise from the $^3\Pi$ and $^3\Sigma^-$ states of InN: 2, 1, 0^+ and 0^- (corresponding to the $^3\Pi$ state) and 1 ,0^+ (corresponding to the $^3\Sigma^-$ state). In Tab. 5.6 we also present basic spectroscopic constants of this molecule, the electronic equilibrium bond length R_e, the harmonic vibrational frequency ω_e, and the excitation energy T_e. The relativistic ground state is 0^+, with almost the same R_e and T_e as for the spin–free ground state $^3\Sigma^-$. Two avoided crossings, corresponding to 1 and 0^+ states can be seen in Fig. 5.5. Without these crossings the spin–orbit effects on the InN molecule would be negligible. Instead, three pairs of similar states are produced. The first pair includes two lowest states 0^+ and 1, with spectroscopic properties being very close to the $^3\Sigma^-$ state. The second pair (2, 0^-) is not affected by the avoided crossings, leading to almost the same R_e and ω_e as in the $^3\Pi$ state. The third pair includes second 0^+ and 1 states, which have avoided crossings in the vicinity of their their minima. Their properties are thus strongly affected by these crossings. Bond lengths of these states are closer to the $^3\Pi$ state than to $^3\Sigma^-$, but the respective harmonic frequencies are higher by 220–330 cm^{-1} when compared to both spin–free low–lying states. This feature can be clearly seen in Fig. 5.5, avoided crossing leads to the narrower potential energy curves.

5.3 Electric properties – dipole moments and dipole polarizabilities

Calculations of electric properties in general can be performed in two different ways, either as an expectation value of the given operator or by so called derivatives methods. *Conditio sine qua non* to apply the first method is to have a wave function which satisfies the Hellmann–Fyenman theorem [51]. This is fulfilled for, *e.g.*, variational wave functions in which all parameters are fully optimized (like in SCF or CASSCF methods). When using correlated methods, only the full CI or CC with all excitation operators guarantees that the Hellmann–Fyenman theorem is satisfied. This is possible only for really small molecules. For more realistic applications we are very rarely dealing with wave functions fulfilling this theorem. Therefore, even when using highly sophisticated correlated methods we are usually relying on energy derivatives methods (numerical or analytical) with respect to the external perturbation which defines the pertinent property. The analytical derivatives methods need derivatives of atomic and molecular one– and two–electron integrals and excitation amplitudes with respect to the external field. There are many well elaborated methods of this category, see, *e.g.*, Refs. [39, 40]. Analytical derivatives may be a problem for some relativistic operators. Generally applicable and straightforward is the so called finite field method [37] which exploits the expansion of the energy with respect to an electric external field, F_a (or, for some properties, also other external fields) along the a–direction,

$$E = E^0 - \mu_i F_i - \frac{1}{2}\alpha_{ij}F_iF_j - \frac{1}{6}\beta_{ijk}F_iF_jF_k - \frac{1}{24}\gamma_{ijkl}F_iF_jF_kF_l - \cdots . \tag{5.1}$$

Tab. 5.6. Spectroscopic properties of the relativistic states of the InN molecule. CASPT2/RASSI–SO/ANO–RCC calculations[a]. Data from Ref. [294].

State	R_e (bohr)	ω_e (cm^{-1})	T_e (eV)
Spin-free relativistic results			
$X^3\Sigma^-$	4.163	447.3	-
$1^3\Pi$	3.884	522.3	0.111
SO results			
0^+	4.157	441.1	-
1	4.157	441.6	0.001
2	3.882	522.6	0.100
0^-	3.887	521.6	0.133
1	3.940	789.4	0.133
0^+	3.942	705.6	0.154

[a] Inactive orbitals $12a_1/5b_1/5b_2/2a_2$, active orbitals $7a_1/3b_1/3b_2/1a_2$,18 correlated electrons in CASPT2.

The first order properties like dipole and quadrupole moments, electric field gradient, *etc.* are calculated as the first order derivatives,

$$\mu_a = -\left(\frac{\partial E}{\partial F_a}\right)_{F_a=0} = -\frac{E(+F_a) - E(-F_a)}{2F_a}. \tag{5.2}$$

The second order properties like dipole, quadrupole polarizabilities, force constants, geometry derivatives of the first order properties, *etc.* are calculated as the second order derivatives, *e.g.*,

$$\alpha_{aa} = -\left(\frac{\partial^2 E}{\partial F_a^2}\right)_{F_a=0} = -\frac{E(+F_a) + E(-F_a) - 2E(0)}{2F_a^2}. \tag{5.3}$$

In this way we can calculate also first and second hyperpolarizabilities. We would like to stress the importance of theoretical and computational methods in this area since particularly nonlinear optical properties are frequently not available from experiment. One problem with the finite–field method is a numerical accuracy which depends on the careful selection of the intensity of an external field. It should be small enough to avoid contamination by higher order properties, so that the accuracy with which the energy is calculated must be very high. For accurate calculations the series of fields with different strength and more complicated numerical derivative methods must be used.

In this Section we will document the impact of relativistic effects on dipole moments and polarizabilities. First, we should mention that when calculating atomic and molecular electric properties, two– and one–component relativistic methods suffer from the change of picture effect, see Section 4.6.4. Tab. 5.7 gives example of the magnitude of this effect in the case of dipole moments of coinage metal hydrides. There is a growing relativistic contribution going from copper to gold. While the CCSD(T) value, with the change of picture effect included, for Cu

Tab. 5.7. Change of picture effect on dipole moments of CuH, AgH, and AuH [a.u.]. Data from Ref. [257].

Method		μ_e		
		CuH	AgH	AuH
Nonrelativistic results				
SCF		1.593	1.808	1.660
CCSD(T)		1.136	1.362	1.223
Relativistic results				
DKH–SCF	no-CP[a]	1.519	1.588	0.830
DKH–SCF	CP[b]	1.526	1.618	0.980
DKH–CCSD(T)	no-CP[a]	1.042	1.102	0.400
DKH–CCSD(T)	CP[b]	1.052	1.135	0.522

[a] Douglas–Kroll–Hess calculations with the change of picture not included.
[b] Douglas–Kroll–Hess calculations with the change of picture included.

was diminished by 7%, for Au it was 57% already. The electron correlation effect is significantly more uniform here and accounts for 30% to 47%. The change of picture effect is rather small here, what is a typical behaviour of valence–determined properties. Compare it with electric field gradients, Section 5.4, where it is a serious issue.

Dipole moments of GeO, SnO, and PbO are collected in Tab. 5.8. Before we will concentrate on relativistic effects throughout the group we note that the lowering of dipole moments due to the electron correlation is more important than are relativistic effects. Quite small relativistic change of the dipole moment of PbO is particularly surprising. As it is usually the case, the electron correlation and the relativistic effects are not additive [295]. In general, the agreement of theoretical and experimental results is good, especially for GeO. Dipole moments for SnO and PbO are systematically lower than experimental ones by about 5.9% and 3.8%, respectively. The spin–orbit effect is rather small even for PbO, as it follows from results obtained by Roos and Malmqvist [297]. Theoretical values presented in Tab. 5.8 are uncorrected for vibrational effects, but their accuracy is still sufficient for discussion of trends within the group of molecules.

Good agreement of theoretical dipole moments with experiment gives some confidence to theoretical polarizabilities presented in Tab. 5.9. For GeO and SnO experimental data are missing. The only experimental values are available for PbO from the optical measurements for the

Tab. 5.8. Dipole moments of GeO, SnO, and PbO [a.u.]. Data from Ref. [21].

Method[a]	μ_e		
	GeO	SnO	PbO
nr–CCSD(T)	1.263	1.565	1.669
DKH–SCF	1.681	2.114	2.374
DKH–CCSD(T)	1.280	1.598	1.764
Experiment[b]	1.291	1.70	1.83

[a] The HyPolf basis set, which is the HyPol set extended by two f functions, was used, see Ref. [295]. In DKH calculations bases with the DKH contractions were used.
[b] Ref. [296].

Tab. 5.9. Dipole polarizabilities of GeO, SnO, and PbO [a.u.]. Data from Ref. [21].

Method[a]	α_{zz}			α_{xx}		
	GeO	SnO	PbO	GeO	SnO	PbO
nr–CCSD(T)	40.52	57.18	65.76	28.23	40.34	45.85
DKH–SCF	35.02	47.89	53.39	28.19	37.19	34.97
DKH–CCSD(T)	40.33	56.29	62.55	27.62	37.75	37.46

[a] See footnote in Tab. 5.8.

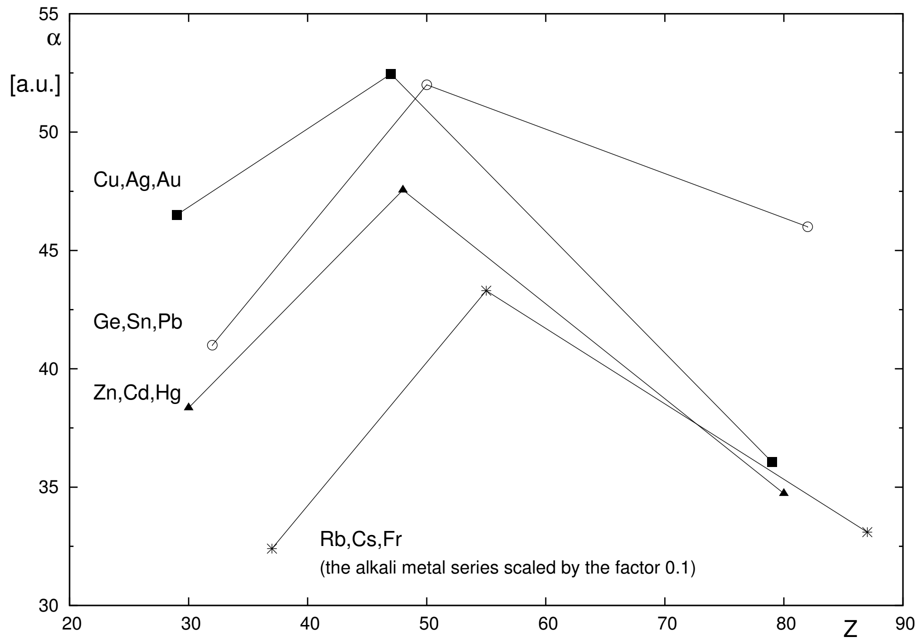

Fig. 5.6. Theoretical atomic dipole polarizabilities, relativistic effects included. Data from Refs. [16, 33, 258, 259, 277].

solid state [298]. As with dipole moments of all the group 14 oxide molecules, parallel component of the polarizability is less affected by relativistic effects than by the electron correlation. The electron correlation for α_{zz} of PbO (9.16 a.u. or 14% of the final DKH–CCSD(T) value) is almost three times larger than is the scalar relativistic effect for α_{zz} of PbO (3.21 a.u. or 5.1% of the final DKH–CCSD(T) value). Again, as with dipole moments, the signs of electron correlation and relativistic effects, respectively, are opposite. Similar compensation of relativistic and electron correlation effects is observed in calculations of α_{xx}. This time, however, the α_{xx} component of the PbO polarizability is more affected by scalar relativistic effects than by the electron correlation. Indeed, results in Tab. 5.9 show, that relativistic effects lower α_{xx} of PbO by 8.39 a.u. (22.3% of the final value) at the CCSD(T) level. With the electron correlation α_{xx} increases by 2.49 a.u. Both relativistic and electron correlation effects in α_{xx} of GeO and SnO are much smaller than in PbO but relativistic effects remain more important than are correlation effects even for the molecules containing relatively lighter atoms.

The appearance of the non monotonic pattern of, *e.g.*, atomic dipole polarizabilities, is quite general. Fig. 5.6 shows polarizabilities for the group 1, 11, 12, and 14 elements (we restrict ourselves to the three heaviest elements in each group). We note that the pattern of polarizabilities is the same for all four groups. Since all elements in the Zn, Cd, and Hg group and in the Rb, Cs, and Fr groups have similar valence electronic structure (valence s–electrons) as the group 11 elements, the interpretation of the pattern remains the same. The group 14 elements are characterized by the valence np^2 electronic structure. For these elements, especially for properties of Pb, the spin–orbit interaction can not be ignored. Polarizabilities of Ge, Sn, and Pb were taken from the review of Schwerdtfeger [16]. In this review the discussion on polarizabilities in the spin–orbit split states can be found. The SO contribution to the dipole polarizability is known also for the group 1 elements, even if estimated at the uncorrelated level [277]. Dirac–Hartree–Fock calculations revealed that the spin–orbit contribution to the polarizability of Rb is negligible. The SO coupling lowers the polarizability of Cs very slightly, by 2.7 a.u., while for Fr its magnitude is 13.0 a.u. It further supports the tendency to the non monotonic pattern. In any case these values are too small to affect our discussion of the general trends within the group 11 elements. To proceed further, Lim *et al.* [277] calculated the polarizability of the superheavy element 119. It is as low (185 a.u.) as the polarizability of the Na atom (165 a.u.). The SO contribution is not negligible but still no larger than 16 a.u. Electric dipole polarizabilities of the halogen atom in the $^2P_{1/2}$ and $^2P_{3/2}$ spin–orbit split states have been investigated by Fleig and Sadlej [299]. They used the two–component variational treatment and showed that for heaviest homologues it is necessary to replace averaged values by individual component polarizabilities. Calculations of electric properties for separated atomic SO states are rather unique. Full account of atomic polarizabilities throughout the Periodic Table was reviewed by Schwerdtfeger [16]. His analysis shows that the group 1 elements have the largest polarizabilities, followed by the group 2 elements polarizabilities. The polarizability then decreases within one period of the Periodic Table.

The trend for polarizabilities of the group of the coinage metal cations is shown in Fig. 5.7. After ionization, the valence electronic structure in all these cations is (n-1)d^{10}. Valence d–electrons are relativistically destabilized and, consequently, their polarizabilities increase [254, 258]. The same trend is observed in the group of CuF, AgF and AuF molecules. Analogous arguments are used in the explanation of trends in the group RbF, CsF, and FrF. However, the valence electronic structure of their metal element cations corresponds to the noble gas element and is (n-1)p^6. Valence p–electrons are relativistically stabilized, and the polarizability of Rb^+, Cs^+, and Fr^+ ions relativistically decreases. The same trend is, again, observed in polarizabilities of RbF, CsF, and FrF molecules. Analogous interpretation, with some reservation, is also valid for GeO, SnO, and PbO molecules. Polarizabilities of these molecules also increase monotonically with an increasing atomic number of the metal element, Tab. 5.9. If we could interpret these molecules as ionic species with the charge of the metal Me^{2+}, the polarizability of PbO should decrease by relativistic effects much more than it is observed in Tab. 5.9. The valence electronic structure of the Ge^{2+}, Sn^{2+}, and Pb^{2+} ions is ns^2np^0. These electrons are relativistically stabilized and their polarizabilities relativistically decrease [295] (like in isoelectronic elements Zn, Cd, and Hg, Fig. 5.6). This is qualitatively in line with relativistic effects in GeO, SnO, and PbO, but the effect in ions is larger and the Z dependence is not monotonic. The change of α_{zz} polarizability due to relativistic effects in PbO is 3.21 a.u., while in Pb^{2+} it is 7 a.u. This quantitative discrepancy is explained by the fact, that PbO can not be completely represented as $Pb^{2+}O^{2-}$; the charge on participating atoms is actually lower. This can be supported by the Mulliken population analysis (with all the reservation to any interpretation based on the HF orbital picture) which shows that there is the charge transfer of about 1.5 electrons from the metal atom to the oxygen atom. We note that the polarizability of the O^{2-} anion is estimated by DKH–CCSD(T) as 75.3 a.u.

To demonstrate the trends of dipole moments for a series of a heavy metal element contain-

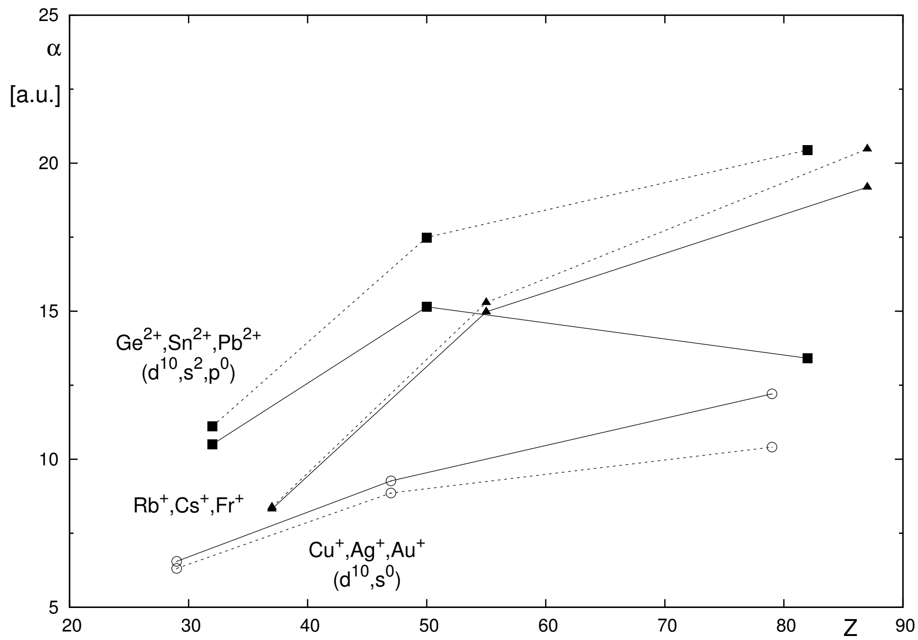

Fig. 5.7. Nonrelativistic (dashed lines) and DKH (full lines) dipole polarizabilities of ions calculated in the CCSD(T) approximation using the Pol family bases. Data from Ref. [21].

ing molecules we will discuss data in Fig. 5.8 for CuF, AgF, AuF, and the series of inter metallic compounds, CuAl, AgAl, AuAl. Relativistically calculated dipole moments in the highly polar MeF series [300] (polarity is $Me^{(+)}F^{(-)}$) are much smaller than are their nonrelativistic counterparts. This should be related to the relativistic increase of IP particularly for the gold element which hinders the charge transfer from the metal element to fluorine, in spite of high electron affinity of the F element. The AuF molecule becomes less ionic due to relativistic effects which, in turn, reinforce the covalent character of the bond in AuF. Opposite situation is encountered in the MeAl series [255]. The polarity at the CCSD(T) level is $Me^{(-)}Al^{(+)}$ in this case. Consequently, huge relativistic increase of the electron affinity supports enhanced polarity of all MeAl molecules, particularly of AuAl. We note that the convention used within this review is that if the left atom of a diatomic molecule has a positive charge and the right–hand atom is negative, the dipole moment has a positive sign. It should be mentioned here, that experimentalists have problems to determine the sign of the dipole moment. Recently, Gijsbertsen *et al.* [301] reported a novel experimental direct approach for determining the sign of permanent dipole moments. Of course, in calculations of theoreticians there are no problems to get the sign.

The number of chemical elements is increasing considerably. The heaviest, man–made elements at the far–end of the Periodic Table are located in the area of the long–awaited superheavy elements [303]. From the theory follows that these heavy elements should exhibit largest relativistic effects. It would be worthwhile to look at it. In Tab. 5.10 we presented CCSD(T)

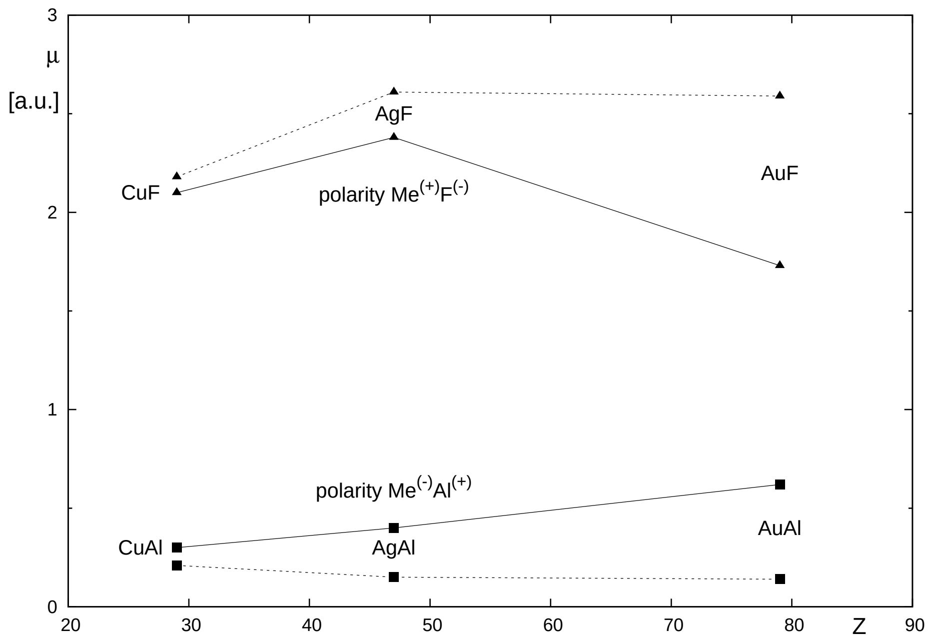

Fig. 5.8. Nonrelativistic (dashed lines) and DKH (full lines) dipole moments of the MeF and MeAl (Me = Cu, Ag, Au) series calculated in the CCSD(T) approximation using the Pol family bases. Data from Ref. [22].

calculations of dipole moments for superheavy–elements hydrides. There are manifested two interesting features. The total relativistic effect for s–block element hydrides 111H and 119H is considerable larger than for p–block element hydrides 113H and 117H, while the spin–orbit effect is larger for p–block element hydrides. The explanation of these two opposite effects is rather simple. The largest relativistic contraction is for s–orbitals and, naturally, the spin–orbit coupling should be larger for p– than for s–orbitals.

Tab. 5.10. Dipole moments of superheavy elements hydrides [a.u.] icalculated at the CCSD(T) level of approximation. Data from Ref. [302].

Method	μ_e			
	111H	113H	117H	119H
Nonrelativistic	1.658	0.322	-0.028	3.633
Scalar relativistic	0.055	0.971	0.243	2.159
Dirac–Coulomb	0.005	-0.026	0.765	2.205

5.4 Determination of nuclear quadrupole moments

All nuclei with the nuclear spin $I \geq 1$ have nonzero nuclear quadrupole moments Q, which means that the electric charge is not spherically symmetric. The knowledge of reliable nuclear quadrupole moments is of considerable interest in nuclear physics for testing nuclear models for stable isotopes and also in chemical and solid state spectroscopy [304, 305].

The electric field at the given nucleus X produced by all electrons and other nuclei of the molecule is not uniform and has a non–vanishing electric field gradient q. For quadrupolar nuclei this leads to the interaction between nuclear quadrupole moment Q of the nucleus X and the electric field gradient q resulting from the distribution of other charges. This interaction might be observed as splittings of lines in atomic spectra [306], microwave rotational spectra of molecules [307], and nuclear quadrupole resonance or Mössbauer spectra of solid state systems [308]. The measured value of the $Q - q$ interaction is often called the nuclear quadrupole coupling constant ν_Q. The electric field gradient q, which from the point of view of the given nucleus is a measure of the inhomogeneity of the external electric field of all other charges, is therefore a molecular property of the first order and can be determined from the knowledge of the electronic wave function and positions of nuclei. Thus combination of experimental nuclear quadrupole coupling constant and theoretical electric field gradient provides us with nuclear quadrupole moment values. This is the currently best way [304,305,309], at least for light elements. According to the source of the experimental data, the nuclear quadrupole moment values are referred to as: atomic, molecular or solid–state. Another approach was the mesonic method, based on measuring the hyper–structure of essentially Coulombic energy levels of μ or π mesons near the nucleus. No such experiments have been published for more than two decades, however, these mesonic nuclear quadrupole moment values still stand as the benchmarks for heavier elements [304, 305]. Low–precision determinations of Q are also available from nuclear Coulomb scattering, nuclear rotational energy levels and from nuclear theory [304, 305].

To obtain the nuclear quadrupole moment of the given nucleus we can either calculate the electric field gradient for the given atom and to combine it with experimental data of the nuclear quadrupole coupling constant of given atom or calculate the electric field gradient at the given nucleus in a molecule, preferably diatomic, for which the nuclear quadrupole coupling constant is available. From the computational point of view the highest accuracy of the electric field gradients can be achieved in atomic calculations. The spherical symmetry greatly simplifies the computational problems and permits to go much beyond the present accuracy limits in molecular calculations. Of course, a special computer code for atoms is required. On the other hand, the atomic nuclear quadrupole coupling constants are usually known with rather low accuracy due to the significant line broadening and the high accuracy of the electric field gradient may not be very helpful.

In this review we will concentrate ourselves on molecular values of the nuclear quadrupole moment since we have been involved in these calculations for two decades [220, 310–324]. In contrast to the atomic experimental data the nuclear quadrupole coupling constant of the nucleus determined from molecular rotational spectra are usually of very high accuracy. In order to profit from this advantage of the molecular microwave spectra it is necessary to calculate electric field gradient values with a very high accuracy also, which might be very tough task, even for diatomic molecules.

The nuclear quadrupole moment Q(X) of the quadrupolar nucleus X in a diatomic molecule in the vibrational state v with the z–axis along the bond becomes (in milibarns; $1\mathrm{mb} = 10^{-31}\ \mathrm{m}^2$)

$$Q(\mathrm{X}) = \frac{\nu^{\mathrm{X}}(v)}{0.2349647 q^{\mathrm{X}}(v)}, \tag{5.4}$$

where $\nu^{\mathrm{X}}(v)$ is the nuclear quadrupole coupling constant for the nucleus X and the vibration state v given in MHz, and $q^{\mathrm{X}}(v)$ is the axial (zz) component of the electric field gradient tensor at the nucleus X and the vibration state v given in atomic units. The vibrational corrections to the equilibrium value of the electric field gradient are usually done via the approximate formula by Buckingham [325]

$$q^{\mathrm{X}}(v) = q_e^{\mathrm{X}} + q_{vib}^{\mathrm{X}} \approx q_e^{\mathrm{X}} + q_1^{\mathrm{X}} \left(v + \frac{1}{2}\right), \tag{5.5}$$

where $q_e^{\mathrm{X}} = q^{\mathrm{X}}(R_e)$ and

$$q_1^{\mathrm{X}} = \frac{B_e}{\omega_e}\left[3(1 + \frac{\alpha_e \omega_e}{6B_e^2})\left(\frac{\partial q^{\mathrm{X}}}{\partial \xi}\right)_{\xi=0} + \left(\frac{\partial^2 q^{\mathrm{X}}}{\partial \xi^2}\right)_{\xi=0}\right]. \tag{5.6}$$

The symbols ω_e, B_e, and α_e denote the usual spectroscopic constants in cm^{-1} taken from experiment [296] and $\xi = (R - R_e)/R_e$. This formula requires only the knowledge of the first and second order derivatives of q with respect to the interatomic distance R evaluated at R_e.

The methodology of calculating electric field gradient at the nucleus X in a diatomic molecule at the equilibrium bond distance R_e is based on partitioning of the total value to individual contributions. First, it is expressed as a sum of the electronic contribution, $q_{e,\mathrm{el}}^{\mathrm{X}}$ and the nuclear one, $q_{e,\mathrm{nucl}}^{\mathrm{X}}$

$$q_e^{\mathrm{X}} = q_{e,\mathrm{el}}^{\mathrm{X}} + q_{e,\mathrm{nucl}}^{\mathrm{X}}. \tag{5.7}$$

Further, the electronic term is divided into Hartree–Fock, $q_{e,\mathrm{HF}}^{\mathrm{X}}$ and electron correlation $q_{e,\mathrm{corr,M}}^{\mathrm{X}}$ contributions

$$q_{e,\mathrm{el}}^{\mathrm{X}} = q_{e,\mathrm{HF}}^{\mathrm{X}} + q_{e,\mathrm{corr,M}}^{\mathrm{X}}. \tag{5.8}$$

In order to reach the required accuracy, highly sophisticated electron correlation methods have to be used. The CCSD(T) method what is a coupled cluster approximation with iterative solution for T_1 and T_2 amplitudes (CCSD) with noniterative T_3 amplitudes [40] is the method of the choice in this area [305]. Later we will discussed also a role of the T_3 contribution $q_{e,\mathrm{corr,T_3}}^{\mathrm{X}}$

$$q_{e,\mathrm{corr,CCSD(T)}}^{\mathrm{X}} = q_{e,\mathrm{corr,CCSD}}^{\mathrm{X}} + q_{e,\mathrm{corr,T_3}}^{\mathrm{X}}. \tag{5.9}$$

5.4.1 Change of picture

Inclusion of relativistic effects in calculation of electric field gradients is inevitable. If one– or two–component relativistic methods (*e.g.* DKH, IOTC) are exploited, the usual method of

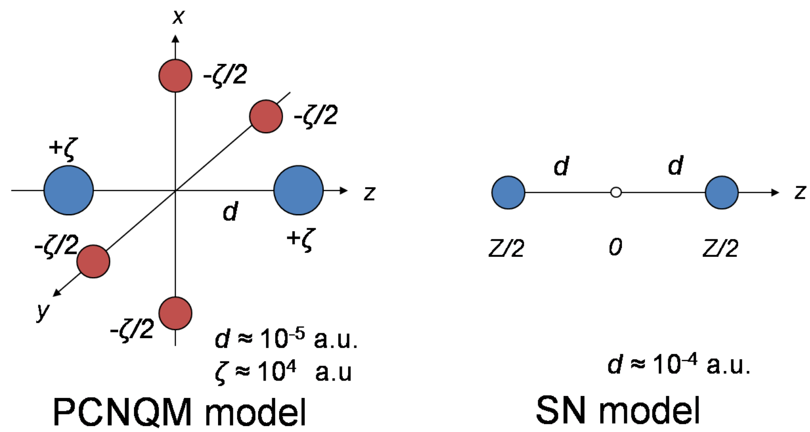

Fig. 5.9. The point charge nuclear quadrupole moment (PCNQM) model [329] and shifted nucleus (SN) model [321].

computing expectation values, which is just a counterpart of the nonrelativistic scheme leads to the change of picture effect [220, 221] manifested by significant inaccuracies of the calculated property values. The physical background of this effect was mentioned in Section 4.6.4 already. The way how to overcome this obstacle is to properly transform also the electric field gradient operator. Reiher *et al.* recently published such calculations [326–328].

Of course, computing expectation values of properties is relevant only if our wave function satisfies Hellmann–Fyenman theorem. If this is not the case we can use the finite field method, see Section 5.3. Pernpointer *et al.* [329] proposed a numerical procedure, named the point charge nuclear quadrupole moment (PCNQM) model, which might be easily used within finite field calculations. The PCNQM model is based on placing a finite nuclear quadrupole moment built of 6 point charges in the octahedral arrangement in the nearest vicinity of the nucleus, see Fig. 5.9. Such artificial quadrupole moment Q placed at the nucleus typically is of the order 10^{-6} a.u., and its interaction energy with the electric field gradient at the nucleus represented by the axial component q_{zz}^{X} is

$$U_{\mathrm{int}} = \frac{3}{2} Q q_{zz}^{\mathrm{X}} = \frac{3}{2} \zeta d^2 q_{zz}^{\mathrm{X}}. \tag{5.10}$$

In nonrelativistic calculations the PCNQM model does not seem to offer any particular advantages over the direct use of the perturbation. On the contrary, it brings a disadvantage of the determination of its two parameters, the value of point charges ζ and the distance of these point charges from the nucleus d, which requires a considerable amount of numerical testing. However, since the PCNQM model introduces a perturbation operator defined in terms of the usual nuclear–attraction operators, it becomes very useful in approximate relativistic calculations as a simple way to avoid the explicit change of picture transformation [330]. This appears to be the most important feature of the PCNQM model. However, the problem of the determination of the most suitable values of the two parameters, which might be in an interval $10^2 - 10^{11}$ a.u. for ζ and $10^{-4} - 10^{-6}$ a.u. for d remains.

Kellö and Sadlej proposed an alternative shifted nucleus (SN) model [321], which also removes the change of picture effect in one– and two–component relativistic methods. The idea of the SN model is to build up a small quadrupole moment by splitting the original nuclear charge Z into two halves and shifted them by a small distance, see Fig. 5.9. If $\mathrm{E}_\mu(d^2)$ denotes the energy calculated with $V_\mu(d^2)$, $\mu = x, y, z$, *i.e.*, with the shifts of half–charge nuclei along the μ–th direction, the value, q_{zz}, of the field gradient operator will be given by:

$$q_{zz}^{\mathrm{X}} = -\frac{4}{3Z_{\mathrm{X}}}\left(\frac{\partial\Delta(d^2)}{\partial(d^2)}\right)_{d=0}, \tag{5.11}$$

where

$$\Delta(d^2) = E_z(d^2) - \frac{1}{2}[E_x(d^2) + E_y(d^2)] = a_1 d^2 + a_2 d^4 + \dots \tag{5.12}$$

can be approximated by fitting to a polynomial in d^2. In the case of diatomic molecules $E_x(d^2) = E_y(d^2)$ and in order to obtain the first derivative we have to perform two calculations, one for $E_z(d^2)$ and other for $E_x(d^2)$. Similarly in the PCNQM model, two calculations for two Q differing by the sign have to be carried out. The important difference between these two approaches is that while the PCNQM model requires two parameters (ζ and d), the SN model needs just one (d).

5.4.2 Examples of calculations

In the next paragraphs we will show and discuss a magnitude of the change of picture effect in approximative relativistic calculations. While the change of picture effect in valence–determined properties is rather small, see Tab. 5.7 in Section 5.3, this effect becomes very large for operators which assume large values in the vicinity of nuclei, *e.g.*, electric field gradient. In Tab. 5.11 are collected calculated values of the q_{zz} component of electric field gradient of hydrogenic ions of rare gas atoms. In the column $q_{\mathrm{no-CP}}$ are the expectation values without the change of picture and in the column q_{CP} are values calculated using the PCNQM model, which takes into account the change of picture. While for $Z = 9$ the difference between the no–CP and CP value is only 0.5%, we can see that going to $Z = 85$, this difference is almost 80%. Here we present values

Tab. 5.11. Change of picture effect on the electric field gradients in one-electron ions as calculated in DKH-SCF approximation [a.u.]. Data from Ref. [220].

Ion	Term	$q_{\mathrm{no-CP}}$	q_{CP}
Ne^{+9}	$2p^1,{}^2\mathrm{P}$	-33.614	-33.449
Ar^{+17}	$2p^1,{}^2\mathrm{P}$	-199.73	-196.58
Kr^{+35}	$2p^1,{}^2\mathrm{P}$	-1735.05	-1624.69
Xe^{+53}	$2p^1,{}^2\mathrm{P}$	-6777.89	-5760.44
Rn^{+85}	$2p^1,{}^2\mathrm{P}$	-44728.2	-25171.8

just for the lowest ^{2}P electronic state, where is the largest effect. In the original paper [220] are presented also values for higher electronic states.

Well, one can argue that hydrogenic ions are little bit artificial systems, so let us have a more ”chemical” example, hydrogen halides. In Tab. 5.12 are presented electronic contributions to electric field gradient at the halogen nucleus in hydrogen halides calculated within the DKH–SCF approximation. We can see that while for HCl the change of picture effect accounts for less than 1%, in the case of astatine it is 30% already. Of course, if we would calculate it nonrelativistically, there should be no differences between these two ways of the calculation.

In Tab. 5.13 are presented values of the electric field gradient for Br and I nuclei calculated within the CCSD(T) approximation with correlated 8 and 18 electrons. We can see that the change of picture amounts for 4% in HBr and for 9% for HI. This is precisely the same trend as for the SCF data presented in Tab. 5.12. Increase of the number of correlated electrons from 8 to 18 electrons has a marginal effect which is an indication of properly chosen active space. In the

Tab. 5.12. Change of picture effect on the electronic contribution to electric field gradients at the halogen nucleus in hydrogen halides as calculated in DKH–SCF approximation [a.u.]. Data from Ref. [220].

Molecule	$q_{\mathrm{no-CP}}$	q_{CP}
HCl	3.540	3.511
HBr	7.806	7.520
HI	12.657	11.683
HAt	34.621	26.656

Tab. 5.13. Values for the nuclear quadrupole moments of the ^{79}Br and ^{127}I nuclei. Data from Refs. [311, 320].

System		q [a.u.]	Q [mb]
^{1}H^{79}Br, (v=0)			
no-CP	CCSD(T) 8 el.	7.579	299
CP	CCSD(T) 8 el.	7.308	310
CP	CCSD(T) 18 el.	7.313	310
4–component CCSD(T)^a		7.035	322
Recommended value this work^b			313±3
^{1}H^{127}I, (v=0)			
no-CP	CCSD(T) 8 el.	11.935	-651
CP	CCSD(T) 8 el.	11.013	-707
CP	CCSD(T) 18 el.	11.038	-705
4–component CCSD(T)^a		10.751	-724
Recommended value this work^c			-710±10

^{a} Ref. [331].
^{b} Considering the atomic value of 314.
^{c} Considering the atomic value of -717.

paper by Bieroń *et al.* [320], which is the source of data for Tab. 5.13, are presented also atomic multiconfigurational Dirac–Fock calculations, which lead to the nuclear quadrupole moment data 314 mb for bromine and -717 mb for iodine. Taking into account both molecular and atomic values the 'recommended' value for ^{79}Br is 313±3 mb and for ^{127}I it is -710±10 mb. While the bromine value is still the 'recommended' one [305], for ^{127}I the present 'recommended' value is -696±12 mb by van Stralen and Visscher [332].

In Tab. 5.14 we want to show the effect of the electron correlation (20 electrons correlated), which amounts about 20%. There is also a rather large effect of triply excited configurations which is about 5%. Concerning this table it should be stressed that GeO and GeS represent completely independent sources of the data and thus the good agreement between Q obtained from these two diatomics supports a reliability of the new recommended value, -196±1 mb. The new value falls in the error bars of the older reference atomic value, however, it is shifted towards the upper bar.

Tab. 5.15 is a nice example how theoretical data on the nuclear quadrupole moment are improving during the years. In 1982 there was a muonic value of 150±6 mb. In 1984 Sundholm *et al.* [335] published atomic value 140.3±1.0 mb, which was rather off the muonic one. In 1999 we published a paper [313] in which molecular data calculated on systems AlF and AlCl were in a perfect agreement with new atomic calculations. The present recommended value is 146.6±1.0 mb.

In Tab. 5.16 are combined DKH–CCSD(T) with fully relativistic 4–component CCSD(T) calculations for ZrO. Using Dirac–Fock and DKH–SCF values calculated in the same basis set we estimated the spin–orbit contribution to the electric field gradient as -0.0056 a.u. For the nuclear quadrupole moment we got the value of 179 mb from DKH–CCSD(T) calculation on ZrO, while from 4–component CCSD(T) it was 176 mb. DKH–CCSD(T) value from ZrS is 173 mb. The reference atomic values are significantly higher. Our present recommended value is set to 176±3 mb.

Tab. 5.17 represents another interesting "time dependence" of nuclear quadrupole moment values. The old ^{121}Sb atomic value of Murokawa from 1955 was -530±100 mb [344], the 2001–

Tab. 5.14. Values for the nuclear quadrupole moment of the ^{73}Ge nucleus. Data from Ref. [314].

System	$\nu_Q{}^a$ [MHz]	electronic^b contributions to q [a.u.]			Q [mb]
		DKH-SCF	DKH-CCSD	DKH-(T)^c	
^{73}Ge^{16}O, $(v=0)$	208.33	-6.332	0.947	0.335	-195
^{73}Ge^{32}S, $(v=0)$	186.72	-5.742	0.861	0.289	-197
Reference 'atomic' value^d					-173±26
Present recommended value					-196±1

^{a} Data from Ref. [333].
^{b} Nuclear contributions to q are 0.533 and 0.582 for GeO and GeS respectively.
^{c} Contribution of noniterative triples.
^{d} Ref. [334].

Tab. 5.15. Values for the nuclear quadrupole moment of the ^{27}Al nucleus. Data from Ref. [313].

System	$\nu_Q{}^a$ [MHz]	q^b [a.u.]	Q [mb]
'Molecular' values			
^{27}Al^{19}F, R_e	-37.75±0.08	-1.099	146.2
^{27}Al^{19}F, $(v = 0)$	-37.53±0.12	-1.091	146.4
^{27}Al^{35}Cl, $(v = 0)$	-30.4081±0.0027	-0.879	147.2
^{27}Al^{37}Cl, $(v = 0)$	-30.4112±0.0028	-0.879	147.2
'Atomic' value			
^{27}Al(^{2}P$_{3/2}$)	18.91526±0.0007	-0.5493	146.6
Reference 'atomic' value^c			140.3±1.0
Reference 'muonic' value^d			150±6
Present recommended value			146.6±1.0

^{a} The molecular data from Refs. [333, 336] and the atomic data from Refs. [337, 338].
^{b} Molecular values are of DKH–CCSD(T) quality, atomic ones are relativistically corrected numerical MCHF calculations.
^{c} Ref. [335].
^{d} Ref. [339].

Tab. 5.16. Values for the nuclear quadrupole moment of the ^{91}Zr nucleus. Data from Ref. [316].

System	$\nu_Q{}^a$ [MHz]	q [a.u.]	Q [mb]
^{91}Zr^{16}O, $(v = 0)$	130.5499±0.0046	-3.11^b	-179
		-3.16^c ($\Delta_{\mathrm{SO}} = -0.0056$)	-176
^{91}Zr^{32}S, $(v = 0)$	116.4609±0.0047	-2.86^b	-173
Reference 'atomic' values			-206±10^d
			-257^e
			-230±20^f
Present recommended value			-176±3

^{a} Data from Ref. [340].
^{b} The DKH–CCSD(T) values, 28 respectively 34 electrons correlated.
^{c} The 4–component CCSD(T) values.
^{d} Ref. [341].
^{e} Ref. [342].
^{f} Ref. [343].

year standard [304] value is 360±40 mb, and in 2003 has appeared a solid state value of -669±15 mb [345]. In 2005 Steve Cooke sent us new experimental antimony nuclear quadrupole coupling constant values for diatomics SbN, SbP, SbF, SbCl [346, 347]. So we did CCSD(T) calculations of electric field gradient with scalar relativistic effects covered by the spin–free IOTC method, which led to our recommended value with rather conservative error bars of -556±24 mb. Just few months later Haiduke *et al.* published paper [348] based on the same experimental nuclear quadrupole constants [346, 347] and DC–CCSD–T electric field gradient calculations. Their recommended value is -543±11 mb in a perfect agreement with our result and considerably different from 2001 and 2003 values. Since Haiduke *et al.* used the fully relativistic method and have a lower error limit, their value was adopted by Pyykkö as the 2008–year standard [305]. It is amusing that old Murakawa's value [344], of course within its very large error bars, agrees with it.

So far we did not discussed questions concerning the basis set choice, which is a crucial issue in electric field gradients calculations. Usually completely uncontracted Gaussian function basis sets are exploited. In calculations presented in this review extended even tempered basis sets based on Huzinaga and Klobukowski paper [349] were used. In Tab. 5.18 is presented a basis set dependence study for calculation of the electric field gradient at the nitrogen nucleus in the NP molecule [324]. We can say that the phosphorous atom is a "spectator" atom here and nitrogen is an "actor" atom. The "spectator" atom basis is rather fast saturated, there is very little effect going from the B set to C set on phosphorous, while extending the C set of nitrogen is significant. Let us discuss behaviour of the "actor" basis set. Going from the E set to H set of the "actor" brings the q contribution of -0.0026 a.u., while using the B or C set on the "spectator" brings no change. It has also been found that the atomic basis set for the "quadrupolar" atomic centre needs to be carefully augmented with high–exponent polarization

Tab. 5.17. Values for the nuclear quadrupole moment of the ^{121}Sb nucleus. Data from Ref. [323].

System	$\nu_Q{}^a$ [MHz]	q [a.u.]	Q [mb]
SbN	649.669	-5.199	-532
SbP	620.350	-4.931	-535
SbF	-586.802	4.407	-567
SbCl	-515.124	3.788	-579
1955 atomic value^b			-530±100
2001 "recommended" value^c			-360±40
2003 solid state value^d			-669±15
2006 IOTC-CCSD(T) value, this work			-556±24
2006 DC-CCSD-T value^e			-543±11

^{a} Refs. [346, 347].
^{b} Ref. [344].
^{c} Ref. [304].
^{d} Ref. [345].
^{e} Ref. [348].

functions. The rules established for valence properties do not apply in the case of electric field gradients. The consequence of this finding is that one needs to use very large basis sets on the "quadrupolar" centre. However, it has been simultaneously found that the diffuse part of the polarization subset used for the "quadrupolar" centre and the "spectator" atom is less significant. These findings give some guiding rules for the generation of basis sets for accurate calculations of electric field gradients in molecules.

The presented results clearly proved that accurate *ab initio* calculations of electric field gradients at nuclei in combination with nuclear quadrupole coupling constants obtained from microwave spectra are reliable source of nuclear quadrupole moments. This is an outstanding example of the synergy effect of experiment and theory in contemporary science.

5.5 Dissociation and reaction energies

Relativistic effects on dissociation and reaction energies are described in several reviews, see, *e.g.*, Refs. [9, 10, 19, 20, 350]. Relativistic effects may affect the structure of compounds, they lead to unusual thermochemistry and to relativistically controlled reactivity patterns, relativistically affected properties of atoms explain unexpected catalytic effects of heavy metals, they explain synthesis of interesting new compounds, including large inorganic complexes and nanostructures [351]. Particularly important and interesting is the role of relativistic effect in catalysis [20]. Remarkable is the gold chemistry, (particularly metal–metal bonding and other phenom-

Tab. 5.18. Basis set dependence of electric field gradient q calculated at N in the NP molecule [a.u.]. Data from Ref. [324].

Basis set on N	Basis set on P	q_{HF}	$q_{corr,\mathrm{CCSD(T)}}$	q^a
Study of the "spectator" atom basis set				
A-16s11p5d	A-19s14p7d	-2.7312	0.3103	-1.0793
C-16s12p7d6f	A-19s14p7d	-2.7385	0.3104	-1.0865
C-16s12p7d6f	B-19s14p9d8f	-2.7415	0.2973	-1.1026
C-16s12p7d6f	C-19s15p10d9f	-2.7416	0.2973	-1.1027
E-16s14p9d8f	B-19s14p9d8f	-2.7114	0.2885	-1.0813
E-16s14p9d8f	C-19s15p10d9f	-2.7115	0.2885	-1.0814
E-16s14p9d8f	E-19s17p12d11f	-2.7115	0.2885	-1.0814
Study of the "actor" atom basis set				
C-16s12p7d6f	B-19s14p9d8f	-2.7415	0.2973	-1.1026
E-16s14p9d8f	B-19s14p9d8f	-2.7114	0.2885	-1.0813
H-16s15p12d11f	B-19s14p9d8f	-2.7079	0.2876	-1.0787
C-16s12p7d6f	C-19s15p10d9f	-2.7416	0.2973	-1.1027
E-16s14p9d8f	C-19s15p10d9f	-2.7115	0.2885	-1.0814
H-16s15p12d11f	C-19s15p10d9f	-2.7079	0.2876	-1.0787

^{a} The total value of q which includes the nuclear contribution 1.3416 a.u.

ena frequently described as the "aurophilicity", Au is considered sometimes as a pseudohalogen) [12, 13, 351–353]. Strong tendency of gold to form metal–metal interactions, particularly with electropositive ligands, which donate electron density to the relativistically contracted and stabilized the $6s$ orbital of gold, may lead to creation of remarkable complexes and nanostructures [351].

In the first part of this Section we will show the importance of scalar relativistic effects using an example of a series of bond dissociation energies (BDE) of simple coinage metal fluorides, MF and coinage metal aluminium molecules, MAl, with M=Cu, Ag, and Au. The interpretation of the magnitude of BDE and the effect of relativity on this basic molecular property will be based on previous information of relativistic effects on ionization potentials and electron affinities of the metal. We also employ the knowledge of the polarity of MF and MAl molecules as discussed in Section 5.3. Our selection of the two series combines molecules composed of a common coinage metal atom and atoms having very different electronegativities, namely the most electronegative atom, fluorine, with electron affinity as high as 3.40 eV, and aluminium with much lower EA, 0.441 eV. MAl molecules also serve as a group of intermetalics of great interest in materials sciences. Results of DKH–CCSD(T) calculations are collected in Tab. 5.19. For comparison, we present also BDE's of analogous diatomics, as mercury fluorides and oxides [354]. These results were obtained differently, by DFT calculations, with scalar relativistic effects calculated by the Normalized Elimination of the Small Component method (NESC) which is related to the DKH method. For AuF both methods give sufficiently similar results that allow to study the trends of BDE's of the whole series as presented in Tab. 5.19. Good agreement of DFT with CCSD(T) results also confirms the applicability of DFT in similar calculations which gives an argument for using these methods for interpretation and prediction of bonding situation in large molecules which are not amenable to sophisticated CC or other wave function calculations.

Understanding of the trends [21] in calculated D_e in the CuF, AgF, and AuF series [300], and another group, CuAl, AgAl, and AuAl [255], is facilitated by the analysis of relativistic contribution to BDEs, as shown in the sixth column of Tab. 5.19. We can follow essentially the same physical arguing as was used in our discussion on dipole moments and dipole polarizabilities. CuF, AgF, and AuF molecules have large dipole moment and the polarity is M^+F^-. CuAl, AgAl, and AuAl have small dipole moments and the polarity is opposite, M^-Al^+. The charge transfer between the metal and the ligand, like the polarity, is mainly determined by the electronegativity of participating elements. Some other aspects, particularly relativistic effects in the bond length should be considered as well. Using simple arguments, relativistic changes in D_e can be understood easily. Ionization potential of the coinage element, which determines the charge transfer to the fluorine relativistically increases, especially in gold, and hinders the charge transfer to the ligand. In accord with lower electron affinity of Al and the sign of the dipole moment of MAl, the charge transfer from aluminium to the coinage element in MAl molecules is supported by the relativistically increased electron affinity of M, especially gold. Thus, relativistic effects act in the two groups differently, *destabilizing* MF bonds and *stabilizing* MAl bonds. The relativistic destabilization of the AuF bond is very large, 0.46 eV. Enormous, however, is the relativistic stabilization in AuAl, 1.7 eV. This means that D_e is twice as large at the relativistic level in comparison with the nonrelativistic CCSD(T) result. Due to relativity, D_e of AuAl is even larger than that of AuF. Without considering relativistic effects, D_e of AuAl would be about half of D_e of AuF.

Up to now our main interest was focused on relativistic effects in this Section. Obviously, electron correlation must not be forgotten in the discussion of bond energies. Like as relativistic effects are unavoidable in understanding the underlying coinage metal properties, the one electron Hartree–Fock picture is completely useless in interpreting EA's and IP's of these species. Therefore, it is not surprising that the electron correlation plays so important role in BDE's in MeF and MeAl molecules. Electron correlation is essentially equally important in all molecules presented in Tab. 5.19. It behaves monotonically, always increasing the bond dissociation energy by about 1.35 – 1.55 eV in MF molecules and by 1.2 – 1.5 eV in MAl molecules. It is imperative that both, the electron correlation and relativistic effects must be considered at highly sophisticated level together, to avoid inaccuracies caused by the nonadditivity of both contributions.

Quantitative explanation of the pattern of dissociation energies of the coinage diatomic molecules can not be achieved solely by arguments used so far. Other effects, including the exchange repulsion which is connected with the relativistic shrinking of valence orbitals plays a role as well. Also, there is the difference in the bonding character in MeF and MeAl molecules. All are characterized by the bonding valence $\sigma(s\text{–}p)$ orbital. MeF bods are more ionic, which is demonstrated not only by larger dipole moments, but also by the dipole moment curves, which are almost linear [300] and correspond to what can be expected from the Coulomb law. Just AuF becomes more covalent and less polar due to the relativistically enhanced ionization potential of Au. The MeAl bonds are more covalent. Due to the stabilization of the metal valence s electrons, the valence MeAl σ orbital can be relativistically stabilized as well. This further contributes to the enhancement of D_e of MAl molecules, with M being a coinage metal.

Tab. 5.19. Electron correlation and scalar relativistic effects in dissociation energies ΔE_e[eV] of diatomic molecules. Data from Refs. [255, 300, 354].

Molecule	nr-SCF	nr-CCSD(T)	ΔE_{correl}	DKH-CCSD(T)	ΔE_{relat}	Exper.
CuF ($^1\Sigma^+$)	2.53	4.08	1.55	4.04	-0.04	4.4 [a]
AgF ($^1\Sigma^+$)	2.17	3.55	1.38	3.32	-0.17	3.6 [a]
AuF ($^1\Sigma^+$)	2.04	3.39	1.35	2.93	-0.46	3.01 [b]
CuAl ($^1\Sigma^+$)	0.59	2.08	1.49	2.25	0.17	2.32 [c]
AgAl ($^1\Sigma^+$)	0.41	1.58	1.17	1.95	0.37	2.22 [c]
AuAl ($^1\Sigma^+$)	0.51	1.68	1.17	3.41	1.73	3.34 [c]
		nr-DFT		NESC-DFT	ΔE_{relat}	
AuI ($^1\Sigma^+$) [d]		2.53		2.47	-0.06	
AuO ($^2\Pi$) [d]		1.86		2.27	0.31	2.31
HgO ($^3\Pi$) [d]		1.16		0.41	-0.75	
HgF ($^2\Sigma^+$) [d]		2.70		1.44	-1.26	

[a] Ref. [296].
[b] Ref. [355].
[c] See data in Ref. [255].
[d] Scalar relativistic effects calculated by the Normalized Elimination of the Small Component (NESC) B3LYP DFT data, Ref. [354].

The overall pattern for D_e of all molecules presented in Tab. 5.19 corresponds to available experimental data only when relativistic effects are considered. In general, the agreement between theory and experiment is very good even for heaviest members of both groups. The thermodynamic stability of AuF, Au_2F_2 and related compounds has been subjected to many discussions [20,356]. Reliable experimental evidence and accurate experimental D_e of AuF was not available until 2002 when Okabayashi *et al.* [355] have observed AuF in the $X^1\Sigma^+$ ground state by employing a source–modulated microwave spectrometer. In fact, they were motivated by theoretical papers cited above. Their D_e, 3.01 eV, agrees with theoretical data (compare to our value 2.93 eV) very well.

Pioneering analysis of the relativistic bond stabilization and destabilization of diatomic gold molecules was published by Schwerdtfeger *et al.* [357] who pointed out that it depends on the electronegativity of the ligand. They also showed that the largest relativistic destabilization of gold containing diatomics holds for AuF, like in our gold compounds and the largest stabilization was calculated for AuLi (-174 kJ/mol).

Comparison of the gold bonding with the mercury bonding in diatomic molecules was published recently by Kraka *et al.* [354]. They analysed the scalar relativistic effects at the DFT level considering different bonding situation in the series of molecules, residual π–bonding, lone pair repulsion, and the d–block effect. The interplay of the various electronic effects leads to strongly differing trends in calculated BDEs, which can be rationalized with a simple MO model based on electronegativity differences, atomic orbital energies and their change due to scalar relativity. A relativistic increase or decrease in BDE is directly related to relativistic changes in the $6s$ orbital energy and density. An increase in BDE upon including scalar relativistic effects is found when charge transfer occurs from X to M due to the low electronegativity of X, like it was described in our comparison of the MF and MAl series for coinage metals above.

Valence electronic structure of molecules treated in the MF and MAl series, as presented in Tab. 5.19, is relatively simple. More complicated picture exhibit molecules in which the valence electronic structure is determined by, *e.g.*, π orbitals. A good example is the PbO molecule and its anion, PbO^-. Recently both species were studied [286] utilizing CCSD(T), CASSCF/CASPT2, and the Fock space FS–CCSD methods. Relativistic effects were treated by the spin–free, two–component infinite-order Douglas–Kroll–Hess, Dirac–Coulomb and the Restricted Active Space State Interaction RASSI–SO methods. The potential energy curve for the ground $X^1\Sigma^+/0^+$ state is presented in Fig. 5.2 in Section 5.1 together with the potential energy curve of the $^2\Pi_{1/2}$ state of the PbO anion (see Section 5.1 on electron affinities). The anion splits due to the spin–orbit effect into the $^2\Pi_{1/2}$ and $^2\Pi_{3/2}$ states, respectively. The PbO molecule in its ground state exhibit no split spin–orbit states. Nevertheless dissociation energies of both species are significantly affected by spin–orbit effects. As it is clearly demonstrated in Fig. 5.2, the large SO contribution in both PbO and PbO^- arises from the SO splitting of the product, the Pb atom. The lowest energy state of the neutral lead element, $j_1 = 1/2$, $j_2 = 1/2$ (X^3P_0), was obtained at the CCSD level by inserting two $6p$ electrons into two shells with quantum numbers $m_j = 1/2$ and $m_j = -1/2$. It lies by 8526 cm^{-1} lower than the spin–averaged state of Pb. This contributes to D_e of both PbO and PbO^- significantly. The oxygen $^3P_2$ ground state is affected by the SO effect much less (the same is valid for the O^- anion). Data collected in Tab. 5.20 demonstrate that spin–orbit effects reduce D_e by 1.06 – 1.36 eV (see also Refs. [207,297,358,359]). The magnitude of SO effects as obtained utilizing the RASSI–SO method [102] method (see Section 4.7.2) in which spin–orbit relativistic effects are treated *a posteriori*, do not differ significantly from results in which SO effects are treated inherently within two– and four–component calculation working with spinors. Theoretical dissociation energies D_e of PbO and PbO^- (3.91 eV and 3.20 eV) obtained by the BSS–CCSD(T) method with the ANO–RCC basis set agree with experiment perfectly, within 0.04 and 0.07 eV, respectively. Referring to BSS and BSSsf–CCSD(T) results [286] for R_e and ω_e of PbO one concludes that the bonding situation of PbO is affected by SO effects very little at the correlated level. Consequently, the lowering of D_e is due almost exclusively by SO effects of the lead element. The electron correlation, relativistic scalar and spin–orbit effects are crucial for obtaining good agreement of theoretical and experimental data for EA and D_e. Contributions to the spin–orbit effect on D_e of a series of diatomics were discussed *e.g.*, in Ref. [207]. The contribution to D_e arising from SO effects in the molecule, in the reaction product, or as the effect arising from an inherent SO interaction within spinors depend on a specific bonding situation in each molecule.

Challenging are scalar relativistic and four–component treatments of spin–orbit effects in closed–shell superheavy element monohydrides or their cations, AH or AH^+, with A= $111 - 120$. Thierfelder *et al.* [302] presented dissociation energies, electron affinities, and spectroscopic constants of these properties and trends within the series of these molecules.

Tab. 5.20. Dissociation energies D_e of the PbO molecule and the PbO^- anion [eV].

Method	spin–free	spin–orbit included
PbO molecule		
Pol–DK basis set		
ZORA[a]	5.51	4.15
CASPT2[b]	5.10	4.04
BSS–CCSD(T)[c]	4.85	3.63
DC–CCSD(T)[c]	4.82	3.69
ANO–RCC basis set		
BSS–CCSD(T)[c]	5.20	3.91
Experiment[d]		3.87
PbO^- anion		
ANO–RCC basis set		
BSS–CCSD(T)[c]	4.31	3.20
Experiment[e]		3.13

[a] Ref. [207], GGA functional.
[b] Spin–orbit effect included using RASSI–SO method, D_e recalculated from D_o using ω_e, [297].
[c] Ref. [286].
[d] Using experimental D_o (3.83 eV) and experimental ω_e, [296].
[e] Recalculated from D_o (3.09 eV $\pm$0.07) and experimental ω_e, [287].

5.5.1 Quadruple, quintuple or sextuple bonds?

Our discussion of unusual chemical bonds resulting from relativistic effects can be introduced by a few examples describing a strong multiple bond in gold compounds. Two main effects leading to strong Au bonds are the stabilization of the $6s$ shell and the destabilization of the $5d$ shell. Barysz and Pyykkö [360] have reported in 1998 about $AuBe^+$, AuC^+, and $AuSi^+$, and $AuMg^+$ cations, that time experimentally unknown. First three species have dissociation energies larger than any other D_e known for gold. At the same time, the strikingly short bond length and population analysis of AuC^+ suggest that this diatomic cation may approach the first known triple bond to gold with dissociation energy 3.815 eV and a bond length 1.766 Å. Similarly, PtSi and PtTh also form triple bonds, while $AuTh^+$ does not show any evidence of a multiple bond. In triple bonds of Au and Pt compounds a decisive role is played by their $6s_\sigma$ and $5d_\pi$ orbitals. Particularly strong Au–C and Au–F bonds (D_e 387 and 390 kJ/mol, respectively) were reported [361] also in XAuC molecules (X is an halogen atom, F, Cl, Br, I).

The existence of unprecedented quadruple bonds between two metal atoms dates from 1965, when Cotton and Harris [362] have reported on the crystal structure of $K_2Re_2Cl_8{\cdot}2H_2O$. This discovery affected inorganic chemistry considerably. Inorganic quadruple bond is, however, not the end of the story, in which, as stressed by Ritter [363], theory plays an important role. Theoreticians, particularly Roos and coworkers [364, 365] have investigated Cr_2 compounds which can form quintuple or even sextuple bonds. In 2005, Power and coworkers [366] reported evidence for the first quintuple bond between two chromium atoms in R–Cr–Cr–R compounds. Theoretical calculations [367] on the model compound, phenyl–Cr–Cr–phenyl essentially confirms the picture which describes a quintuple bond between the transition metal atoms. As analysed by Gagliardi and Roos in their review [368], the chromium atom, which has the ground state with six unpaired electrons, $3d^54s^1$ (^{7}S), can offer altogether 12 electrons in the dimer, which have a potential of creating even sextuple bonds. Nevertheless, an effective bonding order is 4.46 and the dissociation energy D_0 of Cr_2 is relatively low, 1.65 eV. The problem is that there is large difference in size between the $3d$ and $4s$ orbitals of Cr. When $3d$ orbitals reach an effective bonding distance, the orbital constructed from $4s$ electrons is already far up on the repulsive part of the potential energy curve [368]. The difference in size decreases for heavier atoms. For this reason compounds with participation of Mo or W where the relativistic contraction of the $6s$ orbital and the relativistic expansion of $5d$ orbitals makes their bonds much stronger, the effective bond order is about 5.2.

The joint effort of experimentalists and theoreticians working in a fascinating chapter of quintuple and possibly sextuple bonds is described by Ritter [363] and Power [366]. Particularly interesting is the prediction of a quintuple bond in the U_2 molecule by Gagliardi and Roos [368, 369]. The ground quintet state of the uranium atom has the $5f^36d^17s^2$ valence electronic structure. All valence electrons of the U atom are energetically close to one another. The energy cost of unpairing the $7s$ electrons is low and consequently, uranium has in fact six electrons available for creation of the sextuple bond. Involved are σ, π, δ, and ϕ orbitals. Calculations [369] involve electron correlation and scalar relativistic effects at the DKH–CASPT2 level, spin–orbit effects coupling was included by allowing the 16 CASSCF wave functions of the gerade symmetry to mix under the influence of the SO Hamiltonian. The analysis of valence orbitals and the bond order analysis indicate that the molecule exhibits a quintuple bond. Similar quantum chemistry methods predict multiple bonded stable diuranium compounds as diuranium chlorides and three different carboxylates [365]. Multiple bonds exhibit also Th_2 and Pa_2 diatomics [370]. Unusual bonding situation and stabilities of all these novel compounds clearly result from striking relativistic effects.

5.6 Intermolecular interactions

The literature on interaction energies in which participate atoms with high atomic numbers is very rich. It includes both strong closed–shell and van der Waals type interactions in inorganic chemistry [11, 12], various metal–ligand interactions up to interactions which represent the nonconventional hydrogen bonds in which gold participates as an electronegative atom [371, 372]. Clearly, this is related to the relativistic enhancement of the Au electron affinity. Much attention is focused on properties of model metallic complexes [352, 373, 374] since the knowledge of the bonding properties of such species can be used in materials sciences with possible technological applications. One area is the construction of Self–Assembled Monolayers (SAMs) which are typically formed from a coinage element interacting with a ligand, like alkylthiolates with different alkyl chains adsorbed on a metal surface [375–379]. Among important characteristics of the functionality of SAMs belongs the bond strength between the metal and the alkylthiolate ligand. Much attention is paid to the relativistic origin of the difference between Cu, Ag, and Au. Relativistic effects in model systems related to the construction of SAMs were studied by Hirao, Marx, Štich *et al.* [376, 377, 380]. Potential applications of SAMs based on the metal–organic ligand interaction include nanofabrication, corrosion prevention, and the development of biocompatible materials. Interactions of heavy metals with different ligand molecules are also important in many biological processes or in developments of drugs in human medicine. [381–384]. Famous are platinum complexes (cis–platinum) with applications as anticancer drugs. There is an indication about possible role of relativistic effects in the anticancer activity of these drugs [383].

Realistic theoretical models relevant for construction of SAM's and other metal–ligand organic or inorganic complexes are usually too large to be accessible to accurate highly correlated methods. Therefore, most frequently used methods for research in this area are DFT techniques [375, 378]. Nevertheless, for the basic knowledge underlying the bonding mechanism of such species and their geometric features accurate high level *ab initio* data may be very useful.

In this Section we present several examples in which differences between nonrelativistic and relativistic interaction energies of small metal–ligand complexes are related to relativistically affected properties of the heavy metal. It is clear that physically relevant are only results considering both electron correlation and relativistic effects. However, our aim is not only presenting data on structural and energetic features of interacting species. We will rather try to demonstrate that relativistic effects may contribute to the understanding of some trends of stabilities of different complexes involving a heavy metal element. In this sense comparing the relativistic and nonrelativistic models may serve as a useful tool for achieving our goals. We will focus our attention primarily on complexes with Cu, Ag, and Au employing data presented in previous Sections of this paper, particularly ionization potentials, electron affinities and polarizabilities of these atoms (see Section 5.1 and 5.3). Nevertheless we hope that data presented in Tab. 5.21 [385–387] are sufficiently instructive and can be generalized to other complexes as well (at least to those which have analogous valence electronic structure).

Initially we were prompted to undergo a comparative study of Ag interacting with H_2O and NH_3 by experimentalists [389, 390] who could indicate the existence of the $AgNH_3$ complex in the Resonantly Enhanced Multiphoton Ionization (REMPI) spectra. In contrast to the data for $AgNH_3$, the REMPI spectrum for the similar complex of Ag with the water molecule does not exist. According to the dipole moment data (1.85 Debye for H_2O and 1.47 Debye for NH_3) [32] the leading dipole–induced–dipole contribution to the interaction energy should favour the $AgOH_2$ complex over the $AgNH_3$ complex. This contradicts experimental observations. Also,

Tab. 5.21. BSSE corrected DKH–CCSD(T) relativistic and nonrelativistic interaction energies [mhartree] of $M\cdots OH_2$, $M\cdots SH_2$, $M\cdots NH_3$, and $M\cdots PH_3$ complexes[a] (doublet states) and the $Cu\cdots SCH_3$ complex in triplet and singlet states. Pol–DK and Pol basis sets are used for DKH and nonrelativistic calculations, respectively. $Cu\cdots SCH_3$ calculated with the aug–cc–pVTZ–DK basis. Data from Refs. [385–388].

Complex	ΔE_{DKH}	ΔE_{NR}	Δ_{rel}[b]
$Cu\cdots OH_2$	-3.78	-3.79	0.01
$Ag\cdots OH_2$	-1.81	-2.13	0.32
$Au\cdots OH_2$	-1.77	-1.62	-0.15
$Cu\cdots SH_2$	-5.99	-4.53	-1.46
$Ag\cdots SH_2$	-1.99	-1.53	-0.46
$Au\cdots SH_2$	-9.08	-1.40	-7.68
$Cu\cdots NH_3$	-16.68 (18.9, -21.4[c])	-14.86	-1.82
$Ag\cdots NH_3$	-6.87 (-8.7, -10.7)	-6.52	-0.35
$Au\cdots NH_3$	-14.64 (17.9, -20.4)	-5.23	-9.41
$Cu\cdots PH_3$	-9.89 (-12.53[c])	-7.25	-2.64
$Ag\cdots PH_3$	-2.24 (-4.40)	-1.15	-1.09
$Au\cdots PH_3$	-18.31 (-25.42)	-1.05	-17.26
$Cu\cdots SCH_3$, $^3A''$	-20.5[c]		
$Ag\cdots SCH_3$	-6.9		
$Au\cdots SCH_3$	-28.4		
$Cu\cdots SCH_3$, $^1A'$	-94.4[c]		
$Ag\cdots SCH_3$	-75.1		
$Au\cdots SCH_3$	-87.2		

[a] Qualitative description of the main structural features of M-L complexes: Optimized structures of $M\cdots OH_2$ and $M\cdots SH_2$ complexes are nonplanar, with the out–of–plane angle θ 58, 55, and 67 deg for $M\cdots OH_2$ and 80, 89, and 81 deg (almost) perpendicular structure of C_s symmetry for $M\cdots SH_2$. $M\cdots NH_3$, and $M\cdots NH_3$ complexes have linear $M\cdots N$ (or $M\cdots P$) bonds in the main axis of the complex with the C_{3v} symmetry.
[b] Relativistic contribution to the interaction energy $\Delta_{\mathrm{rel}} = \Delta E_{\mathrm{DKH}} - \Delta E_{\mathrm{NR}}$.
[c] Results with relativistic augi–cc–pVTZ–DK basis sets [387] and complete basis set limit [388] in parentheses.

the model based on the long–range expression for the induction energy,

$$\Delta E^I = -\frac{1}{2}\alpha_M \mu_L^2 (3\cos^2\theta + 1)R^{-6} \tag{5.13}$$

(α_M and μ_L are the polarizability of the metal atom and the dipole moment of the ligand, respectively), would lead to the planar $M\cdots OH_2$ structures with M interacting with C_{2v} molecules in the direction of their principal axis. Theoretical calculations [391] suggest that it is in fact non–planar. Prompted by the puzzling character of the REMPI experimental data we decided [385] to perform DKH–CCSD(T) calculations for all three coinage atoms and their complexes with H_2O and NH_3. Rigorous theoretical information about the structure and energetics was until recently scarce, see *e.g.*, Refs. [391,392] and any systematic comparison of all these complexes was missing. Calculations were performed by the so called supermolecule method. For the weakly bound dimer AB we can assume that the deformation of geometries of participating subsystems, A and B, would be small. The interaction potential, $V_{\rm AB}$ depends, under this assumptions, only on inter–monomer coordinates (that is, the M…O or M…N bond distance and the orientation of M with respect to the ligand L) and is calculated as:

$$V_{\rm AB} = E_{\rm AB}({\rm AB}) - E_{\rm A}({\rm AB}) - E_{\rm B}({\rm AB}), \tag{5.14}$$

where (AB) denotes that the calculated energies refer to the basis set of the complex. In other words, the complex (supersystem) and both subsystems are calculated with the same basis set. This approach [393] eliminates the basis set superposition error (BSSE) and leads to balanced energies of all participating species. Results are collected in Tab. 5.21. Along with interaction energies presented in former studies on $M\cdots OH_2$ and $M\cdots NH_3$ complexes [385] we also summarize interaction energies in $M\cdots SH_2$, $M\cdots PH_3$ and $M\cdots SCH_3$ complexes [386, 387, 394]. The structures of the complexes are schematically presented in Fig. 5.10 (for details see the original literature [385–387]). $M\cdots OH_2$ and $M\cdots SH_2$ complexes are nonplanar, with M approaching the O or S atom in the direction of the lone pair of the ligand. It is interesting that nonplanar structures were found not only for interactions of neutral atoms with lone–pair ligands like H_2O but also with cations of M [395–398] in which one expects a dominating charge$\cdots$dipole interaction, with planar structure of $M^+\cdots XH_2$ complexes. Analogously in $M\cdots SCH_3$ complexes a metal element approaches the SCH_3 molecule in the direction of the lone–pair on the sulphur atom, leading to the M–S–C angle of 76 up to 82 deg, depending on the metal and the spin state of the resulting complex. These structural features point out on the inadequacy of the induction model of interactions to correctly describe differences in the structure and energetics of metal atom complexes with lone–pair ligands. $M\cdots NH_3$ and $M\cdots PH_3$ complexes preserve the C_{3v} structure of isolated molecules. Again, the metal element is oriented towards the lone electron pair of the ligand.

Returning back to the missing evidence of the existence of the $Ag\cdots OH_2$ complex by the REMPI spectroscopy, as contrasted to the $Ag\cdots NH_3$ complex, the interaction energies in Tab. 5.21 seem to offer the explanation of this observation. Nonrelativistic CCSD(T) interaction energy in $Ag\cdots NH_3$ is 3.1 times larger than in $Ag\cdots OH_2$, the DKH relativistic ratio of the two energies is slightly higher, 3.8. This is just a computational observation of higher stability of NH_3 complexes, not yet the explanation. More interesting is similar ratio of interaction energies in $Au\cdots NH_3$ and $Au\cdots OH_2$ complexes. The nonrelativistic ratio of interaction energies of the

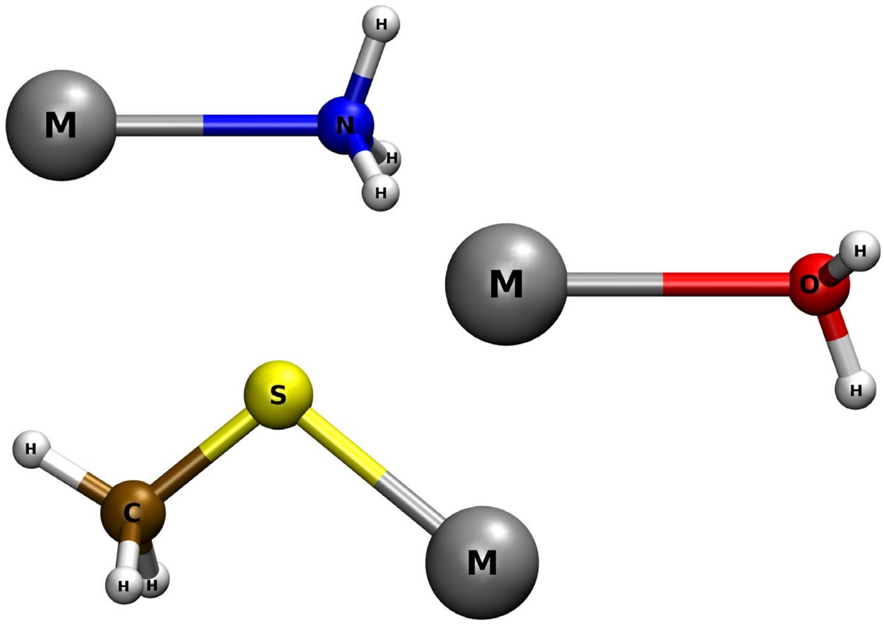

Fig. 5.10. Schematic structures of complexes $M\cdots OH_2$ (and $M\cdots SH_2$), $M\cdots NH_3$ (and $M\cdots PH_3$) and $M\cdots SCH_3$.

two Au complexes is 3.2, about the same as with $Ag\cdots NH_3$ and $Ag\cdots OH_2$. However, when considering scalar relativistic effects the ratio enhanced to 8.2. Also, relativistic interaction energy is much higher for $Au\cdots NH_3$ than for $Ag\cdots NH_3$ (for complexes with water both values are almost the same). One could think about a dispersion interaction as another contributing energy component to the stability of complexes under consideration. With the same ligand interaction energies should be proportional to the magnitude of atomic polarizabilities of the metal atom. Clearly, dispersion forces, which depend on the product of polarizabilities of the metal and the ligand, respectively, do not explain observed order of stabilities for Ag and Au. Nonrelativistic polarizabilities are similar for Ag and Au. Correspondingly, interaction energies for the Ag and $Au\cdots L$ complexes at the nonrelativistic level, see Tab. 5.21, are also similar. Relativistic effects reduce the polarizability of gold from 64 a.u. to about 36 a.u., so that the relativistic polarizability of Ag is the largest from among all coinage elements, (see Section 5.3). However, interaction energies of Au with all ligands relativistically increase (albeit only a little for $Au\cdots OH_2$). Clear indication of different mechanisms of interactions in which participate water and ammonia and other ligands provide different relativistic contributions to the interaction energy, last column of Tab. 5.21. For all $M\cdots SH_2$, $M\cdots NH_3$ and $M\cdots PH_3$ complexes is the relativistic contribution large and negative. For complexes with Au is the relativistic effect *highly stabilizing*. The stability of $Au\cdots PH_3$ is practically completely caused by relativistic effects. For this reason we call the bond in this complex as a *relativistic bond* [387]. For $Cu\cdots OH_2$ and $Ag\cdots OH_2$ complexes,

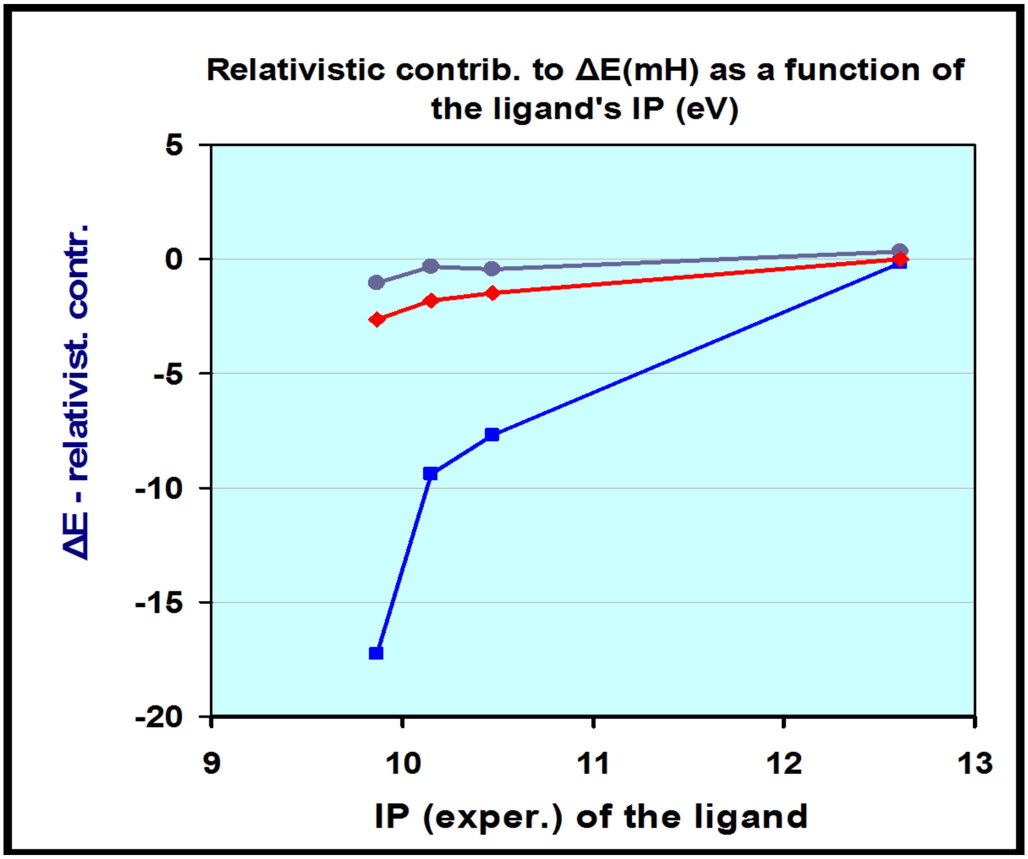

Fig. 5.11. Relativistic contributions to the interaction energies of Cu (middle line), Ag (upper line), and Au (the lowest line) as a function of the IP of the ligand L, PH_3 (IP= 9.87 eV), NH_3 (IP= 10.07 eV), H_2S (IP= 10.46 eV), and H_2O (IP= 12.61 eV). Interaction energies from Refs. [385–387], ionization potentials of ligands from the NIST database [399].

in contrast, is the relativistic contribution *destabilizing*. $Au\cdots OH_2$ is relativistically stabilized very little.

Our hypothesis on the interpretation of the interaction energies pattern for complexes of the coinage metals with different ligands is based on the idea that the basic mechanism behind interaction energies in $M\cdots L$ complexes is the charge transfer form the ligand to the coinage metal. It is mediated by the lone pair of the ligand directed towards the metal, which explains linear $M\cdots X$ bonds in $M\cdots XH_3$ complexes and the nonplanarity of $M\cdots OH_2$ complexes. Hence, we expect that relativistic contributions to interaction energies should be more important for ligands which have low ionization potentials, as is shown in Fig. 5.11. Charge transfer is substantially enhanced by the relativistic contribution to the electron affinity of the metal. This expectation should hold particularly for complexes with Au, which has the far highest electron affinity out of the three coinage metals. High stability of $Au\cdots SH_2$, $Au\cdots NH_3$ and particularly $Au\cdots PH_3$ complexes is therefore linked with a large relativistic enhancement of the electron affinity of Au.

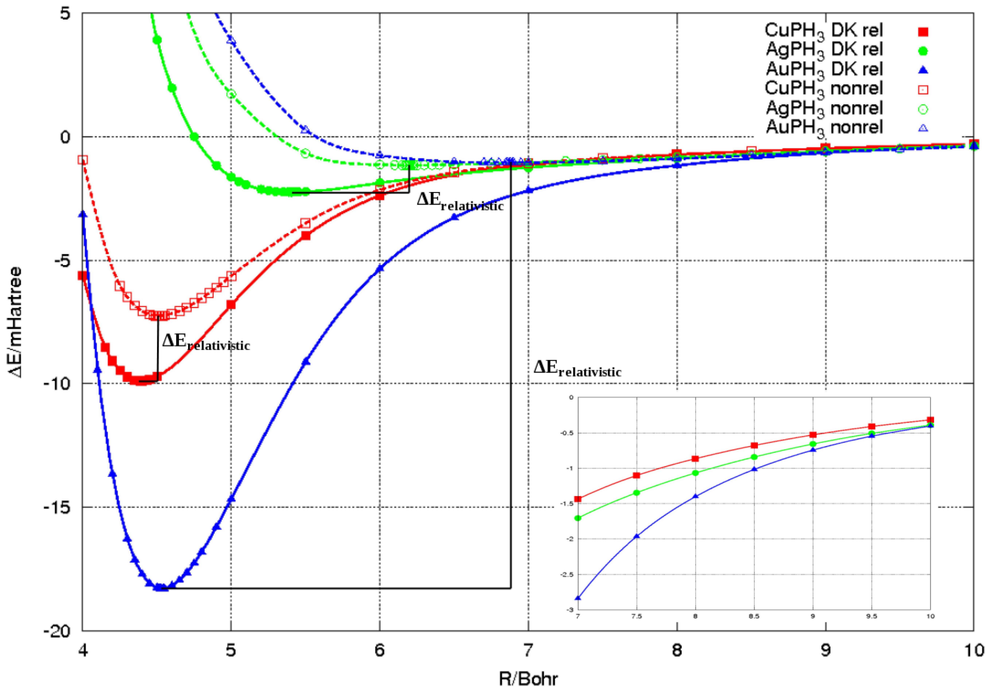

Fig. 5.12. Interaction energies of Cu, Ag, and Au complexes with PH_3. Comparison of nonrelativistic (empty symbols, dotted lines) and DKH–CCSD(T) relativistic (full lines) potential energy curves. Relativistic contribution $\Delta E_{\mathrm{relativistic}}$ at the equilibrium M. . . P bond distance is shown by full vertical lines. Inserted is a long–range part of the DKH–CCSD(T) potential energy curves. See Ref. [387].

Clearly, the charge transfer from the ligand to the metal is hindered in $M\cdots OH_2$ complexes since the ionization potential of water is too large. This is compensated by large relativistic EA of gold in $Au\cdots OH_2$ so that relativistic contribution to ΔE becomes negative, but very small.

The high stability of the $Au\cdots PH_3$ complex (Tab. 5.21) is considerable. Interaction energy in $Au\cdots PH_3$ is much higher than in $Au\cdots NH_3$. To ensure that relative stabilities are not affected by basis set effects relativistic DKH–CCSD(T) calculations with Pol–DK basis set [385] were supplemented [387] with calculations with much larger aug–cc–pVTZ–DK basis sets. The picture remains the same, just interaction energies are higher upon extending the basis set. The crucial observation that the bond strength in $Au\cdots PH_3$ is about twice as large as in $Cu\cdots PH_3$ holds with both relativistic basis sets. Also, the interaction energy in $Au\cdots PH_3$ is higher than in $Au\cdots NH_3$ (note, however, that interaction energies in $Cu\cdots NH_3$ and $Ag\cdots NH_3$ are higher than in their $Cu\cdots PH_3$ and $Ag\cdots PH_3$ counterparts).

The bond strength in $Au\cdots PH_3$ with aug–cc–pVTZ–DK basis set is as high as 67 kJ/mol, nearing the bond strength of a regular chemical bond. We stress that with the DKH–Hartree–Fock relativistic approximation all $M\cdots PH_3$ complexes are *repulsive*. Upon including the electron correlation by the high–level CCSD(T) method but neglecting relativistic effects the $Au\cdots PH_3$ complex exhibits low attractive interaction energies corresponding just to the long–range van der Waals weak interaction (with a shallow minimum at the $M\cdots P$ distance of 6.9 bohr). As it is demonstrated in Fig. 5.12, considerable bond strength results only upon considering (scalar) relativistic effects on top of the electron correlation. Hence we characterize the interaction between Au and PH_3 as a *"relativistic bond"*. The enhancement of the bond strength is accompanied by considerable shortening of the $M\cdots P$ bond distance, see Fig. 5.12. In $Au\cdots PH_3$ is the $Au\cdots P$ bond length shortened by about 2 bohr due to relativistic effects. This is related to relativistic shrinking of the valence $6s$ orbital of Au. Experimental data for interaction energies in $M\cdots PH_3$ complexes are missing. For analogous $Cu\cdots NH_3$ and $Ag\cdots NH_3$ complexes Li *et al.* [388] present DKH–CCSD(T) interaction energies extrapolated to the CBS limit. Both our calculations with larger aug–cc–pVTZ–DK basis set and the CBS limits (50 – 56 kJ/mol for $Cu\cdots NH_3$ and 18 – 28 kJ/mol for $Ag\cdots NH_3$) agree fairly well with experimental values, 47 $\pm$ 15 and 8 $\pm$ 13 kJ/mol for the two complexes, respectively, as presented in Ref. [388].

Another interesting relativistic effect is shown in the inset in Fig. 5.12. It represents a long–range region of the potential energy curves of $M\cdots PH_3$ complexes. The long–range van der Waals bonding region in $M\ldots PH_3$ is governed mainly by electric properties of participating species. We remind that the highest polarizability out of the three coinage metals was calculated for the silver atom, see Section 5.3. The potential energy curves and the inset displayed in Fig. 5.12 show that beyond R=6.0 bohr is the $Ag\ldots PH_3$ complex more stable than $Cu\ldots PH_3$ and beyond of about R=10 bohr it tends to be the most stable $M\ldots PH_3$ species, in line with the highest polarizability of Ag. At R=10.0 bohr are relativistic binding energies of all $M\ldots PH_3$ complexes smaller than nonrelativistic ones, which is attributed to the fact that relativistic effects reduce the dipole polarizability of all coinage metals. Long–range induction and dispersion forces based on relativistic alterations of dipole polarizabilities and ionization potentials of the metal elements and electric properties of ligands were discussed in detail in Ref. [385].

The analysis of energy contributions due to polarization forces and partial charge transfer from the lone pair of the ligand molecule to the ns valence orbital of M provides a uniform interpretation of the interaction energy data and explains some irregularities in the energetics and structures of the investigated systems. Similar interpretation can be also forwarded to explain the bonding and structure of complexes between ligands and heavy metal cations [395, 397, 398, 400, 401]. Analogous mechanism applies to interesting $X(AuPH_3)_2$ complexes [402] with X representing an electronegative atom.

Straightforward insight into the interplay between the electron correlation and relativistic effects can be demonstrated by excitation amplitudes obtained by the nonrelativistic and relativistic treatment of the electron correlation, respectively. CCSD single excitation amplitudes of Ag and Au, see Fig. 5.13, are very similar in the nonrelativistic case, confirming once again that the "nonrelativistic" gold would behave like silver. Enhancement of the CCSD excitation amplitudes resulting from the relativistic DKH calculations is attributed to a large mixing of electron correlation and relativistic effects. Note that relativistically treated Au amplitudes behave similarly as amplitudes of Cu. Relativistic effects in Au diminish the energy gap between valence $5d$ and $6s$ orbitals. Therefore, we may say that from the point of view of the electron correlation the relativistically treated Au becomes similar to Cu. In a sense, both behave like "transition metal" elements. Relatively large excitation CC amplitudes occurring in $Cu\ldots NH_3$ are close to the limit at which the single reference CCSD(T) can still be safely used. In general, large amplitudes are characteristic for quasidegenerate systems in which the energy gap between different states (typically between the ground state and a low–lying excited state) are not sufficiently separated. For such systems iterative calculation of higher than single and double excitation amplitudes

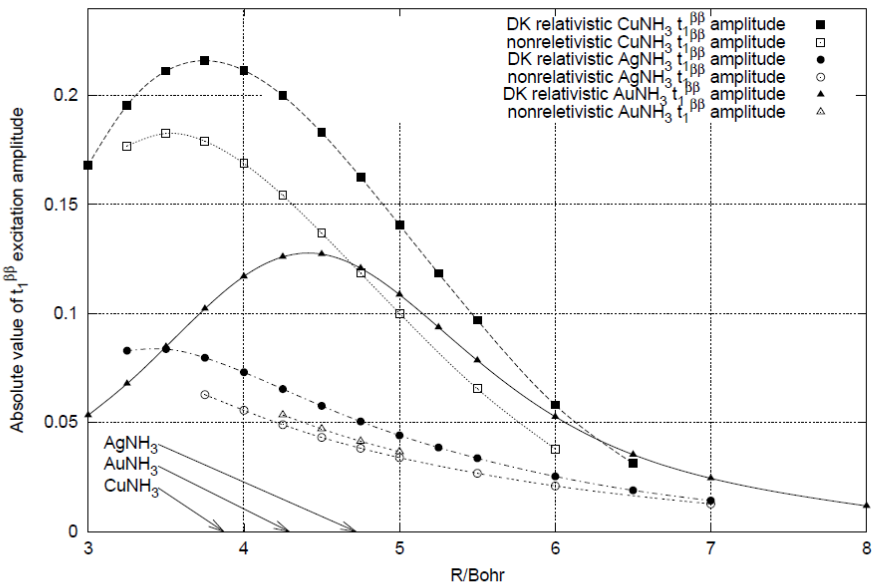

Fig. 5.13. Nonrelativistic and relativistic CCSD single excitation amplitudes of Cu, Ag, and Au (M) complexes with NH_3 as the function of the M–N bond length. Equilibrium M. . . P bond distances of M. . . NH_3 are shown by arrows. Based on data from Ref. [385].

(*i.e.* triples and particularly quadruples) is needed when we stay within the single determinant reference scheme, or we can use multireference MR–CC or MR–CI approach, but all these alternatives are very expensive. This topic [38, 40] is beyond the scope of the present paper. More practical alternative is using the RASSI and CASPT2 method mentioned in Section 4.6.3.

Larger metal–ligand complexes are usually tractable only with DFT methods. Therefore, it may be instructive to compare DFT and CCSD(T) results, when available. In the case of Au. . . PH_3, the present interaction energy is quite different from the Local Density Functional (LDF) value calculated by Häberlen *et al.* [403] (124 kJ/mol $\approx$ 47.2 mhartree). Similarly, Bernhardt *et al.* [404] found that all DFT predicted binding energies of CO and O_2 with small anionic gold clusters are much larger than energies obtained from the gas–phase kinetic data for the oxygen and CO adsorption on small mass–selected coinage metal cluster anions. Solely, the relativistic CCSD(T) result by Schwerdtfeger *et al.* [405] coincides favourably with binding energies deduced from the temperature dependent rate constants. Both underestimated and overestimated binding energies were found in an elaborated investigation of the performance of DFT with various exchange–correlation functionals by Li *et al.* [388] for M. . . NH_3 complexes (M=Na, Al, Ga, In, Cu, Ag, Au and their cations). The analysis of the performance of DFT methods employing different functionals [406] shows that simple local density functionals perform quite well in molecules containing the Au–Au aurophilic bonds.

An example of the different bonding mechanisms related to the relativistic effects represent

M... SCH_3 complexes (M= Cu, Ag, and Au) [394]. These complexes may serve as the simplest representatives of compounds participating in the creation of SAMs. Optimized structures of M... SCH_3 complexes (the C_s symmetry) are schematically shown in Fig. 5.10. The methylthio radical SCH_3 is an open–shell species having the two lone–pairs at the sulphur atom, one of which is doubly occupied, another one is singly occupied. The first ionization potential calculated by the CCSD(T) method is 9.18 eV (lower than of other ligands discussed previously). It agrees fairly well with the experimental value of 9.262 eV obtained by the photoionization mass spectrometry [407]. Applying the same symmetry as considered in M... SCH_3 complexes it represents the process $^2A^{'}$—$^3A^{''}$. The second IP representing ionization of the electron from the singly occupied (the $^2A^{'}$—$^1A^{'}$ process) is 10.57 eV. The structure of SCH_3 is not strictly C_{3v} since it is deformed by the Jahn–Teller effect. This effect (95 cm^{-1}) is much smaller than the spin–orbit splitting of the two states, the $X^2E_{3/2}$ ground state and the $^2E_{1/2}$ state, respectively, which differ by 356 cm^{-1} [408]. We were able to reproduce this value by the RASSI method within 10 cm^{-1}.

Two different states of the M... SCH_3 complex have similar structures (Fig. 5.10). Interaction energies for both states are compared in Tab. 5.21 with M... L interactions discussed above. A weaker bonding results from the metal element approaching the doubly occupied lone–pair orbital of SCH_3. The second lone–pair remains singly occupied and thus the complex is the triplet $^3A^{''}$. The interaction energy is higher than in Au$\cdots PH_3$. In accord with the dominating charge transfer mechanism this corresponds to lower IP of SCH_3 than is IP of PH_3 and other closed–shell ligands. Again, as with Au$\cdots PH_3$ complexes, the M... SCH_3 interaction energy is the highest for Au... SCH_3. Preliminary calculations [394] indicate, that relativistic effects stabilize the $^3A^{''}$ state of the Au... SCH_3 complex even more than Au... PH_3, as is should be if our interpretation of the bonding mechanism is correct. The bonding character of the $^1A^{'}$ state of M... SCH_3 is different than for its $^3A^{''}$ state. It is essentially the σ bond created by the ns electron of the coinage metal and the singly occupied lone–pair valence orbital of SCH_3. For all M... SCH_3 it is quite strong, 248 kJ/mol for Cu... SCH_3 and slightly less, 229 kJ/mol for Au... SCH_3. Structural and energy characteristics of these complexes are relevant for constructing SAMs [375–379].

To summarize, it is appropriate to note that the interpretation of the structural and energy pattern of metal–ligand complexes based on the charge transfer mechanism represents just a principal driving force of their interaction. The basic properties of heavy metal properties participating in their interactions are the enhancement of EA and IP, the relativistic stabilization and contraction of valence s– and p–electrons, destabilization and expansion of d–electrons, lowering of the dipole polarizability, and the overlap of valence orbitals of the metal element and the orbitals of the ligand. In a particular case of the binding energy in Au... PH_3 as compared with Au... NH_3 it may increase also due to the participation of the π bond reinforced in M... PH_3 complexes (back donation). This idea goes back to Mulliken and Person [409] who call such mechanism as a "two–way donor–acceptor action". The bonding model of M... L neutral and charged clusters focuses on the donor–acceptor σ donation and acceptor–donor π back donation [374, 410, 411]. Lim *et al.* [410] have compared the geometries and interaction energies of the series of M$\cdots NH_3$ (M=K, Rb, Cs, and Fr and their cations) with coinage metal$\cdots NH_3$ complexes, analysed the character of highest doubly occupied bonding orbitals (HOMO–1) and the highest singly occupied antibonding orbitals within the two series. They pointed out a significant $5d$ admixture in the HOMO–1 orbital in Au... NH_3, which appears to be even more important in Au. . . PH_3. The σ donation and acceptor–donor π back donation mechanism was used by Li *et al.* [374] in their DFT relativistic calculations and the analysis of relative stabilities of metal–phosphorus $WAu_{12}PX_3$ (with X=H, F, Cl, Br, I, Me, and OMe) and various metal–Au cationic $MAu_{12}PH_3$ complexes. Similar clusters are powerful catalysts and have potential application in nanoelectronics, nanosensors, and as biological markers [351]. Complexes of adenine and adenosine monophosphate with gold were investigated experimentally and theoretically by Kundu *et al.* [412]. The central focus was on understanding of these interactions in relation to the development of functional biomedical nanodevices and accurate biosensors.

An interesting comparison of molecular gold halides with molecular mercury halides and their complexes was published by Hargittai [413]. Differences between dimers, like Au_2X_2 and Hg_2X_4 (X is a halide atom) are attributed to relativistic effects. The peculiar structure of the Hg_2X_4 dimers and the crystal structure of mercury halides is also a consequence of relativistic effects [414]. Kryachko and Remacle [415] studied different neutral and charged $Au_n^Z(NH_3)_m$ complexes ($Z = 0, \pm 1$). They have proposed such complexes as simple logic gates based on gold–ammonia bonding patterns using the conformational manifold of these complexes with conventional Au. . . N and the hydrogen N–H. . . Au bonds.

So far we did not mention explicitly spin–orbit interactions in describing the metal–ligand complexes. As an example of the importance of spin–orbit contributions may serve interactions of the superheavy element 112 (E112, eka-Hg) interacting with Au, Au_4 and Au_6 (and comparison of these complexes with HgAu, $HgAu_4$ and $HgAu_6$) [416]. These complexes are considered as simple models of adsorption of E112 and Hg on the Au(111) surface. Comparative analysis also indicates a strong underestimation of scalar relativistic binding energies by conventional relativistic DFT methods. In complexes involving a group of metals, like lanthanides, the consideration of spin–orbit interactions is unavoidable.

5.7 NMR properties of molecules

Relativistic effects have a profound influence on a wide scale of molecular properties. Here we focus on nuclear magnetic resonance (NMR) shielding constants. Review papers on NMR properties discussing also relativistic effects, let us name a few, are by Helgaker *et al.* [417], or by Vaara [418].

We present the relativistic methodology for computing NMR properties and will briefly show how to remove the gauge–origin dependence and will report few demonstrative results. Likewise we will mention the importance of the electronic correlation on NMR properties.

5.7.1 Four–component calculations of NMR shielding constants

Individual components of the NMR shielding tensor for the nucleus K are calculated within the Born–Oppenheimer approximation as the second derivative of the electronic energy at the zero perturbation strength:

$$\sigma_{pq}^K = \left.\frac{d^2E}{dm_{K,p}dB_q}\right|_{\{\mathbf{m}_K\}=\mathbf{0},\ \mathbf{B}=\mathbf{0}}, \qquad (pq) = xx, xy, xz, yy, yz, zz. \tag{5.15}$$

In our implementation in Ref. [419] we are using the Dirac–Hartree–Fock wave function. To evaluate the second derivative, Eq. 5.15, one has to provide the one–electron Dirac Hamiltonian, Eq. 4.35, with perturbations created by both, a uniform external magnetic field, $\mathbf{B}$, and internal nuclear magnetic moments, $\mathbf{m}_K$. These are represented through the vector potential $\mathbf{A}$ in accordance with the principle of a minimal electromagnetic coupling [127, 420]:

$$\mathbf{A} = \mathbf{A}_B + \sum_K \mathbf{A}_{m_K}. \tag{5.16}$$

The vector potential of a uniform external magnetic field $\mathbf{B}$ is usually chosen in the gauge

$$\mathbf{A}_B(\mathbf{r}) = \frac{1}{2}\mathbf{B} \times \mathbf{r}_G; \quad \mathbf{r}_G = \mathbf{r} - \mathbf{R}_G\ , \tag{5.17}$$

where $\mathbf{R}_G$ is the selected gauge origin. The vector potential associated with a point magnetic dipole at nucleus K is conveniently written as

$$\mathbf{A}_{m_K}(\mathbf{r}) = \frac{1}{c^2}\frac{\mathbf{m}_K \times \mathbf{r}_K}{r_K^3}. \tag{5.18}$$

The perturbed one–electron Hamiltonian has the form as follows:

$$\hat{h}_D(\mathbf{A}) \;=\; \beta mc^2 + c(\hat{\boldsymbol{\alpha}} \cdot \hat{\boldsymbol{\pi}}) + \hat{V}_{nuc} \;=\; \hat{h}_D + c(\hat{\boldsymbol{\alpha}} \cdot \mathbf{A}). \tag{5.19}$$

With the vector potentials defined above, the Dirac Hamiltonian takes the form

$$\hat{h}_D(\mathbf{B}, \{\mathbf{m}_K\}) \;=\; \hat{h}_D \;+\; \mathbf{B} \cdot \hat{h}_{\mathbf{B}} \;+\; \sum_K \mathbf{m}_K \cdot \hat{h}_{\mathbf{m}_K}, \tag{5.20}$$

where the Zeeman operator, $\hat{h}_{\mathbf{B}}$, appears as

$$\hat{h}_{\mathbf{B}} = \frac{1}{2}(\mathbf{r}_G \times c\boldsymbol{\alpha}), \tag{5.21}$$

and the hyperfine operator, $\hat{h}_{\mathbf{m}_K}$, takes the form

$$\hat{h}_{\mathbf{m}_K} = \frac{1}{c^2}\frac{\mathbf{r}_K \times c\boldsymbol{\alpha}}{r_K^3}. \tag{5.22}$$

The resulting perturbed Dirac Hamiltonian, Eq. 5.19, is *linear* in both, the magnetic field, $\mathbf{B}$, and the magnetic dipoles, $\mathbf{m}_K$. It contrasts to its nonrelativistic Schrödinger counterpart, containing the term $(\hat{\boldsymbol{\sigma}} \cdot \hat{\boldsymbol{\pi}})^2$ (or $(\hat{\boldsymbol{\sigma}} \cdot \mathbf{p})^2$ without the perturbation). Likewise in the relativistic four–component theory there is no explicit diamagnetic term, although such a contribution can be obtained from the positive energy–negative energy coupling terms of the linear response function as demonstrated in Ref. [421].

The formula in Eq. 5.15 together with the Hamiltonian carrying perturbations, Eq. 5.20, is the prescription for the so called linear response method, Ref. [232]. It is used for calculating a wide scale of second order molecular properties. Without going into more details, for NMR shielding constants it is written in the short form of

$$\sigma^A = \left\langle\left\langle \hat{h}_{\mathbf{m}_A}; \hat{h}_{\mathbf{B}} \right\rangle\right\rangle_0\ . \tag{5.23}$$

5.7.2 Gauge including atomic orbitals in the four–component theory

The term of Eq. 5.21 contains the gauge origin reference, $\mathbf{r}_G$, which complicates calculations of properties depending on external magnetic fields. This is removed by the introduction of physically motivated London atomic orbitals (LAOs) [422], also called as gauge including atomic orbitals (GIAOs), what ensures that these properties are independent of the choice of the gauge origin [423]. At the four–component level the gauge origin problem was solved by implementing London atomic orbitals as was reported by one of us (MI) in Ref. [419]. The definition of the magnetic field dependent LAO employed within the four–component framework is

$$\omega_\mu^{M,X}(\mathbf{r}_M, \mathbf{B}) = \exp\left\{-\mathrm{i}\mathbf{A}_B\left(\mathbf{R}_M\right)\cdot\mathbf{r}\right\}\chi_\mu^{M,X}(\mathbf{r}_M); \quad X = L\alpha, L\beta, S\alpha, S\beta \ , \tag{5.24}$$

where the extended superscript "M, X" designates that $\chi_\mu^{M,X}(\mathbf{r}_M)$ is an atomic scalar basis function of type X centred at position $\mathbf{R}_M$, see also Section 4.4.6. Operating with the Dirac operator on a London atomic orbital of any type – $L\alpha$, $L\beta$, $S\alpha$, or $S\beta$, Eq. 5.24, gives

$$\begin{aligned} \hat{h}(\mathbf{B})\omega_\mu^M(\mathbf{B}) &= \left[\hat{h}_D + \tfrac{1}{2}\mathbf{B}\cdot(\mathbf{r}_G \times c\boldsymbol{\alpha})\right]\omega_\mu^M(\mathbf{B}) \\ &= \exp\left\{-\mathrm{i}\mathbf{A}_B(\mathbf{R}_M)\cdot\mathbf{r}\right\}\left[\hat{h}_D + \tfrac{1}{2}\mathbf{B}\cdot(\mathbf{r}_M \times c\boldsymbol{\alpha})\right]\chi_\mu^M, \end{aligned} \tag{5.25}$$

showing that the reference to the gauge origin, $\mathbf{r}_G$, in the operator is replaced with the reference to the centre of the orbital, $\mathbf{r}_M$. All formulas for computing NMR shielding constants therefore became gauge origin free.

As an example of usefulness of London atomic orbitals, in Tab. 5.22 we collected a series of computed ^{127}I iodine NMR shielding constants in six increasing basis sets (these are explained in Tab. I of Ref. [419]). Note that the preferential approach is the unrestricted kinetic balance (UKB) [424] in combination with LAO, where the convergence of NMR shielding constants is smoother than in the common gauge origin (CGO) approach, where the gauge origin has to be chosen arbitrarily. The UKB method generates small component basis function according to Eq. 4.46 without any restrictions and the number of small component basis functions is approximately twice as much as the number of large component basis functions. On the contrary, in order to make number of positive and negative states in the DHF solution equal, the restricted kinetic balance (RKB) [128,225] is giving 1:1 ratio between the large and small component functions. This choice make the basis set 'magnetically unbalanced'. To overcome this drawback the so called 'restricted magnetic balance' (RMB) approach was adopted by Komorovský and coauthors [425], which leads to the introduction of perturbation–dependent basis functions, what is a different problem than the gauge–origin dependence. Combination of both treatments, *i.e.* of RMB and LAO, was reported recently by Cheng *et al.* [426] and very recently by Komorovský *et al.* [427]. Note that the relativistic LAO–UKB approach significantly improves values of NMR shielding constants with respect to nonrelativistic LAO–LL values. In the best basis set VI, the relativistic increase makes about 1368 ppm.

Another stream of four–component relativistic property oriented methods can treat, for instance, electronic g–tensors, as is reported by Repiský *et al.* [428].

5.7.3 Electron correlation in NMR calculations

The Hartree–Fock method is one–electron approximation and NMR properties calculated from the four–component DHF wave function, Section 4.4.3, are missing an important contribution of the electron correlation, which is essential to obtain results in agreement with experiment. However, correlation methods for NMR properties based on the DHF wave function as reference are not yet implemented, moreover, the calculations would be computationally intractable for larger systems due to a prohibitive scaling.

In the wave function domain of quantum chemistry, there were formulated perturbation approaches for MCSCF correlation method to incorporate relativistic effects for NMR shielding constants [429]. Comparison of perturbation relativistic contributions calculated at SCF and MCSCF levels shows that the relativistic correction at the correlated MCSCF level differs from the relativistic correction at the SCF level by very small values [429, 430]. Of course, one should take into account that the MCSCF method insufficiently incorporate the dynamic part of correlation, but at least for weakly correlated systems containing lighter atoms, correlation effects and relativistic contribution to the NMR shielding can be treated as additive. This fact opens the possibility to incorporate relativistic effects for NMR shielding constants in an approximate way, where relativistic corrections are estimated as difference between the DHF value and the corresponding nonrelativistic Hartree–Fock value of the NMR shielding. This correction is then

Tab. 5.22. Isotropic ^{127}I iodine NMR shielding constants [ppm] in hydrogen iodide calculated with nonrelativistic (LL), RKB–relativistic, and UKB–relativistic methods; each both with common gauge origin (CGO) on "GO" and with London atomic orbitals (LAO). The difference of each value to the corresponding value in the largest basis set VI is given in parenthesis. Data and basis sets are from Ref. [419].

		I	II	III	IV	V	VI
UKB–CGO	GO=I	5673.0	5808.9	5817.8	5852.0	5854.4	5860.4
		(-187.4)	(-51.5)	(-42.6)	(-8.4)	(-6.0)	
	GO=(0,0,7)	6306.1	5839.5	6184.6	5889.4	5851.7	5857.2
UKB–LAO		5905.2	5961.4	5951.6	5921.7	5960.3	5907.2
		(-2.0)	(+54.2)	(+44.4)	(+14.5)	(+53.1)	
RKB–CGO	GO=I	4753.3	4890.6	5239.4	5278.7	5322.8	5378.2
	GO=(0,0,7)	5388.8	4920.4	5608.9	5317.7	5320.2	5375.4
RKB–CGO [a]	GO=I	6556.9	6690.1	6732.9	6765.1	6769.5	6774.8
		(-217.9)	(-84.7)	(-41.9)	(-9.7)	(-5.3)	
	GO=(0,0,7)	7185.3	6716.3	7095.2	6798.2	6762.4	6767.3
RKB–LAO		4975.3	5027.3	5367.1	5343.9	5422.1	5423.2
LL–CGO [a]	GO=I	4390.4	4538.6	4506.4	4546.8	4541.3	4539.0
		(-148.6)	(-0.4)	(-32.6)	(+7.8)	(+2.3)	
LL–LAO [a]		4536.5	4573.3	4549.8	4548.9	4541.5	4539.0
		(-2.5)	(+43.3)	(+10.8)	(+9.9)	(+2.5)	

[a] Diamagnetic term calculated as expectation value of the nonrelativistic diamagnetic operator. Otherwise obtained from the "-+" linear response function. For details see Ref. [419].

added to the nonrelativistic value of the NMR shielding obtained from a high–level correlation method like the coupled cluster method [431]. This approach was used for relativistic corrections of NMR shielding constants for third row hydrides [432] and the results differ by fraction of ppm from MCSCF perturbation corrections [430]. Although, spin–spin coupling constants (defined as the second derivative of the energy with respect to magnetic dipoles) correspond to principally different perturbations in the Hamiltonian, this approach is successfully applicable for these NMR properties as well. The test was performed on spin–spin coupling constants of the group 14 XH_4 hydrides [433], where authors showed that adding relativistic corrections calculated using the described approximate method to vibrationally corrected nonrelativistic coupled cluster values of spin–spin coupling constants, J^1(XH) (X=C, Si, Ge), leads to an excellent agreement with gas–phase experimental results. The relativistic correction brought theoretical prediction of the spin–spin coupling constant in SnH_4 closer to experimental value but the value was overestimated by about 10%. Although the approach based on additivity of correlation and relativistic effects gives in some cases better results for NMR properties than relativistic DFT approaches even for relatively heavy compounds (see, *e.g.*, NMR properties of xenon fluorides [434]), the usage is obviously limited to lighter systems. Moreover, the calculations are quite expensive due to a slow convergence of the relativistic correction to the basis set limit.

Apart from the mentioned *ab initio* methods for computing NMR properties there is a large group of methods dealing with the electronic correlation and effects of relativity within the two–component DFT approach, see Refs. [435–440].

5.8 From relativistic effects in atoms and molecules to gas–phase properties and the condensed phase

Relativistic effects, as demonstrated in previous Sections, concern primarily properties of isolated atoms or molecules. However, real chemistry and physics proceeds in the gas phase, or, mostly, in the condensed phase. Clearly, the understanding of basic trends in molecular structures, in the bonding character, bonding energies and atomic and molecular properties is unavoidable for understanding the processes in the gas phase, in solutions and in the solid state, too.

An example of relativistic effects beyond isolated molecules is the investigation of sublimation enthalpies of metals in groups 10, 11, and 14 linked with different molecular properties by Pershina *et al.* [441, 442]. Particularly interesting is clear correlation between binding energies of homonuclear and heteronuclear MM′ diatomics of group 10, 11, and 14 elements with their sublimation enthalpies. In previous Sections we have presented several examples of a typical V–shaped pattern of some molecular properties in the series of elements down in the Periodic Table. The V–shaped pattern characterizes binding energies of the group 10 elements (Ni, Pd, and Pt) and coinage metal elements (Cu, Ag, Au, the group 11). Experimental sublimation enthalpies ΔH_{sub} precisely copy the same pattern. Different picture exhibit the group 14 elements. Their binding energies in the Ge, Sn, Pb, and the 114 element series smoothly diminish with increasing atomic number and precisely the same trend is observed for experimental sublimation enthalpies. The behaviour of a series of binding energies of homonuclear and heteronuclear diatomics and relation of these energies to ΔH_{sub} is analysed using relativistic effects in participating valence orbitals and their relativistic stabilization (particularly s and $p_{1/2}$ orbitals) or destabilization (particularly (n-1)d–orbitals in Hg and the element 112 containing molecules).

Comparison of relativistic and nonrelativistic properties of compounds in atomic properties and volatility of the element 112 and Cd and Hg containing molecules and the V–shaped pattern of their properties were treated in detail also in former papers of Pershina *et al.* [442, 443]. Relativistic effects also affect the adsorption of inert gases, Ne up to Xe, Rn and the element 118 on noble metal and other surfaces, including quartz, ice, graphite and teflon [444].

A typical V–shaped trend exhibit transfer Gibbs energies of the coinage and alkali metal cations in the combined theoretical and experimental (Secondary Ion Mass Spectrometry, SIMS) research [445] on ion transfer properties in water and acetonitrile. The theoretical ΔG^0_{298K} were based on the binding energies of the coinage metal Cu^+, Ag^+, and Au^+ cations with water and acetonitrile obtained from CCSD(T) and DKH–CCSD(T) calculations. Relativistic data do nicely correlate with experimental transfer Gibbs energies while the nonrelativistic data are significantly off this trend. The highest binding energy was found for the Au^+ interaction with acetonitrile. This results from the dative sigma–bonding accompanied by the charge transfer from N to Au^+, like it was discussed in detail in Section 5.6 and a significant back–donation of the electron density from the Au^+ $5d$ to N $2p$ shell suggesting the existence of a multiple bond between the nitrogen atom and the gold cation. Ilčin *et al.* [446] performed relativistic CCSD(T) and perturbational calculations of interatomic and intermolecular interactions in complexes of CdZn, HgZn, and HgCd, and used these data for the temperature dependence of the viscosity for low–density binary mixtures of the group 12 elements. CCSD(T) spectroscopic constants of Zn_2, Cd_2, and Hg_2 calculated by the DC Hamiltonian give support for an acceptable agreement of theoretical and experimental dynamic viscosities of the Zn, Cd, and Hg vapours [447]. Similar approach has been used for calculations of diffusion coefficients and stability of $Hg\cdots N_2$ complexes [448].

Vogt *et al.* [449] synthesised and studied experimentally and theoretically the low– and high–temperature modifications of Sc_3RuC_4 and Sc_3OsC_4 carbides. They analysed the local electronic structure of the $T(C_2)_2$ moieties and discussed an interplay between chemical bonding and relativistic effects which is responsible for the "V"–shaped pattern of the C–C bond length in crystals with T=Fe, Ru, and Os. Their interpretation includes the $T \rightarrow \pi^*$(C–C) back donation in line with model $M(C_2H_2)$ benchmark systems (M=Ni, Pd, and Pt) studied by Ziegler *et al.* and Eickerling *et al.* [450, 451].

Another new species, the icosahedral WAu_{12} nanoparticle is a stable multiply bonded system representing a new structural principle in gold chemistry. Based on the idea of the "aurophilicity" and relativistically strengthened W–Au and Au–Au bonds its existence and properties was predicted by Pyykkö and Runeberg [452] in 2002. The existence of this species was experimentally confirmed in the same year [453]. Later on, Pyykkö and coworkers [454] studied the finite–temperature dynamics of this species.

At this occasion we wish to cite the title of the paper "Gold goes nano – from small clusters to low–dimensional assemblies" in which Schwerdtfeger [351] emphasised that bulk gold is a noble metal but the atomic and nanocrystalline gold compounds can be very reactive and reach applications in different areas. It was not until 1987 that the interest in gold nanostructures was really awakened through the report of Haruta *et al.* [455] on CO oxidation on supported gold catalysts. Since then nanocrystalline gold compounds have been the subject of intense research and have found far reaching applications in areas as catalysis, sensors, molecular electronics or as bioconjugate probes for amplification tags in gene analysis, antibody or antigen detection, DNA sequencing, or gene mapping [351]. Catalytic properties of gold, its ability to create metal–metal bonds, aurophilicity and other phenomena linked with relativistic effects in chemical bonds as pioneered in groups of Pyykkö, Schwarz, Schmidbaur, Schwerdtfeger,Schröder and other were discussed in Section 5.5, see, *e.g.*, Refs. [12, 13, 20, 350–353]. The role of the gold nanofilms in biomedical applications was analysed by Tokonami *et al.* [456].

Extremely interesting is discussion of the relation between molecular properties and the solid–state symmetry. It may help in understanding of experimental observations and some trends within a group of analogous compounds and their solid state structures, but in any case it is not straightforward. In two papers dealing with the Cu, Ag, and Au halides Schwerdtfeger *et al.* [457, 458] compared the structures calculated with and without relativistic effects. Along with the bonding characteristics of molecules involved in solid–state structures they also calculated sublimation energies for different most stable crystal modifications and their low– and high– temperature stabilities and their transitions. Some crystals, like the fluorides CuF, are experimentally unknown since they easily disproportionate at normal conditions. In general, the coinage halides crystallize in the zinc blende, rock salt or in the chainlike structures. At the nonrelativistic correlated level the cubic structures are favoured. Relativity stabilizes chainlike structures particularly for the AuX crystals. This is linked with the relativistic increase of the covalency in Au–X (X is F, Cl, Br, or I) molecules and disfavours in this way ionic structure types for which the rock salt crystals are more typical. Different from the AuX compounds, the CuX and AgX halides can be regarded as mainly ionic. How relativity reduces the polarity of MX molecules is demonstrated in Fig. 5.8. Considerable reduction of the dipole moment is observed particularly for AuF. The silver halides, which have highest dipole moments, all crystallize at room temperatures and low pressures in the simple rock salt structure. The most interesting situation is found for the gold halides [458], for which the unusual chainlike structures with short Au–Au distances are favoured compared to the cubic structures. The main message is [457] that relativistic effects drastically influence the solid–state symmetry.

It appears that similar analysis as was presented for the group 11 monohalides is also applicable to the group 12 solid–state oxides, ZnO, CdO, and HgO [459]. The solid–state HgO at low pressure is analogous with the AuF structure. It is represented by the chainlike montroydite and cinnabar structures in contrast with ZnO and CdO structures which have typically hexagonal wurtzite or rock salt structures. This marked difference is caused by relativistic effects. There is some analogy between the bonding situation in AuF and HgO. As it is presented in Tab. 5.19, the bond strength of both molecules is significantly relativistically reduced, and, also, both molecules become less polar, *i.e.* their dipole moments diminish due to relativistic effects, see Fig. 5.8 and Refs. [300, 459]. Besides of changes in the solid–state structure, relativistic effects also reduce the cohesive energy of HgO. It appears that the unusual yellow to red colour of HgO is a relativistic effect as well [459].

Exceptional position of Hg containing crystals in the group 12 dihalides is also attributed to relativistic effects by Donald *et al.* [414]. Their analysis is based on DFT calculations of monomers and dimers of MX_2 molecules (M = Zn, Cd, Hg and X = F, Cl, Br, I). The zinc and cadmium dihalide dimers have the usual D_{2h} symmetry geometry, whereas the mercury dihalide dimers are loosely–bound units with the C_{2h} symmetry. Donald *et al.* found an obvious connection between the structures and characteristics of monomers, their dimers, and the crystals they form. The crystal structures of the group 12 MX_2 dihalides exhibit a wide range of structural types, from three–dimensional extended solids to molecular crystals. Since the ionization potential of Hg is high due to the relativistic stabilization of its valence $6s^2$ electrons, somewhat surprising is the structure of HgF_2, which becomes an ionic solid. The crystals of $HgCl_2$ and $HgBr_2$ are molecular solids which is connected with smaller electronegativity of Cl and Br so that extended structures cannot be formed.

Calculations [460] of the interatomic interaction energies for the Hg dimer and small clusters of the mercury atoms allowed to develop a many–body expansion of the correlation energy which is added to the solid state HF energy [461]. The Hg dimer is more strongly bound than the Zn and Cd dimers due to relativistic effects. The cluster studies were extended to the solid state and optimized lattice parameters and cohesive energies for bulk mercury. For smaller clusters the highly accurate CCSD(T) method was still applicable. DFT methods applicable to larger clusters lead to diverse results for, *e.g.*, the cohesive energies for bulk mercury. Accurate interaction potentials including at least three–body effects are critically needed for reliable description of the bulk properties by Monte Carlo simulations [462]. Accurate interaction potentials, based on the fitting of CCSD(T) data, lead to excellent agreement of the bulk melting temperature of argon, 84.7 K, within less than 1 K of the experimental value. Such accuracy is not yet achievable for metallic systems or molecular solids, but preliminary results results are at least very promising.

A cluster modelling of the interaction of the eka-Hg (element 112) and eka–Pb atom (element 114) with the stable Au(111) surface using accurate small–core relativistic pseudopotentials and two–component non–collinear DFT was published by Zaitsevskii *et al.* [416, 463].

6 Conclusions

Real life of molecules is a relativistic quantum mechanical life. This holds for all atoms and molecules throughout the Periodic Table. In light elements are relativistic effects visible in fine structure effects and are growing dramatically for molecules containing elements with increasing atomic number. We have demonstrated that relativistic effects alter many atomic and molecular properties not only quantitatively but also qualitatively. Most important aspect of this paper is understanding of trends within the Periodic Table. For specific groups of elements in the Table we analyse trends of ionization potentials, electron affinities, geometries, electric properties, magnetic properties, interaction and reaction energies. When going to heavier atoms relativistic effects lead frequently to characteristic ”V” shaped behaviour of properties with respect to the atomic number. These relativistic changes are related to the electronic structure of atoms and molecules. We also discuss briefly the link between relativistic changes in properties of individual atoms or molecules and their behaviour in the condensed phase.

We are witnessing vigorous progress in the development of new relativistic theoretical approaches and methods, which allow treating of gradually larger many–electron molecules at the correlated relativistic level with a reasonable accuracy. Both wave function and density functional theories participate on the extension of applicability to a wide scale of problems which need and can be treated by relativistic methods of quantum chemistry.

Acknowledgments

This research was supported by the Slovak Grant Agency, grant VEGA–1/0520/10 and grants of the Slovak Research and Development Agency APVV (Contracts No. LPP–0110–07 and LPP–0155–09). We are grateful to Professor Maria Barysz, Dr. Lukáš Bučinský, Assoc. Professor Pavel Neogrády, and Professor Ján Pišút for careful reading the manuscript, for their valuable suggestions and their kind help in correcting inaccuracies in the text. We also acknowledge the effort of Professor Vladimír Bužek for his enthusiastic pushing for finishing this paper.

Appendix: Atomic units

Introducing atomic units, $e = m_0 = \hbar = 4\pi\epsilon_0 = 1$, considerably simplifies all formulae of quantum mechanics. In Tab. 0.1 we present SI values of atomic units.

Tab. 0.1. The conversion factors of atomic units to SI and other units based on the 2006 CODATA adjustment of the value of constants [45].

a.u. of	Symbol	Numerical value	Unit
charge: elementary charge	e	$1.602\,176\,487(40)\times10^{-19}$	C
mass: electron mass	m_e	$9.109\,382\,15(45)\times10^{-31}$	kg
action: reduced Planck constant	$\hbar$	$1.054\,571\,628(53)\times10^{-34}$	J s
length: Bohr radius (bohr)	a_0	$0.529\,177\,208\,59(36)\times10^{-10}$	m
		$0.529\,177\,208\,59(36)\times10^{-10}$	Å
energy: Hartree energy (hartree)	E_h	$4.359\,743\,94(22)\times10^{-18}$	J
		$27.211\,383\,86(68)$	eV
		$2.194\,746\,313\,705(15)\times10^{5}$	cm^{-1}
		$2.625\,499\,617\times10^{3}$	kJ mol^{-1}
time	$\hbar/E_\mathrm{h}$	$2.418\,884\,326\,505(16)\times10^{-17}$	s
force	E_h/a_0	$8.238\,722\,06(41)\times10^{-8}$	N
velocity	$a_0E_\mathrm{h}/\hbar$	$2.187\,691\,2541(15)\times10^{6}$	m s^{-1}
momentum	$\hbar/a_0$	$1.992\,851\,565(99)\times10^{-24}$	kg m s^{-1}
current	$eE_\mathrm{h}/\hbar$	$6.623\,617\,63(17)\times10^{-3}$	A
charge density	e/a_0^3	$1.081\,202\,300(27)\times10^{12}$	C m^{-3}
electric potential	E_h/e	$27.211\,383\,86(68)$	V
electric field	E_h/ea_0	$5.142\,206\,32(13)\times10^{11}$	V m^{-1}
electric field gradient	E_h/ea_0^2	$9.717\,361\,66(24)\times10^{21}$	V m^{-2}
electric dipole moment	ea_0	$8.478\,352\,81(21)\times10^{-30}$	C m
		$2.541\,746\,23$	Debye
electric quadrupole moment	ea_0^2	$4.486\,551\,07(11)\times10^{-40}$	C m^2
electric polarizability	$e^2a_0^2/E_\mathrm{h}$	$1.648\,777\,2536(34)\times10^{-41}$	C^2 m^2 J^{-1}
1st hyperpolarizability	$e^3a_0^3/E_\mathrm{h}^2$	$3.206\,361\,533(81)\times10^{-53}$	C^3 m^3 J^{-2}
2nd hyperpolarizability	$e^4a_0^4/E_\mathrm{h}^3$	$6.235\,380\,95(31)\times10^{-65}$	C^4 m^4 J^{-3}
magnetic flux density	$\hbar/ea_0^2$	$2.350\,517\,382(59)\times10^{5}$	T
magnetic dipole moment	$\hbar e/m_\mathrm{e}$	$1.854\,801\,830(46)\times10^{-23}$	J T^{-1}
magnetizability	$e^2a_0^2/m_\mathrm{e}$	$7.891\,036\,433(27)\times10^{-29}$	J T^{-2}
permitivity	e^2/a_0E_h	$1.112\,650\,056...\times10^{-10}$	F m^{-1}

References

[1] S. L. Glashow, B. Bova: *Interactions : a journey through the mind of a particle physicist and the matter of this world*: Warner Books, New York, NY (1988)

[2] P. A. M. Dirac: *Proc. Roy. Soc. Lond. A* **123** (1929) 714

[3] W. Heitler, F. London: *Z. Phys.* **44** (1927) 455

[4] P. A. M. Dirac: *Proc. Roy. Soc. Lond. A* **117** (1928) 610

[5] W. Kołos, L. Wolniewicz: *Acta Phys. Polon.* **20** (1961) 129

[6] B. Swirles: *Proc. Roy. Soc. Lond. A* **152** (1935) 625

[7] I. P. Grant: *Proc. Roy. Soc. Lond. A* **262** (1961) 555

[8] J. P. Desclaux: *At. Data Nucl. Data Tabes* **12** (1973) 311

[9] P. Pyykkö, J. P. Desclaux: *Accounts Chem. Res.* **12** (1979) 276

[10] P. Pyykkö: *Chem. Rev.* **88** (1988) 563

[11] P. Pyykkö: *Chem. Rev.* **97** (1997) 597

[12] P. Pyykkö: *Angew. Chem.-Int. Edit.* **41** (2002) 3573

[13] P. Pyykkö: *Angew. Chem.-Int. Edit.* **43** (2004) 4412

[14] W. Kutzelnigg: *Phys. Rev. A* **54** (1996) 1183

[15] J. Almlöf, O. Gropen: In: *Reviews in computational chemistry*, eds. K. B. Lipkowitz, D. B. Boyd, vol. 8, pp. 203–244. Willey-VCH, New York (2001)

[16] P. Schwerdtfeger: In: *Atoms, Molecules and Clusters in Electric fields: Theoretical Approaches to the calculation of electric polarizability*, ed. G. Maroulis, pp. 1–32. Imperial College Press, London (2006)

[17] P. Schwerdtfeger, M. Seth: In: *Encyclopedia of Computational Chemistry*, ed. P. v. R. Schleyer, pp. 2480–2499. Wiley, Chichester (1998)

[18] B. A. Hess: In: *Encyclopedia of Computational Chemistry*, ed. P. v. R. Schleyer, pp. 2499–2508. Wiley, Chichester (1998)

[19] W. H. E. Schwarz, A. Rutkowski, S. G. Wang: *Int. J. Quantum Chem.* **57** (1996) 641

[20] H. Schwarz: *Angew. Chem.-Int. Edit.* **42** (2003) 4442

[21] M. Urban, V. Kellö: *Adv. Quantum Chem.* **50** (2005) 249

[22] M. Urban, V. Kellö: *Comput. Lett.* **2** (2006) 259

[23] P. Schwerdtfeger (ed.): *Relativistic electronic structure theory. Part 1. Fundamentals.*: Theoretical and computational chemistry v. 11. Elsevier, Amsterdam (2002)

[24] P. Schwerdtfeger (ed.): *Relativistic electronic structure theory. Part 2. Applications.*: Theoretical and computational chemistry v. 14. Elsevier, Amsterdam (2004)

[25] K. G. Dyall, K. Fægri: *Introduction to relativistic quantum chemistry*: Oxford University Press, New York (2007)

[26] M. Reiher, A. Wolf: *Relativistic quantum chemistry : the fundamental theory of molecular science*: Wiley-VCH, Weinheim (2009)

[27] P. A. M. Dirac: *Proc. Roy. Soc. Lond. A* **118** (1928) 351

[28] I. P. Grant, H. M. Quiney: *Int. J. Quantum Chem.* **80** (2000) 283

[29] K. Pachucki, J. Komasa: *Phys. Rev. Lett.* **92** (2004) 213001

[30] D. Mendeleev: *Zhurnal Russkoe Fiziko-Khimicheskoe Obshchestvo* **1** (1869) 66

[31] D. Mendelejeff: *Zeitschrift für Chemie* **12** (1869) 405

[32] D. R. Lide (ed.): *CRC handbook of chemistry and physics, CD-ROM Version 2005*: CRC Press, Boca Raton (2005)

[33] P. Neogrády, V. Kellö, M. Urban, A. J. Sadlej: *Int. J. Quantum Chem.* **63** (1997) 557

[34] J. Gažo, J. Kohout, M. Serátor, T. Šramko, M. Zikmund: *Všeobecná a anorganická chémia*: Alfa, Bratislava (1974)

[35] M. Urban, J. Noga, S. J. Cole, R. J. Bartlett: *J. Chem. Phys.* **83** (1985) 4041

[36] K. Raghavachari, G. W. Trucks, J. A. Pople, M. HeadGordon: *Chem. Phys. Lett.* **157** (1989) 479

[37] M. Urban, I. Černušák, J. Noga, V. Kellö: In: *Methods in Computational Chemistry*, ed. S. Wilson, vol. 1, pp. 117–250. Plenum Press, New York (1987)

[38] J. Paldus, X. Z. Li: *Adv. Quantum Chem.* **110** (1999) 1

[39] T. Helgaker, P. Jørgensen, J. Olsen: *Molecular electronic-structure theory*: Wiley, Chichester ; New York (2000)

[40] I. Shavitt, R. J. Bartlett: *Many-body methods in chemistry and physics : MBPT and coupled-cluster theory*: Cambridge molecular science. Cambridge University Press, Cambridge ; New York (2009)

[41] J. P. Desclaux, Y. K. Kim: *J. Phys. B-At. Mol. Opt. Phys.* **8** (1975) 1177

[42] N. Bohr: *Philos. Mag.* **26** (1913) 1

[43] A. Einstein: *Ann. Phys.-Berlin* **17** (1905) 891

[44] J. C. Maxwell: *Philos. Mag.* **21** (1861) 161

[45] P. J. Mohr, B. N. Taylor, D. B. Newell: *Rev. Mod. Phys.* **80** (2008) 633

[46] J. F. Harrison: *Spin–orbit interaction* (2006): http://www.cem.msu.edu/˜cem987/spin_orbit.pdf

[47] E. Schrödinger: *Phys. Rev.* **28** (1926) 1049

[48] W. Gerlach, O. Stern: *Z. Phys.* **9** (1922) 353

[49] G. E. Uhlenbeck, S. Goudsmit: *Nature* **117** (1926) 264

[50] J. Pišút, R. Zajac: *O atómoch a kvantovaní*: FMFI UK, Bratislava (2009)

[51] L. Piela: *Ideas of quantum chemistry*: Elsevier, Amsterdam ; Boston (2007)

[52] G. E. Uhlenbeck, S. Goudsmit: *Naturw.* **13** (1925) 953

[53] W. Pauli: *Z. Phys.* **43** (1927) 601: See footnote 2 on page 607

[54] M. Born, R. Oppenheimer: *Ann. Phys.-Berlin* **84** (1927) 0457

[55] J. C. Slater: *Phys. Rev.* **34** (1929) 1293

[56] V. Fock: *Z. Phys.* **61** (1930) 126

[57] D. R. Hartree, W. Hartree: *Proc. Roy. Soc. Lond. A* **150** (1935) 9

[58] D. R. Hartree: *Nature* **138** (1936) 1080

[59] C. C. J. Roothaan: *Rev. Mod. Phys.* **32** (1960) 179

[60] J. A. Pople, R. K. Nesbet: *J. Chem. Phys.* **22** (1954) 571

[61] S. F. Boys: *Proc. R. Soc. London Ser. A* **200** (1950) 542

[62] P. Čársky, M. Urban: *Ab initio calculations : methods and applications in chemistry*: Lecture notes in chemistry 16. Springer-Verlag, Berlin ; New York (1980)

[63] C. C. J. Roothaan: *Rev. Mod. Phys.* **23** (1951) 69

[64] F. Aquilante, L. De Vico, N. Ferré, G. Ghigo, P.-Å. Malmqvist, P. Neogrády, T. B. Pedersen, M. Pitoňák, M. Reiher, B. O. Roos, L. Serrano-Andrés, M. Urban, V. Veryazov, R. Lindh: *J. Comput. Chem.* **31** (2010) 224

[65] M. Urban, P. Neogrády, I. Hubač: In: *Recent Advances in Computational Chemistry*, ed. R. J. Bartlett, vol. 3, pp. 275–306. World Scientific, Singapore (1997)

[66] J. D. Watts, J. Gauss, R. J. Bartlett: *J. Chem. Phys.* **98** (1993) 8718
[67] P.-O. Löwdin: *Phys. Rev.* **97** (1955) 1509
[68] C. D. Sherrill, H. F. Schaefer: *Adv. Quantum Chem.* **34** (1999) 143
[69] B. Roos: *Chem. Phys. Lett.* **15** (1972) 153
[70] M. Barbatti, H. Lischka: *J. Phys. Chem. A* **111** (2007) 2852
[71] T. D. Crawford, H. F. Schaefer: In: *Reviews in Computational Chemistry*, eds. K. B. Lipkowitz, D. B. Boyd, pp. 33–136. Wiley-VCH, Inc., Hoboken (2007)
[72] M. Gell-Mann, K. A. Brueckner: *Phys. Rev.* **106** (1957) 364
[73] H. A. Bethe: *Phys. Rev.* **103** (1956) 1353
[74] F. Coester: *Nucl. Phys.* **7** (1958) 421
[75] F. Coester, H. Kümmel: *Nucl. Phys.* **17** (1960) 477
[76] J. Čížek: *J. Chem. Phys.* **45** (1966) 4256
[77] J. Čížek: *Adv. Chem. Phys.* **14** (1969) 35
[78] J. Paldus, I. Shavitt, J. Čížek: *Phys. Rev. A* **5** (1972) 50
[79] R. J. Bartlett: *J. Phys. Chem.* **93** (1989) 1697
[80] J. Paldus, J. Čížek: *Adv. Quantum Chem.* **9** (1975) 105
[81] J. Paldus: In: *Methods in Computational Molecular Physics*, eds. S. Wilson, G. H. F. Diercksen, vol. 293 of *NATO Advanced Science Institutes Series, Series B, Physics*, pp. 99–194. Plenum Press, New York (1992)
[82] S. A. Kucharski, R. J. Bartlett: *Theor. Chim. Acta* **80** (1991) 387
[83] I. Lindgren, S. Salomonson, D. Hedendahl: In: *Recent progress in coupled cluster methods: Theory and applications*, eds. P. Čársky, J. Paldus, J. Pittner, pp. 357–374. Springer, Berlin (2010)
[84] E. Eliav, U. Kaldor: In: *Recent progress in coupled cluster methods: Theory and applications*, eds. P. Čársky, J. Paldus, J. Pittner, pp. 113–144. Springer, Berlin (2010)
[85] P. Čársky, J. Paldus, J. Pittner (eds.): *Recent progress in coupled cluster methods: Theory and applications*: Springer, Berlin (2010)
[86] G. D. Purvis, R. J. Bartlett: *J. Chem. Phys.* **76** (1982) 1910
[87] J. Noga, R. J. Bartlett: *J. Chem. Phys.* **86** (1987) 7041
[88] R. J. Bartlett, M. Musial: *Rev. Mod. Phys.* **79** (2007) 291
[89] M. Kallay, P. R. Surjan: *J. Chem. Phys.* **115** (2001) 2945
[90] S. A. Kucharski, R. J. Bartlett: *J. Chem. Phys.* **108** (1998) 5243
[91] M. Musial, S. A. Kucharski, R. J. Bartlett: *J. Chem. Phys.* **116** (2002) 4382
[92] X. Z. Li, J. Paldus: *J. Chem. Phys.* **101** (1994) 8812
[93] P. Neogrády, M. Urban: *Int. J. Quantum Chem.* **55** (1995) 187
[94] M. Douglas, N. M. Kroll: *Ann. Phys. (N.Y.)* **82** (1974) 89
[95] B. A. Hess: *Phys. Rev. A* **32** (1985) 756
[96] J. Noga, W. Kutzelnigg: *J. Chem. Phys.* **101** (1994) 7738
[97] X. Z. Li, J. Paldus: *J. Chem. Phys.* **119** (2003) 5320
[98] J. Pittner, P. Piecuch: *Mol. Phys.* **107** (2009) 1209
[99] O. Demel, J. Pittner, P. Čársky, I. Hubač: *J. Phys. Chem. A* **108** (2004) 3125
[100] B. O. Roos, K. Andersson, M. P. Fülscher, P.-Å. Malmqvist, L. Serrano-Andrés, K. Pierloot, M. Merchán: *Adv. Chem. Phys.* **93** (1996) 219

[101] K. Andersson, P.-Å. Malmqvist, B. O. Roos, A. J. Sadlej, K. Wolinski: *J. Phys. Chem.* **94** (1990) 5483

[102] B. O. Roos, P.-Å. Malmqvist: *Phys. Chem. Chem. Phys.* **6** (2004) 2919

[103] P.-Å. Malmqvist, B. O. Roos, B. Schimmelpfennig: *Chem. Phys. Lett.* **357** (2002) 230

[104] Z. Azizi, B. O. Roos, V. Veryazov: *Phys. Chem. Chem. Phys.* **8** (2006) 2727

[105] B. O. Roos, R. Lindh, P.-Å. Malmqvist, V. Veryazov, P. O. Widmark: *J. Phys. Chem. A* **108** (2004) 2851

[106] B. O. Roos, R. Lindh, P.-Å. Malmqvist, V. Veryazov, P. O. Widmark: *J. Phys. Chem. A* **109** (2005) 6575

[107] H. A. Lorentz: *Proc. Acad. Science Amsterdam* **1** (1899) 427

[108] H. Poincaré: *Comptes rendus de l' Académie des Sciences de Paris* **140** (1905) 1504

[109] A. Einstein: *Ann. Phys.-Berlin* **18** (1905) 639

[110] W. Gordon: *Z. Phys.* **40** (1926) 117

[111] O. Klein: *Z. Phys.* **41** (1927) 407

[112] W. Pauli, V. Weisskopf: *Helv. Phys. Acta* **7** (1934) 709

[113] P. A. M. Dirac: In: *History of twentieth century physics*, ed. C. Weiner, pp. 109–146. Academic Press, New York (1977)

[114] C. D. Anderson: *Phys. Rev.* **41** (1932) 405

[115] C. G. Darwin: *Proc. Roy. Soc. Lond. A* **118** (1928) 654

[116] H. A. Bethe, E. E. Salpeter: *Quantum mechanics of one-and two-electron atoms*: Plenum Press, New York (1977)

[117] R. E. Moss: *Advanced molecular quantum mechanics; an introduction to relativistic quantum mechanics and the quantum theory of radiation*: Chapman and Hall, London (1973)

[118] M. E. Rose: *Relativistic electron theory*: Wiley, New York (1961)

[119] A. Messiah: *Quantum mechanics*: North-Holland, Amsterdam (1961)

[120] H. E. White: *Phys. Rev.* **38** (1931) 514

[121] A. Szabo: *J. Chem. Educ.* **46** (1969) 678

[122] C. W. Sherwin: *Introduction to quantum mechanics*: Holt, Rinehart and Winston, New York (1959)

[123] I. P. Grant, H. M. Quiney: *Adv. At. Mol. Phys.* **23** (1988) 37

[124] Y. Ishikawa, H. M. Quiney: *Int. J. Quantum Chem. Suppl.* **21** (1987) 523

[125] O. Visser, P. J. C. Aerts, D. Hegarty, W. C. Nieuwpoort: *Chem. Phys. Lett.* **134** (1987) 34

[126] L. Visscher, K. G. Dyall: *At. Data Nucl. Data Tables* **67** (1997) 207: see also http://www.chem.vu.nl/˜visscher/FiniteNuclei/FiniteNuclei.htm

[127] M. Gell-Mann: *Nuovo Cimento Suppl.* **4** (1956) 848

[128] T. Saue, L. Visscher: In: *Theoretical chemistry and physics of heavy and superheavy elements*, eds. U. Kaldor, S. Wilson, vol. 11 of *Progress in theoretical chemistry and physics*, p. 211. Kluwer, Dordrecht (2003)

[129] P. A. M. Dirac: In: *Structure et Propertietes des Noyaux Atomiques. Septieme Conseil du Physique Solvay, Bruxelles, 22–29 October 1933*, eds. J. Cockcroft, J. Chadwick, F. Joliot, J. Joliot, N. Bohr, G. Gamov, P. A. M. Dirac, W. Heisenberg, pp. 203–230. Gautier-Villars, Paris (1934)

[130] G. Breit: *Physical Review* **34** (1929) 553

[131] J. A. Gaunt: *Proc. Roy. Soc. Lond. A* **122** (1929) 513

[132] P. M. Kozlowski, L. Adamowicz: *Chem. Rev.* **93** (1993) 2007

[133] G. E. Brown, D. G. Ravenhall: *Proc. Roy. Soc. Lond. A* **208** (1951) 552

[134] M. H. Mittleman: *Phys. Rev. A* **24** (1981) 1167

[135] H. M. Quiney: *Private communication; the information is provided in a letter from Lady Jeffreys (born Swirles) to H.M.Q., 3 March 1997* ()

[136] G. Malli, J. Oreg: *J. Chem. Phys.* **63** (1975) 830

[137] R. E. Stanton, S. Havriliak: *J. Chem. Phys.* **81** (1984) 1910

[138] P. J. C. Aerts, W. C. Nieuwpoort: *Chem. Phys. Lett.* **113** (1985) 165

[139] K. G. Dyall, I. P. Grant, S. Wilson: *J. Phys. B-At. Mol. Opt. Phys.* **17** (1984) 493

[140] L. Visscher, P. J. C. Aerts, O. Visser: In: *The effects of relativity in atoms, molecules, and the solid state*, eds. S. Wilson, I. P. Grant, B. L. Gyorffy, p. 197. Plenum Press, New York (1991)

[141] J. Thyssen: *Develompment and applications of methods for correlated relativistic calculations of molecular properties*: Phd. thesis, University of Southern Denmark, Odense (2001)

[142] H. J. Aa. Jensen, K. G. Dyall, T. Saue, K. Fægri: *J. Chem. Phys.* **104** (1996) 4083

[143] J. Thyssen, T. Fleig, H. J. Aa. Jensen: *J. Chem. Phys.* **129** (2008) 034109

[144] T. Fleig, C. M. Marian, J. Olsen: *Theor. Chem. Acc.* **97** (1997) 125

[145] H. A. Kramers: *Proc. Acad. Sci. Amsterdam* **33** (1930) 959

[146] P. Hafner: *J. Phys. B-At. Mol. Opt. Phys.* **13** (1980) 3297

[147] H. A. Bethe: *Annal. Phys.* **3** (1929) 133208

[148] S. L. Altmann: *Rotations, quaternions, and double groups*: Clarendon Press, Oxford (1986)

[149] C. J. Bradley, A. P. Cracknell: *The mathematical theory of symmetry in solids; representation theory for point groups and space groups*: Clarendon Press, Oxford, (1972)

[150] P. J. C. Aerts: *Chem. Phys. Lett.* **104** (1984) 28

[151] A. Rosen: *Int. J. Quantum Chem.* **13** (1978) 509

[152] J. Meyer: *Int. J. Quantum Chem.* **33** (1988) 445

[153] J. Meyer, W. D. Sepp, B. Fricke, A. Rosen: *Comput. Phys. Commun.* **54** (1989) 55

[154] L. Visscher: *Chem. Phys. Lett.* **253** (1996) 20

[155] T. Saue, H. J. Aa. Jensen: *J. Chem. Phys.* **111** (1999) 6211

[156] K. Rykhlinskaya, S. Fritzsche: *Comput. Phys. Commun.* **171** (2005) 119

[157] T. Yanai, R. J. Harrison, T. Nakajima, Y. Ishikawa, K. Hirao: *Int. J. Quantum Chem.* **107** (2007) 1382

[158] D. L. Peng, J. Y. Ma, W. J. Liu: *Int. J. Quantum Chem.* **109** (2009) 2149

[159] B. A. Hess, C. M. Marian: In: *Computational molecular spectroscopy*, eds. P. Jensen, P. R. Bunker, p. 169. Wiley, Chichester ; New York (2000)

[160] K. Balasubramanian: *Relativistic effects in chemistry. Part A: Theory and techniques*: Wiley Interscience, New York (1997)

[161] K. G. Dyall: *Theor. Chem. Acc.* **115** (2006) 441

[162] K. G. Dyall: *Theor. Chem. Acc.* **117** (2007) 483

[163] K. G. Dyall: *J. Phys. Chem. A* **113** (2009) 12638

[164] K. G. Dyall, A. S. P. Gomes: *Theor. Chem. Acc.* **125** (2010) 97

[165] A. Gomes, K. Dyall, L. Visscher: *Theor. Chem. Acc.* (2010): DOI 10.1007/s00214-009-0725-7

[166] L. Visscher: *Theor. Chem. Acc.* **98** (1997) 68

[167] M. Abe, T. Yanai, T. Nakajima, K. Hirao: *Chem. Phys. Lett.* **388** (2004) 68

[168] C. Møller, M. Plesset: *Phys. Rev.* **46** (1934) 618

[169] J. K. Laerdahl, T. Saue, K. Fægri: *Theor. Chem. Acc.* **97** (1997) 177

[170] DIRAC: *a relativistic ab initio electronic structure program, release dirac08* (2008): written by L. Visscher, H. J. Aa. Jensen, and T. Saue, with new contributions from R. Bast, S. Dubillard, K. G. Dyall, U. Ekström, E. Eliav, T. Fleig, A. S. P. Gomes, T. U. Helgaker, J. Henriksson, M. Iliaš, Ch. R. Jacob, S. Knecht, P. Norman, J. Olsen, M. Pernpointner, K. Ruud, P. Sałek, and J. Sikkema, see http://dirac.chem.sdu.dk

[171] M. Abe, T. Nakajima, K. Hirao: *J. Chem. Phys.* **125** (2006) 234110

[172] L. Visscher, T. J. Lee, K. G. Dyall: *J. Chem. Phys.* **105** (1996) 8769

[173] M. Pernpointner, L. Visscher: *J. Comput. Chem.* **24** (2003) 754

[174] L. Visscher, K. G. Dyall, T. J. Lee: *Int. J. Quantum Chem. Suppl.* **29** (1995) 411

[175] A. Landau, E. Eliav, Y. Ishikawa, U. Kaldor: *J. Chem. Phys.* **121** (2004) 6634

[176] L. Visscher, E. Eliav, U. Kaldor: *J. Chem. Phys.* **115** (2001) 9720

[177] A. Landau, E. Eliav, U. Kaldor: *Chem. Phys. Lett.* **313** (1999) 399

[178] A. Landau, E. Eliav, U. Kaldor: *Int. J. Mod. Phys. B* **17** (2003) 5335

[179] E. Eliav, M. J. Vilkas, Y. Ishikawa, U. Kaldor: *J. Chem. Phys.* **122** (2005) 224113

[180] T. Fleig, J. Olsen, C. M. Marian: *J. Chem. Phys.* **114** (2001) 4775

[181] T. Fleig, J. Olsen, L. Visscher: *J. Chem. Phys.* **119** (2003) 2963

[182] T. Fleig, H. J. Aa. Jensen, J. Olsen, L. Visscher: *J. Chem. Phys.* **124** (2006) 104106

[183] S. Knecht, H. J. Aa. Jensen, T. Fleig: *J. Chem. Phys.* **132** (2010) 014108

[184] T. Fleig: *Phys. Rev. A* **77** (2008) 062503

[185] Y. S. Lee: In: *Relativistic electronic structure theory. Part 2. Applications.*, ed. P. Schwerdtfeger, Theoretical and computational chemistry v. 14, pp. 352–416. Elsevier, Amsterdam (2004)

[186] K. A. Peterson, D. Figgen, E. Goll, H. Stoll, M. Dolg: *J. Chem. Phys.* **119** (2003) 11113

[187] D. Figgen, K. A. Peterson, M. Dolg, H. Stoll: *J. Chem. Phys.* **130** (2009) 164108

[188] H. Stoll: *Chem. Phys. Lett.* **429** (2006) 289

[189] D. Figgen, A. Wedig, H. Stoll, M. Dolg, E. Eliav, U. Kaldor: *J. Chem. Phys.* **128** (2008) 024106

[190] L. L. Foldy, S. A. Wouthuysen: *Phys. Rev.* **78** (1950) 29

[191] B. A. Hess, C. M. Marian, S. D. Peyerimhoff: In: *Modern electronic structure theory, Part I*, ed. D. R. Yarkony, Advanced series in physical chemistry, Vol. 2, pp. 152–278. World Scientific, Singapore (1995)

[192] B. A. Hess: *Phys. Rev. A* **33** (1986) 3742

[193] T. Nakajima, K. Hirao: *J. Chem. Phys.* **113** (2000) 7786

[194] T. Nakajima, K. Hirao: *J. Chem. Phys.* **119** (2003) 4105

[195] C. Park, J. E. Almlöf: *Chem. Phys. Lett.* **231** (1994) 269

[196] C. van Wüllen: *J. Chem. Phys.* **120** (2004) 7307

[197] M. Reiher, A. Wolf: *J. Chem. Phys.* **121** (2004) 2037

[198] M. Reiher, A. Wolf: *J. Chem. Phys.* **121** (2004) 10945

[199] J. L. Heully, I. Lindgren, E. Lindroth, S. Lundqvist, A. M. Mårtensson-Pendrill: *J. Phys. B-At. Mol. Opt. Phys.* **19** (1986) 2799

[200] W. Kutzelnigg: *J. Chem. Phys.* **110** (1999) 8283

[201] W. Kutzelnigg, W. J. Liu: *J. Chem. Phys.* **123** (2005) 241102

[202] E. van Lenthe, E. J. Baerends, J. G. Snijders: *J. Chem. Phys.* **105** (1996) 2373

[203] K. G. Dyall: *J. Chem. Phys.* **106** (1997) 9618

[204] K. G. Dyall: In: *Theoretical chemistry and physics of heavy and superheavy elements*, eds. U. Kaldor, S. Wilson, p. 325. Kluwer, Dordrecht (2003)

[205] C. Chang, M. Pelissier, P. Durand: *Phys. Scr.* **34** (1986) 394

[206] E. van Lenthe, E. J. Baerends, J. G. Snijders: *J. Chem. Phys.* **101** (1994) 9783

[207] E. van Lenthe, J. G. Snijders, E. J. Baerends: *J. Chem. Phys.* **105** (1996) 6505

[208] K. G. Dyall, E. van Lenthe: *J. Chem. Phys.* **111** (1999) 1366

[209] R. van Leeuwen, E. van Lenthe, E. J. Baerends, J. G. Snijders: *J. Chem. Phys.* **101** (1994) 1272

[210] Y. Nakatsuka, T. Nakajima, M. Nakata, K. Hirao: *J. Chem. Phys.* **132** (2010) 054102

[211] M. Barysz, A. J. Sadlej, J. G. Snijders: *Int. J. Quantum Chem.* **65** (1997) 225

[212] M. Barysz, A. J. Sadlej: *Theochem-J. Mol. Struct.* **573** (2001) 181

[213] M. Barysz: *J. Chem. Phys.* **114** (2001) 9315

[214] M. Barysz, A. J. Sadlej: *J. Chem. Phys.* **116** (2002) 2696

[215] M. Barysz: In: *Theoretical Chemistry and Physics of Heavy and Super-Heavy Elements.*, eds. U. Kaldor, S. Wilson, vol. 11 of *Progress in Theoretical Chemistry and Physics*, pp. 349–397. Kluwer Academic Publishers, Dordrecht (2003)

[216] M. Barysz: In: *Relativistic methods for chemists*, eds. M. Barysz, Y. Ishikawa, vol. 10 of *Challenges and advances in computational chemistry and physics*, pp. 165–190. Springer, Dordrecht (2010)

[217] R. D. Cowan, D. C. Griffin: *J. Opt. Soc. Am.* **66** (1976) 1010

[218] J. H. Wood, A. M. Boring: *Phys. Rev. B* **18** (1978) 2701

[219] S. Komorovský, M. Repiský, O. L. Malkina, V. G. Malkin, I. Malkin, M. Kaupp: *J. Chem. Phys.* **124** (2006) 084108

[220] V. Kellö, A. J. Sadlej: *Int. J. Quantum Chem.* **68** (1998) 159

[221] M. Barysz: *Pol. J. Chem.* **74** (2000) 1329

[222] D. Kędziera, M. Barysz, A. J. Sadlej: *Struct. Chem.* **15** (2004) 369

[223] J. Seino, W. Uesugi, M. Hada: *J. Chem. Phys.* **132** (2010) 164108

[224] M. Iliaš, T. Saue: *J. Chem. Phys.* **126** (2007) 064102

[225] L. Visscher, T. Saue: *J. Chem. Phys.* **113** (2000) 3996

[226] K. G. Dyall: *J. Chem. Phys.* **100** (1994) 2118

[227] H. J. Aa. Jensen, M. Iliaš in preparation

[228] W. J. Liu, D. L. Peng: *J. Chem. Phys.* **125** (2006) 044102

[229] D. Kędziera, M. Barysz: *Chem. Phys. Lett.* **446** (2007) 176

[230] M. Barysz, L. Mentel, J. Leszczynski: *J. Chem. Phys.* **130** (2009) 164114

[231] C. E. Moore: *Ionization Potentials and Ionization Limits Derived from the Analyses of Optical Spectra*: Natl. Stand. Ref. Data Ser. U.S. Natl. Bur. Stand. (1970)

[232] T. Saue, H. J. Aa. Jensen: *J. Chem. Phys.* **118** (2003) 522

[233] C. M. Marian: In: *Reviews in computational chemistry*, eds. K. B. Lipkowitz, D. B. Boyd, vol. 17, pp. 99–204. Willey-VCH, New York (2001)

[234] B. A. Hess, C. M. Marian, U. Wahlgren, O. Gropen: *Chem. Phys. Lett.* **251** (1996) 365

[235] M. Iliaš, V. Kellö, L. Visscher, B. Schimmelpfennig: *J. Chem. Phys.* **115** (2001) 9667

[236] L. Visscher, O. Visser, P. J. C. Aerts, H. Merenga, W. C. Nieuwpoort: *Comput. Phys. Commun.* **81** (1994) 120

[237] H. N. Russel, F. A. Saunders: *Astrophys. J.* **61** (1925) 38

[238] W. E. Lamb, R. C. Retherford: *Phys. Rev.* **72** (1947) 241

[239] H. A. Bethe: *Phys. Rev.* **72** (1947) 339

[240] J. P. Briand, P. Chevallier, P. Indelicato, K. P. Ziock, D. D. Dietrich: *Phys. Rev. Lett.* **65** (1990) 2761

[241] I. Goidenko, L. Labzowsky, E. Eliav, U. Kaldor, P. Pyykkö: *Phys. Rev. A* **67** (2003) 020102

[242] K. G. Dyall, C. W. Bauschlicher, D. W. Schwenke, P. Pyykkö: *Chem. Phys. Lett.* **348** (2001) 497

[243] M. J. Vilkas, Y. Ishikawa, K. Hirao: *Chem. Phys. Lett.* **321** (2000) 243

[244] T. H. Dunning, K. A. Peterson, D. E. Woon: In: *Encyclopedia of Computational Chemistry*, ed. P. v. R. Schleyer, pp. 88–115. Wiley, Chichester (1998)

[245] A. J. Sadlej: *Collect. Czech. Chem. Commun.* **53** (1988) 1995

[246] A. J. Sadlej: *Theor. Chim. Acta* **79** (1991) 123

[247] A. J. Sadlej, M. Urban: *Theochem-J. Mol. Struct.* **234** (1991) 147

[248] A. J. Sadlej, M. Urban, O. Gropen: *Phys. Rev. A* **44** (1991) 5547

[249] A. J. Sadlej: *Theor. Chim. Acta* **81** (1991) 45

[250] A. J. Sadlej: *Theor. Chim. Acta* **81** (1992) 339

[251] V. Kellö, A. J. Sadlej: *Theor. Chim. Acta* **83** (1992) 351

[252] V. Kellö, A. J. Sadlej, K. Fægri: *Phys. Rev. A* **47** (1993) 1715

[253] V. Kellö, A. J. Sadlej: *Theor. Chim. Acta* **91** (1995) 353

[254] P. Neogrády, V. Kellö, M. Urban, A. J. Sadlej: *Theor. Chim. Acta* **93** (1996) 101

[255] M. Urban, A. J. Sadlej: *Mol. Phys.* **92** (1997) 587

[256] I. Černušák, V. Kellö, A. J. Sadlej: *Collect. Czech. Chem. Commun.* **68** (2003) 211

[257] V. Kellö, A. J. Sadlej, B. A. Hess: *J. Chem. Phys.* **105** (1996) 1995

[258] V. Kellö, A. J. Sadlej: *Theor. Chim. Acta* **94** (1996) 93

[259] I. Miadoková, V. Kellö, A. J. Sadlej: *Theor. Chem. Acc.* **96** (1997) 166

[260] V. Kellö, A. J. Sadlej, K. Fægri: *J. Chem. Phys.* **108** (1998) 2056

[261] I. Miadoková, V. Kellö, A. J. Sadlej: *Mol. Phys.* **96** (1999) 179

[262] Z. Benková, A. J. Sadlej: *Mol. Phys.* **102** (2004) 687

[263] K. Fægri, K. G. Dyall: In: *Relativistic electronic structure theory, Part 1. Fundamentals*, ed. P. Schwerdtfeger, Theoretical and computational chemistry. Vol. 11, pp. 259–290. Elsevier, Amsterdam (2002)

[264] N. B. Balabanov, K. A. Peterson: *J. Chem. Phys.* **123** (2005) 064107

[265] K. A. Peterson, C. Puzzarini: *Theor. Chem. Acc.* **114** (2005) 283

[266] P. Hohenberg, W. Kohn: *Phys. Rev.* **136** (1964) B864

[267] W. Kohn, L. J. Sham: *Phys. Rev.* **140** (1965) A1133

[268] A. K. Rajagopal, J. Callaway: *Phys. Rev. B* **7** (1973) 1912

[269] A. K. Rajagopal: *J. Phys. C* **11** (1978) L943

[270] E. Engel, S. Keller, A. F. Bonetti, H. Müller, R. M. Dreizler: *Phys. Rev. A* **52** (1995) 2750

[271] E. K. U. Gross, R. M. Dreizler (eds.): *Density functional theory*: Plenum Press, New York (1995)

[272] C. J. Cramer: *Essentials of computational chemistry: theories and models*: Wiley, Chichester, 2nd edn. (2004)

[273] T. Saue, T. Helgaker: *J. Comput. Chem.* **23** (2002) 814

[274] O. Fossgaard, O. Gropen, M. C. Valero, T. Saue: *J. Chem. Phys.* **118** (2003) 10418

[275] P. Salek, T. Helgaker, T. Saue: *Chem. Phys.* **311** (2005) 187

[276] N. Gaston, P. Schwerdtfeger, T. Saue, J. Greif: *J. Chem. Phys.* **124** (2006) 044304

[277] I. S. Lim, M. Pernpointner, M. Seth, J. K. Laerdahl, P. Schwerdtfeger, P. Neogrády, M. Urban: *Phys. Rev. A* **60** (1999) 2822

[278] I. S. Lim, P. Schwerdtfeger, B. Metz, H. Stoll: *J. Chem. Phys.* **122** (2005) 104103

[279] E. Eliav, U. Kaldor, Y. Ishikawa: *Phys. Rev. A* **50** (1994) 1121

[280] W. C. Martin, A. Musgrove, S. Kotochigova, J. E. Sansonetti: *Ground Levels and Ionization Energies for the Neutral Atoms*: National Institute of Standards and Technology, Gaithersburg (2003): http://physics.nist.gov/IonEnergy

[281] I. S. Lim, P. Schwerdtfeger: *Phys. Rev. A* **70** (2004) 062501

[282] F. E. Jorge, A. C. Neto, G. G. Camiletti, S. F. Machado: *J. Chem. Phys.* **130** (2009) 064108

[283] M. Iliaš, P. Neogrády: *Chem. Phys. Lett.* **309** (1999) 441

[284] P. Neogrády, M. Medveď, I. Černušák, M. Urban: *Mol. Phys.* **100** (2002) 541

[285] A. Borschevsky, V. Pershina, E. Eliav, U. Kaldor: *Chem. Phys. Lett.* **480** (2009) 49

[286] M. Iliaš, H. J. Aa. Jensen, V. Kellö, B. O. Roos, M. Urban: *Chem. Phys. Lett.* **408** (2005) 210

[287] M. L. Polak, M. K. Gilles, R. F. Gunion, W. C. Lineberger: *Chem. Phys. Lett.* **210** (1993) 55

[288] L. Demovič, V. Kellö, M. Urban to be published

[289] Y. Ralchenko, A. E. Kramida, J. Reader: *NIST Atomic Spectra Database (version 3.1.5)*: National Institute of Standards and Technology, Gaithersburg, MD (2008): http://physics.nist.gov/asd3

[290] F. Wang, T. Ziegler, E. van Lenthe, S. van Gisbergen, E. J. Baerends: *J. Chem. Phys.* **122** (2005) 204103

[291] S. Yamamoto, H. Tatewaki: *J. Chem. Phys.* **132** (2010) 054303

[292] M. Urban, J. D. Watts, R. J. Bartlett: *Int. J. Quantum Chem.* **52** (1994) 211

[293] R. Pou-Amerigo, M. Merchán, I. Nebotgil, P. O. Widmark, B. O. Roos: *Theor. Chim. Acta* **92** (1995) 149

[294] L. Demovič, I. Černušák, G. Theodorakopoulos, I. D. Petsalakis, M. Urban: *Chem. Phys. Lett.* **447** (2007) 215

[295] V. Kellö, A. Antušek, M. Urban: *J. Comput. Methods Sci. Eng.* **4** (2004) 753

[296] K. Huber, G. Herzberg: *Molecular Spectra and Molecular Structure IV. Constants of Diatomic Molecules*: Van Nostrand Reinhold Co., New York (1979)

[297] B. O. Roos, P.-Å. Malmqvist: *Adv. Quantum. Chem.* **47** (2004) 37

[298] R. R. Reddy, Y. N. Ahammed, K. R. Gopal, P. A. Azeem, B. S. Devi, T. V. R. Rao, S. H. Behere: *Opt. Mater.* **22** (2003) 7

[299] T. Fleig, A. J. Sadlej: *Phys. Rev. A* **65** (2002) 032506

[300] M. Iliaš, P. Furdík, M. Urban: *J. Phys. Chem. A* **102** (1998) 5263

[301] A. Gijsbertsen, W. Siu, M. F. Kling, P. Johnsson, P. Jansen, S. Stolte, M. J. J. Vrakking: *Phys. Rev. Lett.* **99** (2007) 213003

[302] C. Thierfelder, P. Schwerdtfeger, A. Koers, A. Borschevsky, B. Fricke: *Phys. Rev. A* **80** (2009) 022501

[303] M. Schädel: *Angew. Chem.-Int. Edit.* **45** (2006) 368

[304] P. Pyykkö: *Mol. Phys.* **99** (2001) 1617

[305] P. Pyykkö: *Mol. Phys.* **106** (2008) 1965

[306] E. Arimondo, M. Inguscio, P. Violino: *Rev. Mod. Phys.* **49** (1977) 31

[307] W. Gordy, R. L. Cook: *Microwave molecular spectra*: Wiley, New York (1984)

[308] D. A. Shirley: *Rev. Mod. Phys.* **36** (1964) 339

[309] P. Pyykkö: *Z. Naturforsch.* **47a** (1992) 189

[310] M. Urban, A. J. Sadlej: *Chem. Phys. Lett.* **173** (1990) 157

[311] V. Kellö, A. J. Sadlej: *Mol. Phys.* **89** (1996) 127

[312] V. Kellö, A. J. Sadlej: *Chem. Phys. Lett.* **292** (1998) 403

[313] V. Kellö, A. J. Sadlej, P. Pyykkö, D. Sundholm, M. Tokman: *Chem. Phys. Lett.* **304** (1999) 414

[314] V. Kellö, A. J. Sadlej: *Mol. Phys.* **96** (1999) 275

[315] V. Kellö, A. J. Sadlej: *Phys. Rev. A* **60** (1999) 3575

[316] V. Kellö, P. Pyykkö, A. J. Sadlej, P. Schwerdtfeger, J. Thyssen: *Chem. Phys. Lett.* **318** (2000) 222

[317] V. Kellö, A. J. Sadlej: *J. Chem. Phys.* **112** (2000) 522

[318] V. Kellö, A. J. Sadlej, P. Pyykkö: *Chem. Phys. Lett.* **329** (2000) 112

[319] V. Kellö, P. Pyykkö, A. J. Sadlej: *Chem. Phys. Lett.* **346** (2001) 155

[320] J. Bieroń, P. Pyykkö, D. Sundholm, V. Kellö, A. J. Sadlej: *Phys. Rev. A* **64** (2001) 052507

[321] V. Kellö, A. J. Sadlej: *J. Chem. Phys.* **120** (2004) 9424

[322] P. Schwerdtfeger, R. Bast, M. C. L. Gerry, C. R. Jacob, M. Jansen, V. Kellö, A. V. Mudring, A. J. Sadlej, T. Saue, T. Söhnel, F. E. Wagner: *J. Chem. Phys.* **122** (2005) 124317

[323] L. Demovič, V. Kellö, A. J. Sadlej, S. A. Cooke: *J. Chem. Phys.* **124** (2006) 184308

[324] V. Kellö, A. J. Sadlej: *Collect. Czech. Chem. Commun.* **72** (2007) 64

[325] A. D. Buckingham: *J. Chem. Phys.* **36** (1962) 3096

[326] A. Wolf, M. Reiher: *J. Chem. Phys.* **124** (2006) 064102

[327] A. Wolf, M. Reiher: *J. Chem. Phys.* **124** (2006) 064103

[328] R. Mastalerz, G. Barone, R. Lindh, M. Reiher: *J. Chem. Phys.* **127** (2007) 074105

[329] M. Pernpointner, M. Seth, P. Schwerdtfeger: *J. Chem. Phys.* **108** (1998) 6722

[330] M. Barysz, A. J. Sadlej: *Theor. Chem. Acc.* **97** (1997) 260

[331] L. Visscher, T. Enevoldsen, T. Saue, J. Oddershede: *J. Chem. Phys.* **109** (1998) 9677

[332] J. N. P. van Stralen, L. Visscher: *Mol. Phys.* **101** (2003) 2115

[333] F. J. Lovas, E. Tiemann: *J. Phys. Chem. Ref. Data* **3** (1974) 609

[334] A. F. Oluwole, S. G. Schmelling, H. A. Shugart: *Phys. Rev. C* **2** (1970) 228

[335] D. Sundholm, P. Pyykkö, L. Laaksonen, A. J. Sadlej: *Chem. Phys. Lett.* **112** (1984) 1

[336] K. D. Hensel, C. Styger, W. Jager, A. J. Merer, M. C. L. Gerry: *J. Chem. Phys.* **99** (1993) 3320

[337] N. J. Martin, P. G. H. Sandars, G. K. Woodgate: *Proc. Roy. Soc. A* **305** (1968) 139

[338] J. S. M. Harvey, L. Evans, H. Lew: *Can. J. Phys.* **50** (1972) 17191727

[339] R. Weber, B. Jeckelmann, J. Kern, U. Kiebele, B. Aas, W. Beer, I. Beltrami, K. Bos, G. de Chambrier, P. F. A. Goudsmit, H. J. Leisi, W. Ruckstuhl, G. Strassner, A. Vacchi: *Nucl. Phys. A* **377** (1982) 361

[340] S. A. Beaton, M. C. L. Gerry: *J. Chem. Phys.* **110** (1999) 10715

[341] S. Büttgenbach: *Hyperfine structure in 4d- and 5d-shell atoms*: Springer tracts in modern physics 96. Springer-Verlag, Berlin ; New York (1982): p. 83

[342] L. Young, C. A. Kurtz, D. R. Beck, D. Datta: *Phys. Rev. A* **48** (1993) 173

[343] S. Bouazza, J. Dembczynski, E. Stachowska, G. Szawiola, J. Ruczkowski: *Eur. J. Phys. D* **4** (1998) 39

[344] K. Murakawa: *Phys. Rev.* **100** (1955) 1369

[345] A. Svane: *Phys. Rev. B* **68** (2003) 064422

[346] S. A. Cooke, M. C. L. Gerry: *Phys. Chem. Chem. Phys.* **6** (2004) 4579

[347] S. A. Cooke, M. C. L. Gerry: *J. Mol. Spectrosc.* **234** (2005) 195
[348] R. L. A. Haiduke, A. B. F. da Silva, L. Visscher: *J. Chem. Phys.* **125** (2006) 064301
[349] S. Huzinaga, M. Klobukowski: *Theochem-J. Mol. Struct.* **167** (1988) 1
[350] J. Roithová, D. Schröder: *Coord. Chem. Rev.* **253** (2009) 666
[351] P. Schwerdtfeger: *Angew. Chem.-Int. Edit.* **42** (2003) 1892
[352] P. Pyykkö, P. Zaleski-Ejgierd: *J. Chem. Phys.* **128** (2008) 124309
[353] H. Schmidbaur: *Gold Bull.* **33** (2000) 3
[354] E. Kraka, M. Filatov, D. Cremer: *Croat. Chem. Acta* **82** (2009) 233
[355] T. Okabayashi, Y. Nakaoka, E. Yamazaki, M. Tanimoto: *Chem. Phys. Lett.* **366** (2002) 406
[356] P. Schwerdtfeger, J. S. McFeaters, M. J. Liddell, J. Hrušák, H. Schwarz: *J. Chem. Phys.* **103** (1995) 245
[357] P. Schwerdtfeger, M. Dolg, W. H. E. Schwarz, G. A. Bowmaker, P. D. W. Boyd: *J. Chem. Phys.* **91** (1989) 1762
[358] B. Metz, H. Stoll, M. Dolg: *J. Chem. Phys.* **113** (2000) 2563
[359] W. Liu, C. van Wüllen, Y. K. Han, Y. J. Choi, Y. S. Lee: *Adv. Quantum Chem.* **39** (2001) 325
[360] M. Barysz, P. Pyykkö: *Chem. Phys. Lett.* **285** (1998) 398
[361] C. Puzzarini, K. A. Peterson: *J. Chem. Phys.* **122** (2005) 084323
[362] F. A. Cotton, C. B. Harris: *Inorg. Chem.* **4** (1965) 330
[363] S. Ritter: *Chem. Eng. News* **83** (2005) 9
[364] B. O. Roos: *Collect. Czech. Chem. Commun.* **68** (2003) 265
[365] B. O. Roos, L. Gagliardi: *Inorg. Chem.* **45** (2006) 803
[366] T. Nguyen, A. D. Sutton, M. Brynda, J. C. Fettinger, G. J. Long, P. P. Power: *Science* **310** (2005) 844
[367] M. Brynda, L. Gagliardi, P. O. Widmark, P. P. Power, B. O. Roos: *Angew. Chem.-Int. Edit.* **45** (2006) 3804
[368] L. Gagliardi, B. Roos: In: *Lecture Series on Computer and Computational Sciences*, ed. G. Maroulis, vol. 6, pp. 6–22. Brill Academic Publishers, Leiden (2006)
[369] L. Gagliardi, B. O. Roos: *Nature* **433** (2005) 848
[370] B. O. Roos, P.-Å. Malmqvist, L. Gagliardi: *J. Am. Chem. Soc.* **128** (2006) 17000
[371] E. S. Kryachko, F. Remacle: *J. Chem. Phys.* **127** (2007) 194305
[372] E. S. Kryachko: *J. Mol. Struct.* **880** (2008) 23
[373] P. Pyykkö, N. Runeberg: *Chem. Asian J.* **1** (2006) 623
[374] J. Li, Y. X. Qiu, S. G. Wang: *J. Phys. Chem. A* **113** (2009) 1646
[375] I. Štich: *Acta Phys. Slovaca* **57** (2007) 1
[376] M. Konôpka, R. Rousseau, I. Štich, D. Marx: *J. Am. Chem. Soc.* **126** (2004) 12103
[377] M. Konôpka, R. Turanský, M. Dubecký, D. Marx, I. Štich: *J. Phys. Chem. C* **113** (2009) 8878
[378] H. Grönbeck, H. Häkkinen: *J. Phys. Chem. B* **111** (2007) 3325
[379] V. De Renzi: *Surf. Sci.* **603** (2009) 1518
[380] Y. Akinaga, T. Nakajima, K. Hirao: *J. Chem. Phys.* **114** (2001) 8555
[381] A. Casini, C. Hartinger, C. Gabbiani, E. Mini, P. J. Dyson, B. K. Keppler, L. Messori: *J. Inorg. Biochem.* **102** (2008) 564
[382] J. V. Burda, M. Zeizinger, J. Leszczynski: *J. Comput. Chem.* **26** (2005) 907
[383] H. Chojnacki, J. Kuduk-Jaworska, I. Jaroszewicz, J. J. Janski: *Pol. J. Chem.* **83** (2009) 1013

[384] N. P. Labello, A. M. Ferreira, H. A. Kurtz: *J. Phys. Chem. A* **110** (2006) 13507
[385] A. Antušek, M. Urban, A. J. Sadlej: *J. Chem. Phys.* **119** (2003) 7247
[386] J. Granatier, M. Urban, A. J. Sadlej: *J. Phys. Chem. A* **111** (2007) 13238
[387] J. Granatier, M. Urban, A. J. Sadlej: *Chem. Phys. Lett.* **484** (2010) 154
[388] S. Li, K. A. Peterson, D. A. Dixon: *J. Chem. Phys.* **128** (2008) 154301
[389] P. Archirel, V. Dubois, P. Maitre: *Chem. Phys. Lett.* **323** (2000) 7
[390] J. Miyawaki, K. Sugawara, H. Takeo, C. Dedonder-Lardeux, S. Martrenchard-Barra, C. Jouvet, D. Solgadi: *Chem. Phys. Lett.* **302** (1999) 354
[391] V. Dubois, P. Archirel, P. Maitre: *Chem. Phys. Lett.* **323** (2000) 1
[392] N. A. Lambropoulos, J. R. Reimers, N. S. Hush: *J. Chem. Phys.* **116** (2002) 10277
[393] S. F. Boys, F. Bernardi: *Mol. Phys.* **19** (1970) 553
[394] J. Granatier, M. Urban, A. J. Sadlej (2010): to be published
[395] H. M. Lee, S. K. Min, E. C. Lee, J. H. Min, S. Odde, K. S. Kim: *J. Chem. Phys.* **122** (2005) 064314
[396] H. M. Lee, M. Diefenbach, S. B. Suh, P. Tarakeshwar, K. S. Kim: *J. Chem. Phys.* **123** (2005) 074328
[397] C. Gourlaouen, J. P. Piquemal, T. Saue, O. Parisel: *J. Comput. Chem.* **27** (2006) 142
[398] J. Hrušák, D. Schröder, H. Schwarz: *Chem. Phys. Lett.* **225** (1994) 416
[399] S. G. Lias: In: *NIST Chemistry WebBook, NIST Standard Reference Database Number 69*, eds. P. J. Linstrom, W. G. Mallard. National Institute of Standards and Technology, Gaithersburg (): http://webbook.nist.gov
[400] M. Barysz, J. Leszczynski, A. Bilewicz: *Phys. Chem. Chem. Phys.* **6** (2004) 4553
[401] M. Barysz, D. Kędziera, J. Leszczynski, A. Bilewicz: *Int. J. Quantum Chem.* **106** (2006) 2422
[402] H. Fang, S. G. Wang: *Theochem-J. Mol. Struct.* **773** (2006) 15
[403] O. D. Häberlen, N. Rösch: *J. Phys. Chem.* **97** (1993) 4970
[404] T. M. Bernhardt, J. Hagen, S. M. Lang, D. M. Popolan, L. D. Socaciu-Siebert, L. Woste: *J. Phys. Chem. A* **113** (2009) 2724
[405] P. Schwerdtfeger, M. Lein, R. P. Krawczyk, C. R. Jacob: *J. Chem. Phys.* **128** (2008) 124302
[406] S. G. Wang, W. H. E. Schwarz: *J. Am. Chem. Soc.* **126** (2004) 1266
[407] B. Ruscic, J. Berkowitz: *J. Chem. Phys.* **97** (1992) 1818
[408] G. D. Bent: *J. Chem. Phys.* **89** (1988) 7298
[409] R. S. Mulliken, W. B. Person: *Molecular complexes; a lecture and reprint volume*: Wiley-Interscience, New York, (1969)
[410] I. S. Lim, P. Botschwina, R. Oswald, V. Barone, H. Stoll, P. Schwerdtfeger: *J. Chem. Phys.* **127** (2007) 104313
[411] G. Frenking: *J. Organomet. Chem.* **635** (2001) 9
[412] J. Kundu, O. Neumann, B. G. Janesko, D. Zhang, S. Lal, A. Barhoumi, G. E. Scuseria, N. J. Halas: *J. Phys. Chem. C* **113** (2009) 14390
[413] M. Hargittai: *Accounts Chem. Res.* **42** (2009) 453
[414] K. J. Donald, M. Hargittai, R. Hoffmann: *Chem.-Eur. J.* **15** (2009) 158
[415] E. S. Kryachko, F. Remacle: *Mol. Phys.* **106** (2008) 521
[416] A. Zaitsevskii, C. van Wüllen, A. V. Titov: *J. Chem. Phys.* **132** (2010) 081102
[417] T. Helgaker, M. Jaszuński, K. Ruud: *Chem. Rev.* **99** (1999) 293
[418] J. Vaara: *Phys. Chem. Chem. Phys.* **9** (2007) 5399
[419] M. Iliaš, T. Saue, T. Enevoldsen, H. J. Aa. Jensen: *J. Chem. Phys.* **131** (2009) 124119

[420] T. Saue: In: *Relativistic electronic structure theory, Part 1. Fundamentals*, ed. P. Schwerdtfeger, Theoretical and computational chemistry. Vol. 11, pp. 332–400. Elsevier, Amsterdam (2002)

[421] G. A. Aucar, T. Saue, L. Visscher, H. J. Aa. Jensen: *J. Chem. Phys.* **110** (1999) 6208

[422] F. London: *J. Phys. Radium* **8** (1937) 397

[423] T. Helgaker, P. Jørgensen: *J. Chem. Phys.* **95** (1991) 2595

[424] T. Saue, K. Fægri, T. Helgaker, O. Gropen: *Mol. Phys.* **91** (1997) 937

[425] S. Komorovský, M. Repiský, O. L. Malkina, V. G. Malkin, I. M. Ondík, M. Kaupp: *J. Chem. Phys.* **128** (2008) 104101

[426] L. Cheng, Y. Xiao, W. Liu: *J. Chem. Phys.* **131** (2009) 244113

[427] S. Komorovský, M. Repiský, O. L. Malkina, V. G. Malkin: *J. Chem. Phys.* **132** (2010) 154101

[428] M. Repiský, S. Komorovský, E. Malkin, O. L. Malkina, V. G. Malkin: *Chem. Phys. Lett.* **488** (2010) 94

[429] P. Manninen, P. Lantto, J. Vaara, K. Ruud: *J. Chem. Phys.* **119** (2003) 2623

[430] M. Jaszuński, K. Ruud: *Mol. Phys.* **104** (2006) 2139

[431] J. Gauss, J. F. Stanton: *Adv. Chem. Phys.* **123** (2002) 355

[432] A. Antušek, M. Jaszuński: *Mol. Phys.* **104** (2006) 1463

[433] A. Antušek, D. Kędziera, K. Jackowski, M. Jaszuński, W. Makulski: *Chem. Phys.* **352** (2008) 320

[434] A. Antušek, M. Pecul, J. Sadlej: *Chem. Phys. Lett.* **427** (2006) 281

[435] V. G. Malkin, O. L. Malkina, D. R. Salahub: *Chem. Phys. Lett.* **261** (1996) 335

[436] M. Bühl, M. Kaupp, O. L. Malkina, V. G. Malkin: *J. Comput. Chem.* **20** (1999) 91

[437] M. Kaupp, M. Bühl, V. G. Malkin: *Calculation of NMR and EPR parameters : theory and applications*: Wiley-VCH, Weinheim (2004)

[438] S. K. Wolff, T. Ziegler, E. van Lenthe, E. J. Baerends: *J. Chem. Phys.* **110** (1999) 7689

[439] S. K. Wolff, T. Ziegler: *J. Chem. Phys.* **109** (1998) 895

[440] R. Bouten, E. J. Baerends, E. van Lenthe, L. Visscher, G. Schreckenbach, T. Ziegler: *J. Phys. Chem. A* **104** (2000) 5600

[441] V. Pershina, J. Anton, B. Fricke: *J. Chem. Phys.* **127** (2007) 134310

[442] V. Pershina, T. Bastug: *Chem. Phys.* **311** (2005) 139

[443] V. Pershina, J. Anton, T. Bastug: *Eur. Phys. J. D* **45** (2007) 87

[444] V. Pershina, A. Borschevsky, E. Eliav, U. Kaldor: *J. Chem. Phys.* **129** (2008) 144106

[445] I. Černušák, M. Aranyosiová, O. Vollárová, D. Velič, O. Kirdajová, J. Benko: *Int. J. Quantum Chem.* **109** (2009) 2365

[446] M. Ilčin, V. Lukeš, V. Laurinc, S. Biskupič: *Collect. Czech. Chem. Commun.* **72** (2007) 363

[447] L. Bučinský, S. Biskupič, M. Ilčin, V. Lukeš, V. Laurinc: *J. Comput. Chem.* **30** (2009) 65

[448] M. Ilčin, V. Lukeš, L. Bučinský, V. Laurinc, S. Biskupič: *Int. J. Quantum Chem.* **108** (2008) 2150

[449] C. Vogt, R. D. Hoffmann, U. C. Rodewald, G. Eickerling, M. Presnitz, V. Eyert, W. Scherer, R. Pottgen: *Inorg. Chem.* **48** (2009) 6436

[450] J. A. Li, G. Schreckenbach, T. Ziegler: *Inorg. Chem.* **34** (1995) 3245

[451] G. Eickerling, R. Mastalerz, V. Herz, W. Scherer, H. J. Himmel, M. Reiher: *J. Chem. Theory Comput.* **3** (2007) 2182

[452] P. Pyykkö, N. Runeberg: *Angew. Chem.-Int. Edit.* **41** (2002) 2174

[453] X. Li, B. Kiran, J. Li, H. J. Zhai, L. S. Wang: *Angew. Chem.-Int. Edit.* **41** (2002) 4786

[454] K. Manninen, P. Pyykkö, H. Häkkinen: *Phys. Chem. Chem. Phys.* **7** (2005) 2208

[455] M. Haruta, T. Kobayashi, H. Sano, N. Yamada: *Chem. Lett.* (1987) 405

[456] S. Tokonami, H. Shiigi, T. Nagaoka: In: *Nanostructured thin films and surfaces*, ed. C. S. S. R. Kumar, pp. 175–202. Wiley-VCH, Weinheim (2010)

[457] T. Söhnel, H. Hermann, P. Schwerdtfeger: *Angew. Chem.-Int. Edit.* **40** (2001) 4382

[458] T. Söhnel, H. Hermann, P. Schwerdtfeger: *J. Phys. Chem. B* **109** (2005) 526

[459] S. Biering, A. Hermann, J. Furthmüller, P. Schwerdtfeger: *J. Phys. Chem. A* **113** (2009) 12427

[460] N. Gaston, P. Schwerdtfeger: *Phys. Rev. B* **74** (2006) 024105

[461] B. Paulus, K. Rosciszewski, N. Gaston, P. Schwerdtfeger, H. Stoll: *Phys. Rev. B* **70** (2004)

[462] E. Pahl, F. Calvo, P. Schwerdtfeger: *Int. J. Quantum Chem.* **109** (2009) 1812

[463] A. Zaitsevskii, C. van Wüllen, E. A. Rykova, A. V. Titov: *Phys. Chem. Chem. Phys.* **12** (2010) 4152

Miroslav Iliaš born in Bojnice, Slovakia (1975), graduated in Physical Chemistry at the Comenius University in Bratislava (1998). At the same institution he received his PhD. degree in Chemical Physics (2002). Afterwards he spent more than 4 years at various institutions abroad (Denmark, France, Israel) as a post-doctoral fellow, working on the development and applications of methods of relativistic quantum chemistry with professors L. Visscher, T. Saue, H. J. A. Jensen, U. Kaldor. Up to 2009 he worked at the University of Žilina, presently he is a faculty member at the Matej Bel University in Banská Bystrica, Slovakia.

Vladimr Kellö was born in Bratislava, Czechoslovakia (1947). He studied chemistry at the Comenius University Bratislava, where he graduated in 1972 and in 1977 he received PhD. from the same institution working with Miroslav Urban on a topic ab initio calculations of equilibrium constants of chemical reactions. He has been on the faculty of the Comenius University since 1978. He was a postdoctoral fellow at Max-Planck Institute of Astrophysics in Garching, Germany with Geerd H. F. Diercksen in the period 1981-1982 and later was a frequent visitor and spent many months at this institute. A close scientific collaboration with Andrzej J. Sadlej began during the Garching postdoctoral stay and lasted for 30 years. In the frame of this collaboration he many times visited University of Lund, Sweden and later the Copernicus University Torun, Poland. He became Associated Professor in 1991, received the D.Sc. degree in 1995, and was promoted to Full Professor at the Comenius University in 1998. His research centers on calculations of atomic and molecular properties by means of highly electron correlated methods with inclusion of relativistic effects, with particular interest in electric dipole moments, polarizabilities and field gradients.

Miroslav Urban (1942) is a Professor at the Slovak University of Technology in Bratislava, Faculty of Materials Science and Technology in Trnava, Slovakia. Since 1964 he worked at the Comenius University, Faculty of Natural Sciences, up to January 2009 as a Full Professor of Theoretical and Computational Chemistry. He received his master degree in Physical chemistry at the Comenius University (1964), Phd. Degree at the Charles University in Prague (1972; supervisors J. Koutecký, J. Paldus and R. Polák). He worked repeatedly as a visiting scientist/visiting Professor at the Quantum Theory Project, University of Florida, Gainesville, USA (with Professor R. J. Bartlett), Max-Planck Institute for Astrophysics, Garching, Germany (with Professor G. H. F. Diercksen), Department of Theoretical Chemistry, University of Lund, Sweden (with Professor A. J. Sadlej), Center for Computational Quantum Chemistry, University of Georgia, Athens, USA (with Professor H. F. Schaefer). He published 108 scientific papers, 3 books, 3 chapters in monographs. His scientific interests are focused to the development of the Many-Body Perturbation Theory and Coupled Cluster methods, developments of efficient computer codes, applications to accurate calculations of, e.g., electric and optical properties, electron affinities, reaction and interaction energies, relativistic and electron correlation effects in molecular properties. He is a member of the scientific board of the World Association of Theoretical and Computational Chemists, a member of the International Academy of Quantum Molecular Science, Slovak Academic Society, and Learned Society of the Slovak Academy of Sciences.